Antibody Targeted Nanoparticles for Imaging and Therapy of Cancer

Kim Louise Vigor

A thesis submitted to the University College London for the degree of Doctor of Philosophy in the faculty of Biomedical Sciences,

Department of Oncology,
UCL Cancer Institute,
University College London

February 2010

Abstract

The central hypothesis for this thesis is that antibody-targeted superparamagnetic iron oxide nanoparticles (SPIONs) can be used for diagnosis and therapy of cancer. The hypothesis is based on the knowledge that firstly, recombinant single chain Fv antibody fragments (scFv) are effective targeting reagents and second, SPIONs can substantially improve the sensitivity of magnetic resonance imaging (MRI). Furthermore, SPIONs can be induced to generate heat when subjected to an alternating magnetic field (AMF).

The aim of the thesis was to test the cancer imaging and therapeutic potential scFv-functionalised nanoparticles by: (1) Generating scFvs reactive with carcinoembryonic antigen (CEA) a cell surface tumour marker. (2) Developing conjugation methods to attach the scFv, in functional form, to SPIONs. (3) Evaluating the cellular interaction (targeting and specificity) of functionalised SPIONs and (4) Measuring the imaging and therapeutic heating effect of the targeted SPIONs.

ScFvs reactive to CEA were generated in *Pichia pastoris* and conjugation chemistries optimised for attachment of purified scFv to SPION surface. Targeting efficacy of the scFv functionalised SPIONs was tested by ELISA, cellular uptake, confocal microscopy and MRI. Results demonstrated unequivocal CEA-specific cellular uptake and CEA-specific MRI, using SPIONs conjugated with Sm3E, a high affinity humanized anti-CEA scFv. Cellular interaction of the Sm3E-SPIONs was found to be influenced by size and surface properties; neutrally charged Sm3E functionalised dextran SPIONs localised preferentially to the outside of the cell membrane, whilst negatively charged Sm3E functionalised PEGylated SPIONs showed evidence of intracellular uptake. The SPIONs were shown to be effective generators of heat when exposed to AMF of 150V, 0.74A and 1MHz. AMF treatment of Sm3E-SPION targeted cells was found to induce expression of the stress protein HSP70 and lead to hyperthermic cell death *in vitro*.

These results indicate that scFv-SPION conjugates have potential for selective tumour imaging and therapy.

Declaration of Originality

I Kim Vigor declare that the research for this thesis is original and that the ideas were developed by me in conjunction with my supervisors. Where information has been derived from other sources; I confirm that this has been indicated in the thesis.

Contents

Title page……..... I
Abstract……..... II
Declaration……..... III
Contents……..... IV
List of Figures……..... X
List of Tables……..... XIII
List of Equations……..... XIV
List of Abbreviations……..... XV
Acknowledgements……..... XX

CHAPTER 1 · Introduction

1.1 Cancer ……. 2
1.2 Carcinoembryonic antigen …….. 3
1.3 Antibodies and their use in cancer therapy…….. 5
1.3.1 Antibody structure and function……..... 5
1.3.2 Hybridoma technology…….. 8
1.3.3 Humanisation…… 8
1.3.4 Treatment of cancer with antibodies …… 9
1.3.4.1 Non-conjugated mAbs ……..... 9
1.3.4.2 Immunoconjugates……..... 11
1.4 Recombinant antibody technology……... 12
1.4.1 Phage display technology……..... 12
1.4.2 Recombinant antibody fragments …… 14
1.4.2.1 Fab ……..... 14
1.4.2.2 scFv …… 15
1.4.2.3 Domain antibodies…….. 15
1.4.2.4 Multivalency…….. 17
1.5 Anti CEA scFv MFE-23 and Sm3E……..... 17
1.6 Superparamagnetic iron oxide nanoparticles (SPIONs)……..... 19
1.6.1. Stabilising coating ……. 20

1.6.1.1 Adsorption of dextran 20
1.6.2. Stealth coatings 20
1.6.2.1 Incorporation into liposomes 21
1.6.2.2 Addition of polyethylene glycol chain 21
1.6.3. Surface functionalisation 22
1.7 Magnetic resonance imaging..... 24
1.7.1. Application of SPIONs in MRI 25
1.8 Hyperthermic therapy 27
1.8.1. Application of SPIONs in hyperthermia 29
1.9 Research aims..... 31

CHAPTER 2 · Materials and Methods

2.1 Materials..... 33
2.1.1. Microbial strains..... 37
2.1.2. Proteins..... 38
2.1.3. Human cell lines..... 38
2.1.4. Antibodies 38
2.1.5 Superparamagnetic iron oxide nanoparticles..... 39
2.2 Methods..... 40
2.2.1. Protein expression..... 40
2.2.1.1 Fermentation of Pichia pastoris X-33 cells..... 40
2.2.2. Protein purification 41
2.2.2.1 Expanded-bed adsoption immobilised metal affinity chromatography 41
2.2.2.2 Size exclusion chromatography..... 42
2.2.3. Protein characterisation 43
2.2.3.3 Western Blot Analysis 44
2.2.3.4 Enzyme linked immunosorbant Assay..... 45
2.2.4. Antibody-SPION conjugation chemistry..... 46
2.2.4.1 Sodium periodate conjugation 46
2.2.4.2 Carbodiimide conjugation 46

2.2.4.3 Cyanogen bromide conjugation ……..... 47
2.2.5. ScFv-SPION conjugation analysis…… 47
2.2.5.1 Ratio of scFv-SPION in conjugate solution ……..……... 47
2.2.5.2 Ferrozine assay to estimate iron concentration …….. 49
2.2.5.3 Magnetic resonance imaging potential of SPIONs …… ….. 50
2.2.5.4 Alternating magnetic field heating potential of SPIONs …….. 50
2.2.5.5 Zeta potential of SPIONs ……... 50
2.2.6. Cell culture……... 50
2.2.6.1 Taking cell lines into culture…… 50
2.2.6.2 Propagation of adherent cell lines LS174T and A375M …….. 51
2.2.6.3 Cryogenic storage…… 51
2.2.7. *In vitro* analysis of scFv-SPIONs ……..... 51
2.2.7.1 Ferrozine assay to measure cell SPION uptake……..... 51
2.2.7.2 MTT toxicity assay……...……..... 52
2.2.7.3 Immunostaining of adherent cells incubated in scFv-SPIONs…… 53
2.2.7.4 Magnetic resonance imaging (MRI) of adherent cells incubated in scFv-SPIONs …… 54
2.2.8. Hyperthermic *in vitro* studies …… 54
2.2.8.1 Incubator heating of adherent cells: viable cell counts……..... 54
2.2.8.2 Incubator heating of adherent cells: MTT assay…….. ……..... 55
2.2.8.3 Incubator heating of adherent cells: heat shock protein 70 immunocytochemistry staining……..... 56
2.2.8.4 AMF heating of adherent cells: viable cell counts……..... 56
2.2.8.5 AMF heating of adherent cells incubated in SPIONs: MTT assay…… 57
2.2.8.6 AMF heating of adherent cells incubated in SPIONs: heat shock protein 70 immunocytochemistry staining……... 58
2.2.9. *In vivo* biodistribution study …….. 59
2.2.9.1 LS174T colorectal tumour xenografts…….…….....…….....…… 59
2.2.9.2 Biodistribution of Sm3E-SPION conjugates …….. ……..... 59
2.2.9.3Prussion blue staining from frozen tissue sections ……. 60

CHAPTER 3 · Conjugation of Anti CEA scFvs to Superparamagnetic Iron Oxide Nanoparticles

3.1 Introduction…… 62

3.2 Objectives…….... 63

3.3 Results…….…….... 64

3.3.1. Generation of anti CEA scFv …… 64

3.3.2.1 MFE-23 ……..…….... 64

3.3.2.2 Sm3E ……..…….... 64

3.3.2 SPION stability ……..... 67

3.3.3 SPION iron content ……..... 71

3.3.4 Sodium periodate conjugation of MFE-23 to SPIONs ……..... 72

3.3.5 Optimisation of MFE-23-SPION conjugation.……..... 75

3.3.6 Application of optimised conjugation chemistry to Sm3E ……..……... 78

3.3.6.1 DX-SPIONs ……..…….... 78

3.3.6.2 dSPIONs ……..…….... 78

3.3.7 Cyanogen bromide conjugation of Sm3E to DX-SPIONs.……..... 81

3.3.8 Carbodiimide conjugation of Sm3E scFv to SPIONs……... 84

3.3.8.1 CMX-SPIONs ……..…….... 85

3.3.8.2 PEG-dSPIONs ……..…….... 85

3.4 Discussion……... 90

3.5 Summary……..... 94

CHAPTER 4 · Interaction of Functionalised SPIONs with Cancer Cells

4.1 Introduction…… 97

4.2 Objectives……... 98

4.3 Results…….. 99

4.3.1 Quantification of SPION uptake …..... 99

4.3.2 Specificity of SPION uptake …..... 101

4.3.3 Effect of SPION surface chemistry …..... 103

4.3.4 Intracellular trafficking …..... 105

4.3.5 Surface charge…. 107
4.4 Discussion…… 108
4.5 Summary……. 111

CHAPTER 5 · Imaging Potential of Functionalised SPIONs

5.1 Introduction…… 113
5.2 Objectives…….. 114
5.3 Results…….. 115
5.3.1 *In vitro* cytotoxicity…. 115
5.3.2 Magnetic resonance imaging potential of SPIONs …. 116
5.3.3 *In vitro* MRI of Sm3E-SPIONs …. 117
5.3.2.1 Sm3E-d50 ……..…….. 117
5.3.3.2 Sm3E-PEG-d50…….. 118
5.3.3.3 Sm3E-PEG-d20 ……..…….. 118
5.3.4 Biodistribution of Sm3E-SPIONs …. 120
5.4 Discussion…… 122
5.5 Summary……. 125

CHAPTER 6 · Therapeutic Potential of Functionalised SPIONs

6.1 Introduction…… 128
6.2 Objectives……... 129
6.3 Results…….. 130
6.3.1 Temperature effect on cell viability …… 130
6.3.2 Temperature effect on cellular HSP70 response……... 131
6.3.3 Magnetic fluid hyperthermia using AMF system 1 …… 132
6.3.3.1 AMF induced heating of d100 and DX100 ……..…….. 132
6.3.3.2 Cell viability following magnetic fluid hyperthermia……..…….. 133
6.3.3.3 Induction of HSP by magnetic fluid hyperthermia ……..…….. 135
6.3.4 Magnetic fluid hyperthermia using AMF system 2 …… 137
6.3.4.1 AMF induced heating of d100 ……..…….. 138
6.3.4.2 AMF induced heating of d50, PEG-d50 and PEG-d20……..…….. 139

6.3.4.3 AMF induced heating of DX100……..139
6.3.4.4 Cell viability following magnetic fluid hyperthermia……..140
6.3.5 Effect of cellular uptake of SPIONs on magnetic fluid hyperthermia……..144
6.3.5.1 Cell loading ……..144
6.3.5.2 Heating mechanism……..145
6.4 Discussion……..147
6.5 Summary……..152

CHAPTER 7 · Conclusion and future directions

7.1 Conclusion and future directions……154

APPENDIX 1. References……158
APPENDIX 2. Presentations and Publications……184

List of Figures

Chapter 1		**Page**
Figure 1.1	Commonly diagnosed cancers…….....	2
Figure 1.2	Structure of Immunoglobulin G …….	6
Figure 1.3	Humanisation of a whole antibody……..	9
Figure 1.4	Genetically engineered antibody fragments…….	16
Figure 1.5	SPION coatings……	23
Figure 1.6	Neél and Brownian rotation……	30
Chapter 2		
Figure 2.1	Protein standards……	37
Chapter 3		
Figure 3.1	SDS-PAGE and ELISA of purified MFE-23……..	64
Figure 3.2	SDS-PAGE analysis of large scale EBA-IMAC purification of Sm3E……	65
Figure 3.3	SEC profile of EBA-IMAC purified Sm3E…….	66
Figure 3.4	SDS-PAGE and Western blot analysis of SEC purified Sm3E…..	66
Figure 3.5	ELISA of SEC purified Sm3E ……	67
Figure 3.6	Magnetic separation of DX-SPIONs and CMX-SPIONs……	68
Figure 3.7	SEC profile of d50, DX100 and CMX50……	69
Figure 3.8	Ferrozine iron assay analysis of SPIONs…….	71
Figure 3.9	Evaluation of SPION concentration by absorbance readings at 490nm……..	72
Figure 3.10	Schematic representation of sodium periodate conjugation chemistry……..	73
Figure 3.11	SEC profile of MFE-23-d50……	74
Figure 3.12	CEA ELISA of purified MFE-23-d50…….	74
Figure 3.13	Western blot analysis of MFE-23-d50 ……	75

Figure 3.14 SEC profile of MFE-23-d50 after optimisation……... 76
Figure 3.15 Western blot analysis of MFE-23-d50 SEC fraction after optimization……. 77
Figure 3.16 ELISA of MFE-23-d50 SEC fraction after optimisation …… 77
Figure 3.17 SEC profile of Sm3E-dSPIONs …… 79
Figure 3.18 ELISA of SEC purified Sm3E-dSPIONs……. 80
Figure 3.19 Schematic representation of cyanogen bromide conjugation chemistry……. 81
Figure 3.20 Stability analysis of Sm3E-DX-SPIONs…… 82
Figure 3.21 ELISA of magnetically purified Sm3E-DX-SPIONs……. 83
Figure 3.22 Schematic representation of carbodiimide conjugation chemistry.. 84
Figure 3.23 SEC profile of Sm3E-PEG-dSPION…… 86
Figure 3.24 ELISA of SEC purified Sm3E-PEG-dSPION……. 87

Chapter 4

Figure 4.1 Standard curve of Ferrozine assayed……... 101
Figure 4.2 Confocal microscopy analysis of Sm3E-d50 …….. 102
Figure 4.3 Confocal microscopy analysis of Sm3E-d100 …… 103
Figure 4.4 Confocal microscopy analysis of Sm3E-PEG-d50 …… 104
Figure 4.5 Confocal microscopy analysis of Sm3E-PEG-d20 ……. 105
Figure 4.6 Endosomal localization of Sm3E-PEG-d50……... 106

Chapter 5

Figure 5.1 SPION cytotoxicity…… 115
Figure 5.2 MRI Phantom…….. 116
Figure 5.3 MRI analysis of SPIONs……. 117
Figure 5.4 MRI analysis of Sm3E functionalised SPIONs *in vitro*……... 119
Figure 5.5 Biodistribution of Sm3E functionalised SPIONs ……... 121

Chapter 5

Figure 6.1 Affect of heat on cell survival…….. 130

Figure 6.2	Confocal analysis of HSP70 expression following heating…….	131
Figure 6.3	AMF heating system 1…….	132
Figure 6.4	Heating profile of SPIONs in AMF system 1….....	133
Figure 6.5	Cell viability following MFH in AMF system 1…….	134
Figure 6.6	Confocal analysis of HSP70 expression following MFH in AMF system 1……...	136
Figure 6.7	AMF heating system 2…….	137
Figure 6.8	Heating profile of d100 in AMF system 2…….....	138
Figure 6.9	Heating profile of d100, d50, PEG-d50 and PEG-d20 in AMF system 2…….....	139
Figure 6.10	Heating profile of DX100 in AMF system 2…….....	140
Figure 6.11	Cell viability following MFH with d100 and DX100…….	142
Figure 6.12	Cell viability following MFH with d50, PEG-d50 and PEG-d20…	143
Figure 6.13	Cellular uptake of Sm3E-DX100 as quantified by Ferrozine assay	144
Figure 6.14	Cell viability following MFH of cells loaded with Sm3E-DX100..	145
Figure 6.11	AMF heating of d100nm and DX100 in water or glycerol……..	146

List of Tables

Chapter 1		**Page**
Table 1.1	FDA approved recombinant antibodies for the treatment of cancer…….	10
Table 1.1	FDA approved immuno-conjugates for the treatment of cancer…	11
Chapter 2		
Table 2.1	Microbial culture media and solutions for yeast fermentation …..	33
Table 2.2	Solutions for EBA-IMAC purification……...	34
Table 2.3	Buffers for protein manipulation……	34
Table 2.4	Solutions for scFv-SPION sodium periodate conjugation…….	35
Table 2.5	Solutions for scFv-SPION carbodiimide conjugation……	35
Table 2.6	Solutions for scFv-SPION cyanogen bromide conjugation ……	36
Table 2.7	Solutions for tissue culture……	36
Table 2.8	Solutions for immunostaining adherent cells……	36
Table 2.9	Solutions for ferrozine assay…….	36
Table 2.10	Solutions for Prussian blue staining……...	37
Table 2.11	SPION nomenclature…….	39
Table 2.12	Flow rates for the addition of glycerol and methanol during yeast fermentation……...	41
Table 2.13	Antibody dilutions…….	45
Chapter 3		
Table 3.1	Summary of successful purification protocols……..	70
Table 3.2	Estimation of scFv:SPION binding ratio……...	88
Table 3.3	Summary of results……	89
Chapter 4		
Table 4.1	Cellular uptake of Sm3E functionalized SPIONs …….	100

Table 4.2 Summary of results……..... 107

List of Equations

Chapter 1 **Page**

Equation 1.1 $SAR = C\,\Delta T/\Delta t$……. 30

Chapter 2

Equation 2.1 $A_{280}=\varepsilon_{280} \times c \times l$…… 43

Equation 2.2 $moles = \frac{[Sm3E][\mu g/ml]}{MW[kDa]}$ ……. 48

Equation 2.3 $nSm3E/ml = moles \times N_A$ ……. 48

Equation 2.4 $nSPION/ml = [SPION][mg/ml] \times nSPION/mg$ ……..... 49

Equation 2.5 $nSm3E/nSPION = \frac{nSm3E/ml}{nSPION/ml}$ …….. 49

Equation 2.6 $SPION/cell[\mu g] = \frac{[SPION][\mu g/well]}{nCell/well}$ ……. 52

Equation 2.7 $nCell = 2 \times 1 \times 10^4 [cells/ml] \times Tvol[ml]$……. 55

.

List of Abbreviations

A	Amplitude
ADCC	Antibody dependant cellular cytotoxicity
ADEPT	Antibody directed enzyme prodrug therapy
AMF	Alternating magnetic field
Anti-HIS	monoclonal antibody raised against the hexahistidine tag
Anti-MFE-23	Rabbit polyclonal antibody raised against MFE-23
A375M	Human melanoma cell line
B_0	Magnetic field
bp	Base pair
C	Constant domain
C_L	light chain constant domain
C_H	heavy chain constant domain
CDC	Complement dependent cytotoxicity
CDR	Complementarity determining region
CEA	Carcinoembryonic antigen
CMX-SPION	Carboxymethylated dextran coated SPION from chemicell GMbH
COOH	Carboxyl group
CT	Computer tomography
Da	Dalton
DAB	3,3'-Diaminobenzidine
dH_2O	Double-distilled water
DNA	Deoxyribonucleic acid
DMSO	
dSPION	Dextran coated SPION from micromod GMbH
DTPA	Diethylenetriaminepentaacetic acid
DX-SPION	Dextran coated SPION from chemicell GMbH
EBA-IMAC	Expanded bed adsorption immobilised metal affinity

	chromatography
EDC	N-ethyl-N'-(3-diethyl-aminopropyl)-carbodiimide
E. coli	*Escherichia coli*
EDTA	Ethylenediamine tetraacetic acid
EGFR	Epidermal growth factor reecptor
ELISA	Enzyme-linked immunosorbent assay
EU	Europe
Fab	Fragment released from papain digestion of an IgG
Fc	Constant fragment
FDA	Federal drug association
Fe	Iron
FPLC	Fast pressure liquid chromatography
Fv	Variable region fragment
g	gram
Gd	Gadolilium
GO	Gemtuzumab ozogamicin
hr	hour
H	Heavy chain
HAMA	Human anti-mouse antibodies
HR	High resolution
HRP	Horseradish peroxidase
HSP	Heat Shock Protein
Hz	Hertz
Ig	immunoglobulin
IMAC	Immobilised metal affinity chromatography
K_D	Dissociation constant
kDa	kiloDalton
κ	kappa
l	litre
L	Light chain
LSM	Laser scanning microscope

λ	lambda
LHRH	Luteinizing hormone releasing hormone
LS174T	Human colorectal adenocarcinoma cell line
N	Nitrogen
NH_2	Amine group
NIR	Near infra-red irradiation
nm	nanometers
M	molar
MAb	Monoclonal antibody
MCL	Magnetic cationic liposomes
MES	2-(4-morpholino) ethanesulphonic HCL
MFH	Magnetic fluid hyperthermia
MHC	Major histocompatibility complex
MRI	Magnetic resonance imaging
MTT	3-(4,5-Dimethylthiazol-2-yl)-2,5-diphenyltetrazolium
MW	Molecular weight
MHz	Mega hertz
µg	Microgram
mg	Milligram
min	minute
µM	micromolar
mM	millimolar
µl	microlitre
ml	millilitre
NHS	N-hydroxysuccinimide
OD	Optical density
OPD	O-phenylenediamine dihydrochloride
PBS	Phosphate buffered saline
PCR	Polymerase chain reaction
PEG	Poly(ethylene) glycol
PEG-dSPION	PEGylated dextran coated SPION from Micromod GMbH

PET	Positron emission tomography
PM	Paramagnetic material
P. pastoris	*Pichia pastoris*
PVDF	Polyvinylidene difluoride
RAID	Radio-immunodetection
RES	Reticuloendothelial system
RF	Radiofrequency
RIGS	Radio-immunoguided surgery
RIT	Radioimmunotherapy
RNA	Ribonucleic acid
rpm	Revolutions per minute
RT	Room temperature
s	second
SAR	Specific absorption rate
ScFab	Single chain Fab
scFv	Single chain fragment variable
SDS	Sodium dodecyl sulphate
SDS-PAGE	SDS-polyacrylamide gel electrophoresis
SEC	Size exclusion chromatography
SPIONs	Superparamagnetic iron oxide nanoparticles
T	Tesla
T_1	Longitudinal relaxation
T_2	Transverse relaxation
TAA	Tumour associated antigen
T_c	Cytotoxic T cells
TE	Echo time
TR	Repetition time
UV	ultraviolet
V	Variable domain
V	Voltage
V_H	Heavy chain variable domain

V_HH	Variable heavy domains from camelids
V_L	Light chain variable domain
V-NAR	Variable heavy domains from sharks
v/v	Volume to volume
w/v	Weight to volume

Acknowledgements

I would like to thank Professor Kerry Chester for her encouragement, advice and support throughout my PhD. I also thank Professor Richard Begent for allowing me to pursue my PhD in his laboratory and Professor Quentin Pankhurst for his supervision and helpful discussions in particle physics. I would also like to acknowledge the Trustees of the Restoration of Appearance and Function Trust and Rosetree Trust for their financial support of my studentship.

Thanks to everyone I have worked alongside during my PhD in the Department of Oncology. In particularly I would like to thank Dr. Berend Tolner (especially for critical, last-minute proof-reading), Lynda Robson, Helen Lowe, Dr Noelia Sainz, Dr Heide Kogelberg, Bettina Berndl and Natalie Griffith for their constant support. Thanks also goes to Professor Barbara Pedley, Matthew Robson and Uzma Quesh for help with the *in vivo* work. Dr. Mark Lythgoe and Panagiotis Kyrtatos at the Centre of Advance Biomedical Imaging UCL, Dr Shane Minogue at the Centre of Molecular Biology UCL, Dr Kostas Kostarelos and Dr Khuloud Al-Jamal at the Centre for Drug Delivery Research (University of London), Dr Kerstin Rolfe and Janette Richardson at RAFT and Dr Paul Southern and Mathew Kallumadil at the Royal Institution of Great Britain.

Finally, I would like to thank my family, especially my husband Chris and sister Charlotte for constant encouragement and for always being there.

Chapter 1

Introduction

1.1 Cancer

Cancer is one of the major causes of illness and death worldwide. One in 3 people will develop malignancies in their lifetime, with half the people diagnosed with cancer dying within 5 years (cancerresearchuk.org). Cancer occurs in a wide range of tissues with different outcomes. For example, in the UK there are over 200 types of cancers, with lung, breast, prostate and colon cancer accounting for the majority of deaths (Fig. 1.1).

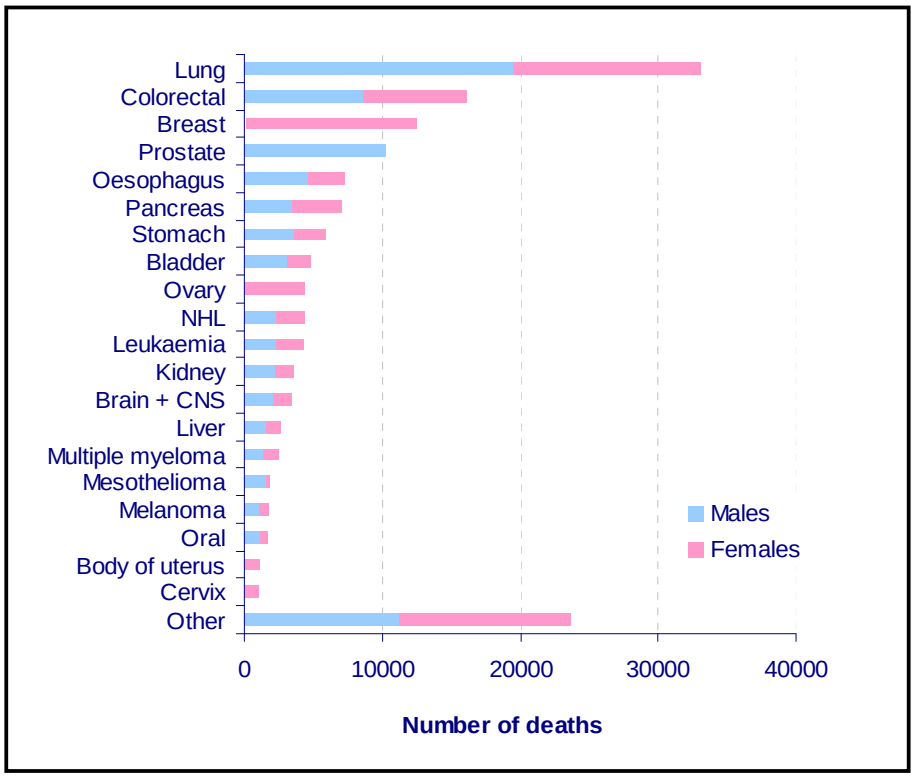

Fig. 1.1. The 20 most commonly diagnosed cancers in the UK in 2005 (www.cancerresearchuk.org)

Cancer arises from an accumulation of genetic and epigenetic alterations within proto-oncogenes and tumour suppressor genes, which consequently leads to disruptions in numerous signalling pathways (Grady & Carethers, 2008; Smith & Theodorescu, 2009). The deregulation of these tightly controlled signalling pathways causes a breakdown in the cell cycle, causing the cells to present unscheduled

proliferation and genomic and chromosomal instability, key properties in the transformation of normal cells into cancerous cells (Malumbres, 2009).

The uncontrolled proliferation, further mutations and a process of Darwinian evolution allows the development of the primary tumour (Stratton *et al*., 2009; Klein, 2009). Infiltration of cancerous cells from the primary tumour to other organs in the body (metastasis) is governed by their ability to leave the primary tumour, invade through membranes and tissues, survive in circulation by avoiding immune attack, seed at distant organs and eventually establishing themselves in surrounding tissues (Smith & Theodorescu, 2009; Joyce & Pollard, 2009). Furthermore, to maintain growth, cancer cells require the capacity to initiate the formation of new blood vessels (angiogenesis) (Hanahan & Weinberg, 2000), providing a constant supply of nutrients. Once tumour cells have metastasised and taken over distant organs, they become difficult to treat and often results in the patient mortality (Klein, 2009). Although treatments for cancers are improving, the survival rate has only increased by 10% therefore; there is still a great need to develop new therapies.

As normal cells transform into cancerous cells their cell surface properties change, showing unique expression or over-expression of certain antigens and receptors. The over-expression of these molecules relative to normal cells makes them attractive targets for targeted therapies. A number of targets have already been exploited, these include: HER2, a mutated epidermal growth factor receptor (EGFR) over-expressed on 25% of breast cancers; EGFR1, over-expressed in lung, breast, colorectal, prostate and head and neck cancers; CEA (*see section*: Carcinoembryonic antigen); VEGF (vascular endothelial growth factor) a target for angiogenesis; and CD20, CD22 and CD52, that are targets for the treatment of lymphoma (Adams & Weiner *et al*., 2005) (*see section:* Treatment of cancer with antibodies).

1.2 Carcinoembryonic antigen

Gold and Freedman first described CEA in 1965 and thought it to be a specific marker for adenocarcinoma (Gold & Freedman, 1965b). They hypothesised CEA to only be expressed during embryonic development stages then switched off and only

re-expressed in cancerous tissues (Gold & Freedman, 1965b) hence the name. However, subsequent studies have revealed CEA to be up-regulated in 50-70% of all human cancer including colorectal, lung, breast and stomach cancer (Bates *et al.*, 1992; Hammerstrom *et al.*, 1999; Chan *et al*., 2007), although, the level of CEA expression does vary between cancers (Chung *et al*., 1994). In addition, normal tissues have been found to express CEA but at a less differentiative level (Hammerstrom *et al*., 1999).

CEA is a highly glycosylated cell surface protein with a MW between 180-200 kDa and its carbohydrate content makes up over half of its weight (Kamark *et al.*, 1987; Hefta *et al.*, 1988; Takami *et al.*, 1988; Bates *et al.*, 1992). From nucleotide sequence analysis it was deduced that CEA contains 668 amino acids residues; containing a leader sequence, an NH_2 terminal domain, 3 homologous repeating domains, which individually contain 2 immunoglobulin domains (A and B) and a COOH terminal domain (Oikawa *et al*., 1987c; Zimmermann *et al*., 1988; Hefta *et al*., 1988; Takami *et al.*, 1988; Bates *et al.*, 1992). CEA is anchored to the cancer cell membrane via linkage to glycosylphospalidylinositol moiety (Sack *et al.*, 1988; Hefta *et al.*, 1988; Takami *et al*., 1988). When cleaved by phospholipace C, CEA secretes into the body (Sack *et al.*, 1988; Takami *et al.*, 1988). The typical domain structure of CEA is N-A1-B1-A2-B2-A3-B3-GPI (Beauchemin *et al.*, 1987; Thompson *et al*., 1987; Hammarstrom *et al*., 1999). Sequence analysis has shown CEA to have similarities to the variable and constant domains of immunoglobulins, making CEA and the other members of the CEA gene family, members of the immunoglobulin super-family (Paxton *et al.*, 1987; Berling *et al.*, 1990).

Since the discovery of CEA other antigens have been identified that are structurally similar. These include non-specific cross reacting antigen (NCA or CEACAM6) (von Kleist *et al.*, 1972; Oikawa *et al.*, 1987b; Thompson *et al.*, 1987; Hefta *et al*., 1988; Neumaier *et al.*, 1988; Arakawa *et al.*, 1990), biliary glycoprotein (BGP or CEACAM1) (Svenberg *et al.*, 1976; Hefta *et al.*, 1988; Hinoda *et al.*, 1988), Pregnancy specific glycoprotein (PSG) (Khan *et al.*, 1990) and faecal antigen (Kamarck *et al.*, 1987). These genes are collectively part of the CEA gene family, at present there are approximately 29 characterised gene members (Olsen *et al.*, 1994;

Teglund *et al.,* 1994) and all are on chromosome 19q13.2 (Kamarck *et al.,* 1987; Zimmermann *et al*., 1988; Inazawa *et al*., 1989).

The actual function of CEA in cancerous tissues is still un-clear. Reports have suggested it to have a role in cell differentiation, disruption of cell architecture, cell-cell adhesion and recognition, promotion of cell survival through release of IL-6 and IL-10 and inhibition of caspase mediated anoikis resistance (Hefta *et al.,* 1988; Eidelman *et al*., 1993; Benchimol *et al.,* 1989; Hostetter *et al.,* 1990; Virji, 2001; Ilantzis *et al*., 2002; Taheri *et al*., 2003; Chan *et al*., 2007; Camacho-Leal *et al*., 2008). The high expression of CEA in cancerous tissues in addition to its role in cancer development makes it an ideal target for imaging and therapy.

1.3 Antibodies and their use in cancer therapy

1.3.1 Antibody structure and function

Antibodies, also known as immunoglobulins (IgG, IgM, IgA, IgE and IgD) exhibit exceptional targeting ability and can initiate immune responses crucial in the bodies defence against pathogenic organisms and toxins. Due to these properties, antibodies have become a desirable molecule for use as a selective cancer therapeutic. The most abundant of the immunoglobulins is IgG, generally depicted as a Y shape format (Fig. 1.2), it is the main immunoglobulin structure used in the design of therapeutic antibodies.

Antibodies were first identified in 1939 by Kabat and Tiselius (Tiselius *et al.,* 1939). Subsequently, their structure was discovered by Porter and Edelman in the 1950s (Edelman 1958; Porter, 1958). The basic antibody structure consists of two identical light chains (L) of approximately 250 residues and two identical heavy chains (H) of approximately 450 residues (Porter *et al.,* 1962; Edelman *et al.,* 1975). These four chains are held together by covalent disulphide bridges and non-covalent forces (Edelman 1973). Within the first 110 amino acids of the L and H chain there are large variations between immunoglobulins, this region was therefore denoted the variable region (V) and constitutes the antigen-binding site of the immunoglobulin

(Riechmann *et al*., 1988; Skerra & Pluckthun, 1988). The variation in amino acid sequence allows for different binding specificities, creating a diverse population of antibodies.

The basic IgG format can be de-associated into two fragments via proteolytic cleavage by papain digestion (Porter, 1958). The first fragment, known as the Fab fragment consists of the V_L-C_L and the first two domains of the heavy chain V_H-C_{H1}. The Fab region is primarily involved in the antigen binding property of the antibody. The second fragment is the Fc fragment, which contains the rest of the constant heavy chains C_{H2}-C_{H3} (Fig. 1.2). The Fc domain is responsible for maintaining the structure of the IgG, as well as initiating the biological effector function (Tao & Morrison, 1989; Krapp *et al*., 2003).

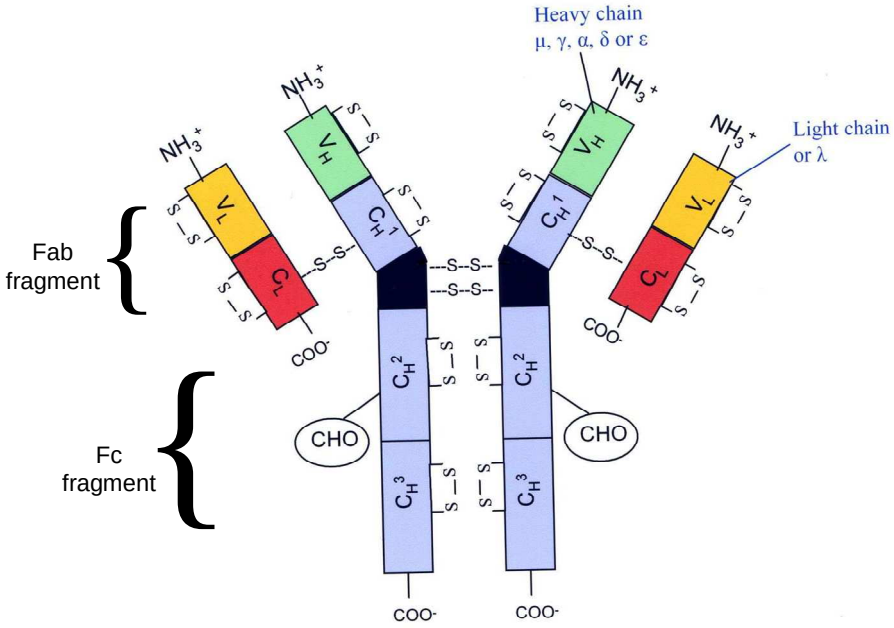

Fig. 1.2. Schematic diagram of the structure of immunoglobulins IgG shows it consists of two identical heavy chains and two identical light chains. The heavy chain consists of four domains, V_H, C_{H1}, C_{H2}, and C_{H3}, a flexible hinge region separates the C_{H1} and C_{H2} domains of the heavy chain. The light chain consists of only two domains, V_L and C_L. The heavy and light chains are linked together through a disulphide bridge formed between a cysteine residue in the hinge region and the C-terminal cysteine on the light chain. Carbohydrate chains (CHO) are attached to the C_{H2} group.

Characterisation of the Fab fragment by sequence analysis revealed the difference in the amino acid sequence within the V domains to be confined to six regions, 3 within the V_H and 3 within the V_L. These regions are termed the hypervariable regions, also known as complementarily determining regions (CDRs). The CDRs are responsible for the antibodies vast array of antigen binding specificity (Wu & Kabat, 1970). The region within the V_H and V_L chains where there is less amino acid variation is termed the framework regions. The conserved sequence in the framework region forms a β sheet structure, which acts as a scaffold to the three hypervariable loops within the V_H and V_L regions. The rest of the Fab arm contains the C_H and C_L regions, these have a number of roles including: assisting in the antigen interaction, increasing the maximum rotation of the Fab arms and holding the V_H and V_L chains together by an inter-chain disulfide bond.

Further sequence analysis found the light chain family to consist of two basic amino acid sequences denoted lambda (λ) and kappa (κ); a single antibody can only contain one type of light chain (Cook & Tomlinson, 1995; Tonegawa, 1983). In comparison, the heavy chain family contains five different amino acid sequences, with each of these isotypes being denoted μ, δ, γ, ε and α. The five different heavy chain isotypes gives rise to the five different subgroups of immunoglobulins, IgM (μ), IgD (δ), IgG (γ), IgE (ε) and IgA (α), which ultimately determines the function of the immunoglobulin. The length of the isotypes amino acid sequence also varies, with δ, γ and α having 330 amino acids, which constitutes three C regions C_H1, C_H2, C_H3 and a hinge region. Where as, the isotypes μ and ε have 440 amino acids, constituting four C regions C_H1, C_H2, C_H3 and C_H4 and no hinge region. The hinge region is a flexible proline rich region, found between the C_H1 and C_H2 domain, giving the Fab arm extra flexibility when binding to antigens (Harris *et al*., 1997).

The understanding of how diverse antibodies are produced *in vivo* through combinational rearrangement (Tonegawa, 1983) and somatic hypermutations (Neuberger, 2008), has allowed the development of genetic engineering technology (Hoogenboom *et al*., 2005). Antibody engineering has advance at a fast rate; enabling the generation and construction of large-scale amounts of high specificity and affinity monoclonal antibodies to be produced, for diagnostic and therapeutic applications.

1.3.2 Hybridoma technology

The concept of antibody-targeted therapeutics took momentum in the 70s, with the development of hybridoma technology in 1975 by George Kohler and Cesar Milstein (Kohler *et al.*, 1975). This development was a massive step forward in Paul Ehrlich vision of the "magic bullet" (Strebhardt & Ullrich, 2008). The progress of hybridoma technology paved the way for the mass production of monoclonal antibodies (mAbs) that react with specific antigens. Hybridoma technology makes use of B cells clones, that produce antibodies specific for a single epitope, fused to immortalised myeloma cells (malignant plasma cells) to form hybridomas (B cell / myeloma hybrids*)* (Kohler *et al.*,1975). These hybridomas can grow continuously, secreting the specific antibody, in large quantities against virtually every antigen. However, owing to their murine origin the development of effective mAb based therapeutics has proved difficult. Murine antibodies when used in humans induce human anti mouse antibodies (HAMA) response (Tjandra *et al*., 1990; Mountain *et al.*, 1992), resulting in accelerated clearance of mAbs and therefore lower efficacy of treatment. In addition, murine mAbs are also poor recruiters of effector functions (Adams *et al.*, 2005).

1.3.3 Humanisation

To overcome the immunogenicity murine mAbs presents, chimeric and humanised mAbs were genetically engineered. The generation of chimeric mAbs involves fusing all of the murine variable regions into the human IgG framework (Boulianne *et al*., 1984; Colcher *et al*., 1998). In comparison, humanisation of mAbs only involves grafting of the murine CDR regions into the human IgG framework (Fig. 1.3) (Jones *et al*., 1986; Adams *et al*: 2005). These advances in antibody engineering have led to the development of a number of therapeutically promising mAbs pre-clinically and clinically.

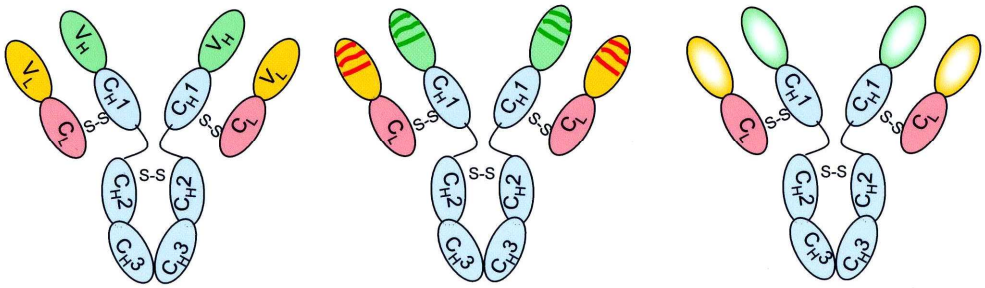

Fig. 1.3. Schematic image of a fully human IgG, a humanised IgG, where the CDR regions are of mouse origin and a chimeric IgG, where the variable domains are of mouse origin.

1.3.4 Treatment of cancer with antibodies

1.3.4.1 Non-conjugated mAbs

The first mAb to gain FDA approval for the treatment of cancer was Rituximab in 1997, a chimeric mAb for the treatment of B-cell non-hodgkin's lymphoma. Trastuzumab, in 1998, a humanised mAb for the treatment of HER2 expressing breast cancer, quickly followed. Since then 2 more humanised mAbs, Alemtuzumab for chronic lymphocytic leukaemia and Bevacizumab for colorectal cancer, 1 chimeric mAb, Cetuximab for colorectal cancer and 1 fully human mAb, Panitumumab also for the treatment of colorectal cancer have received FDA approval (Table 1.1) (Magdelaine-Beuzelin *et al*., 2007).

The mechanisms of action of these FDA approved mAbs are still under investigation, but are likely to act in multiple ways (Adams & Weiner 2005). Reports have suggested Rituximab, Cetuximab, Tastuzamab and Alemtuzumab are involved in mediating antibody dependent cellular cytotoxicity (ADCC). (Adams & Weiner 2005; Arnould *et al.*, 2006; Frieze *et al*., 2006; Golay *et al.*, 2006; Nahta *et al.*, 2006; Magdelaine-Beuzelin *et al*., 2007). In addition, complement dependent cytotoxicity (CDC) has been found to play a significant role in the therapeutic effect of Rituximab (Di *et al.*, 2003; Adams *et al.*, 2005; Golay *et al.*, 2006), showing reduced toxicity in C1q knock out mice (Golay *et al.*, 2006). Another mechanism of action is

the inhibition of signalling pathways and angiogenesis. Anti EGFR mAbs Cetuximab, Trastuzumab and Panitumumab have been reported to be potent inhibitors of a number of downstream signalling pathways (Adams & Weiner 2005; Arnould *et al.*, 2006; Frieze *et al.*, 2006; Nahta *et al.*, 2006); thus ultimately inhibiting tumour growth (Jean *et al*., 2008; Capdevila *et al*., 2009). Where as Bevacizumab targets and blocks vascular endothelial growth factors (VEGF), preventing the proliferation of new tumour blood vessels (Sharkey *et al*., 2006).

Table 1.1 FDA approved recombinant mAbs currently used in the treatment of cancer.

Non conjugated mAbs	**Format**	**Target**	**Main indication**	**Date of FDA approval**
Rituximab (Mabthera®)	Chimeric	CD-20	Treatment of non-hodgkins lymphoma	26th Nov 1997
Trastuzumab (Herceptin®)	Humanised	EGFR2 /HER2	Metastatic breast cancer	25th Sept 1998
Alemtuzumab (MabCampath®)	Humanised	CD-52	B cell chronic lymphocytic leukaemia	5th July 2001
Cetuximab (Erbitux®)	Chimeric	EGRF /HER1	Treatment of advanced colorectal cancer	12th Feb 2004
Bevacizumab (Avastin®)	Humanised	VEGF	Colorectal cancer	26th Feb 2004
Panitumumab (Vectibix®)	Fully Human	EGFR	Metastatic colorectal cancer	27th Sept 2006

More recently, in April 2009 a mouse/rat mAb Catumaxomab gained EU approval (www.trionpharma.de). Catumaxomab is a bi-specific trifunctional mAb with two different antigen-binding sites, binding the epithelial cell adhesion molecule antigen (Ep-CAM) on tumour cells and CD3 on T lymphocytes (Sebastian *et al*., 2009). The intact Fc region provides a third functional binding site; binding and activating immune effector cells leading to specific tumour cell kill (Sebastian *et al*., 2009).

Despite the early success of antibody therapeutics, they are yet to be curative and are generally used in combination with chemotherapy regimes (Sharkey *et al*; 2006). Promising results have been demonstrated with Rituximab in combination with chemotherapy, showing improvements in response rate, time to progression and event-free survival, similar results were was also reported for Trastuzumab (Sharkey *et al*; 2006).

1.3.4.2 Immunoconjugates

To improve the therapeutic potency of mAbs, immunoconjugates, where antibodies are linked to cytotoxic drugs, toxins, cytokines or radionuclides, have been developed. So far, three immunoconjugates have received FDA approval (Table 1.2).

Table 1.2 FDA approved Immunoconjugates currently used in the treatment of cancer.

Immunoconjugates	**Format**	**Target**	**Main indication**	**Date of FDA approval**
Gemtuzumab (Mylotarg)	Humanised conjugated with calicheamicin	CD33	Acute myeloid leukemia	May 2000
Ibrutumomab tuixetan (Zevalin)	Murine conjugated to ^{90}Y	CD20	B-cell non-Hodgkin lymphoma	Feb 2002
Tositumomab (Bexxar)	Murine conjugated to ^{131}I	CD20	Non-hodgkin lymphoma	June 2003

The first immunoconjugate to gain FDA approval for cancer treatment was the antibody drug conjugate Gemtuzumab ozogamicin (GO). GO is a humanised anti CD-33 mAb linked to the anti tumour antibiotic calicheamicin, a potent DNA binding agent (Tsimberidou *et al.*, 2005; Wu *et al.*, 2005). The overall response rate of GO has been reported to be 30% (Wu *et al.*, 2005).

The other two immunoconjugates to have FDA approval are radioimmunotherapies (RAIT), Yttrium-90 ibritumomab tiuxetan (Zevalin) and Iodine-131 tositumomab (Bexxar). Both are specific for the CD-20 surface antigen expressed on over 90% of

B cell lymphomas and have shown an overall response rate of 60-80% (Lemieux *et al.,* 2005; Pohlman *et al.,* 2006). Yttrium-90, used in Zevalin RAIT is a pure β-emitter linked to ibritumomab mAb by the chelator tiuxetan and has a half life of 2.7 days. The advantage of using ^{90}Y β particles is its long path length making it effective against tumours with heterogeneous or low distribution of antigens enabling delivery bystander effects, killing directly targeted cells as well as neighbouring tumour cells (Wu *et al.,* 2005). On the other hand, Iodine-131 used in Bexxar RAIT emits β particles with a shorter path length, making this therapy more appropriate for diseases where there is minimal residual (Lemieux *et al.,* 2005).

Another form of targeted therapy is antibody directed enzyme pro-drug therapy (ADEPT). This form of therapy was designed by Bagshawe and Senter in 1988 (Bagshawe *et al.,* 1988*;* Senter *et al*., 1988; Senter, 1990; Bagshawe *et al.,* 1995). Principally ADEPT involves a three-step approach. Firstly, the mAb-enzyme conjugate is administered intraveneously, the mAb targets and localises the enzyme at the tumour site. When the mAb-enzyme is cleared from the plasma a non-toxic prodrug is administered. This pro-drug is processed by the pre-localised enzyme, causing a potent cytotoxic agent to be produced only at the tumour site, which in turn causes cell death. Its short half-life allows for occurrence of a bystander effect; thus minimising the killing of more distantly located healthy cells.

Though mAb therapy has shown some success, its effectiveness has been limited due to poor tumour penetration (due to size), long circulatory half-life (increasing their toxicity to other tissues) and immunogenecity (HAMA response and activation of unwanted immune effector functions). These limiting factors are presently being addressed through advances in recombinant antibody engineering.

1.4 Recombinant antibody technology

1.4.1 Phage display

Progress in technologies such as the polymerase chain reaction (PCR), bacterial expression systems and DNA manipulation, cloning, expression and selection

systems has enabled the development and use of phage display libraries. Phage display libraries can be used to engineer customised humanised antibodies with defined affinity, specificity and less immunogenic, bypassing the need to make hybridomas (Winter *et al*., 1994; Mao *et al*., 1999; Nilsson *et al*., 2000). Antibody Phage display was first described in 1985 by George Smith and largely mimics the *in vivo* process of antibody generation (Smith, 1985). Phage display involves the presentation of a library of peptides on the surface of filamentous phage, by fusing the peptide gene to the phage genome. Affinity selection of peptide-phage by binding to an antigen (panning), elution of bound peptide-phage, several rounds of selection and re-amplification of the selected peptide-phage, generates a large amount of specific antibodies (McCafferty *et al*., 1990). Phage technology is far more efficient in producing antibodies than hybridoma technology. So far, naïve scFv chain and Fab libraries have been generated with a diversity of over 10^{10} clones (Sblattero & Bradbury, 2000; Hoogenboom, 2005). At present one human antibody "Humira" generated by phage display has been FDA approved. Humira is an anti TNFα antibody used in patients with arthritis and is currently in phase 2/3 clinical trials for other applications (Hoogenboom, 2005).

The selection of an antibody phage library can be done using cells, tissue sections, immune sera or live animals (George *et al*., 2003), but usually purified or recombinant antigens are used to enable conditions to be controlled and minimise non-specific binding (Yip *et al.*, 2002; Hoogenboom, 2005). The antibodies selected from a phage display library are generally more amendable to genetic engineering and can be further modified via chain shuffling, error prone PCR or CDR centred mutagenesis to create higher affinity binding antibodies (Yip *et al.*, 2002).

Ribosomal display is another library system used for the selection of proteins and peptides. Ribosomal selection technology is performed entirely *in vitro* and therefore offers two main advantages; firstly, diversity is not limited by transformation efficiency and second, random mutations can be introduced easily (Zahnd *et al.*, 2007). Yeast display using *Saccharomyces cerevisiae* has also shown promise as a selection platform and has enabled the selection of high affinity antibodies (Boder *et al.*, 2000).

1.4.2 Recombinant antibody fragments

The development of phage library technology has made possible the generation of recombinant antibodies with different binding affinities, kinetics, and biophysical properties. Library technology has also made it easier to generate a variety of antibody fragment formats, including Fab, scFv and V_H domains. Whole antibodies have shown excellent target binding specificity, however, their long blood half life results in poor contrast in imaging applications and their ability to initiate effector functions can lead to toxic effects, preventing repeat administration (Holliger *et al*; 2005). Studies in recombinant antibody fragments have become increasingly more popular for their use in therapeutic and diagnostic application. Firstly, because of the ease and cost effectiveness in producing them, they are able to be expressed at high yields in a variety of hosts such as bacteria, yeast and plant (Worn *et al*., 2001) and secondly their size. Fab, scFv and V domain fragments are 55 kDa, 27 kDa and 15 kDa respectively, compared to a whole antibody of 150 kDa. This smaller size can be advantageous in imaging applications since these molecules are below the renal threshold and consequently are rapidly cleared via the kidneys. This in contrast to mAbs, where the tumour to blood ratio is a limiting factor in the use of mAbs as imaging tools (Adams *et al*., 1999).

1.4.2.1 Fab

Fab fragments are attractive platforms for antibody-based therapies. So far, three have received FDA approval, however not for cancer indications (Nelson *et al*., 2009). Fabs are made up of the antigen binding V_H and V_L domains bound to C_{H1} and C_L chains (Fig. 1.2 and 1.4). A disulphide bond covalently holds both chains together. Although Fab fragments express well in bacteria, the presence of two chains can make genetic manipulation and large-scale production difficult (Carter *et al*., 1992**;** Skerra, 1993). Recently, the single chain Fab (scFab) antibody format has been developed, which has been successfully produced in *E.coli*, *Bacillus megaterium* and *Pichia pastoris* (Hust *et al*., 2007; Jordan *et al*., 2007). The scFab is composed of the V_H-C_{H1} and V_L-C_L domains connected by a 34 amino acid linker and combine the advantages of scFv and Fab fragments.

1.4.2.2 ScFv

Single chain Fv (27kDa) (Fig. 1.4) currently account for 53% of recombinant antibody fragments being taken through the clinical pipeline, dominating mAb fragment clinical development (Nelson *et al*., 2009). ScFvs consist of 1 V_H and 1 V_L domain held together by a flexible, polypeptide linker (Huston *et al.,* 1988, Bird *et al*., 1988). The choice of linker can affect the solubility, expression and stability of the scFv. The most common linker used is the $(Gly_4Ser)_3$ motif (Huston *et al*., 1988), due to its flexibility, neutral charge and solubility (Turner *et al*., 1997; Kortt *et al*., 2001). However, other linkers have been investigated (Bird *et al.,* 1988; Pantoliano *et al.,* 1991; Whitlow *et al.,* 1993; Tang *et al.,* 1996; Deonarain *et al.,* 1997; Turner *et al*., 1997; Hennecke *et al.,* 1998).

Due to the size and ability to retain the specific antigen binding affinity of the parent IgG (Holliger & Hudson 2005), scFvs are ideal platforms for antibody-based therapies. In addition, they are readily obtained to virtually any target using phage display libraries and recombinant antibody technology and furthermore, can be generated for clinical use to high yields in non-mammalian expression systems (Tolner *et al*., 2007).

1.4.2.3 Domain antibodies

Domain antibodies (V_H and V_L) (Fig. 1.4) are 11kDa-15kDa is size and were first isolated in the late 1980's by phage display (Ward *et al*., 1989). In the past, murine and human V_H domains exhibited low binding affinity to their target antigen. Furthermore, they were generally unstable, with tendencies to aggregate *in vivo* due to exposed hydrophobic areas (Ward *et al*., 1989; Muyldermans *et al.,* 2001). However, the discovery of two types of organisms, Camelids and Cartilaginous fish, such as sharks, that can generate antibodies devoid of light chains, has heightened interest in this area (Hamers-Casterman *et al.,* 1993). From sequence and structural analysis of these heavy domain V_HH antibodies from Camelids (also referred to as nanobodies®) (Harmsen & De Haard, 2007) and sharks (V-NAR); extension of the CDR loops is thought to compensate for the absence of the light chains (Muyldermans *et al*., 1994). In comparison to the murine and human V_H domain, the

V_HH domains are produced with good solubility and thermo-stability, attributed to four highly conserved hydrophilic mutations (Holt *et al*., 2003; Jesper *et al*., 2004). Through replacement of these residues (camelisation) and a further five framework substitutions, increase of CDR length and diversity, the solubility of murine and human V_H domains have improved (Holt *et al*., 2003). Furthermore, it is also possible to isolate V_L domains from V_L libraries, generated by DNA shuffling techniques (Van den Beucken *et al*., 2001). Due to the size, domain antibodies (dAbs) are especially effective for targeting enzyme active-site clefts (Holt *et al*., 2003) and cryptic viral epitopes (Stijlemans *et al*., 2004), unattainable by classical antibodies. Advancements in the knowledge of dAbs has enabled the selection of high specificity and affinity dAbs from phage display libraries (Holt *et al*., 2003; Dufner *et al*., 2006).

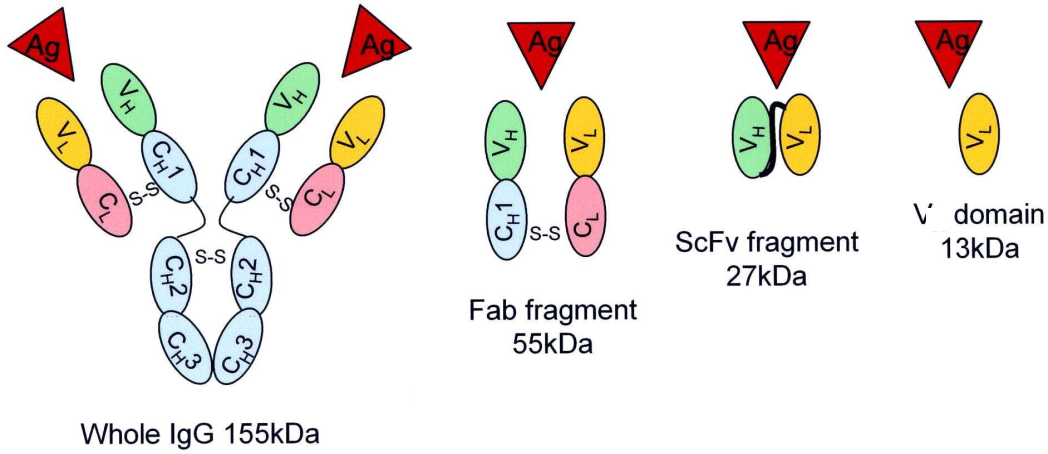

Fig. 1.4. Schematic diagram of genetically engineered antibody constructs. Include monovalent antibody fragments Fab, scFv and V domain (in this image the V_L is depicted) Symbols used: Ag, antigen.

Due to their small size, Fabs, scFvs and dAbs are able to diffuse and penetrate through solid tumours easily. Thus, allowing rapid delivery of toxins, potentially making them more effective at tumour destruction (Yokota et *al*., 1992; Adams et *al*., 2000; Fang et *al*., 2003). However, their monovalency leads to issues of fast dissociation rates and modest retention times on the antigen (Adams *et al*., 1998; Yokota *et al*., 1992; Nielsen *et al*., 2000; Holliger *et al*., 2005; Huang *et al*., 2006). Work is ongoing to overcome these limitations, with strategies to improve the

retention time by affinity maturation and modification of size, through fusion to toxins (Kreitman & Pastan, 1998), enzymes (Michael *et al.*, 1996; Bhatia *et al.*, 2000; Kousparou *et al.*, 2002), cytokines (Scherf *et al.*, 1996; Cooke *et al.*, 2002; Kaspar *et al.*, 2007), drugs (Sun *et al.*, 2003), liposomes (Park *et al.*, 2002; Weng *et al.*, 2008), polyethylene-glycol (Lee *et al.*, 1999; Yang *et al.*, 2003; Kubetzko *et al.*, 2006) and albumin (Holt *et al.*, 2003).

1.4.2.4 Multivalency

Improving the retention time by increasing the valency of Fabs, scFvs and dAbs, through multimerisation, is also under investigation (Adams *et al.*, 1999; Nielsen *et al.*, 2000; Todorovska *et al.*, 2001). Spontaneous multimerisation can be encourage through linker shortening, forcing V domains to pair with complementary domains of another scFv (Atwell *et al.*, 1999; Adams *et al.*, 2000; Dolezal *et al.*, 2000; Kortt *et al.*, 2001). However, bio-stability issues have been reported, with these multimers dissociating into their monomeric forms *in vivo* (FitzGerald *et al.*, 1997; Huang *et al.*, 2006). A more stable method to generate diabodies is through genetically engineering a cysteine residue onto the terminal end of the scFvs. The availability of a free cysteine allows formation of a disulphide bond that covalently cross-links the V_L and V_H domain, creating a stable diabody (FitzGerald *et al* 1997; Huang *et al.*, 2006).

Increasing the valency of scFvs can increase its avidity to target antigens therefore, encouraging more scFv to be taken up by the tumour and retained thus, improving its therapeutic efficacy (Pluckthun *et al.*, 1997).

1.5 Anti CEA scFv MFE-23 and Sm3E

The recombinant antibody fragments investigated in this thesis are the scFvs MFE-23 and its humanised variant Sm3E. Both scFvs are directed against the carcinoembryonic antigen (CEA) (*see section*: Carcinoembryonic antigen), binding predominantly to the N and A1 (N-A1) domains of CEA (Boehm *et al*; 2000; Sainz-Pastor *et al.*, 2006).

MFE-23 is a murine scFv and was the first scFv to be tested in the clinic, showing effective targeting of CEA expressing colorectal carcinoma for radio-immunodetection (Begent *et al*., 1996) and radio-immunoguided surgery (Mayer *et al.,* 2000). MFE-23 has also been used as the targeting arm in antibody-directed prodrug therapy (ADEPT), which has recently undergone phase I clinical trial. (Bagshaw *et al.*, 1995; Sharma *et al.*, 2005; Mayer *et al*., 2006).

MFE-23 was produced from a phage display library made up of anti CEA scFvs, constructed from variable region genes extracted from CEA immunised mice (Chester *et al*., 1994). Selection conditions favoured high affinity scFvs with MFE-23 having a binding affinity of kD 2-4nM (Chester *et al*., 2000b).

Through knowledge of the crystal structure (Boehm *et al*., 2000), MFE-23 was humanised to improve its therapeutic potential, reducing the possibility of HAMA responses and allowing repeat administration of the scFv. Boehm *et al*., found MFE-23 to be structurally similar to the human TR1.9 antibody (Boehm *et al*., 2000). This understanding led to the humanisation of the Fv framework by replacing the residues as mentioned in Boehm *et al* with the corresponding residues in the human TR1.9 antibody (Graff *et al*., 2004). The humanised version of MFE-23 termed hMFE showed no change in its CEA immunoreactivity with a dissociation constant of k_D = 8.5nM (Graff *et al*., 2004). Further genetic manipulation of hMFE increased its tumour retention time and stability. Studies by Graff and Wittrup found that the dissociation rate constant (k_{off}) is an important factor in the tumour retention of antibodies (Graff & Wittrup, 2003). Two rounds of mutagenesis were performed to improve the affinity of hMFE. The first round of affinity maturation involved error prone PCR to produce variants with 10-100 fold improvement in off rates, the second round involved random mutagenesis and DNA shuffling to produce variants with up to a 1000 fold binding improvement. The affinity matured variant m3E was found to be the most promising clone with a $k_{off} = 1x10^{-6}$ s^{-1} and a dissociation half-life of several days at 37^0C, compared to that shown by the original hMFE of 10 min (Graff *et al.,* 2004). However, the excellent binding affinity seen with these mutant variants came with the problem of poor expression, which correlates with poor stability. Further improvement on these affinity-matured variants was achieved by stability maturation, involving 4-5 mutations within the V_L domain. After addressing the

humanisation, affinity and stability of MFE-23 by genetic engineering the scFv Sm3E was produced (Graff *et al*., 2004). The Sm3E scFv has exceptional properties with a dissociation constants of 30pM, effectively irreversible binding to CEA. In addition, Sm3E showed a 100-fold increase in expression compared to hMFE, with a solubility of 8 mg/l compared to 0.08 mg/l (Graff *et al*., 2004).

The experiments in this thesis investigate the development of a new immuno-conjugate, using the MFE-23 and Sm3E scFv conjugated to superparamagnetic iron oxide nanoparticles (*see section*: Superparamagnetic iron oxide nanoparticles), for dual application in cancer imaging (*see section:* Application of SPIONs in MRI) and therapy (*see section*: Application of SPIONs in hyperthermia).

1.6 Superparamagnetic iron oxide nanoparticles (SPIONs)

SPIONs are small nanomaterials consisting of iron oxide core crystals surrounded by a stabilising polymer or polysaccharide shell (Thorek *et al*., 2006). The two most commonly studied iron oxides have been magnetite (Fe_3O_4) and maghemite (γ-Fe_2O_3) (Gupta *et al*., 2005b). There are a number of different chemical methods for synthesizing SPIONs (Peng *et al.,* 2008). The most reported approach is by co-precipitation of Fe2+ and Fe3+ chloride, at pH 9-14, under non oxidising conditions (Gupta *et al.,* 2005b; Peng *et al*., 2008). The balance of these requirements pH, type of salt, Fe2+ and Fe3+ ratio and ionic strength are reported to control the shape, size and composition of the SPIONs (Gupta *et al.*, 2005b).

Due to their magnetic properties SPIONs have been extensively used in a number of bioapplications including magnetic drug and gene delivery (McBain *et al*., 2008), tissue repair, cell separation (Gupta *et al*., 2005), magnetic resonance imaging (MRI) (*see section:* Application of SPIONs in MRI) and magnetic fluid hyperthermia (MFH) (*see section:* Application of SPIONs in hyperthermia).

1.6.1 Stabilising coating

SPIONs have a large surface area, are hydrophobic and at neutral pH have an iso-electric point of zero this can lead to stability issues including agglomeration of the particles and eventual precipitation (Gupta *et al.*, 2005b). For SPIONs to be used in biological situations they are required to be soluble in physiological solutions. Therefore, to prevent destabilisation due to particle-particle interaction, coating of the particles is essential, with the most common being dextran (Gupta *et al.*, 2005b).

1.6.1.1 Adsorption of dextran

Dextran is a hydrophilic and neutrally charged polysaccharide consisting of glucose residues with α-1.6 linkages (Fig. 1.5.). Particles are generally embedded in a matrix of dextran, preventing interaction with neighbouring particles (Moore *et al*., 1997; Mornet *et al.*, 2004). The dextran coat has shown to considerably improve the stability of particles at neutral pH. Another advantage of dextran is that it is non-toxic and biodegradable. When taken up by cells the SPIONs accumulate within the lysosomes, and are eventually broken down, causing no detrimental affect to the cells (Okon *et al*., 1994; Thorek *et al.*, 2006). Dextran is already used for stabilisation of the FDA approved SPIONs Endorem® EU (Ferridex USA; Guerbet/Berlex lab) and Resovist® (Schering AG), furthermore, Sinerem EU (Combidex USA; Guerbet/Advance Magnetics), which is currently in phase III trial (*see section*: Application of SPIONs in MRI for more detail on these SPIONs).

1.6.2 Stealth coatings

SPIONs are rapidly cleared from the blood by the reticuloendothelial system (RES), accumulating mainly in the liver and spleen (Mornet *et al.*, 2004). This happens very fast, in a matter of minutes. In some cases, it is a requirement that the SPIONs accumulate in organs of the RES, referred to as passive targeting (Mornet *et al.*, 2004). However, to enable SPIONs to reach other organs or tissues evasion of the RES is an important requirement. This can be achieved by preventing or reducing opsonisation of the SPIONs, thus delaying recognition by the RES and increasing blood circulation times. A number of reports have demonstrated that SPIONs with

hydrophilic coating and a hydrodynamic diameter below 100nm show reduced levels of opsonisation (Tiefenauer *et al.,* 1996; Gaur *et al.,* 2000; Brannon-Peppas *et al.,* 2004; Gupta *et al.,* 2005b; Mornet *et al.,* 2004). The literature however, is quite conflicting on whether dextran can reduce opsonisation and RES recognition (Berry *et al.,* 2004; Moore *et al*., 2000). Two other coatings investigated for stealth include liposomes and polyethylene glycol.

1.6.2.1 Incorporation into liposomes

Liposomes, are made up of a phospholipid bilayer membrane (Fig. 1.5) and were first proposed as drug carriers in cancer chemotherapy by Gregoriadis *et al.* (Gregoriadis *et al*., 2008). Much research has now gone into encapsulating toxic drugs such as doxorubicin into non-toxic liposomes (Park *et al.,* 2002; Cattel *et al.,* 2004). As drug delivery vehicles, liposomes prevent the toxicity of the drug affecting healthy tissues until it reaches its target site, upon where the drug is released. Shinkai *et al* has reported on the development of magnetoliposomes consisting of a magnetite core coated in phopholipids phosphatidylcholine and phophatidylethanolamine, results showed good aqueous stability (Shinkai *et al.,* 1996b) but poor RES evasion (Yanase *et al.,* 1998b). In addition, studies have reported that liposome coated SPIONs are open to the same RES fate as naked or dextran coated SPIONs, so only a proportion of the injected drug reaches the target (Sofou *et al.,* 2004).

1.6.2.2 Addition of polyethylene glycol chains

Synthetic polymers such as polyethylene glycol, polyethylene oxide and poloxamers are being used to generate a new family of stealth particles (Brigger *et al*., 2002; Berry *et al.,* 2003). PEGylation was first applied to liposomes to increase their blood half-life, studies found that PEG could increase blood residency from seconds to hrs (Panagi *et al.,* 2001; Gabizon *et al.,* 2001; Shmeeda *et al*., 2009). PEG has also been used in a number of FDA-approved biotherapeutics (Bailon *et al*., 2009). Polyethylene glycol polymers are non-immunogenic and can be absorbed onto either unmodified, dextran or liposome stabilised particles, giving a brush like affect (Gref *et al.,* 2000). The PEG chains sterically prevent plasma proteins attaching to the particles, reducing opsonisation and therefore increasing blood circulatory times

(Zhang *et al.,* 2002; Berry *et al.,* 2003). Absorption of PEG chains has shown the most promise in delaying clearance to the RES (Park *et al*., 2002; Owens *et al*., 2006) however, complete RES evasion is still proving difficult. Another property exerted by PEG is its ability to encourage internalisation by membrane fusion, increasing the cellular uptake of cytotoxic drugs or particles *in-vitro* and thus enhancing their detrimental affect to the cells (Yamazaki *et al.,* 1990; Lentz *et al.,* 1999; Zhang *et al*., 2002; Gupta *et al.,* 2004).

1.6.3 Surface functionalisation

Cell uptake of SPIONs can be encouraged by surface functionalisation with a targeting moiety. Coupling of SPIONs to ligands specific for receptors over-expressed on cancers cells has been successfully demonstrated with transferrin (Kresse *et al.,* 1998) and luteinizing hormone releasing hormone (LHRH) (Zhou *et al*., 2006; Leuschner *et al*., 2006). Antibodies and more recently recombinant antibody fragments have also demonstrated the ability to enhance selective SPION uptake into cancer cells *in vitro* and *in vivo* (Weissleder *et al.,* 1992; Tiefenauer *et al.,* 1993; Suzuki *et al.,* 1996; Suwa *et al.,* 1998; Shinkai *et al.,* 2001; Artemov *et al.,* 2003; Funovic *et al.,* 2004; Toma *et al.,* 2005; Reynolds *et al*., 2006; Zhou *et al*., 2007; Natarajan *et al.,* 2008; Yang *et al.,* 2009).

As coating on SPION **Chemical Structure**

A. Dextran

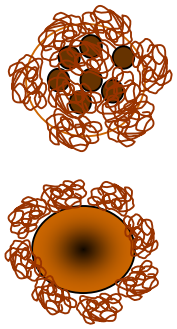

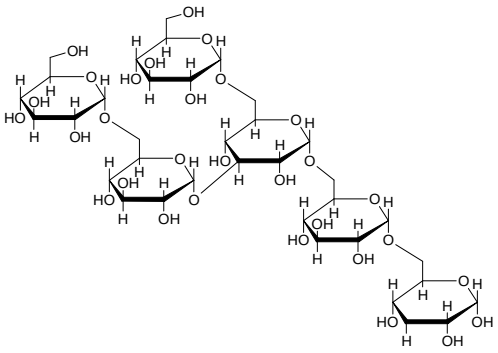

B. Liposome

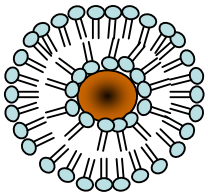

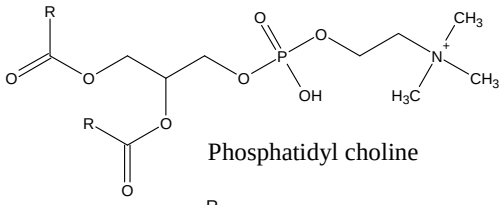

Phosphatidyl choline

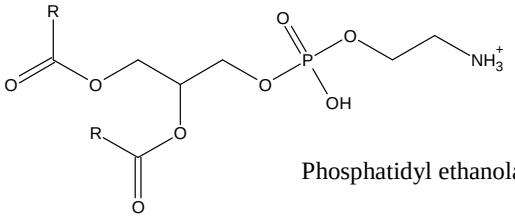

Phosphatidyl ethanolamine

C. Polyetheylene glycol

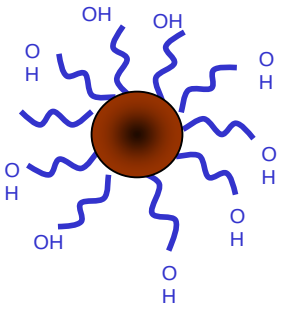

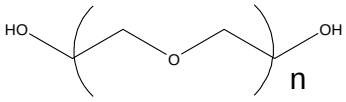

Fig. 1.5 Chemical structure and schematic representations of A) Dextran, B) Liposome (Phosphatidylcholine and phosphatidylethanolamine) and C) Polyethelene glycol (Adapted from Mornet *et al.,* 2004).

1.7 Magnetic resonance imaging

Magnetic Resonance imaging (MRI) was first developed in 1973 and used mainly for brain and spinal cord imaging. Due to the signal to noise ratio caused by breathing and other movements, MRI could not be used to image below the abdomen (Wallis *et al.,* 1999). Over the last 5 years, MRI technology has advanced considerably, with the development of faster imaging sequences, improved gradient and magnet designs, advanced transmit and receiver coils and recently contrast enhancing agents. This has allowed for higher quality hepatic and abdominal images, enhancing its diagnostic potential.

The MRI imager consists of a powerful magnetic field generated by super conducting magnets with a field strength used clinically of 1-1.5 Tesla. To create an image, MRI relies on the nuclear magnetic resonance signal from protons of hydrogen nuclei within water and lipid molecules in tissues, when in a static magnetic field $\boldsymbol{B}_0$ and a radiofrequency field (Pankhurst *et al.,* 2003). In a magnetic field ($\boldsymbol{B}_0$) the protons align against the field generating a net magnetic moment. Through application of radiofrequency (RF) pulses, the net magnetic moment becomes excited at a frequency known as Larmour frequency (Wallis *et al*., 1999; Pankhurst *et al.,* 2003). Through switching off the RF pulse, the protons return to a state of equilibrium known as relaxation (Lanza *et al.*, 2004). There are two types of relaxation signals generated. Firstly, longitudinal relaxation, also termed T_1 spin lattice recovery, involves hydrogen nuclei releasing absorbed energy to surrounding tissues, enabling its return to ground state $\boldsymbol{B}_0$. Secondly, transverse relaxation, which involves the exchange of energy between spinning protons, also termed T_2 decay or spin-spin relaxation (Lanza *et al.,* 2004; Mornet *et al.,* 2004).

To obtain high contrast images various sequence parameters such as repetition time (TR) and echo (delay) time (TE) can be optimised. Relaxation signals from the protons are collected and reconstructed to give a 3-D image (Mornet *et al.,* 2004). The MRI contrast seen from the different tissues is mainly due to the concentration of hydrogen nuclei within the tissues. All tissues have a different concentration of

hydrogen nuclei, causing relaxivity rates to differ, allowing a contrast to be seen (Mornet *et al.,* 2004).

Using contrast agents, MR images can be enhanced. The most common contrast agent used is paramagnetic gadolinium ion complexed with diethylenetriaminepentaacetic acid (DTPA) (Artemov *et al.,* 2003; Mornet *et al.,* 2004). Gadolinium ions directly influence nearby H nuclei atoms causing a shortening in their T_1 relaxation times, leading to enhanced positive contrast of the respective tissue (Artemev *et al.,* 2003; Mornet *et al.,* 2004).

1.7.1 Application of SPIONs in MRI

Advances in superparamagnetic materials (SPM) have shown SPIONs to also exhibit an MRI contrast enhancement potential. SPIONs cause a shortening in the T_2 signals, which leads to a negative contrast (Renshaw *et al.,* 1986; Weissleder *et al.,* 1990; Pankhurst *et al.,* 2003; Pardoe *et al.,* 2003; Bulte *et al*., 2004).

Superparamagnetic materials have a higher magnetic susceptibility compared to paramagnetic material. Upon application of a magnetic field the magnetic moments within the SPIONs align in the direction of the field, this gives rise to a large net magnetic moment, in comparison, paramagnetic material exhibit only a small net magnetic moment (Goshima *et al*., 2004; Mornet *et al.,* 2004). The large magnetic moment generated by SPIONs leads to a disturbance in the local magnetic field, causing a shortening of the hydrogen nuclei relaxation times. This shortening in proton relaxation times leads to a detectible change in the T_2 MRI signal (Mornet *et al.,* 2004). Due to SPM larger magnetic moment, only nanomolar concentrations of SPIONs are needed, compared to millimolar concentrations of Gd complexes to be effective as MRI contrast agents (Kohler *et al.,* 2004).

Currently there are two FDA approved SPION contrast enhancement agents, Endorem® EU (Ferridex USA; Guerbet/Berlex lab) and Resovist® (Schering AG), both used for liver and spleen imaging. Sinerem EU (Combidex USA; Guerbet/Advance Magnetics) is another SPION contrast agent currently in phase III trial for application in lymph node imaging.

Endorem® consists of multiple 5nm iron oxide core crystals embedded in a dextran matrix to give a hydrodynamic diameter of 80-150nm (Wang *et al.,* 2001; Thorek *et al.,* 2006). Resovist® also consists of multiple 5nm iron oxide core crystals but these are embedded in carboxymethylated dextran matrix and have a hydrodynamic diameter of 60nm (Wang *et al.,* 2001; Thorek *et al.,* 2006). Even though Endorem® and Resovist® are stabilised in dextran, the particles are only partially coated, increasing the likelihood of agglomeration. The application of these SPIONs is for liver specific imaging, therefore it is a requirement for the particles to be taken up by the body's RES. The SPIONs accumulate in the organs of the RES, with 80% taken by Kupffer cells within liver and 5-10% in the spleen (Wang *et al.,* 2001).

In comparison to Endorem® and Resovist®, the contrast enhancement agent Sinerem consist of a single 5nm iron oxide core crystal covered more completely in dextran and has a hydrodynamic diameter of 20-40nm (Wang *et al.,* 2001). Due to Sinerem's hydrodynamic radii and its thicker dextran coat, opsonisation by plasma proteins and recognition by RES is reduced. This allows the particles to remain in the blood longer; increasing its blood half-life (Jung *et al.,* 1995a). Whilst in the blood, a percentage of SPIONs can leak into the interstitium, where clearance is via macrophages of the lymphatic system. The accumulation of SPIONs within the lymph nodes in-turn allows for MRI imaging of lymph node metastases (Rockall *et al.,* 2005).

At present, the FDA approved SPION contrast agents work by passive accumulation within healthy macrophages within organs of the RES. However, in areas of organs of the RES that are cancerous the macrophages function is altered, preventing uptake of the SPIONs. Cancerous tissues therefore, appear brighter (positive contrast) as they contain no SPIONs, in comparison the healthy tissues appear darker due to the T_2 negative contrast caused by the uptake of SPIONs.

1.8 Hyperthermic therapy

Tumour cells have shown a greater sensitivity to heat treatments compared to healthy cells (Zee *et al.,* 2002). This has led to the use of thermo-ablation and hyperthermic therapies in the clinic, often in combination with other treatments. The use of heat to treat illnesses dates back to the time of Hippocrates (460-370 BC), who said " Those diseases which medicines do not cure, the knife cures; those which the knife cannot cure, fire cures; and those which fire cannot cure, are to be reckoned wholly incurable" (Ito *et al.,* 2005).

Hyperthermia is classed into two categories; themo-ablation and mild hyperthermia. Thermo-ablation is where a temperature rise exceeds 46^{o}C and causes cell necrosis (Jordan *et al.,* 1999; Gneveckow *et al.,* 2004). Mild hyperthermia is where the temperature increase is between 41^{o}C – 46^{o}C (Lao *et al.,* 2004). This temperature rise is high enough to cause partial cell kill and to damage and sensitise cancer cells to chemotherapy and radiotherapy (Jordan *et al.,* 1999b; Wust *et al.,* 2002; Gupta *et al.,* 2005b; Okayama *et al*., 2009).

The adjuvant affect of hyperthermia with radiotherapy has shown to cause increase blood flow into radio-resistant, hypoxic, low pH areas, causing oxygenation of the tissues, in turn increasing the cells radio-sensitivity (Song *et al*., 1996; Griffin & Corry, 2009). Studies have also shown heat treatments to cause protein denaturation and affect DNA repair mechanisms, preventing the repair of radiation induced DNA damage (Vernon *et al*., 1996; Zee *et al.,* 2002). Furthermore, thermal treatment can enhance the toxicity of chemotherapy (Zee *et al.,* 2002). It is reported that a raise in tissue temperature can cause increased intracellular drug uptake and increased blood flow in turn, raising intra-tumour drug concentrations and enhancing DNA damage (Zee *et al.,* 2002).

In addition, hyperthermia can also activate the immune system through up-regulation of heat shock proteins (HSP) (Ito *et al*., 2003a; Beere 2004; Tabuchi *et al*., 2008). HSP70 has been elucidated to a number of roles including anti-tumour immunity (Srivastava *et al*., 1998; Wang *et al*., 2000; Ito *et al*., 2003). Both Todryk *et al* and

Ito *et al* reported that the induction of HSP70 after hyperthermic treatments encouraged the recruitment of macrophages and dendritic cells into the tumour and furthermore, mediated the up-regulation of the cell surface major histocompatibility class I molecules (MHC-1) (Todryk *et al*., 1999; Ito *et al*., 2001). Tumours have managed to evade immune detection due to a number of reasons including inefficient MHC expression (Costello *et al*., 1999; Garcia-Lara *et al*., 2003). Through up-regulation of the MHC-I expression, increased presentation of functional MHC-I-Ag complexed to cytotoxic T lymphocytes was reported (Tabuchi *et al*., 2008). This suggests HSP70 increases the immunogenicity of the tumour cells by priming them for immune recognition and attack (Ito *et al*., 2001; Tabuchi *et al*., 2008).

Clinical approaches to hyperthermia have included immersion of the body part in question in hot water, the use of hot irons, hot probes, and fever therapy, however, all with limited success (Zee *et al.*, 2002). More conventional thermal therapies used include lasers (Amin *et al*., 1993; ,Vogl *et al*., 1999), focused ultrasound (Jolesz *et al*., 2002), microwaves (Seki *et al*., 1999) and radiofrequency probes that can be placed in the lesion (Gazelle *et al*., 2000; Shinkai *et al.*, 1999, 2002). Though all have shown evidence of cell necrosis, no benefit to patient survival has been reported. There are a number of limiting factors with these macroscopic heating methods including lack of specificity to the tumour cells, heterogeneous distribution of temperature over the target site and poor temperature control leading to a detrimental affect on normal healthy cells (Samanta *et al*., 2008). New approaches are currently under investigation to separate the energy source from the heating source, enabling control over thermal release. Such approaches include near infrared irradiation (NIR) and magnetic induced thermal therapy. Near infrared irradiation involves metal nanoshells (Hirsch *et al*., 2003), nanorods (Huang *et al*., 2006) or nanotubes (Chahraverty *et al*., 2008) being placed in the area of the tumour, followed by irradiation with an infrared laser from outside of the body. However, due to limited penetration depth, NIR is not effective at treating deep-seated tumours (Samanta *et al*., 2008).

1.8.1 Application of SPIONs in hyperthermia

Magnetic induced thermal therapy also known as magnetic fluid hyperthermia (MFH) was first reported by Gilchrist in 1957. Gilchrist *et al* showed that injection of magnetic particles into lymph nodes in dogs, caused a temperature increase during exposure to an alternating magnetic field (AMF) (Gilchrist *et al*., 1957). Over the last decade, MFH has re-emerged. A number of groups have reported promising results *in vivo*, where iron oxide particles were injected directly into the tumour (Jordan *et al*., 1997; Hilger *et al*., 2001, 2005) and more recently in the clinic, where an intra-tumoural temperature rise of 40^{o}C-44^{o}C was achieved and reported to be sufficient for radio-sensitisation (Johannson *et al*., 2007; Maier-Hauff *et al*., 2007).

By exposing SPIONs to an AMF energy is created in the form of heat, this thermal energy dissipates into the surrounding tissues and if the temperature is high enough can destroy or weaken cancerous cells (Berry *et al.*, 2003; Pankhurst *et al*., 2003). Using SPIONs to generate heat can overcome the issue of non-specific tissue heating, as the application of the alternating magnetic field can be localised to the area of the body where the SPIONs have collected. Through varying the frequency, current parameter of the AMF and the size and composition of the SPIONs, the temperature generated from the SPIONs can be controlled (Pankhurst *et al.*, 2003; Okawa *et al*., 2006; Hergt & Dutz, 2007).

Unlike micron sized particles, which exhibit heating through hysterisis loss (Pankhurst *et al*., 2003), SPIONs are thought to generate heat through Néel relaxation and Brownian motion whilst in an AMF (Fig. 1.3) (Maier-Hauff *et al.*, 2006). In the case of Néel relaxation, the AMF causes the magnetic moments within the SPIONs to rotate, generating internal friction. When the field is off the moments return to equilibrium, this is where energy is released in the form of heat (Pankhurst *et al.*, 2003; Mornet *et al*., 2004). Brownian motion requires the rotation of the SPION as a whole therefore, the heat is generated through frictional movement in its surroundings (Mornet *et al.*, 2004). However, SPIONs can become trapped within biological tissues, this in-turn blocks free rotation of the particles, preventing the generation of frictional heat (Hergt *et al.*, 2004a; Mornet *et al.*, 2004).

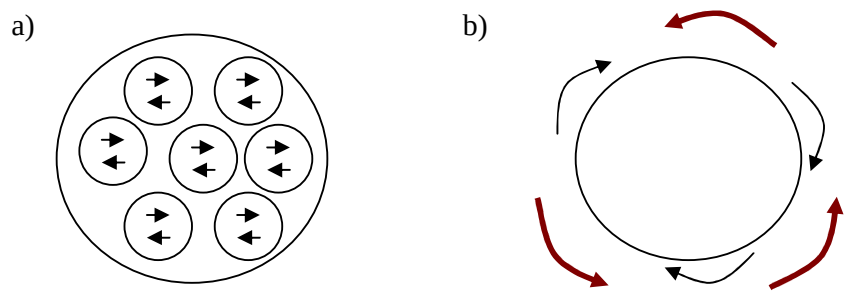

Fig 1.6**.** Schematic representation of **a)** Néel rotation, where magnetic moments **within** the SPION rotate and b) Brownian motion, where the SPION rotates as a **whole.**

The specific absorption rate (SAR) Wg^{-1} is the measurement of thermal energy generated from magnetic particles and is defined as the power of heating of a magnetic material per gram. SAR is measured as:

$$SAR = C\,\Delta T/\Delta t \qquad \text{(Equation 1.2)}$$

Where C is the specific heat capacity of the sample ($Jg^{-1}\ K^{-1}$), ΔT is change in temperature and Δt is change in time. The SAR values are affected by a number of parameters firstly, the specific heat capacities of the surrounding liquid in the body, blood flow and tissue perfusion can act as a cooling mechanism (Mornet *et al.*, 2004). Second, size, physical and chemical composition of the SPIONs can affect heat generated, with the optimum core diameter proposed as 10 nm-20 nm (Hergt *et al.*, 2004b) and third, particle heating can be affected by frequency and amplitude of the alternating magnetic field applied (Hergt *et al.*, 2004b). Above a certain threshold, the field strength can cause physiological problems by inductive heating (Hergt *et al.*, 2004b) such as, stimulation of peripheral, skeletal and cardiac muscles (Mornet *et al.*, 2004). At present, the only AMF coil generated for patient use is limited to 18kA/m at a fixed frequency of 100 kHz (Gneveckow *et al*., 2004).

The concentration of SPIONs delivered to the target site is also a limiting factor in generating toxic levels of heat (Hilger *et al.*, 2001). Direct injection into the tumour

allows for delivery of high concentrations of SPIONs to the target area therefore, allowing other areas of the body to remain unaffected by AMF heating. The first clinical study of magnetic fluid hyperthermia by Johannsen *et al* showed that direct injection of 12.5 ml SPION suspension into the prostate at concentrations of 120 mg/ml was well tolerated (Johannsen *et al*., 2005). Systemic application of SPIONs however, proves more difficult due to their rapid clearance from the blood by the RES and therefore, reducing the concentration of SPIONs reaching the target organ. To improve the systemic application of SPIONs functionalisation with a targeting moiety would be advantageous.

1.9 Research aims

The central hypothesis for this thesis is that SPIONs can be used for diagnosis and targeted therapy of cancer. The aims of this thesis was to generate scFv-SPION conjugates that would selectively target SPIONs to cancer cells and test their imaging potential by MRI and therapeutic potential by magnetic fluid hyperthermia (MFH).

#

Chapter 2

General Materials and Methods

2.1 Materials

Table 2.1 Microbial culture media and solutions for yeast fermentations

Media	**Formula**
YEPD medium/glucose primary culture medium	Dissolve 10 g Bacto yeast extract, 20 g Bacto peptone, 10 g glucose into 1 litre dH_2O. Autoclave
Basic salt medium	Dissolve 5.4 g $CaSO_4$, 88 g K_2SO_4, 70 g $MgSO_4 \cdot 7H_2O$, 54 g $(NH_4)_2SO_4$ and 300 ml glycerol into 5 litre dH_2O. Autoclave.
Sodium hexametaphosphate	Dissolve 150 g in 1 litre dH_2O. Filter sterilise
Trace element solution (PTM1; for 1 litre)	Dissolve 5.99 g $CuSO_4 \cdot (H_2O)_5$, 8 ml 10X NaI stock solution (0.4 g NaI per 40 ml dH_2O), 3g $MnSO_4 \cdot H_2O$, 0.2 g $Na_2MoO_4 \cdot (H_2O)_2$, 0.5 g $CoCl_2 \cdot (H_2O)_6$, 20.04 g $ZnCl_2 \cdot (H_2O)_5$, 65.05 g $FeSO_4 \cdot (H_2O)_7$, 800 µl of 100X H_3BO_3 stock solution (1 g H_3BO_3 per 40 ml dH_2O), 19.2ml 96.2% H_2SO_4, 0.4 g D-biotin in 970 ml dH_2O. Autoclave.
Secondary culture medium	300 ml basic salt medium, 30 ml sodium hexametaphophate, 1 ml trace element solution. Filter sterilise.
Fermentation medium	4.7 litre basic salt medium, 1 litre sodium hexametaphosphate, 1 ml anti-foam, 24 ml trace elements. Autoclave in fermenter.
Limited glycerol feed	300 ml glycerol, 300 ml dH_2O. Autoclave. Add 7 ml trace element solution.
Limited methanol feed	2 litre methanol, 24 ml trace element solution

Table 2.2 Solutions for His tagged protein isolation and purification on expanded bed adsorption immobilized-metal affinity chromatography (EBA IMAC)

Buffer	**Formula**
Copper sulphate	Dissolve 75 g $CuSO_4 \cdot (H_2O)_7$ in 3 litre dH_2O. Autoclave.
1X PBS, 1 M NaCl	Dissolve 96 g PBS powder and 584 g NaCl into 10 litre dH_2O. Autoclave.
2X PBS, 2 M NaCl	Dissolve 192 g PBS powder and 1169 g NaCl into 10 litre dH_2O. Autoclave.
Imidazole wash buffer 40 mM	Dissolve 48 g PBS powder, 292 g NaCl and 13.6 g Imidazole into 5 litre dH_2O.
Imidazole elution buffer 200 mM	Dissolve 48 g PBS powder, 292 g NaCl and 68.01 g into 5 litre dH_2O.
50 mM EDTA	Dissolve 75 g EDTA into 4 litre dH_2O. Autoclave
Sanitizing solution: 1 M NaOH, 1 M NaCl	Dissolve 400 g NaOH and 584 g NaCl into 10 litre dH_2O.
20% (vol/vol) ethanol	Dilute 2 litre 100% ethanol in 8 litre dH_2O.

Table 2.3. Buffers for protein manipulation

Buffers	**Formula**
2X SDS-PAGE loading buffer	1.25 mM Tris-HCL, pH 6.8; 20%(w/v) glycerol; 2% (w/v) β-mercaptoethanol; 0.1% (w/v) bromophenol blue; 0.1% (w/v) SDS
1X SDS-PAGE running buffer	25 mM Tris-HCl, 192 mM Glycine; 0.1% (w/v) SDS
1X transfer buffer	25 mM Tris-HCl, 192 mM Glycine, 20% (w/v) methanol
Coomassie gel stain	0.1% (w/v) coomassie blue R-250, 45% (w/v) methanol, 10% (w/v) glacial acetic acid
Coomassie gel destain	30% (w/v) methanol, 10% (w/v) glacial acetic acid

Table 2.4: Solutions for scFv-SPION sodium periodate conjugation

Buffers	**Formula**
Sodium Acetate 10 mM	Dissolve 5.4 g NaAc into 4 litre dH_2O. Adjust to pH 4 with acetic acid. Filter to sterilise.
Sodium Acetate 0.2 M	Dissolve 2.7g NaAc into 100 ml dH_2O. Adjust to pH 6 with acetic acid. Filter to sterilise
Sodium periodate oxidation buffer 10 mM	Dissolve 0.02 g $NaIO_4$ into 10 mls 0.2 M NaAc buffer. Keep in dark.
Sodium borohydride reduction buffer 0.1 M	Dissolve 0.06 g $NaBH_4$ into 10 mM NaAc buffer.

Table 2.5: Solutions for scFv-SPION carbodiimide conjugation

Buffers	**Formula**
MES buffer 0.5 M	Dissolve 9.75 g 2-(4-morpholino) ethanesulphonic HCl into 100 ml dH_2O. Adjust to pH 6.3 with Na_2CO_3 (sodium carbonate). Filter to sterilise.
MES buffer 0.1 M	Dissolve 78 g 2-(4-morpholino) ethanesulphonic HCl into 4 litre dH_2O. Adjust to pH 6.3 with Na_2CO_3 (sodium carbonate). Filter to sterilise
EDC/ NHS activation buffer	Dissolve 0.6 mg 1-ethyl-3-(3-dimethylaminopropyl)-carbodiimide hydrochloride and 1.2 mg N-hydroxysuccinimide into 200 µl 0.5 M MES buffer
Glycine 25 mM	Dissolve 0.18 g Glycine into 100 mls 1XPBS. Filter to sterilise

Table 2.6 Solutions for scFv SPION cyanogen bromide conjugation

Buffers	**Formula**
Activation Buffer	0.1 M Sodium hydrogen phosphate buffer pH9. Filter to sterilise
Glycine 25 mM	Dissolve 0.18 g Glycine into 100 mls 1XPBS

Table 2.7 Solutions for tissue culture

Buffers	**Formula**
Culture medium	To 500 ml RPMI medium add 1% 100x L-glutamine, 10% Foetal calf serum
Trypsin	Versene EDTA and trypsin
Freezing medium	Mix 1 ml dimethyl sulphoxide (DMSO) with 9ml foetal calf serum

Table 2.8 Solutions for immunostaining adherent cells

Buffers	**Formula**
Fixing buffer	4% Parafilm aldehyde
Quenching buffer	10 mM Tris. Adjust pH 7.5 with HCL
Permeabilisation buffer	0.05% Triton-X-100 in PBS
Blocking buffer	3% BSA in PBS

Table 2.9 Solutions for ferrozine assay

Buffers	**Formula**
$FeCl_3$ standard	Disslove in 1 litre H_2O
Lysis buffer	50 mM NaOH 0.2 g dissolved in 100 ml H_2O
Iron Releasing Buffer	Dilute 3.5 ml of 4 M HCL into 10 ml H_2O add to 10 ml solution of 0.45 g of $KMnO_4$ dissolved in H_2O
Iron Detection Buffer	Dissolve in 5 mls H_2O 0.015 g ferrozine, 0.015 g neocuproine, 0.96 g ammonium acetate and 0.99 g ascorbic acid.

Table 2.10 Solutions for Prussion blue staining

Buffers	Formula
Prussian blue	4g potassium ferrocyanide dissolved in 20ml H_2O added to 20ml and 2% HCL

All chemicals were purchased from Sigma-Aldrich (St Louis, USA Ltd) unless specified. All buffers were filtered through 0.2µm Nalgene filter (VWR International, Leicestershire, UK).

Pre-cast Tris-Glycine SDS-PAGE minigels (10 well, 12% Polyacrylamide, 1mm thick) and protein molecular weight marker "SeeBlue Plus 2®" (Fig.2.1) were obtained from Invitrogen Ltd (Paisley, UK). Sequencing grade 0.45 µm polyvinylidene difluoride (PVDF) membrane and chromatography filter paper was purchased at BioRad laboratories Ltd (Hemel Hempstead, UK).

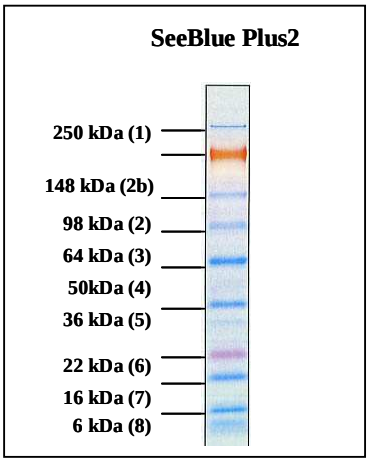

Fig. 2.1. Molecular weight calibrants for gel filtration chromatography were purchased from Bio-Rad laboratories (UK). Apparent molecular weights of SeeBlue Plus2 markers subjected to SDS-PAGE (4-20% Tris-Glycine). Molecular weight markers correspond as follows: (1) Myosin; (2)BSA; (2b) Phosphorylase B; (3) Glutamic Dehydrogenase; (4) Alcohol Dehydrogenase; (5) Carbonic Anhydrase; (6) Myoglobin; (7) Lysozyme; (8) Aprotinin; Taken from Invitrogen catalogue.

2.1.1 Microbial strains

The wild type yeast strain X-33 was obtained from Invitrogen (UK).

2.1.2 Proteins

Laboratory stock of carcinoembryonic antigen (CEA) was kindly donated by Dr Graeme Denton and Professor Alan Perkins (Nottingham University).

2.1.3 Human cell lines

The human CEA expressing colorectal cancer cell line LS174T and human CEA negative melanoma cell line A375M were purchased from the European catalogue of Human and Animal Cell Culture (ECACC; UK).

2.1.4 Antibodies

The murine anti-CEA scFv, MFE-23, was originally selected from a combinational phage display library produced from mice immunised with CEA (Chester *et al.,* 1994). The humanised high affinity anti-CEA scFv, Sm3E, was constructed by site directed mutagenesis of MFE-23 (Graff *et al.,* 2004). MFE-23, and Sm3E were purified by EBA IMAC (Tolner *et al.,* 2006), from induced *Pichia Pastoris* yeast cells transformed with pPICzαA/ MFE-23 HIS and pPICzαA/ Sm3E respectively.

Laboratory stocks of polyclonal antibodies were raised against MFE-23 by immunisation of a rabbit with purified MFE-23. Mouse tetra his (anti-HIS) antibody was obtained from Qiagen (Crawley, West Sussex, UK). Mouse anti dextran was obtained from StemCell research (Stemcell Technologies Inc, Vancouver, Canada). Mouse anti LAMP1 was kindly donated by Dr Shane Minogue (Department of Medicine, Royal Free and University College Medical School).

The conjugated antibody goat anti-rabbit horse rabbit peroxidase (HRP) was purchased from Sigma-Aldrich (St Louis, USA Ltd). Sheep anti-mouse HRP, Goat anti-mouse Alexa Fluor 564 and 488, nuclear stain Hoechst and ProLong gold anti-fade was purchased from Molecular Probes (Invitrogen, Oregan US).

2.1.5 Superparamagnetic iron oxide nanoparticles

Details of the SPIONs investigated are shown in Table 2.10, which gives simplified nomenclature, SPION coating, number of SPIONs per mg, commercial name and supplier.

Table 2.11 Details of SPIONs investigated includes simplified nomenclature of SPIONs used in thesis.

SPIONs	Coating	Commercial name	Supplier	SPIONs /mg	Hydrodynamic diameter
D50	Dextran	50nm nanomag-D-spio	Micromod Partikeltechnologie GMbH	$1x10^{13}$	50nm
d100	Dextran	100nm nanomag-D-spio	Micromod Partikeltechnologie GMbH	$1x10^{12}$	100nm
PEG-d20	Dextran-PEG-COOH	20nm nanomag-D-spio-PEG-COOH	Micromod Partikeltechnologie GMbH	$1x10^{14}$	20nm
PEG-d50	Dextran-PEG-COOH	50nm nanomag-D-spio-PEG-COOH	Micromod Partikeltechnologie GMbH	$1x10^{12}$	50nm
DX200	Dextran	200nm FluidMAG-DX	Chemicell GMbH	$2\ x10^{11}$	200nm
DX100	Dextran	100nm FluidMAG-DX	Chemicell GMbH	$2\ x10^{12}$	100nm
CMX200	Dextran-COOH	200nm FluidMAG-CMX	Chemicell GMbH	$2\ x10^{11}$	200nm
CMX100	Dextran-COOH	100nm FluidMAG-CMX	Chemicell GMbH	$2\ x10^{12}$	100nm
CMX50	Dextran-COOH	50nm FluidMAG-CMX	Chemicell GMbH	$2\ x10^{13}$	50nm

2.2 Methods

2.2.1 Protein expression

2.2.1.1 Fermentation of Pichia pastoris X-33 cells

Fermentation of *Pichia pastoris X-33* cells was performed with the help of Dr. Berend Tolner and Mr Tim Hillyer (Department of Oncology) *(*Tolner B *et al.,* 2006*)* using a BioFlo 3000 Batch/Continuous Bioreactor (New Brunswick Scientific, Edison, NJ, USA). Fermentation medium was prepared in the fermentor and was composed of the components as listed in Table 2.1.1, subsequently the fermentor containing the media was autoclaved. A primary seed lot in a 2 litre conical flask containing 250 ml of YEPD glucose medium was started by inoculation with one frozen vial containing 1 ml of seed lot and grown overnight at 30^{o}C at 200 rpm to an OD_{600} of 12. Upon reaching OD_{600} of 12, 2 ml of the primary culture was used to inoculate the secondary culture medium (Table 2.1.1). The secondary culture was grown overnight at 30^{o}C at 200 rpm to an OD_{600} of 5. Once this was reached the secondary culture was added to the fermentation medium and the fermentation run was started. The pH at the start of the fermentation was set to 5.0 and was automatically maintained by addition of 100% NH_4OH base solution or 10% ortho phosphoric acid solution. The dissolved oxygen probe was set to 40% and the temperature was set to 30 ^{o}C. At 22-24 hrs after inoculation, a sharp increase in dissolved oxygen (spike) was observed, which is indicative of depletion of the glycerol (carbon source) in the vessel. At this point a limited glycerol feed (Table 2.1.1) was started and the pH reset to 6.5. One hour after the start of the limited glycerol feed, 12 ml of limited methanol feed (Table 2.1.1) was directly injected into the fermenter. During the run the flow rates of the glycerol and methanol limited feeds were altered (Table 2.2.1). The fermentation run was stopped after approximately 72 hr post inoculation, ready for protein capture.

Table 2.12 Flow rates for addition of glycerol and methanol during yeast fermentation

Time post limited feed start (hr)	Flow rate glycerol (ml/hr)	Flow rate methanol (ml/hr)
0	120	0
1.0	120	0
1.5	100	0
2.0	80	0
2.5	60	0
3.0	40	0
3.5	20	0
4.0	0	10
6.0	0	20
8.0	0	30
10.0	0	42-45

2.2.2 Protein purification

2.2.2.1 Expanded-bed adsorption immobilized metal affinity chromatography (EBA IMAC)

Large scale purification of the hexahistidine-tagged proteins straight from the *Pichia pastoris* fermentation was performed using the expanded bed adsorption IMAC (GE Healthcare). All application to the column were in an up-flow except for the elution step. Briefly, the EBA column was connected to the spectrophotometer and zeroed with water. The column was charged with 0.1 M copper sulphate solution at flow rate 300 cm/h (Table 2.1.2) and unbound ions were washed off with dH_2O until UV signal returned back to baseline. Ten column volumes of loading buffer (Table 2.1.2) were then run through the column.

The bioreactor contents from the *Pichia pastoris* fermentation was first diluted 1:1 with 2 M NaCl in 2x PBS, then loaded onto the charged EBA column at flow rate 300 cm/h. Once all the bioreactor contents had been applied to the column loading buffer was run through until the UV signal reached baseline. To remove non-specificically bound contaminants, 40 mM Imidazole wash buffer was applied to the column at a flow rate 300 cm/h until the UV signal returned to baseline. Finally, the column flow was reversed and the target hexa-histidine-tagged proteins were eluted off the column by application of 200 mM Imidazole elution buffer to the column at flow rate 150 cm/h fraction. Peak fractions containing protein were determined spectrophotometrically at an OD_{280}, these fractions were collected, pooled, filtered through a 0.2 μM Nalgene filter and dialysed against PBS overnight. Fractions were either stored as 25 ml aliquots at -80^{o}C or further purified by size exclusion chromatography.

The EBA column was washed with sterile dH_2O until the UV signal returned to baseline, and regenerated with 4 litre 50 mM EDTA, removing the copper sulphate. Five column volumes of dH_2O were applied to the column to displace the EDTA solution, the EBA column was further washed in sanitizing solution for 1 hr and stored in 20% ethanol.

2.2.2.2 Size-exclusion chromatography

Proteins were separated according to molecular weight by size exclusion chromatography (SEC) using an AKTA *FPLC™* system (GE-Healthcare, Amershan, UK). For resolution of smaller proteins, a Superdex 75 SEC column (GE-Healthcare) was used. For loads of less than 2mls the Superdex 75, 16/60, (matrix volume 120ml) was used. Protein samples were loaded via the 2 ml injection loop at a constant flow rate of 2 ml/min PBS. For protein samples of up to 25 mls the Superdex 75, 25/60 column (matrix volume 500 mls) was used. Protein samples were loaded onto the column at a flow rate of 5 ml/min PBS. Fractions were collected and peak fractions were pooled. One millilitre aliquots were made and samples stored at -80^{o}C ready for further analysis.

For separation of larger molecules such as magnetic particles, a Sephacryl 300 high resolution SEC column 16/25 (30 ml) and 16/60 (120 ml) (GE-Healthcare) were used. Magnetic particles and protein samples were injected onto the column at a constant flow rate of 0.5 ml/min PBS. Magnetic particle fraction was collected throughout the void volume; peak fractions were pooled and stored at 4^{o}C ready for further analysis.

For calibration, the Gel Filtration Standard kit (Bio-Rad) was prepared and applied to columns as directed by manufacturers.

2.2.3 Protein characterisation

2.2.3.1 Protein quantification

The concentration of proteins was determined spectrophotometrically using the following equation:

$$A_{280}=\varepsilon_{280} \times c \times l \qquad \text{(Equation 2.1)}$$

Where A_{280} is the absorbance at 280 nm of protein samples measured in quartz cuvettes on a Cecil CE2041 2000 series spectrophotometer, ε_{280} is the extinction coefficient (0.1%, 280 nm, 1 cm path length) of the protein calculated based on the protein primary amino acid sequence using the Expasy Protparam web tool (http://www.expasy.ch/tools/protparam.htlm), c is the protein concentration, l is the path length of the cuvette (cm). For MFE-23, ε_{280} = 1.9; for Sm3E, ε_{280} = 1.9

2.2.3.2 Sodium dodecyl sulphate-polyacrylamide gel electrophoresis (SDS-PAGE)

Electrophoresis of proteins was performed under reducing conditions. Samples were prepared by the addition of 2X SDS-PAGE reducing buffer (Table 2.1.3) followed by denaturation at 95^{o}C for 5 min. Samples were loaded onto 12% Tris-Glycine pre-cast mini-gels (Invitrogen) and separated on an XCell II™ Mini-Cell system (Invitrogen) in 1x SDS-PAGE Running buffer (Table 2.1.3) on an automated

program of 90 min at 35 mA (125 V, 5 W) using a PowerEase® 500 power supply (Invitrogen). Following electrophoresis, proteins were either stained with coomassie blue (Table 2.1.3) or subjected to Western blotting (section 2.2.4.3).

Gels were stained with Coomassie blue stain for 2-4 hrs at room temperature. To enable visualisation of proteins the gels were de-stained with de-stain solution (Table 2.1.3) for 2-4 hrs with repeated de-stain solution changes. Gels were rinsed in dH_2O followed by 15 min incubation in Gel drying solution (Invitrogen) in preparation for drying using the Invitrogen Gel drying kit. Two gel drying plastic sheets (Invitrogen) were soaked in the Gel drying solution, the gel was sandwich between them and left to dry in a drying rack overnight at room temperature.

2.2.3.3 Western blot analysis

Following electrophoresis proteins were transferred to polyvinylidene difluoride (PVDF) membrane (Bio-Rad Laboratories Ltd), pre-treated by soaking in methanol for 10 min. Gels were sandwiched with the PVDF membrane between several sheets of pre-wetted chromatography filter paper (Whatmen, Maidstone, UK) and sponges. This was submerged in an XCell II Blot Module (Invitrogen) filled with 1x Transfer buffer (Table 2.1.3). Proteins were transferred using an automated program of 90 min at 125 mA (25 V, 17 W).

Following electro-transfer, PVDF membranes were blocked in 5% (w/v) Marvel skimmed milk powder (Marvel, UK) in PBS for at least 1 hr. The blocked blots were washed in PBS and incubated on a rocker at room temperature for 1 hr in the appropriate primary antibody diluted in 1% (w/v) Marvel/PBS. The blots were then washed with 3x 0.1% (v/v) Tween-20 in PBS, then 3x PBS followed by incubation on a rocker at room temperature for 1 hr in the appropriate secondary horseradish peroxidase (HRP)-conjugate antibody diluted in 1% (w/v) Marvel/PBS. Following incubation, the blots were washed as before and proteins visualised with DAB substrate solution (0.25 mg/ml 3, 3'-Diaminobenzidine tetrahydrochloride, 0.5 µl/ml H_2O_2 in dH_2O). The reaction was stopped by rinsing the membrane in dH_2O. The membrane was left to dry at room temperature.

Table 2.13 Antibody dilutions

Primary Antibody (dilutions)	**Secondary Antibody (dilutions)**
Tetra His 1/1000 (Qiagen)	Sheep anti-mouse-HRP 1/500 (GE-Healthcare)
Anti-MFE-23 rabbit sera 1/1000 (Laboratory generated stock)	Goat anti-rabbit-HRP 1/1000 (Sigma-Aldrich)
Anti-dextran 1/1000 (Stemcell)	Sheep anti-mouse-HRP 1/500 (GE-Healthcare)

2.2.3.4 Enzyme-linked immunosorbent assay (ELISA)

ELISAs were performed on 96-well micro-titre plates (Costa, High Wycombe, UK) coated for 1-2 hr with 100 µl 1 µg/ml CEA in PBS or PBS. Wells were washed 2x with PBS and blocked with 200 µl 5% (w/v) Marvel/PBS for 2-16 hrs. Fifty to one hundred micro-litres of samples (neat supernatant or purified proteins diluted in PBS) were applied to CEA or PBS coated wells in triplicate and incubated for 1 hr. After incubation the wells were washed 3x with PBS. Wells were then incubated for 1 hr with 100 µl primary antibody diluted in 1% (w/v) Marvel/PBS. Following incubation wells were washed 3x in PBS/0.1% (v/v) Tween-20 followed by 3x PBS, then incubated for 1 hr with 100 µl HRP-conjugated secondary antibody diluted in 1% (w/v) Marvel/PBS. Wells were washed as before and 100 µl OPD (O-phenylenediamine dihydrochloride; 0.4 mg/ml dissolved in phosphate citrate buffer, pH 5.0) was added. Reactions were stopped with 50 µl 4 M HCL and the absorbances were measured at 490 nm using Opsys MR™ Microplate Reader (Dynex Technologies). See Table 2.2.2 for antibody dilutions.

2.2.4 Antibody-SPION conjugation chemistry

2.2.4.1 Sodium periodate conjugation

Conjugation of the available OH groups on the dSPIONs to the available NH_3 groups on the scFvs was achieved by adaptation of the sodium periodate method (Molday *et al*., 1982). Briefly, 5 mg/ml of the dSPION (1 ml) was added to 1 ml 10 mM sodium periodate (Sigma-Aldrich) and incubated at room temperature for 1 hr in the dark on a rotating shaker to allow partial oxidation of the dextran. The oxidation reaction was terminated by application to a PD-10 desalting column (GE-Healthcare) equilibrated with 10 mM sodium acetate buffer pH 4. The same buffer was used for elution of the SPIONs. Conjugation was achieved by addition of the eluted oxidised dSPION (3 ml at 3 mg/ml) to the scFv (1 ml of 0.1 mg/ml in 10 mM sodium acetate buffer pH 4) and incubation on a rotating shaker for 24 hrs at room temperature. Subsequently the mixture was reduced by addition of 0.5 ml at 0.1 M sodium borohydride (Sigma-Aldrich) for 15 min at room temperature. The reaction was terminated by application to a PD-10 desalting column as described above for the oxidation reaction. The scFv-dSPION conjugate (7 ml) was concentrated to 2 ml using Vivaspin 15R concentrators with a 5000 MW cut off (Sartorios Stedim Biotech GmbH, Germany) at 3082 g and purified by size exclusion chromatography (SEC) using Sephacryl 300HR (GE Healthcare) in PBS buffer (Section *2.2.3.2.*).

2.2.4.2 Carbodiimide conjugation.

Conjugation of the available COOH groups on the PEG-dSPIONs to the available NH_3 groups on the scFvs was achieved using a modification of the carbodiimide method (DeNardo *et al*., 2005). Briefly, 5 mg/ml of PEG-dSPION were activated by incubation with EDC/NHS activation buffer (Table 2.1.4) for 1 hr at room temperature on a rotating shaker. The reaction was terminated by application to PD-10 desalting columns equilibrated with 0.1 M MES buffer pH6.3. The same buffer was used for elution of the SPIONs. The activated PEG-dSPIONs (2 ml at 2 mg/ml) was added to the scFv (1 ml of 0.1 mg/ml in 0.1 M MES buffer pH6.3) and the conjugation reaction was achieved by incubation for 24 hrs on a rotating shaker at room temperature. After 24 hr, 0.1 ml of 25 mM Glycine in PBS was added to the

conjugation reaction and the mixture was incubated for a further 30 min at room temperature on the shaker to block remaining reactive sites. The resulting scFv-PEG-dSPION conjugates (3ml) were concentrated to 2ml using Vivaspin 15R concentrators with a 5000 MW cut off at 3082 g and then purified by SEC on Sephacryl 300HR in PBS (Section 2.2.3.2.).

2.2.4.3. Cyanogen bromide conjugation

Conjugation of the available OH groups on the FluidMAG-DX SPIONs (DX-SPION) to the available NH_3 groups on the scFvs was achieved by adaptation of the cyanogen bromide conjugation chemistry from the Chemicell GMbH website. Briefly, 10 mg/ml DX-SPIONs diluted in activation buffer (Table 2.1.6) was activated by incubation with 0.05 ml of CNBr (Sigma-Aldrich). The solution was vortexed and incubated on ice for 10 min. The reaction was stopped by running the particles through a PD-10 desalting column equilibrated with PBS; the same buffer was used for elution of the SPIONs. The activated DX-SPIONs (2 ml at 4.5 mg/ml) were added to the scFv (1 ml of 0.1 mg/ml in PBS) and the conjugation reaction was achieved by incubation for 24 hr on a rotating shaker at room temperature. After 24 hr, 0.1 ml of 25 mM glycine in PBS was added to the conjugation reaction and the mixture was incubated for a further 30 min at room temperature on the shaker to block remaining reactive sites. To remove unbound scFv and glycine, four overnight magnetic washes with PBS were performed. The scFv-DX-SPION conjugate sample was diluted to 6 ml with PBS and placed in 6 x 1 ml holders on the DynalMagnet (Millipore). After the final magnetic wash the pellets were resuspended to 1 ml in PBS and pooled.

2.2.5 ScFv-SPION conjugation analysis

2.2.5.1 Ratio of scFv-SPION in conjugate solution

The protein concentration of the scFv-SPION conjugate was estimated using the Bradford assay. Firstly, (non-conjugated) scFv protein concentration standards were prepared in PBS buffer at concentration 0, 2.5, 5, 7.5 and 10 µg/ml. To 500 µl of each standard 500 µl of Bradford reagent (Sigma-Aldrich) was added and mixed

gently by hand. The samples were left to incubate at room temperature for 15 min. The absorbance of each standard was measured at 595 nm in quartz cuvettes on a Cecil CE2041 2000 series spectrophotometer. The absorbance *vs*. the protein concentration for each standard was plotted.

Subsequently, the concentration of conjugated scFv in the purified scFv-SPION conjugate solutions was determined using the Bradford assay above and the absorbance was measured at 595 nm on the spectrophotometer which was blanked against non-functionalised SPIONs. The absorbance value was then referenced against the standard curve of Bradford assayed serial dilutions of the scFv.

The number of scFv molecules in the scFv-SPION conjugate solution was then calculated following the equations 2.2 and 2.3 below, where nSm3E equals the number of Sm3E molecules and N_A equals Avogadro's constant 6.022 x 10^{23}

$$moles = \frac{[Sm3E][\mu g/ml]}{MW[kDa]} \qquad \text{Equation 2.2}$$

$$nSm3E/ml = moles \times N_A \qquad \text{Equation 2.3}$$

Absorbance readings at 490 nm were performed to estimate the concentration of the SPIONs in scFv-SPION conjugate solutions. Firstly, SPION concentration standards were prepared in PBS buffer at concentrations 0, 0.125, 0.25, 0.375 and 0.5 mg/ml. The absorbance of each standard was measure at OD 490 nm in quartz cuvettes on a Cecil CE2041 2000 series spectrophotometer. The absorbance *vs.* the SPION concentration for each standard was plotted.

The absorbance of the purified scFv-SPION conjugates at 490 nm was subsequently referenced against the standard curve of their respective serial diluted SPIONs, allowing the concentration of the SPIONs to be determined. Following equation 2.4

the number of SPIONs in the conjugate solution can be calculated. See section 2.1.5 for the number of SPIONs per mg *(nSPION)* as stated by the manufacturer.

$$nSPION/ml = [SPION][mg/ml] \times nSPION/mg \qquad \text{Equation 2.4}$$

Finally, the number of Sm3E scFvs bound per SPION was calculated following equation 2.5.

$$nSm3E/nSPION = \frac{nSm3E/ml}{nSPION/ml} \qquad \text{Equation 2.5}$$

2.2.5.2 Ferrozine assay to estimate iron concentration

To quantify the concentration of Fe^{2+} in the SPIONs, $FeCl_3$ standards were firstly prepared. One hundred microlitre $FeCl_3$ standards at concentrations 0, 0.05, 0.1, 0.25, 0.5, 1, 2.5, 5, 7.5 and 10 μg/ml in 10 mM HCL were incubated in 100 μl 50 mM NaOH and 100 μl iron releasing buffer (Table 2.1.9) at 60^{o}C on a heat block for 2 hrs. After incubation the samples were cooled to room temperature for 10 min, 30 μl iron detection buffer (Table 2.1.9) was subsequently added to all the samples. The iron detection buffer forms a complex with ferrous iron that absorbs strongly at 550 nm. The samples were mixed and incubated for 30 min to allow for maximum colour change. Following incubation the absorbance of the standards was read at 550 nm using Opsys MR™ Microplate Reader (Dynex Technologies). The absorbance vs. the Fe^{2+} concentration for each standard was plotted. This assay was then performed for all the SPIONs at concentrations 0, 0.5, 1, 2.5, 5, 10, 2.5, 5, 10, 25, 50 and 100 μg/ml in 10 mM HCL. The absorbance vs. the SPION concentration for each standard was plotted. The SPION concentration was then plotted against its corresponding Fe^{2+} concentration.

2.2.5.3 Magnetic resonance imaging (MRI) potential of SPIONs

To determine the MRI potential of the SPIONs, serial dilutions of the SPIONs were prepared in PBS at concentrations 0, 7.5, 37.5 and 75 μg/ml. The samples were

aliquoted into 250 µl MRI eppendorf tubes and placed in a rack inside a 50 ml falcon tube containing 2.5 g/L $CuSO_4$. The samples were then scanned using a 2.35T horizontal bore SMIS system (3 cm coil, 128 x 128 matrix, 2mm slice along the eppendorf cross section, 2 averages, FOV 40mm, TR = 1s at multiple TEs). T2 values were determined.

2.2.5.4 Alternating magnetic field (AMF) heating potential of SPIONs

To determine the AMF heating potential of the SPIONs, a range of SPION concentrations were prepared in water and placed into the coil of the AMF heating apparatus. Two AMF heating systems were used, applying a field strength of 300V, 0.62 A and 139.8 Hz or 150 V, 0.74 A and 1 MHz. The temperature increase over 20 min was measured using a Luxtron thermometer probe placed in the SPION solution.

2.2.5.5 Zeta Potential of SPIONs

The SPION zeta potential measurements were performed with the help of Dr. Khuloud Al-Jamal (Nanomedicine lab, The school of pharmacy). The hydrodynamic Z-average diameters and zeta potentials of the SPIONs were measured using a Zetasizer Nano ZS (Malvern Instruments, Malvern) at concentration range of 0.01-1mg/ml in deionised water or at pH 7.4. The average of three measurements provided results expressed as zeta potential (mV) ± S.D.

2.2.6 Cell culture

Following standard tissue culture techniques, cell culture procedures were carried out in a class II Hood. Culture medium (see Table 2.1.7), PBS and Trypsin/EDTA were pre-warmed to 37^{o}C before use. All cell cultures were incubated at 37^{o}C in a tissue culture incubator humidified with a CO_2 concentration of 5%.

2.2.6.1 *Taking cell lines into culture*

Cell lines were purchase and stored in frozen aliquots, to bring them into culture the aliquots were thawed at 37^{o}C and resuspended by drop wise addition of 10 ml culture

medium (Table 2.1.7). The cells were pelleted at 1300RPM for 3 min in a bench top centrifuge. The cells were resuspended in 5 ml of culture medium and seeded into T25 culture flasks until confluent.

2.2.6.2 Propagation of adherent cell lines CEA+ve LS174T and CEA-ve A375M

Once confluent, cells were sub-cultured routinely twice weekly in a split ratio of 1:5. Culture medium was poured off and cells washed once in 10 ml PBS. The PBS wash was poured off and cells were released from the flask by incubation in 5 ml trypsin/EDTA for 5 min at 37^{o}C (Trypsinisation). For complete release of cells the flasks were whacked twice and an equal volume of fresh culture medium was added to resuspend the released cells. Two millilitres of resuspended cells was pelleted at 1300 g for 3 min. The cells were resuspened in 2 ml fresh culture medium and seeded into T75 flasks containing 13 ml fresh culture medium.

2.2.6.3 Cryogenic storage

Once cells were confluent, culture medium was poured off and cells washed once in 10 ml PBS. The PBS wash was poured off and cells were releases from the flask by trypsinisation (Section *2.2.7.1).* Equal volume of fresh culture medium was added to resuspend the released cells. Resuspended cells were pelleted at 1300 g for 3 min. The cells were resuspened in 5 ml freezing medium (see Table 2.1.7) and aliquoted into 1 ml cryovial™ (Nalgene). The cryovials were stored at -80^{o}C.

2.2.7 *In-vitro* analysis of scFv-SPIONs

2.2.7.1. Ferrozine assay to measure cell SPION uptake.

Cellular uptake of the scFv functionalised and non functionalised SPIONs were quantified following the adapted ferrozine assay based method (Riemer *et al*., 2004). Briefly exponentially growing cells were trypsonised and seeded at a density of 5x10^{4} cells/ml, 2 ml/well in 24 well plates and incubated in culture medium (Table 2.1.7) for 5 days. On the 5th day, the culture media was removed and replaced with 1

ml filter sterilised scFv functionalised and non-functionalised SPIONs at 0.1 mg/ml in culture media. Cells were incubated overnight followed by 3 x washes in cold PBS. After completely removing the PBS, the cells in three of the media control wells were trypsonised and counted to determine the number of cells per well. The cells in the rest of the wells were frozen and stored at -20^{o}C. Cells were lysed with 300 µl 50 mM NaOH for 2 hrs on a shaker at room temperature. The cell lysates were subsequently transferred to 1.5 ml eppendorf and mixed with 300 µl of 10 mM HCL and 300 µl of the iron releasing reagent (Table 2.1.9), the samples were incubated for 2 hrs at 60^{0}C on a heating block. After incubation the samples were cooled to room temperature, 30 µl iron detection buffer (Table 2.1.9) was then added to all the samples. After gentle mixing by hand the samples were incubated at room temperature for a further 30 min to allow for maximum colour change. Absorbance readings at 550 nm were performed using the Opsys MR™ Microplate Reader (Dynex Technologies), values were referenced against standard curve of ferrozine assayed SPIONs at known concentrations (Section 2.2.5.3). The SPION uptake per cell was calculated following equation 2.6, where nCell equals the number of cells.

$$SPION/cell[\mu g] = \frac{[SPION][\mu g / well]}{nCell/well} \qquad \text{Equation 2.6}$$

2.2.7.2 MTT toxicity assay

Toxicity of the SPIONs was investigated using a cell viability assay based on 3-(4,5-Dimethylthiazol-2-yl)-2,5-diphenyltetrazolium bromide (MTT) (Sigma-Aldrich) (Mosmann 1983). Briefly, exponentially growing cells were trypsonised and seeded at a density of 1x10^{5} cells/ml, 200µl/well in 96 well plates. The plates were incubated in a humidified incubator with a CO_2 concentration of 5% for a minimum of 16 hours to allow adherence of the cells. Once adhered the cells were incubated overnight 0.1ml with culture medium containing non-functionalised SPIONs at particle concentrations of 1mg/ml, 0.5mg/ml and 0.1mg/ml or functionalised scFv-SPIONs at a particle concentration of 0.1mg/ml. The cells were then washed and incubated a further 96 hours in fresh culture media. MTT (20µl; 5mg/ml) was subsequently added to each well and incubation allowed to proceed for a further

4hrs. Media was then carefully removed and the purple formazan crystals (indicating cell viability) were solubilised using 100µl/well of DMSO. Absorbance at 550nm was measured using the Opsys MR™ Microplate Reader (Dynex Technologies). The percentage cell survival was determined by comparison with untreated control wells. All tests were performed in triplicate.

2.2.7.3 Immunostaining of adherent cells incubated in scFv-SPIONs.

The specificity and cellular uptake of scFv functionalised and non functionalised SPIONs to the CEA+ve LS174T or CEA-ve A375M cells were examined by indirect immunofluorescence confocal microscopy. Briefly, cells were seeded onto 13 mm circular coverslips (VWR) in 24 well plates at a density of $1x10^5$ cells/ml, 500 µl/coverslip. The cells were incubated overnight at 37^{o}C in a humidified incubator with a CO_2 concentration of 5%, to allow adherence of the cells. Following adherence the cell medium was removed and the cell coated coverslips were incubated overnight with 500 µl of culture media containing i) no SPIONs ii) filter sterilised non functionalised SPIONs at 0.1 mgSPION/ml or iii) filter sterilised scFv-SPIONs at 0.1 mgSPION/ml. Following incubation cells were washed in PBS and fixed in 4% paraformaldehyde for 20 min. To quench residual paraformaldehyde the cells were washed 3x in PBS followed by incubation in 10 mM Tris/HCL pH 7 for 10 min at room temperature. After incubation the cells were again washed 3x in PBS then blocked in 500 µl blocking buffer (Table 2.1.8) for 20 min at room temperature. The cell coated coverslips were again washed 3x in PBS, the coverslips were removed from the 24 well tissue culture plate using tweezers and incubated cell face down in 50 µl mouse anti-dextran antibody 1/100, on parafilm for 45 min at room temperature. After incubation the coverslips were washed 3x in PBS, placed cell face up in 12 well plates and further incubated with 500 µl goat anti-mouse antibody labelled with Alexa Fluor 564 1/500 (Molecular Probes) and counterstained with nuclei stain Hoechst 1/5000 (Molecular Probes) for 30 min, in the dark, at room temperature, on a rocker. To remove unbound secondary antibody cell coated coverslips were washed 3x in PBS followed by 1 PBS wash on the rocker for 1 min and 1 wash in dH_2O. The coverslips were mounted cell face down on coverslides in

ProLong antifade (GE-Healthcare) imaged by using a Zeiss LSM 510 meta confocal microscope.

For the endosomal co-localisation study the mouse anti-LAMP1 IgG2b antibody was incubated together with the mouse anti-dextran IgG. Following PBS washes, the cells were incubation with the goat anti mouse IgG2b labelled with Alexa Fluor 488 1/500 (Molecular Probes) in addition to the goat anti mouse IgG1 labelled with Alexa Fluor 564 and the nuclei stain Hoechst 33342. Coverslips were mounted and imaged as before.

2.2.7.4 Magnetic resonance imaging (MRI) of adherent cells incubated in scFv-SPIONs

The MRI imaging and specificity of scFv functionalised and non-functionalised SPIONs to the CEA+ve LS174T or CE-ve A375M cells were examined. Cells cultured in a T75 flask were incubated overnight in 10 ml of medium containing i) no SPIONs ii) filter sterilised non-functionalised SPIONs at 0.1 mgSPION/ml or iii) filter sterilised scFv-SPION at 0.1 mgSPION/ml under cell culture conditions. After incubation the cells were washed in PBS, released from the flask with Versene™ followed by 2x PBS washes by centrifugation and fixed in 4% paraformaldehyde for 20 min. Following fixation the cells were washed in PBS and pelleted into 250 μl MRI eppendorf tubes and subsequently placed in a rack inside a 50 ml falcon tube containing 2.5 g/L $CuSO_4$. The samples were then scanned and T_2-weighted images were acquired with a 2DFT spin-echo sequence using a 2.35T horizontal bore scanner interfaced to a SMIS console (3cm RF coil, 256x256 matrix, 1 mm slice, 2 averages, FOV 60 mm, TR=1s, TE=80 ms).

2.2.8 Hyperthermic *in vitro* studies

2.2.8.1 Incubator heating of adherent cells: viable cell counts

To determine at which temperature cell viability becomes affected cell viability counts were performed after heat treatment. The CEA+ve LS174T cells were

cultured to 75% confluency in T25 flasks and incubated in triplicate at temperatures of 37^{o}C, 40^{o}C, 43^{o}C and 47^{o}C for 30 min. Following treatment the cells were left to recover for 1 hr at 37^{o}C. The viability of the cells was determined by cell viability counts using trypan blue stain. Briefly, the treated cells were washed 3 x in PBS and released from the flask by trypsonisation (Section 2.2.6.2). The cells were subsequently centrifuged and the cell pellet was resuspended in 10 ml culture medium, 100 µl of resuspended cells was added to 100 µl Trypan Blue stain and mixed by pipetting. Viable cells were counted using a haemocytometer, under an inverted phase contrast microscope; the total viable cell number was calculated using equation 2.7, where *nCell* equal the average number of viable cells, 2 is the dilution factor when using trypan blue and *Tvol* is the total volume of resuspended cells

$$nCell = 2 \times 1 \times 10^{4} [cells / ml] \times Tvol[ml]$$

Equation 2.7

2.2.8.2 Incubator heating of adherent cells: MTT assay

To determine at which temperature cell viability becomes affected MTT viability assay was performed after heat treatment. The CEA+ve LS174T cells were seeded at a density of 1 x 10^5 cells/ml, 200 µl/well into 96 well plates. The plates were incubated for a minimum of 16 hours to allow the cells to adhere to the wells. Once cells had adhered the plates were incubated at increasing temperatures of 37 ^{o}C, 38 ^{o}C, 39 ^{o}C, 40 ^{o}C, 41 ^{o}C, 42 ^{o}C, 43 ^{o}C, 44 ^{o}C, 45 ^{o}C, 46 ^{o}C and 47 ^{o}C for 1 hr. Following treatment the plates were returned to 37 ^{o}C and left to incubate for a further 96 hr in a tissue culture incubator humidified with a CO_2 concentration of 5%. MTT (20 µl; 5 mg/ml) was subsequently added to each well and incubation allowed to proceed for a further 4 hr. Media was then carefully removed and the purple formazan crystals (indicating cell viability) were solubilised using 100 µl/well of DMSO. Absorbance at 550 nm was measured using the Opsys MR™ Microplate Reader (Dynex Technologies). The percentage cell survival was determined by comparison with untreated control wells. was determined from the control wells.

2.2.8.3 Incubator heating of adherent cells: heat shock protein 70 immunocytochemistry Staining

To determine at which temperature the heat shock protein 70 (HSP70) is expressed, the CEA+ve LS174T cells were heat treated in an incubator and stained for HSP70 expression. Briefly, cells were seeded at a density of $1x10^5$ cells/ml, 500 µl/well onto sterile 13 mm circular coverslips (VWR) placed in 24 well tissue culture plates. Cells were incubated 2 days at 37^{o}C in a tissue culture incubator humidified with a CO_2 concentration of 5%. In triplicate the cell coated cover-slips were incubated at temperatures of 37^{o}C, 38^{o}C, 39^{o}C, 40^{o}C, 41^{o}C, 42^{o}C, 43^{o}C, 44^{o}C, 45^{o}C, 46^{o}C and 47^{o}C for 30 min then left to recover for 1 hr at 37 ^{o}C. Following treatment cells were washed 3x in PBS, then fixed in 500 µl 4% paraformaldehyde for 20 minutes at room temperature. To quench residual paraformaldehyde the cells were washed 3x in PBS followed by incubation in 10 mM Tris/HCL pH 7 for 10 min at room temperature. After incubation the cells were again washed 3x in PBS then blocked in 500 µl blocking buffer (Table 2.1.8) for 20 min at room temperature. The cell coated coverslips were again washed 3x in PBS, the coverslips were removed from the 24 well tissue culture plate using tweezers and incubated cell face down in 50 µl mouse anti-HSP70 antibody 1/100, on parafilm for 45 min at room temperature. After incubation the coverslips were washed 3x in PBS, placed cell face up in 12 well plates and further incubated with 500 µl goat anti-mouse antibody labelled with Alexa Fluor 564 1/500 (Molecular Probes) and counterstained with nuclei stain Hoechst 1/5000 (Molecular Probes) for 30 min, in the dark, at room temperature, on a rocker. To remove unbound secondary antibody cell coated coverslips were washed 3x in PBS followed by 1 PBS wash on the rocker for 1 min and 1 wash in dH_2O. The coverslips were mounted cell face down on coverslides in ProLong antifade (GE-Healthcare) imaged by using a Zeiss LSM 510 meta-confocal microscope.

2.2.8.4. AMF Heating of Adherent Cells Incubated in SPIONs: Viable Cell Counts

Viability cell counts were performed to determine whether AMF activated SPIONs and scFv-SPION conjugates can induce a hyperthermic cell death. Briefly; CEA+ve LS174T cells were grown to 75% confluency in a T25 flask culture medium. The cells were then washed 3 times in PBS and released by trysonisation. The cells were

centrifuged and cell pellet resuspended well in 1ml culture medium containing no SPIONs, 1 mg/ml, 5 mg/ml, 10 mg/ml or 25 mg/ml SPIONs. The samples were placed into AMF system 1. An alternating magnetic field of 300V, 0.62A and 139.8Hz was applied for 20min.

To determine cell viability the cells was centrifuged, washed 3x in PBS and resuspended in 10ml culture medium. One hundred microlitres of resuspended cells was mixed with 100µl Tryphan Blue stain which stains non-viable cells. The cells were counted x3 using a haemocytometer, under an inverted phase contrast microscope. Total viable cell number of was calculated using equation 2.7.

2.2.8.5 AMF heating of adherent cells incubated in SPIONs: MTT assay

MTT viability assay was performed to determine whether AMF activated SPIONs and scFv-SPION conjugates can induce a hyperthermic cell death. Briefly, cells were seeded at a density of $1x10^5$ cells/ml, 200 µl/well into 4 wells of sterile strip-wells (1 stripwell per test). The strip-wells were placed into a 96 well frame.

The cells to be treated with the scFv-SPION conjugates +/- AMF were incubated for 1 day at 37^{o}C in a tissue culture incubator; media was then replaced with 100 µl of filtered sterilised scFv-SPION at 0.1 mgSPION/ml in culture media and incubated for a further 24 hr at 37^{o}C in a tissue culture incubator. After incubation the wells were washed 3x PBS and 100 µl of fresh media was added to each well.

The cells to be treated with non functionalised SPIONs +/-AMF were incubated for 2 days at 37^{o}C in a tissue culture incubator. Following incubation the medium was removed and replaced with 100 µl filter sterilised medium containing 5 mg/ml, 2.5 mg/ml, 1 mg/ml 0.5 mg/ml or 0.1 mg/ml SPIONs, 2x strip-wells per concentration, one to be AMF control and the other to be treated with the AMF.

One strip-well at a time was exposed to the AMF of 150 V, 0.74 A and 1 MHz for 30 min. To remain sterile the cell coated strip-wells was placed into a 15 ml test tube, with the lid screwed loosely on, this was then placed inside the AMF heating coil. Ambient temperature was maintained at 37^{o}C using the Air-Therm. After AMF

treatment the strip-wells were placed back into the 96 well frames, the cells were then washed and incubated a further 96 hr in fresh media. MTT (20 µl; 5 mg/ml) was subsequently added to each well and incubation allowed to proceed for a further 4 hr. Media was then carefully removed and the purple formazan crystals were solubilised using 100 µl/well of DMSO. Absorbance at 550 nm was measured using the Opsys MR™ Microplate Reader (Dynex Technologies). The percentage cell survival was determined by comparison with untreated control wells.

2.2.8.6 AMF heating of adherent cells incubated in SPIONs: heat shock protein 70 immunocytochemistry staining

Confocal microscopy was performed to determine whether AMF treated cells incubated in scFv functionalised or non-functionalised SPION can induce HSP70 expression. Briefly, cells were seeded at a density of $1x10^5$ cells/ml, 500 µl/well onto sterile 13 mm circular coverslips (VWR) placed in 24 well tissue culture plates. Cells were incubated 2 days at 37^{o}C in a tissue culture incubator humidified with a CO_2 concentration of 5%.

In triplicate the cell coated cover-slips were incubated with either filter sterilised media containing scFv-SPIONs (0.1 mgSPION/ml) overnight, followed by PBS washed to remove unbound SPION and incubated in 500 µl fresh medium or filter sterilised media containing 1 mg/ml SPION before AMF treatment. Cell coated cover-slips were exposed to the AMF of 300 V, 0.62 A and 139.8 Hz for 30 min using AMF system 1. To remain sterile the cell coated strip-wells was placed into the lid of a 7 ml bijou tube, immersed in either media or SPIONs, with the tube screwed tightly on, the tube was placed inside the AMF heating coil. The ambient temperature was maintained at 37^{o}C using an Air-Therm. Following AMF treatment the cell coated coverslips were placed into 24 well plates and washed 3x in PBS followed by further incubated in fresh medium for 4 hr in tissue culture conditions. The cells were again washed 3x in PBS, then fixed in 500 µl 4% paraformaldehyde for 20 min at room temperature. To quench residual paraformaldehyde the cells were washed 3x in PBS followed by incubation in 10 mM Tris/HCL pH 7 for 10 min at room temperature. After incubation the cells were again washed 3x in PBS then blocked in

500 µl blocking buffer (Table 2.1.8) for 20 min at room temperature. Once blocked the cell coated cover-slips were washed 3x in PBS, using tweezers the cover-slips were removed and incubated cell face down in 50 µl mouse anti-HSP70 antibody 1/100, on parafilm for 45 min at room temperature. After incubation the cover-slips were washed 3x in PBS, placed cell face up in 12 well plates and further incubated with 500 µl goat anti-mouse antibody labelled with Alexa Fluor 564 1/500 (Molecular Probes) and counterstained with nuclei stain Hoechst 1/5000 (Molecular Probes) for 30 min, in the dark, at room temperature, on a rocker. To remove unbound secondary antibody cell coated cover-slips were washed 3x in PBS followed by 1 PBS wash on the rocker for 1 min and 1 wash in dH_2O. The coverslips were mounted cell face down on coverslides in ProLong antifade (GE-Healthcare) imaged by using a Zeiss LSM 510 meta-confocal microscope.

2.2.9 *In vivo* biodistribution study

All animal work was carried out according to home office license with the help of Mr Matthew Robson (Department of Oncology) in the Comparative Biology Unit at the Royal Free Hospital.

2.2.9.1 LS174T colorectal tumour xenografts

The CEA+ve LS174T cell line was used to develop a xenograft model by subcutaneous implantation of small tumour pieces (~1mm^3) in the left flank of male nude mice and were used at 2-3months old weighing 20-25 g at the start of the experiment. Subsequent passaging was performed under halothane anaesthesia by continuous subcutaneous implantation of the original xenograft. Mice were used 3 weeks after passaging when the mean tumour volume was approx 0.5-1 cm^3.

2.2.9.2 Biodistribution of Sm3E-SPION conjugates

Biodistribution study of the functionalised SPIONs was performed into mice to determine the biodistribution of the SPIONs following systemic injection. Two hundred microlitre of Sm3E functionalised and non functionalised SPIONs were injected intravenously via tail vein in mice bearing CEA+ve LS174T tumour

xenografts. Two mice were used per time point. At 5 min, 1 hr, and 24 hr post administration, mice were sacrificed, the tumours, liver and spleen were removed and snap frozen in liquid nitrogen and stored at -80^{o}C ready for cryo-sectioning.

2.2.9.3 Prussian blue staining of frozen tissue sections

Prussian blue staining was used to stain the SPIONs in tissue section. Using Coplin jars, cryo-sectioned tissue on slides were submerged and fixed in acetone for 10 min. The slides were air dried for 1 min then rehydrated in distilled water for 1 min. To detect the iron of the SPIONs the hydrated tissues were submerged in 25 ml Prussian blue staining solution (see Table 2.10) for 30 min then washed 3x in distilled water. The slides were placed on a tray and covered in 0.1% Nuclear fast red for 5 min following this the cells were washed 3x in distilled water. Once washed the slides were dehydrated in alcohol then washed in histo-clear. Slides were mounted onto coverslips coated with a drop of DPX resin and imaged under light microscope.

.

Chapter 3

Conjugation of Anti CEA ScFvs to SPIONs

3.1 Introduction

The overall aim of the work in this thesis was to generate antibody targeted SPION conjugates for imaging and therapy. The first aim of the work described in this chapter was to develop a system to chemically conjugate recombinant scFv antibody fragments in functional form to SPIONs.

The targeting antibodies used were the anti CEA scFvs MFE-23 and Sm3E. The murine scFv MFE-23 was tested as it has been extensively characterised (Chester *et al*., 2000), the humanised high affinity version Sm3E was tested as it is thought to be more applicable for the clinic, minimising the chance of HAMA responses. The scFvs were conjugated to SPIONs via free amines presented on lysine groups. Amine coupling reactions are one of the most common conjugation methods, generally easy to perform, resulting in good conjugation yields (Haugland *et al*., 2001).

Nine different SPIONs were tested (*see section:* 2.1.5 Superparamagnetic iron oxide nanoparticles). These had different composition, size, and surface chemistry, which could influence the chemistry used for scFv functionalisation. Three conjugation chemistries were evaluated: 1) sodium periodate oxidation, 2) carbodiimide and 3) cyanogen bromide. The stability during purification and storage was investigated and immunoreactivity of the scFv-SPION conjugates to CEA was tested.

3.2 Objectives

The objectives of the research described in this chapter were to:

1. Generate anti CEA scFvs

2. Select suitable SPIONs for this study

3. Establish and optimise conjugation chemistries for SPIONs

4. Establish ELISA method to test immunoreactivity of the scFv-SPION conjugates to CEA

3.3 Results

3.3.1 Generation of anti CEA scFv

3.3.2.1 MFE-23

MFE-23 was kindly donated by Dr Berend Tolner (Cancer Institute UCL) and had been generated using the *Pichia pastoris* expression system. SDS-PAGE/Coomassie and ELISA confirms purity, size and immunoreactivity of MFE-23 (Fig. 3.1).

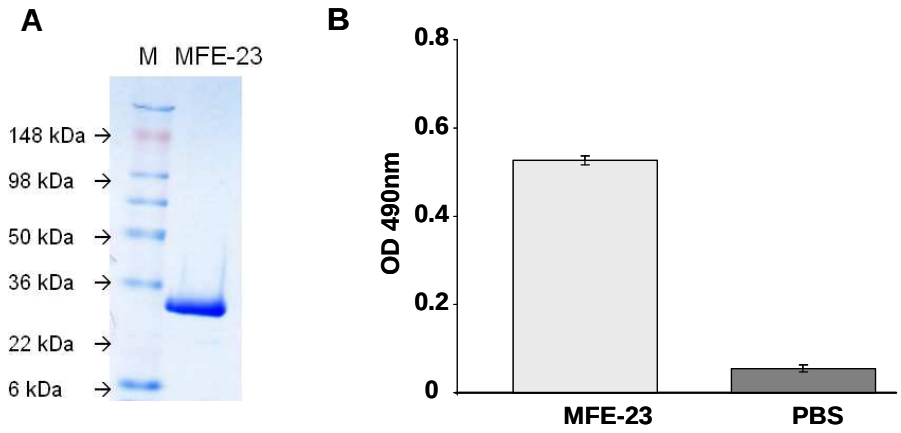

Fig. 3.1. Pooled MFE-23 was tested for purity and CEA binding. A) Coomassie stained 12% Tris glycine SDS-PAGE gel, shows purity of MFE-23. Lane M contains the molecular weight marker. B) CEA ELISA of MFE-23. Detection of binding was performed with a mouse anti-His primary antibody, followed by a sheep anti-mouse HRP. PBS was used as a negative control.

3.3.1.2 Sm3E

Sm3E was expressed and purified from the yeast *Pichia pastoris* in a 10 litre fermenter *(see section:* 2.2.1 Protein expression and 2.2.2 Protein purification). Following EBA-IMAC purification, SDS-PAGE/coomassie gel analysis shows the majority of Sm3E to elute in the 200 mM imidazole fractions 10-15 (Fig. 3.2). Fractions 10-15 were pooled to give a 300 ml Sm3E protein fraction. From absorbance readings at 280 nm the concentration of Sm3E at this point was estimated to be 0.7 mg/ml.

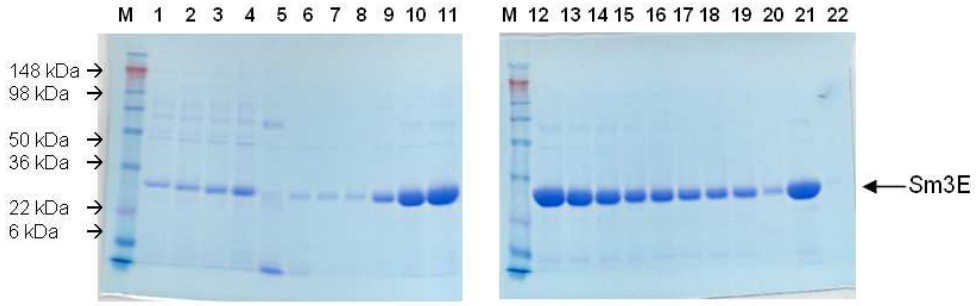

Fig. 3.2. Coomassie stained 12% Tris/glycine gel containing fractions from EBA-IMAC purification of Sm3E. Lane M contains the molecular weight marker. Fractions taken at each purification are shown: lane 1-4, product present in bioreactor at elapsed fermentation times (EFT) of 46, 50, 54 and 72 hrs; lane 5 and 6, wash steps with 40 mM imidazole; lanes 7-20, successive 200 mM imidazole elution fractions; lane 21, pooled fractions 10-15; lane 22, EDTA fraction. There is very little Sm3E in the 40 mM wash and EDTA wash, most of the scFv is in the 200 mM fractions.

Further purification of the Sm3E scFv by SEC using Superdex 75 matrix revealed two peaks (Fig. 3.3). Western blot results (Fig. 3.4) showed the proteins in both peaks to be reactive to the mouse anti His mAb. This result indicates Sm3E is eluted in both peaks. From reference to MW standards used as calibrants on the Superdex 75 column, Sm3E is presumably in dimer and monomer form. From the amino acid sequence of Sm3E-His, the MW of Sm3E is 27 kDa. Therefore, the Sm3E fractions eluted in the 2nd peak, close to the 27 kDa mark, were pooled and assumed to be the monomeric form of the protein. SDS/PAGE/coomassie gels shows the fractions to be pure, giving a single band of approx 27 kDa (Fig. 3.4). From absorbance readings at 280 nm the concentration of the Sm3E was estimated to be 0.3 mg/ml. ELISA of the pooled Sm3E fractions confirms its immunoreactivity to CEA (Fig. 3.5).

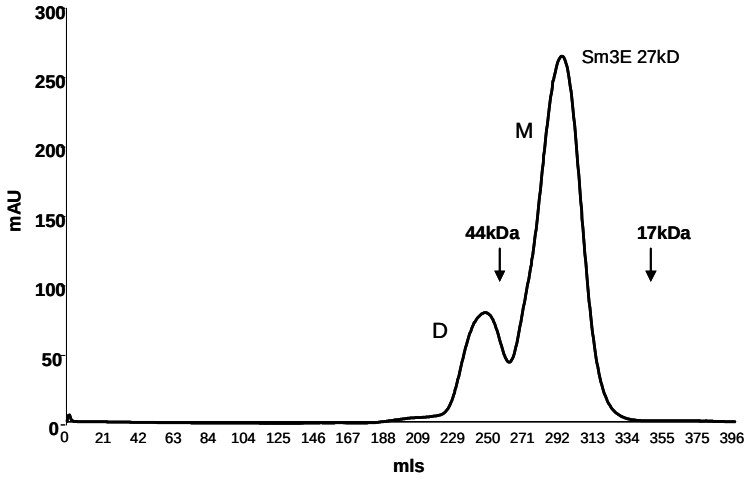

Fig. 3.3 Size exclusion chromatography of *P.pastoris* expressed Sm3E. 25 ml of Sm3E purified from streamline was applied to the 500 ml Superdex 75 column at flow rate 4 ml/min in PBS buffer. Two peaks corresponding to monomeric (M) and dimeric (D) are present with the majority of Sm3E being in the monomeric form. The elution volumes of MW standards are shown.

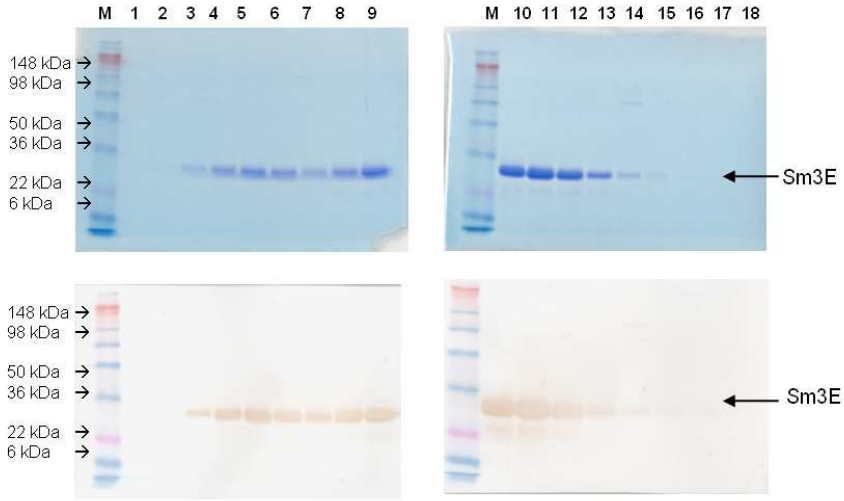

Fig. 3.4. SDS-PAGE of SEC purified Sm3E. Coomassie stained 12% Tris glycine SDS-PAGE gels and Western blot containing fractions from SEC purification. Lane M contains the MW marker. Fractions taken across the 2 elution peaks are shown: lane 1-18 contain fractions 8, 10, 12, 14, 16, 18, 20, 22, 24, 26, 28, 30, 32, 34, 36, 38, 40 and 42. Fraction 14-30 contained majority of monomeric Sm3E and were pooled. The blots were developed with a mouse anti-His mAb as a primary antibody, followed by sheep anti-mouse mAb HRP.

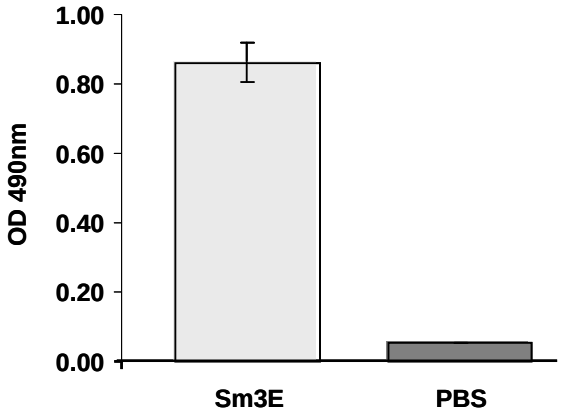

Fig. 3.5 CEA binding analysis of purified *P. pastoris* expressed Sm3E. Pooled Sm3E fraction was tested for binding to CEA by ELISA. Detection of binding was performed with a mouse anti-His as primary antibody, followed by sheep anti-mouse HRP. PBS was used as a negative control.

3.3.2 SPION stability

The stability and solubility of the SPIONs in physiological buffers are important parameters for handling and purification when developing scFv-SPION conjugates. Therefore, the stability and solubility of the SPIONs after three commonly used purification methods, centrifugation, magnetic separation and size exclusion chromatography were assessed prior to attachment experiments. Briefly, SPIONs at 1mg/ml were either centrifuged at 13000 RPM for 30 min, placed on a high field magnet overnight or applied to SEC column. Application to the SEC column was either by gravity, in the case of Sephadex –G25 or by peristaltic pump at a flow rate of 1 ml/min for the Sephacryl 300HR. The solubility of the SPIONs following resuspension or elution was assessed visually.

Results showed that, the d100, d50, PEG-d50, PEG-d20 and CMX50 remained in solution following centrifugation and magnetic separation. In comparison, the DX200, DX100, CMX200 and CMX100 were successfully separated from solution by centrifugal and magnetic force (Fig. 3.6). However, only DX200, DX100, CMX200 and CMX100 SPIONs that were separated out by magnetic force could be resuspended. The SPIONs separated out by centrifugation remained insoluble.

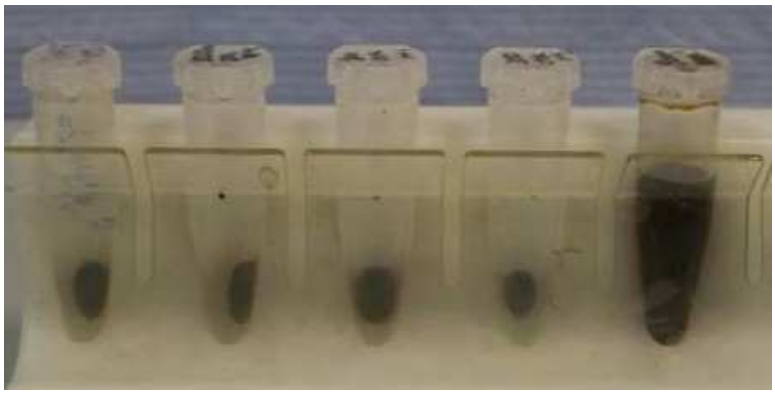

Fig. 3.6. Magnetic separation of SPIONs. From left to right, DX200, DX100, CMX200, CMX100 and CMX50. All SPIONs were successfully pulled out of solution, except the CMX50.

Purification of the SPIONs by size exclusion chromatography (SEC) was investigated with two matrixes, the Sephadex-G25 and the Sephacryl 300HR.

All the SPIONs tested (d50, d100, PEG-d50, PEG-d20, DX100, DX200, CMX50, CMX100, CMX200) moved freely through the Sephadex G-25 and remained soluble after elution. However, due to the low molecular weight filtration threshold (<5kDa) of Sephadex G-25, the matrix appeared to be unsuitable for separating unbound scFvs (27kDa) from the scFv-SPION conjugate solution, as both the unbound scFv and conjugate would appear in the void volume. The Sephacryl 300HR matrix with a filtration threshold of $1.5x10^3$kDa is more appropriate for separation of unbound scFvs from the scFv-SPION conjugates.

Size exclusion chromatography using the Sephacryl 300HR matrix was successful for the d50 (Fig. 3.7), d100, PEG-d20, PEG-d50 and the DX100 (Fig. 3.8). However, the CMX50 appeared to interact with the column as observed by the late elution and retention of the SPIONs on the column. From the elution profile the CMX50 can therefore, not be separated from unbound scFv. Similar results were also found with all other CMX-SPIONs.

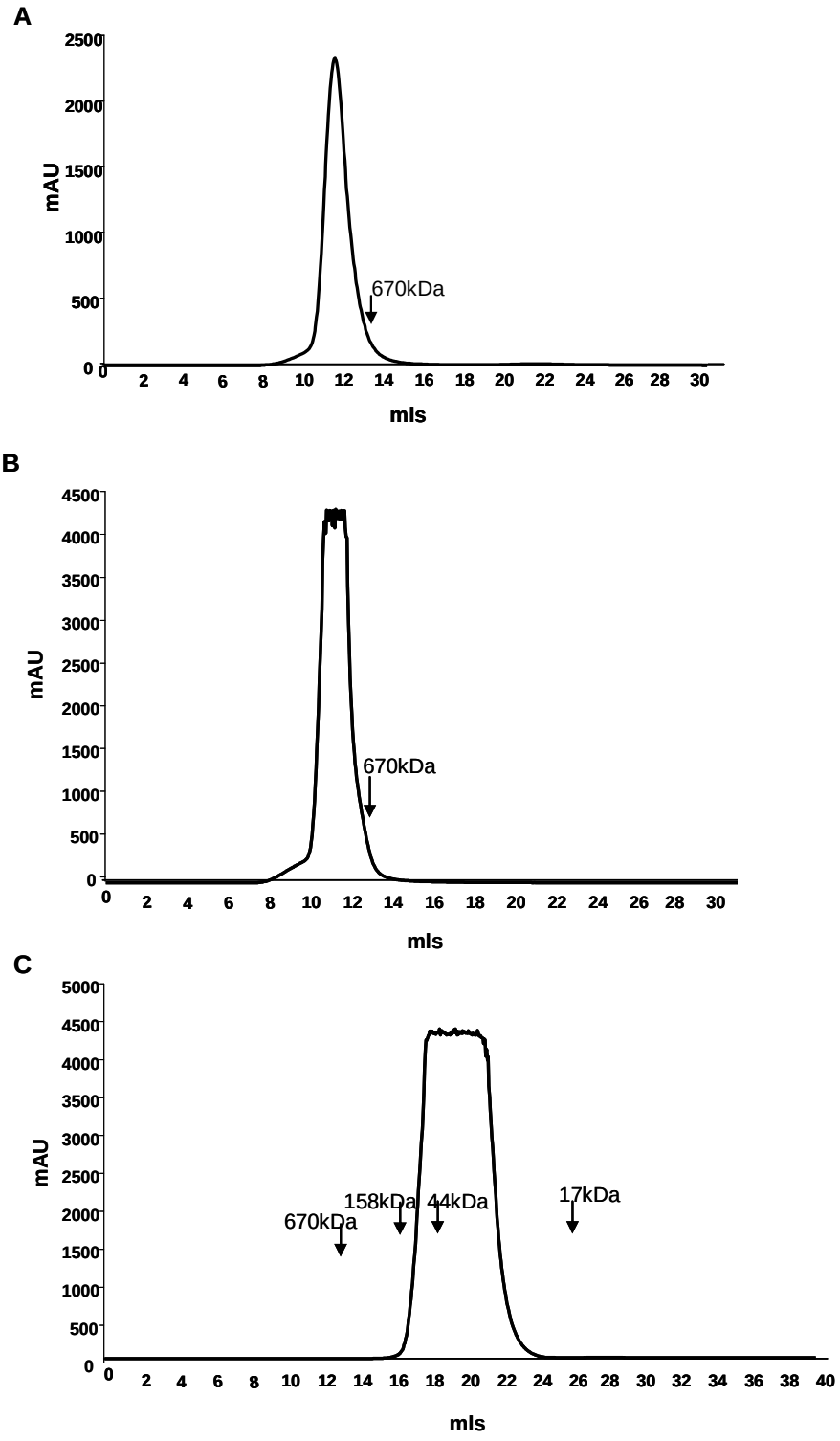

Fig. 3.7 Size exclusion chromatography profile of A) d50, B) DX100 and C) CMX50. 2 ml of 1 mg/ml sample was loaded onto a Sephacryl 300HR 30 ml column at flow rate 1 ml/min in PBS elution buffer. Profile shows the d50 and DX100 to elute off in the void volume, whereas the CMX50 eluted late off the column.

From these results, all the SPIONs except the CMX50 were taken forward to the next stage of scFv functionalisation. See Table 3.1 for summary of results.

Table 3.1. Summary of successful purification procedures and SPIONs taken forward for scFv functionalisation. SPION shaded in red was not taken forward for further investigation.

SPIONs	Successful separation procedures	SPIONs taken Forward
d50	Sephadex G-25 SEC Sephacryl 300HR SEC	YES
d100	Sephadex G-25 SEC Sephacryl 300HR SEC	YES
PEG-d20	Sephadex G-25 SEC Sephacryl 300HR SEC	YES
PEG-d50	Sephadex G-25 SEC Sephacryl 300HR SEC	YES
DX200	Sephadex G-25 SEC Magnetic separation	YES
DX100	Sephadex G-25 SEC Sephacryl 300HR SEC Magnetic separation	YES
CMX200	Sephadex G-25 SEC Magnetic separation	YES
CMX100	Sephadex G-25 SEC Magnetic separation	YES
CMX50	Sephadex G-25 SEC	NO

3.3.3 SPION iron content

For comparability and consistency the SPION concentration (iron oxide plus coating) and the iron oxide, content for all the SPIONs was measured. The SPION (iron oxide plus coating) concentration was measured at an absorbance reading of 490nm and the iron oxide content of the SPIONs was measured using the ferrozine assay (*see section*: 2.2.5.2). Results found the PEG-dSPIONs contained approximately 40% iron oxide (Fig. 3.8), indicating the other 60% to be the dextran-PEG coating. In comparison, the dSPIONs at the same SPION concentration contained approximately 14% iron oxide, under half the amount of iron compared to the PEG-dSPIONs (Fig. 3.8). The concentration of the PEG-dSPIONs and dSPIONs was further analysed by spectrophotometric absorbance readings at 490 nm. Results revealed the PEG-dSPIONs to be twice as concentrated as the dSPIONs (Fig. 3.9). These results therefore, suggest that the dSPIONs were supplied at the same concentration as the PEG-dSPIONs, 5 mg/ml instead of the stated 10 mg/ml. For comparability, the dSPION concentration was assumed to be 5 mg/ml.

Ferrozine assay analysis showed the DX-SPIONs to consist of 60% iron oxide (Fig. 3.10), suggesting the other 40% to be dextran.

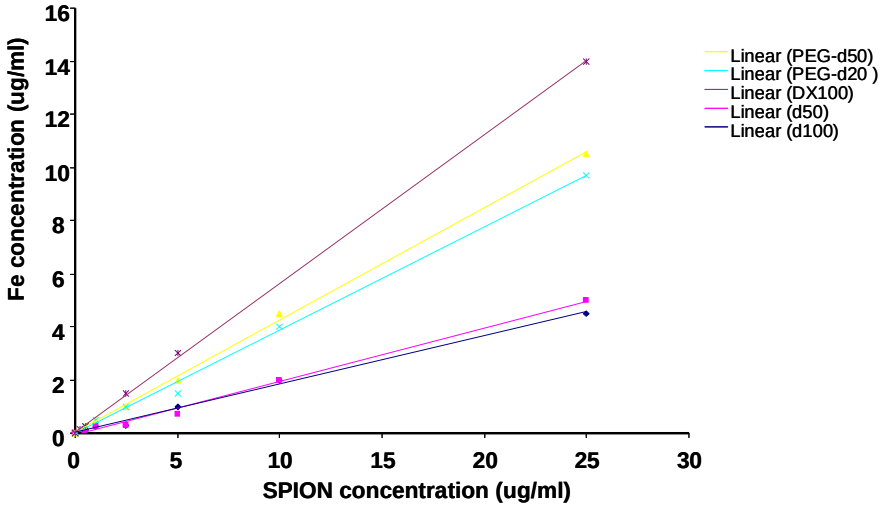

Fig. 3.8. Iron concentration of serial diluted SPIONs as measured by the ferrozine based iron assay. Detection of Fe^{2+} was performed at absorbance of 550 nm. Values were compared against a calibration curve of $FeCl_3$ standards.

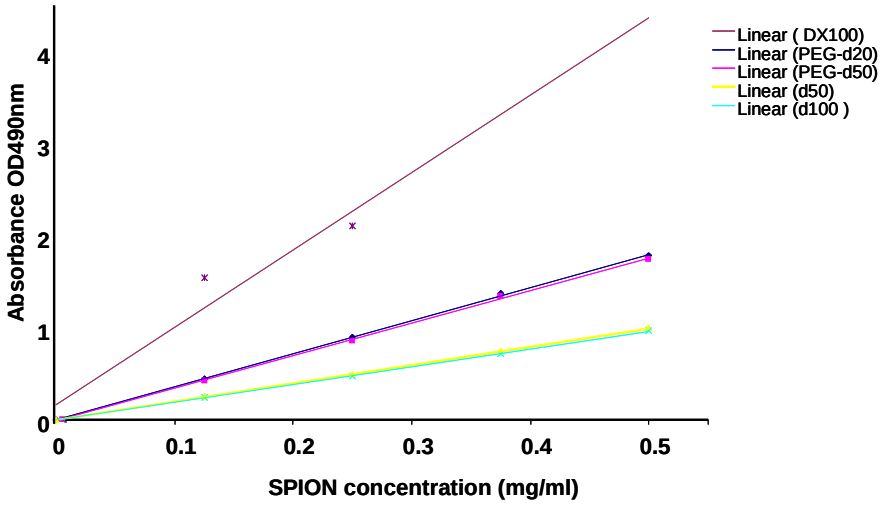

Fig. 3.9. Absorbance readings at 490 nm of serial diluted SPIONs. Absorbance values were used as reference to determine the concentration of the SPIONs in the conjugate solution.

3.3.4 Sodium periodate conjugation of MFE-23 to SPIONs

The feasibility of successfully conjugating scFvs to SPIONs was first investigated using the MFE-23 scFv and the d50 SPION.

The sodium periodate oxidation chemistry, schematically represented in Fig. 3.10 and detailed in section 2.2.4.1 was used to conjugate MFE-23 to the d50. This chemistry was chosen due to the available hydroxyl groups on the d50's dextran coat.

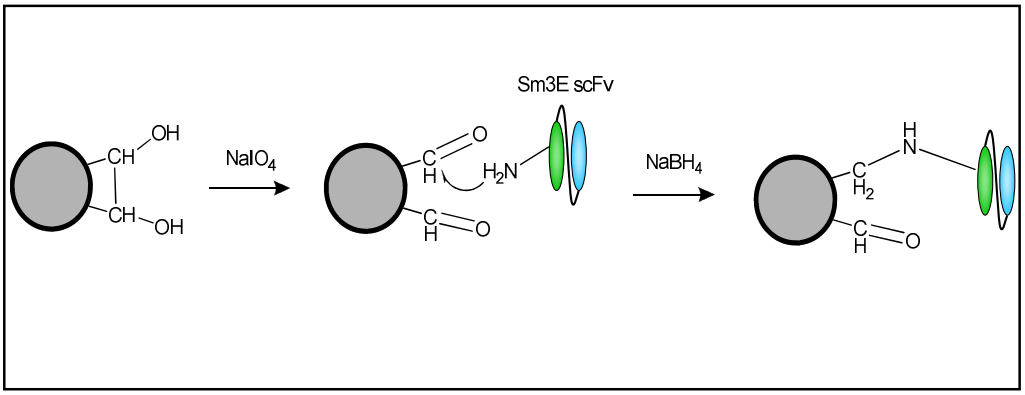

Fig. 3.10. Schematic representation of sodium periodate conjugation chemistry. The available OH groups on the dextran coat are oxidised by sodium periodate creating reactive aldehyde functions, which react with free amine groups on lysines or unblocked N-terminus found in the protein structure of MFE-23. The bond is reduced with sodium borohydride to create a stable covalent bond.

To establish the chemistry, 5 mg/ml of oxidised d50 was incubated with 0.5 mg/ml MFE-23 for 3 hrs. Isolation of MFE-23-d50 conjugates from unbound MFE-23 was performed by SEC using the Sephadex-G25 and Sephacryl 300HR matrix. The elution profile from the Sephacryl 300HR purification (Fig. 3.11) shows two peaks one in the void volume and the other at 27 kDa. The first peak was assumed to be the SPIONs, as the eluate was brown in colour. Fractions were collected and analysed by ELISA (Fig. 3.12) and Western blot (Fig. 3.13) using mouse anti His mAb. Results revealed both peaks to contain MFE-23. This result indicates that the MFE-23 eluted in the first peak was bound to the d50 SPIONs and the protein in the 2nd peak was free MFE-23. This is further supported by the fact the 2nd peak is in the area MFE-23 would elute. These results therefore, demonstrate the feasibility of conjugating MFE-23 to the dextran coated SPIONs via amine conjugation, whilst retaining its immunoreactivity to CEA (Fig. 3.13).

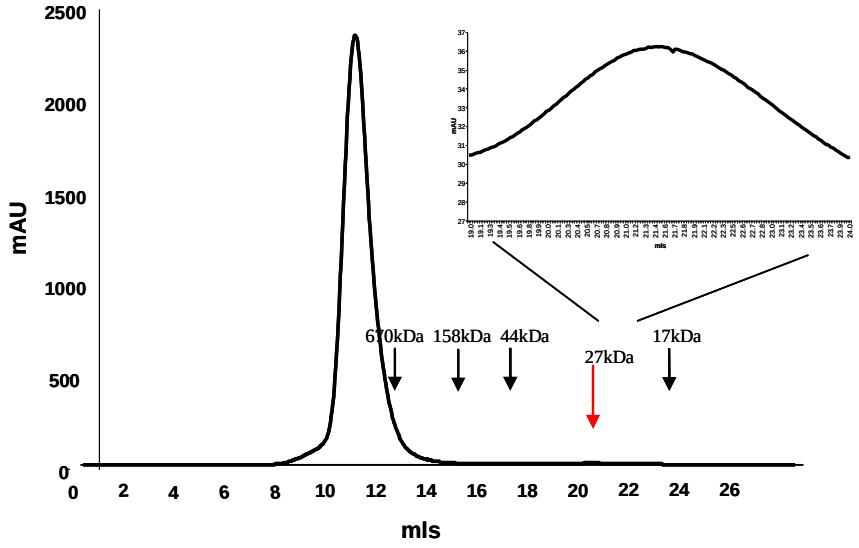

Fig. 3.11. Size exclusion chromatography of MFE-23-d50 at concentration 0.5 mg: 5 mg. 2 ml of the conjugated MFE-d50 were applied to Sephacryl 300HR 30 ml column at flow rate 1 ml/min in PBS elution buffer. The first peak is in the void volume corresponding to the d50. A small peak is seen where unbound MFE-23 has eluted. The elution volumes of MW standards are show.

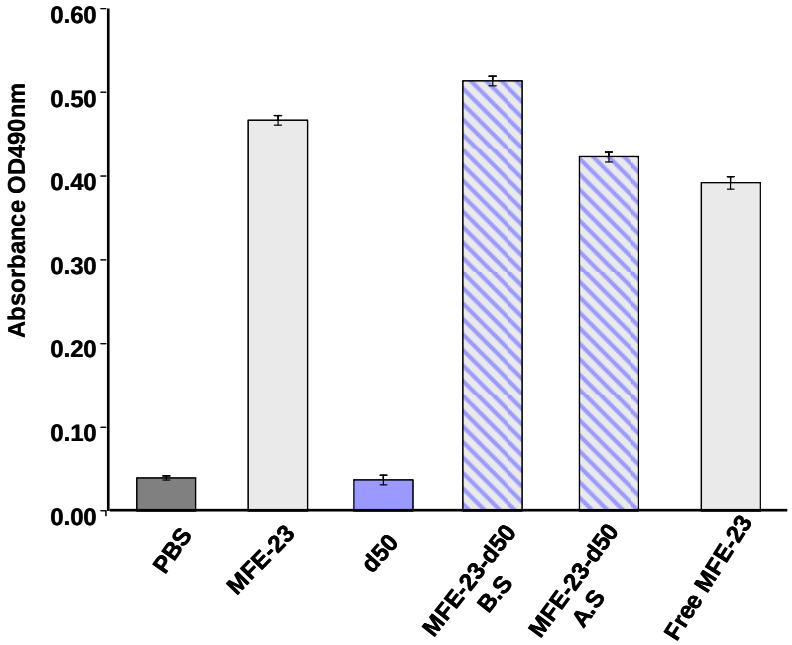

Fig. 3.12. CEA protein ELISA of SEC purified MFE-23-d50. Detection of binding was performed with a mouse anti His primary antibody, followed by a sheep anti mouse HRP. MFE-23 was used as positive control and un-conjugate dSPION and PBS as negative controls. Symbols used: B.S: before separation by SEC; A.S: after separation by SEC.

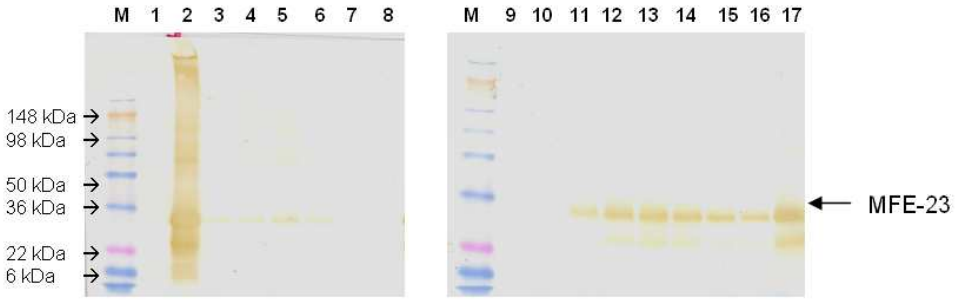

Fig. 3.13. SDS-PAGE of MFE-23-d50 before and after SEC purification. Western blot transferred from 12% Tris glycine SDS-PAGE gel containing fractions from SEC purification. Lane M contains the MW marker. Lane 1: non-functionalised d50, lane 2: MFE-23 functionalised d50 before separation, lane 3-7: Peak fractions at 11-14 mls from SEC elution profile of MFE-23-d50, lanes 8-10: SEC fractions taken at 15-18 mls and lanes 11-16: SEC fractions taken at 19-24 mls showing presence unbound MFE-23. Lane 17: MFE-23 control. The Western blots were developed with a mouse anti-His mAb as a primary antibody, followed by sheep anti-mouse mAb HRP.

3.3.5 Optimisation of MFE-23-SPION conjugation

Results from the MFE-23-d50 conjugation showed that a substantial amount of MFE-23 remained unattached to the SPIONs. Optimisation of the sodium periodate procedure to reduce the amount of unbound MFE-23 was performed. The excess of unbound MFE-23 maybe due to the reactive sites of the d50 being exhausted. It was postulated this could be improved by increasing the number of reactive sites by further oxidation with sodium periodate. However, following incubation with sodium periodate at a concentration of 20 mM the d50 precipitated.

Since it was not possible to increase the number of reactive sites an alternative approach was taken to reduce the loss of MFE-23. The ratio of MFE-23 to d50 was reduced from 0.5 mg: 5 mg to 0.1 mg: 5 mg. Following purification by SEC on the Sephacryl 300HR the elution profile revealed 1 peak in the void volume (Fig. 3.14). The fraction eluted at this peak was brown in colour therefore, was assumed the d50. The fraction was analysed by Western blot using mouse anti His mAb (Fig. 3.15). Results revealed the fraction to contain MFE-23, indicating MFE-23 was attached to

the d50. No peak was seen at the point where unbound MFE-23 would elute, suggesting majority of the MFE-23 to have bound to the d50. However, a small amount of unbound MFE-23 was detected by Western blot (Fig. 3.15).

To test whether increasing the incubation time would further improve the scFv:SPION binding ratio the time for conjugation was increased from 3 hrs to 24 hrs. Following purification, the MFE-23-d50 (24 hr) fractions were analysed in parallel with MFE-23-d50 (3 hr) by CEA ELISA using mouse anti His mAb (Fig. 3.16). The results show the MFE-23-d50 (24 hr) to have a small but significant ($p<0.001$) increase in binding on the ELISA assay compared to the MFE-23-d50 (3 hrs), suggesting 24hr incubation time and a scFv to d50 ratio of 1:50 to be more favourable.

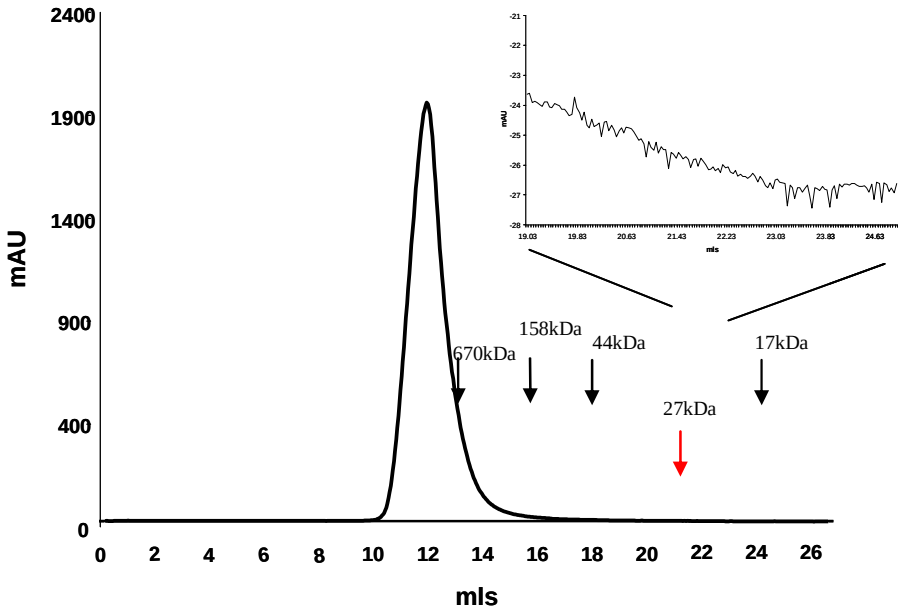

Fig. 3.14. Size exclusion chromatography profile of MFE-23-d50 (0.1 mg: 5 mg), after 3 hr incubation. 2 ml of the conjugated MFE-23-d50 was applied to Sephacryl 300HR 30 ml column at flow rate 1 ml/min in PBS elution buffer. The peak in the void volume corresponds to MFE-23-d50. No peak is seen where unbound MFE-23 should elute. The elution volumes of MW standards are shown.

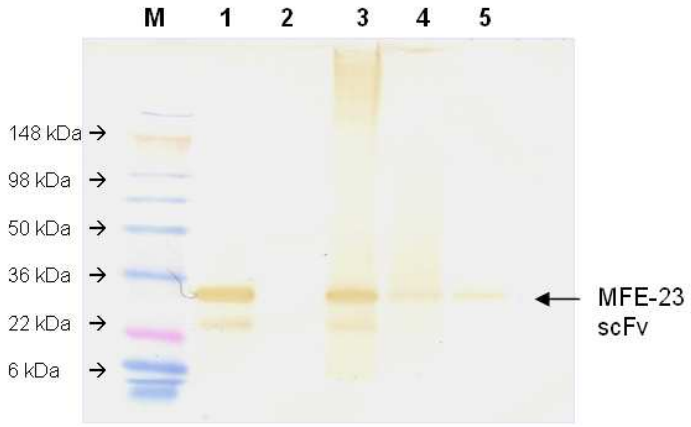

Fig. 3.15. Western Blot analysis of MFE-23-d50 (0.1 mg: 5 mg) after incubation for 3hrs. Western blot transferred from 12% Tris glycine SDS-PAGE gel containing fractions from SEC purification. Lane M contains the MW marker. Lane 1: MFE-23 control, lane 2: Non-functionalised d50, lane 3: MFE-23-d50 before separation, lane 4: MFE-23-d50 pooled SEC fractions and lane 5: unbound MFE-23 pooled SEC fractions. The Western blots were developed with a mouse anti-His mAb primary antibody, followed a sheep anti-mouse mAb HRP.

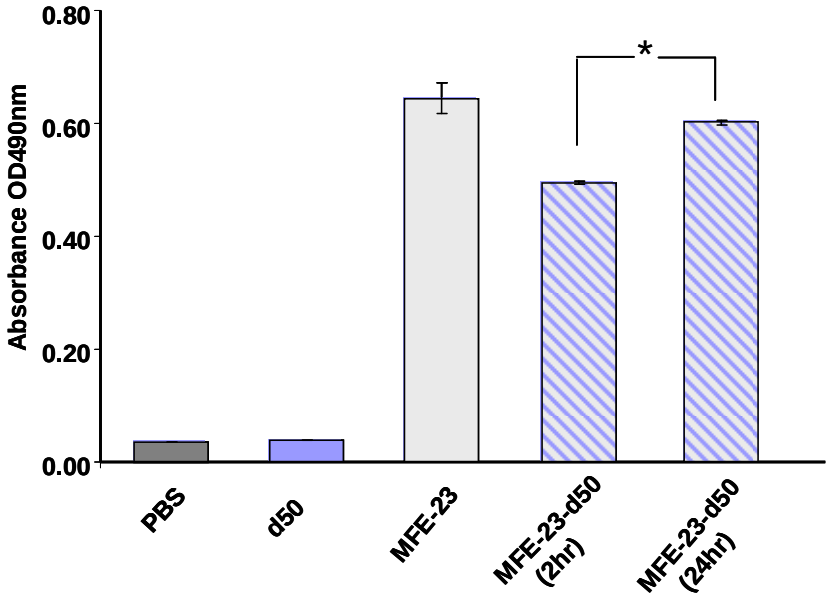

Fig. 3.16. CEA ELISA of the MFE-23-d50 conjugate after SEC purification. Detection of binding was performed with a mouse anti-His primary antibody, followed by a sheep anti-mouse HRP. MFE-23 was used as a positive control and non-functionalised d50 and PBS were used as negative controls * p= <0.001 by T-test analysis.

These results show that for minimal loss of MFE-23 the optimal ratio scFv to d50 is 0.1 mg: 5 mg. To allow for maximal binding of the scFvs to d50 an incubation time of 24 hrs at room temperature was favourable. Therefore, a ratio 1:50 for scFv to SPION and a 24 hr incubation time was used for all subsequent conjugations.

3.3.6. Application of optimised conjugation chemistry to the Sm3E scFv

The feasibility of conjugating Sm3E to the DX100, DX200, d100 and d50 using the optimised sodium periodate conjugation chemistry was also tested. Results are shown below.

3.3.6.1 DX-SPIONs

Oxidation of both the DX100 and DX200 by 10 mM sodium periodate caused the SPIONs to become unstable and precipitate. Even upon reducing the concentration of sodium periodate to 5 mM, destabilisation of the DX-SPIONs was still visually evident. The DX-SPIONs therefore, were unable to be conjugated to the Sm3E scFv via the sodium periodate conjugation chemistry.

3.3.6.2 dSPIONs

The d100 and d50 remained soluble throughout the sodium periodate conjugation procedure. The SEC elution profile showed that both the Sm3E-d100 and Sm3E-d50 eluted in the void volume and that no peak indicative of unbound Sm3E was detected (Fig. 3.17). The SPION elution fraction was analysed by ELISA using anti His mAb and anti dextran mAb (Fig. 3.18). Results confirmed the eluate to contain immuno-reactive Sm3E, assumed to be bound to the dSPIONs. ELISA results also show no detectable binding of non-functionalised SPIONs to CEA. These results indicate that binding of both the Sm3E-d100 and Sm3E-d50 to CEA was via the conjugated Sm3E.

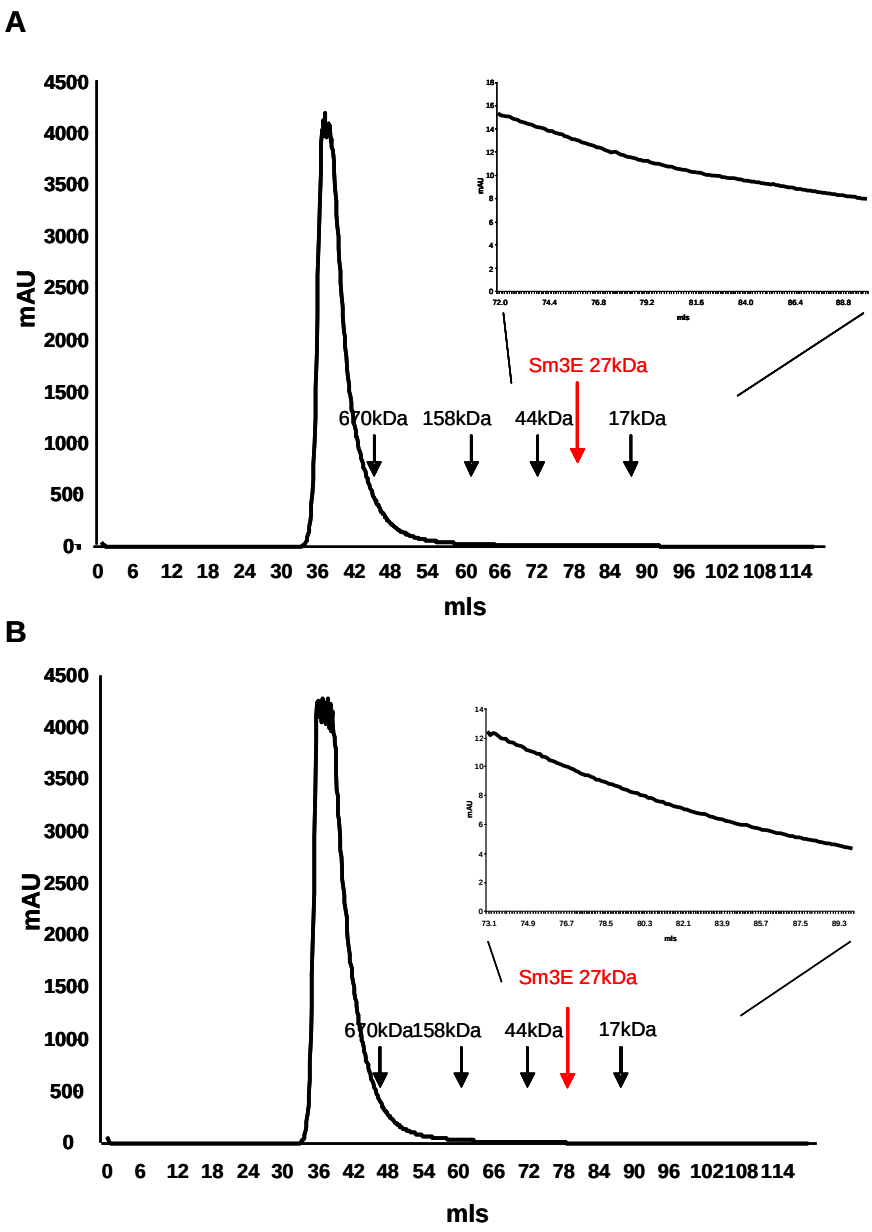

Fig. 3.17 Size exclusion chromatography of A) Sm3E-d100 and B) Sm3E-d50. 2 ml of the Sm3E-dSPION conjugate solution was applied to the Sephacryl 300HR column at a flow rate 1 ml/min in PBS elution buffer. The peak in the void volume corresponds to the Sm3E-dSPIONs, no peak is seen where unbound Sm3E should elute. The elution volumes of molecular weight standards are shown.

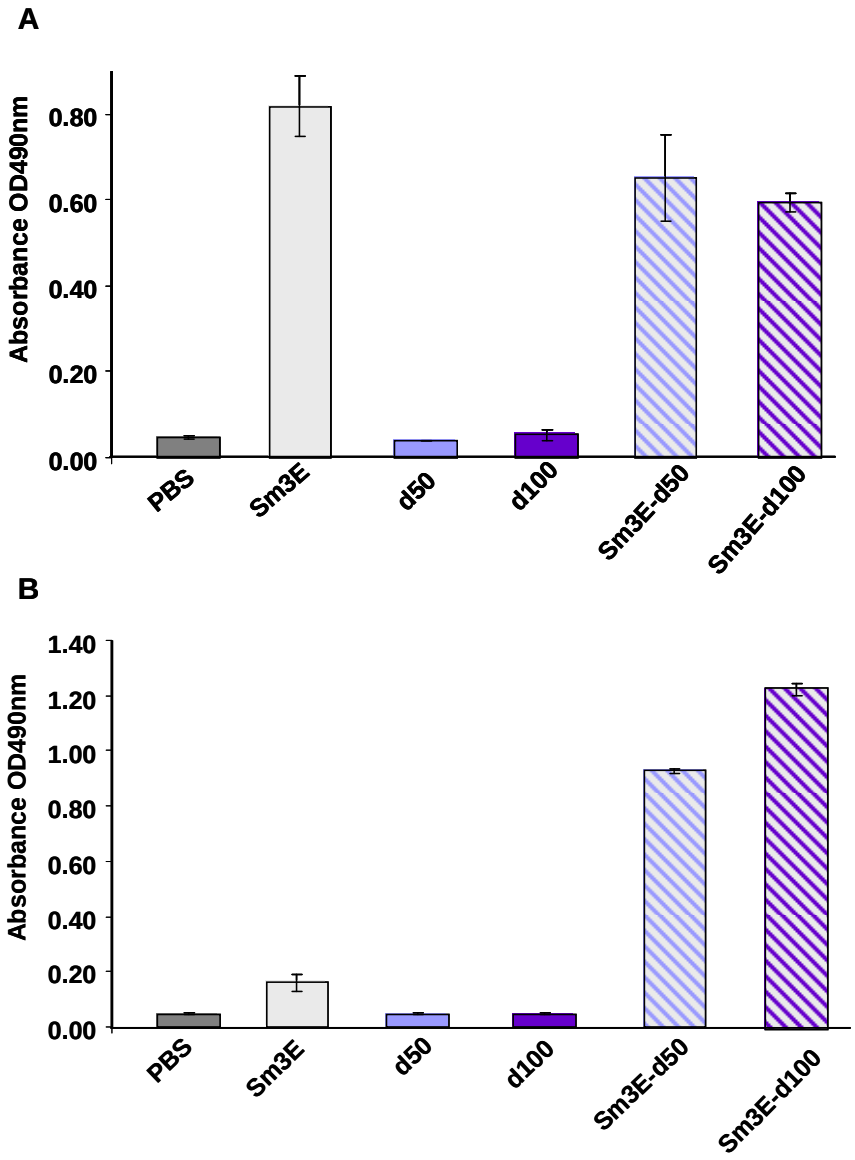

Fig. 3.18. The Sm3E-d100 and Sm3E-d50 conjugates after SEC purification were tested for binding to CEA by ELISA. ELISA A) detected with a mouse anti-His primary antibody, followed by a sheep anti-mouse HRP. Positive control was Sm3E, negative controls were non-functionalised d100 and d50 and PBS. ELISA B) detected with a mouse anti-dextran primary antibody, followed by a sheep anti-mouse HRP. Negative controls were Sm3E, non-functionalised d100 and d50 and PBS.

To further confirm and quantify the attachment of Sm3E to the d100 and d50 SPIONs, the conjugate solutions were analysed by Bradford protein assay and spectrophotometric readings, results were calculated using equation 2.2-2.5 (*see section*: 2.2.5 scFv-SPION conjugation analysis). Results showed approximately 120 and 28 Sm3E scFvs to bind per d100 and d50 (Table 3.2).

One limitation with SEC is the dilution of the eluted fractions. To increase the concentration of the conjugate solutions centrifugation using the Vivaspin 15R concentration tubes was tested. The Sm3E-dSPION solution concentrated successfully, minimal destabilisation was observed and loss was negligible as measured by absorbance at 490nm.

3.3.7 Cyanogen bromide conjugation of Sm3E to DX-SPIONs

The cyanogen bromide (CNBr) conjugation chemistry represented schematically in Fig. 3.19 and detailed in section 2.2.4.3 was investigated as an alternative method for conjugation of the DX100 and DX200 to Sm3E.

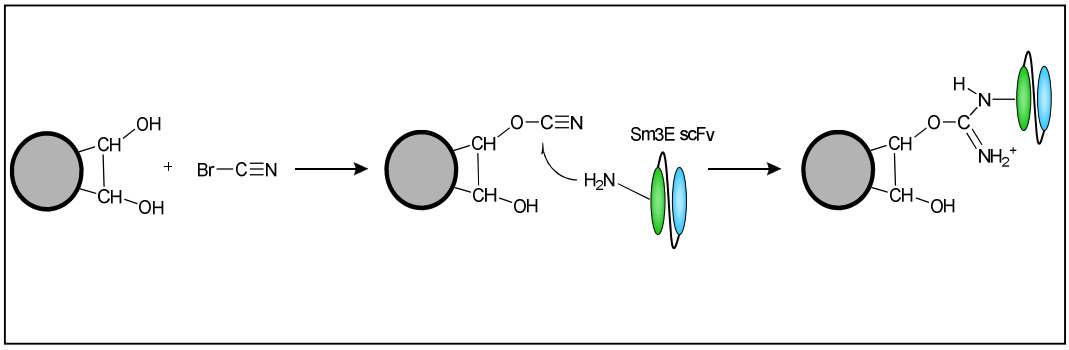

Fig. 3.19. Schematic representation of the cyanogen bromide conjugation chemistry. The available OH groups on the dextran coat are activated by cyanogen bromide, forming cyanate ester groups which react with free amine groups on lysines or unblocked N-terminus found in the protein structure of Sm3E.

Incubation of the DX-SPIONs with CNBr causes activation of the hydroxyl groups on the dextran coat, allowing it to react with free amine groups on Sm3E. SEC using the Sephadex-G25 was used to purify the activated DX-SPIONs from CNBr. Following elution from the Sephadex-G25 column, the DX-SPIONs were found to remain in solution. Isolation of the Sm3E-DX-SPION conjugates was performed by several magnetic washes. Following conjugation to Sm3E, the Sm3E-DX200 became unstable and precipitated. In contrast, the Sm3E-DX100 remained stable upon subjection to this procedure (Fig. 3.20). For this reason, the DX200 was not taken forward for further investigation.

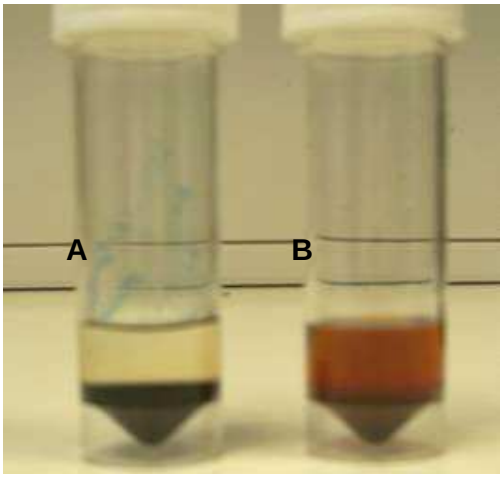

Fig. 3.20. Stability of the Sm3E-DX100 and Sm3E-DX200 following conjugation. A) Sm3E-DX200 showed complete precipitation, B) Sm3E-DX100, the majority remains soluble in PBS.

The supernatant from the magnetic washes and the resuspended Sm3E-DX100 conjugates were analysed by CEA ELISA using anti His mAb and anti dextran mAb (Fig. 3.21). Results showed the Sm3E-DX100 to react with CEA, confirming the presence of immuno-reactive Sm3E. Only a minimal amount of unbound Sm3E was present in the magnetic washes, indicating the majority of the Sm3E to be chemically coupled to the DX100.

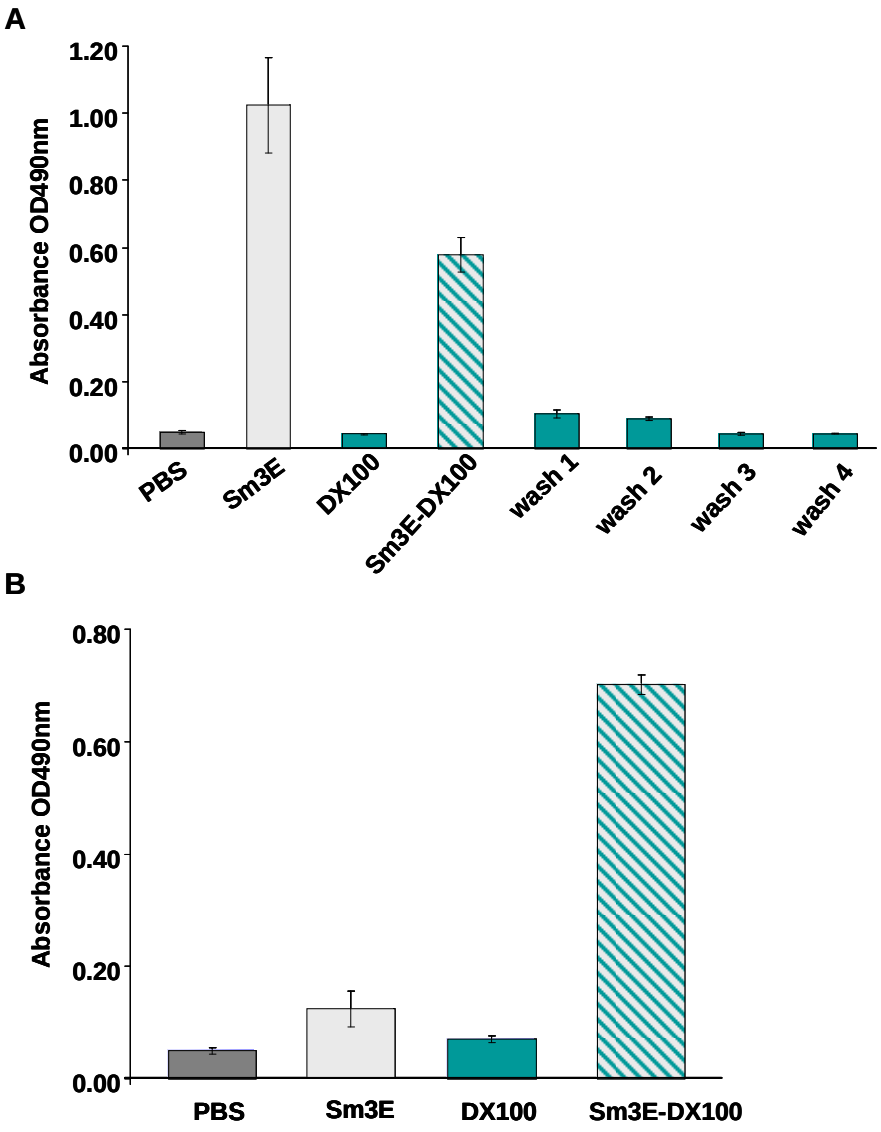

Fig. 3.21. CEA ELISA of the Sm3E-DX100 conjugate ELISA A) also contains magnetic washes 1-4. Binding was detected with a mouse anti-His primary antibody, followed by a sheep anti-mouse HRP. Sm3E was used as positive control, non-functionalised DX100 and PBS were used as negative controls. ELISA B) binding was detected with a mouse anti-dextran primary antibody, followed by a sheep anti-mouse HRP. Negative controls used were Sm3E, non-functionalised DX100 and PBS.

To quantify the attachment of Sm3E to the DX100, the conjugate solutions were analysed by Bradford protein assay and spectrophotometric readings. Results however, were inconclusive because the colour change of the sample due to the Bradford reagents, appeared to be minimal relative to the colour of the actual SPION solution.

3.3.8 Carbodiimide conjugation of Sm3E scFv to SPIONs

Unlike the dSPIONs and DX-SPIONs, which present OH terminal groups the PEG-dSPIONs and CMX-SPIONs present terminal COOH groups. To facilitate the conjugation of Sm3E to the COOH groups presented by the SPIONs the carbodiiminde conjugation chemistry, schematically presented in Fig. 3.22 and detailed in section 2.2.4.2, was investigated.

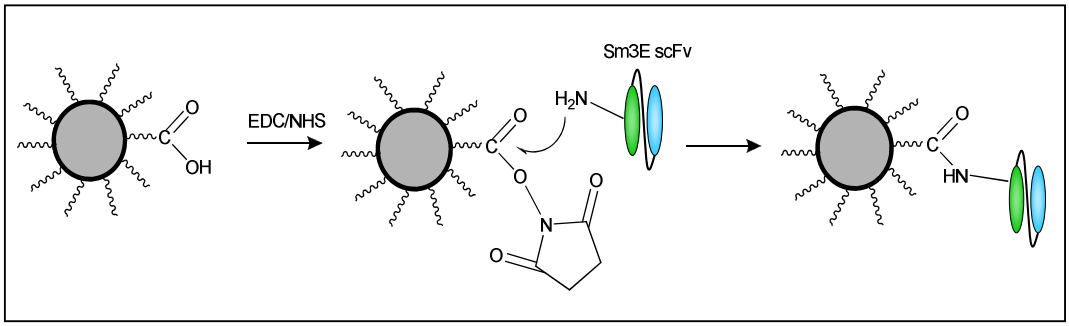

Fig. 3.22. Schematic representation of the carbodiimide conjugation chemistry. The available COOH groups on the PEG and carboxymethylated dextran coat are activated by EDC/NHS to form an ester group which reacts with free amine groups on lysines or unblocked N-terminus found within the protein structure of Sm3E.

3.3.8.1 CMX-SPIONs

Purification of the EDC/NHS activated CMX-SPIONs was achieved by SEC using the Sephadex-G25. Following elution, the CMX-SPIONs were found to remain soluble in solution. Isolation of the Sm3E-CMX-SPION conjugates was performed by several magnetic washes. However, throughout the magnetic washes both the Sm3E-CMX100 and Sm3E-CMX200 precipitated. Due to insolubility, the CMX100 and CMX200 SPIONs were not taken forward for further investigation.

3.3.8.2 PEG-dSPIONs

Isolation of Sm3E-PEG-dSPION conjugates from unbound Sm3E was performed by SEC using the Sephadex-G25 and Sephacryl 300HR matrix. The elution profile from the Sephacryl 300HR purification shows Sm3E-PEG-d20 and Sm3E-PEG-d50 to elute off cleanly in the void volume, no free Sm3E was evident from the SEC profile (Fig. 3.23). The SPION elution fraction was analysed by ELISA using anti His mAb and anti dextran mAb (Fig 3.24). From the results the eluted fractions react with CEA confirming, Sm3E has been successful coupled to both the PEG-d20 and PEG-d50 SPIONs and retained its immunoreactivity to CEA.

To determine whether the incubation time of the activated PEG-dSPIONs with Sm3E affects the number of scFv binding to the PEG-dSPION, incubation times of 3 hrs and 24 hrs were compared. Quantification of the number of Sm3E scFvs bound to the PEG-d20, PEG-d50, following incubation for 3 hrs and 24 hrs, was determined by Bradford protein assay, and spectrophotometric readings and calculated using equation 2.2-2.5. Results showed, after 3 hr incubation approx 0.5 and 10 Sm3E scFvs had bound per PEG-d20 and PEG-d50. However, by increasing the incubation time to 24 hrs approx 2 and 29 Sm3E scFvs bound per PEG-d20 and PEG-d50 (Table 3.2).

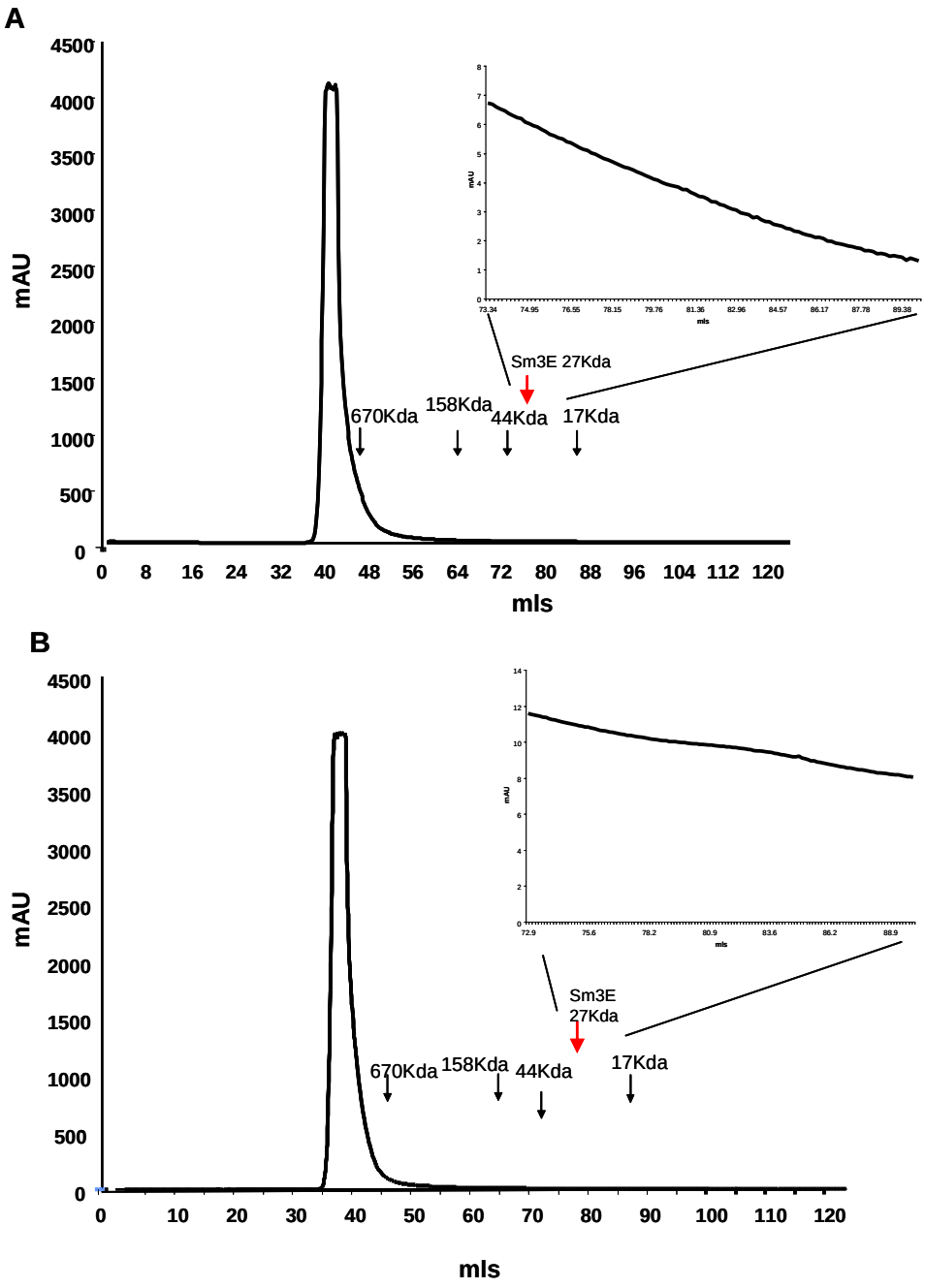

Fig. 3.23 Size exclusion chromatography purification of A) Sm3E-PEG-d20 and B) Sm3E-PEG-d50. 2 ml of the Sm3E-PEG-dSPION conjugates were applied to Sephacryl 300HR column at flow rate 1 ml/min in PBS elution buffer. The peak in the void volume corresponds to the Sm3E-PEG-dSPION conjugates. No peak is seen where unbound Sm3E should elute. The elution volumes of MW standards are shown.

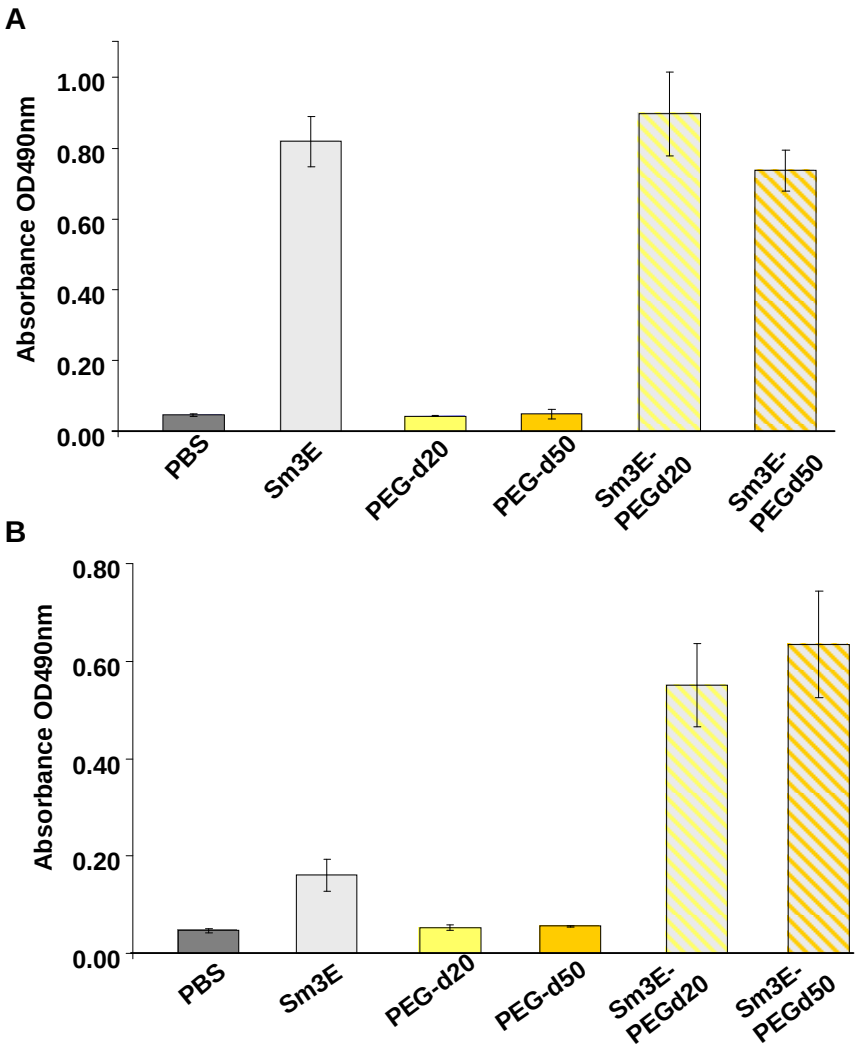

Fig. 3.24. CEA ELISA of SEC purified Sm3E-PEG-d20 and Sm3E-PEG-d50 conjugates. ELISA A) binding was detected with a mouse anti-His, primary antibody, followed by a sheep anti-mouse HRP. Sm3E was used as a positive control, non functionalised PEG-dSPION and PBS were used as negative controls. ELISA B) binding was detected with a mouse anti-dextran primary antibody, followed by a sheep anti-mouse HRP. Sm3E, non-functionalised PEG-dSPION and PBS were used as negative controls.

Table 3.2 Details the concentration of Sm3E as determined by Bradford protein assay and the concentration of d100, d50, PEG-d20 and PEG-d50 as determined by spectrophotometric readings. The number of Sm3E binding per SPION was estimated from these results.

SAMPLE	**SPION** (mg/ml)	**Number SPIONs/mg**	**Sm3E** (ug/ml) (total vol 7mls)	**Number scFv**	**scFv / SPION**	**% bound Sm3E**
Sm3E-d100 (24hr incubation)	0.375	0.25x 10*12	1.4	3 x 10 *13	120	10%
Sm3E-d50 (24hr incubation)	0.35	7 x 10 *12	5	1x10 *14	28	35%
Sm3E-PEG-d50 (3hr incubation)	0.28	2.8 x 10 *12	1.4	3x10 *13	10	10%
Sm3E- PEG-d50 (24hr incubation)	0.3	3 x 10 *12	4	8.9x10*13	29	29%
Sm3E- PEG-d20 (3hr incubation)	0.275	0.43 x 10*14	0.6	1x10 *13	0.5	4%
Sm3E- PEG-d20 (24hr incubation)	0.38	0.6 x 10*14	6	1.3x10 *14	2	42%

.

Results presented in this chapter for the development of MFE-23 and Sm3E functionalised SPIONs are summarised in Table 3.3.

Table 3.3. Summary of results presented in this chapter regarding the preferred washing procedures, conjugation chemistry, stability of the scFv-SPION conjugates and CEA reactivity. The SPIONs shaded in read were not taken forward for further investigation.

SPIONs	Separation method	Conjugation chemistry	Stable	CEA reactive
Sm3E-d50	SEC	Sodium periodate	YES	YES
Sm3E-d100	SEC	Sodium periodate	YES	YES
Sm3E-PEG-d20	SEC	Carbodiimide (EDC/NHS)	YES	YES
Sm3E-PEG-d50	SEC	Carbodiimide (EDC/NHS)	YES	YES
Sm3E-DX200	Centrifuge Magnetic	Cyanogen bromide	NO	Not tested
Sm3E-DX100	Centrifuge Magnetic	Cyanogen Bromide	YES	YES
Sm3E-CMX200	Centrifuge Magnetic	Carbodiimide (EDC/NHS)	NO	Not tested
Sm3E-CMX100	Centrifuge Magnetic	Carbodiimide (EDC/NHS)	NO	Not tested
Sm3E-CMX50	None	Not tested	Not tested	Not tested

3.4 Discussion

The work presented in this chapter has examined the feasibility of stably functionalising SPIONs with anti CEA scFvs. The scFv-SPION conjugates were subsequently used to test the hypothesis that scFv functionalised SPIONs can be targeted and bind specifically to CEA.

The nine SPIONs tested had different characteristics, which can affect their behaviour throughout the conjugation reaction. Fundamental to the conjugation protocol is the development of suitable handling and washing procedures to enable stopping of reactions, removal of excess chemicals and purification of scFv-SPION conjugates whilst maintaining solubility. Therefore, prior to attempting functionalisation the SPIONs solubility, following centrifugation, magnetic separation and SEC was visually assessed.

Due to the solubility of the dSPIONs and PEG-dSPIONs, centrifugation and magnetic separation were unsuitable for separation of these SPIONs from solution and therefore were not used as a method to purify scFv-dSPION and scFv-PEG-dSPION conjugates. The dSPIONs and PEG-dSPIONs however, were successfully purified following SEC with both the Sephadex-G25 and the Sephacryl 300HR matrix. The most likely explanation for the SPIONs solubility is that the dSPIONs and PEG-dSPIONs are ferrofluids. Due to the dSPIONs and PEG-dSPIONs thick dextran coating and small size, Brownian motion enables these SPIONs to stay suspended, therefore preventing the SPIONs settling out of solution (Gupta *et al*., 2005b). A number of groups (Dutton *et al.,* 1979; Tiefenauer *et al*., 1993; Maruyama *et al*.; 1995, Kresse *et al*., 1998; Funovics *et al*., 2004; Toma *et al*., 2005) have also reported the suitability of using SEC as a method to purify SPION-conjugates.

The DX-SPIONs were also found to separated well by SEC. However, purification of the CMX-SPIONs by SEC, proved unsuccessful, with the CMX-SPIONs interacting or agglomerating within the Sephacryl 300HR matrix of the column. The main difference between the DX-SPIONs and CMX-SPIONs is their surface chemistry. The CMX-SPIONs consist of negatively charged carboxyl groups.

Electrostatic interaction of the CMX-SPIONs to the matrix may be a reason for the delay in elution time. In addition, the terminal COOH groups could also be interacting with the N-group of the acrylamide component of the matrix (communication with Dr Nevil Deane GE Healthcare, Amersham, UK), which would cause the retention of the CMX-SPIONs on the column.

Furthermore, purification of the CMX-SPIONs by centrifugation was unsuitable, this was also observed for the DX-SPIONs. Although the CMX and DX-SPIONs separated out of solution, resuspension proved challenging. The likely reason for this behaviour could be due to the harsh conditions of centrifugation. The procedure can cause separation of the adsorbed dextran coating from the denser iron oxide cores, ultimately causing the particles to agglomerate (communication with Dr Cordula Gruettner; Micromod Partikeltechnologie GMbH, Germany), as evident with the CMX-SPIONs and DX-SPIONs. Even so, this may not be the case for all SPIONs as a number of groups (Cerden, 1989; Tiefenauer *et al*., 1993; Suwa *et al*., 1998; Toma *et al*., 2005) have successfully used centrifugation as a method to separate SPION conjugates, reporting no instability of the SPIONs.

Purification using a high magnetic field successfully separated the CMX100, CMX200, DX100 and DX200 SPIONs from their surrounding media. The feasibility of using magnetic separation as a procedure for isolation of SPION conjugates has been previously reported (Mehta *et al*., 1997; Koneracká *et al*., 1999; DeNardo *et al*., 2005). Magnetic separation however, was not suitable for separation of the CMX50.

From these results, all the SPIONs were taken forward for conjugation to the anti CEA scFvs except the CMX-50, due to its inability to undergo any of the purification procedures tested.

Although the DX100 and d100 are of the same hydrodynamic size, their level of solubility was different. A possible explanation could be the composition of the SPIONs. From iron content analysis, the DX100 consists of more iron than the d100 and in turn, consists of less dextran. The dSPIONs increased solubility during purification may therefore, be due to the higher dextran content. This finding

supports evidence that SPIONs embedded in thicker dextran coat exhibit improved stability (Gupta *et al*., 2005; Mornet *et al*., 2004).

Functionalisation of d50 with MFE-23 was successfully performed using the sodium periodate chemistry (Dutton, 1979; Molday *et al*., 1982). The hydroxyl groups of dextran have been reported to be poorly reactive (Bobbit, 1956; Rothfus & Smith 1963). Therefore, to facilitate coupling of the dextran coated SPIONs to the free amine groups present on the MFE-23, the dSPIONs require oxidation with sodium periodate this in turn oxidises the OH groups to create highly reactive aldehyde functions (Bobbit, 1956; Rothfus & Smith 1963). Following conjugation an excess amount of free MFE-23 was found, possibly due to saturation of the reactive aldehyde functions. The oxidation of the dextran hydroxyl groups with sodium periodate affects how many C-C bonds are cleaved and thus how many reactive aldehyde functions are generated (Van Lenten & Ashwell 1971; Lotan *et al.,* 1975). Attempts to increase the number of reactive aldehyde groups per d50 by increasing the concentration of sodium periodate however, proved unsuccessful with the d50 SPIONs precipitating. It is reported that oxidative stress can lead to instability of the dextran polymer (Garden *et al*., 2006), causing unravelling of the dextran matrix from the SPION cores, leading to SPION agglomeration. It was therefore decided that the concentration of sodium periodate was optimal at 10 mM. Further optimisation of the sodium periodate protocol by reducing the ratio of MFE-23 to d50 and increasing the incubation time to 24 hrs did prove successful. The results presented confirm the feasibility of generating CEA reactive MFE-23-d50 conjugates using the sodium periodate chemistry. Furthermore, a number of other groups have also reported success using the sodium periodate conjugation chemistry (Kresse *et al.,* 1998; Funovics *et* al., 2004; Toma *et al*., 2005).

For clinical application of scFv-SPION conjugates attachment of SPIONs to the humanised Sm3E is preferable. Using the optimised sodium periodate protocol the Sm3E, expressed and purified from the yeast *Pichia pastoris*, was successfully attached to the d50 and d100. The ratio of scFvs per dSPION is exceptionally good, with approx 28 Sm3E scFvs binding per d50 and 120 Sm3E scFvs to binding per d100. In comparison, Funovics *et al*., reported a binding ratio of 2 mAbs to 1 SPION (Funovics *et al*., 2004).

The sodium periodate conjugation method however, was not suitable for the conjugation of scFv to the DX-SPIONs. Oxidation of the DX-SPIONs, even at low concentrations of sodium periodate, caused precipitation of the SPIONs. A possible reason for the DX-SPIONs reduced solubility following oxidation, could be the DX-SPIONs low dextran content compared to the dSPION. As mentioned previously the degree of oxidation of the OH groups can cause changes in the structure of dextran, causing it to unravel from the SPION.

The cyanogen bromide conjugation chemistry was investigated as an alternative to the sodium periodate chemistry. Activation of OH with CNBr is a more sensitive method and leads to the conversion of hydroxyl groups to cyanate ester groups, these subsequently react and bind with free amine groups (Axen *et al*., 1967). Activation of the DX-SPIONs with CNBr proved successful with the SPIONs remaining soluble. However, following purification of the conjugates, resuspension of the Sm3E functionalised DX200 proved challenging. For this reason, the DX200 was not investigated further. In comparison, the Sm3E functionalised DX100 remained in solution and showed reactivity to CEA.

Due to the availability of free COOH groups on the PEG-dSPIONs and the CMX-SPIONs the carbodiimide conjugation chemistry was investigated to facilitate the coupling of free amines to the carboxyl groups. Reaction with EDC and NHS converts COOH groups to stable esters enabling the conjugation to amines (Hoare and Koshland 1967; Staros *et al*., 1986; Gilles *et al*., 1990).

Conjugation via the carbodiimide chemistry, proved unsuccessful for the CMX100 and CMX200. In comparison, attachment of Sm3E to the PEG-d20 and PEG-d50 resulted in soluble Sm3E-PEG-dSPION conjugates reactive with CEA. Attachment via the carbodiimide chemistry allows proteins to be conjugated to the distal end of the PEG chains, thus minimising the effect of steric hindrance caused by the PEG chains (Maruyama *et al*., 1995).

The ratio of scFv binding to PEG-dSPION was dependent on incubation time. Following incubation for 3hrs, 0.5 scFvs bound per PEG-d20 and 10 scFvs bound per PEG-d50. After 24hrs, this increased to 2 scFvs per PEG-d20 and 29 scFvs per PEG-

d50. The binding of two scFvs per PEG-d20 is consistent with DeNardo *et al*, who reported conjugation of two ChL6 mAbs to the PEG-d20 by carbodiimide conjugation chemistry (DeNardo *et al*., 2005).

The scFv binding yield also appeared to be dependent on SPION hydrodynamic radius for example, as SPION size increased from 20 nm to 100 nm the number of scFvs bound increased from 2 to 120. This is as expected, as the more surface area available the higher the number of sites for scFvs to bind. Increased multivalency can increase the avidity to target antigens, thus improving uptake and retention by the tumour (Plunkthun *et al*., 1997). This would suggest the larger SPIONs to have higher binding avidity for CEA, assuming all Sm3E scFvs bound are functional. However, the total percentage of scFv bound to the SPIONs actually decreased with hydrodynamic size. For example in 1mg/ml there was a higher number of scFvs in the Sm3E-PEG-d20 sample this is most likely due to there being 10x more 20nm SPIONs in 1mg/ml compared to the 50nm SPIONs and 20x more than the 100nm SPIONs. On the other hand, the SPION coating and conjugation chemistry had little effect on the number of scFvs binding per SPION. For example, the 50 nm SPIONs, whether stabilised in dextran or PEG-dextran both bound approx 28 and 29 Sm3E scFvs respectively.

The advantage of all the chemistries investigated is that no prior ligand modification or activation of the scFv is required, reducing the risk of affecting MFE-23 and Sm3E reactivity to CEA. In conclusion this chapter has shown firstly, that conjugation of dextran and PEG coated SPIONs to both the MFE-23 and Sm3E scFv through different chemistries is possible and secondly, that these scFv-SPION conjugates can effectively target and bind specifically to the target antigen CEA.

3.5. Summary

The aim of this chapter was to establish and optimise suitable conjugation chemistries to attach biocompatible SPIONs to the anti CEA scFvs.

A number of commercially available SPIONs were researched these include, dSPION, PEG-dSPION, DX-SPION and CMX-SPION with hydrodynamic diameter

of 20 nm to 200 nm. Stability of the SPIONs was assessed by magnetic, centrifugation and size exclusion chromatography separation methods. All SPIONs except the CMX50 were able to undergo at least one of the separation procedures used throughout the conjugation chemistry.

The sodium periodate conjugation chemistry, resulted in approx 28 and 120 scFv binding per d50 and d100, respectively. For covalent conjugation of Sm3E to the PEG-d20 and PEG-d50 the carbodiimide EDC/NHS conjugation chemistry was successfully employed, binding approx 2 and 29 scFvs per particle respectively. These two chemistries caused stability issues when attaching the Sm3E scFv to the DX-SPION and CMX-SPION. This stability issue could not be resolved for the CMX-SPIONs. Conjugation however, by the cyanogen bromide method proved successful for conjugation of Sm3E to the DX100. All Sm3E-SPION conjugates retained reactivity to the target antigen CEA by ELISA.

Chapter 4

Interaction of Functionalised SPIONs with Cancer Cells

4.1 Introduction

Having established methods to functionalise SPIONs with scFvs and shown binding on ELISA, I next investigated whether the scFv-SPION conjugates could specifically target and bind cancer cells.

The aim of the work presented in this chapter was to quantify and characterise the interaction of the Sm3E functionalised SPIONs with target CEA expressing cancer cells.

Previous reports have shown functionalisation of SPIONs to encourage specific uptake into target cells (Mailander *et al*., 2008; Villanueva *et al*., 2009), in turn improving their therapeutic and diagnostic potential. The SPIONs surface properties and hydrodynamic radii however, can affect how they interact with the target cells, for example internalisation and their relative specificity (Lentz *et al*., 1999; Zhang *et al*., 2002; Mailänder *et al*., 2008; Wilhelm *et al.,* 2008; Villanueva *et al*., 2009). To test the influence of surface coatings and size, the Sm3E functionalised d100, d50, PEG-d50 and PEG-d20 were investigated.

Furthermore, it has been reported that following intracellular uptake, SPIONs accumulate into endosomal compartments within the cell cytoplasm (Wilhelm *et al*., 2008; Villanueva *et al*., 2009). To determine the cellular fate of the Sm3E functionalised SPIONs co-localisation studies using an endosomal marker were performed.

4.2 Objectives

The objectives of the research described in this chapter were to:

1. Test the specificity of the different scFv-SPION conjugates to CEA expressing cells *in vitro*

2. Quantify uptake of Sm3E functionalised SPIONs using an optimised ferrozine based assay

3. Visualise uptake of Sm3E functionalised SPIONs via confocal microscopy

4.3 Results

4.3.1 Quantification of SPION uptake

To measure the specific binding of the Sm3E functionalised SPIONs to CEA+ve LS174T an *in vitro* cell uptake assay was developed (*see section*: 2.2.7.1). Sm3E functionalised and non-functionalised SPIONs, at a SPION concentration of at 0.1 mg/ml, were incubated with the CEA+ve cell line LS174T. Following incubation the cells were washed and SPION uptake measured using a ferrozine based iron assay adapted and scaled down from Riemer *et al*., 2004.

Results showed the cellular uptake to be dependent on hydrodynamic radii, with uptake increasing with SPION size. The specific uptake of the Sm3E functionalised PEGd20 was 2.4 pgSPION/ml compared to the Sm3E functionalised d100 SPIONs, which gave a specific uptake of 6.6 pgSPION/ml. PEGylation however, showed no benefit to the uptake of SPIONs at the pg range, as both the PEGylated and non PEGylated Sm3E-d50 demonstrated comparable SPION uptake of 4.7 pgSPION/cell and 4.4 pg/cell, respectively. Measurement of non-specific binding was minimal for all non-functionalised SPIONs, demonstrating uptake of less than 0.01 pgSPION/cell (Table 4.1).

From these experiments, results demonstrate that conjugation of Sm3E is essential for specific binding of the SPIONs to CEA+ve LS174T cells.

Table. 4.1. Uptake of SPIONs by CEA+ve LS174T cells as quantified by ferrozine based assay. The absorbance at 550 nm was referenced against standard curve of ferrozine assayed SPIONs (Fig. 4.1) to obtain SPION uptake per well (µgSPION/ml). Concentration per well was divided by cell number 5x10*6 per well to obtain SPION uptake per cell (pgSPION/cell). The number of SPIONs taken up per cell was calculated using known number of SPIONs per mg

SPION	Absorbance 550nm	SPION uptake (pgSPION/cell)	Number Of SPIONs
d100	0.01	0.00	0
Sm3E-d100	0.21	6.63 (+/-0.38)	6.6x 10*3
d50	0.01	0.00	0
Sm3E-d50	0.14	4.43 (+/-0.11)	4.4 x 10*4
PEG-d50	0.04	0.00	0
Sm3E-PEG-d50	0.15	4.73 (+/-0.12)	4.7 x 10*4
PEG-d20	0.04	0.00	0
Sm3E-PEG-d20	0.09	2.43 (+/-0.35)	2.4 x 10*5

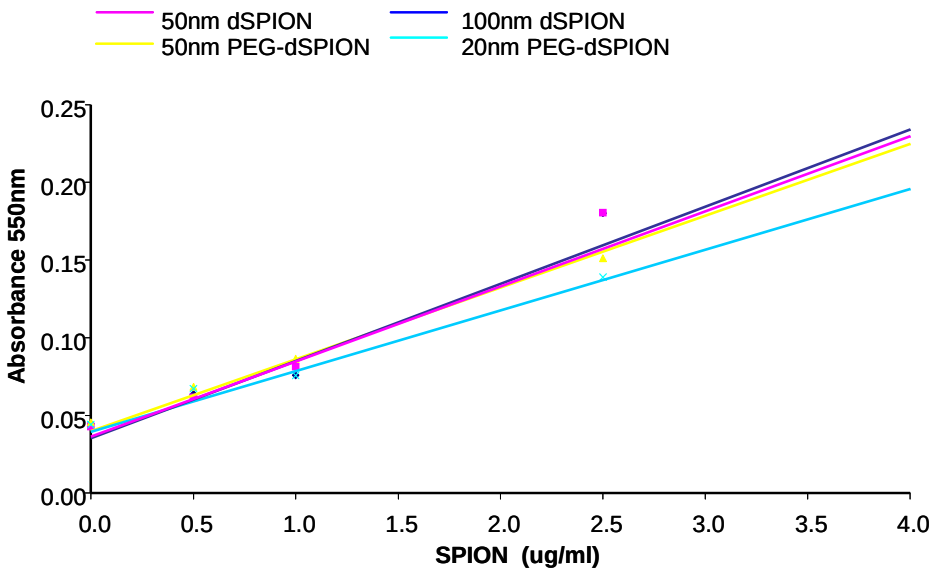

Fig. 4.1. Standard curve of Ferrozine assayed SPIONs, showing absorbance against SPION concentration.

4.3.2 Specificity of SPION uptake

To further confirm and visualise the specificity of the Sm3E functionalised SPIONs to the CEA expressing cells confocal laser scanning microscopy (CLSM) was used. For this experiment the CEA+ve LS174T cell were again incubated with Sm3E functionalised or non functionalised d50 and d100 at a SPION concentration of 0.1mg/ml. Specific binding of the SPIONs was detected with anti-dextran (red) to enable visualisation by CLSM. To show the presence of cells the nuclei stain Hoechst (blue) was used. The CEA-ve A375M cell line was used as a control.

The CLSM results clearly show the dextran coated Sm3E-d50 to specifically target the CEA+ve LS174T cells, preferentially distributing around the cell surface membrane (Fig. 4.2a & 4.2b). In contrast, the non-functionalised d50 SPION showed no binding to the CEA+ve LS174T cells (Fig. 4.2c). Neither Sm3E-d50 nor non-functionalised d50 bound to the control CEA-ve A375M cells (Fig. 4.2e & 4.2f).

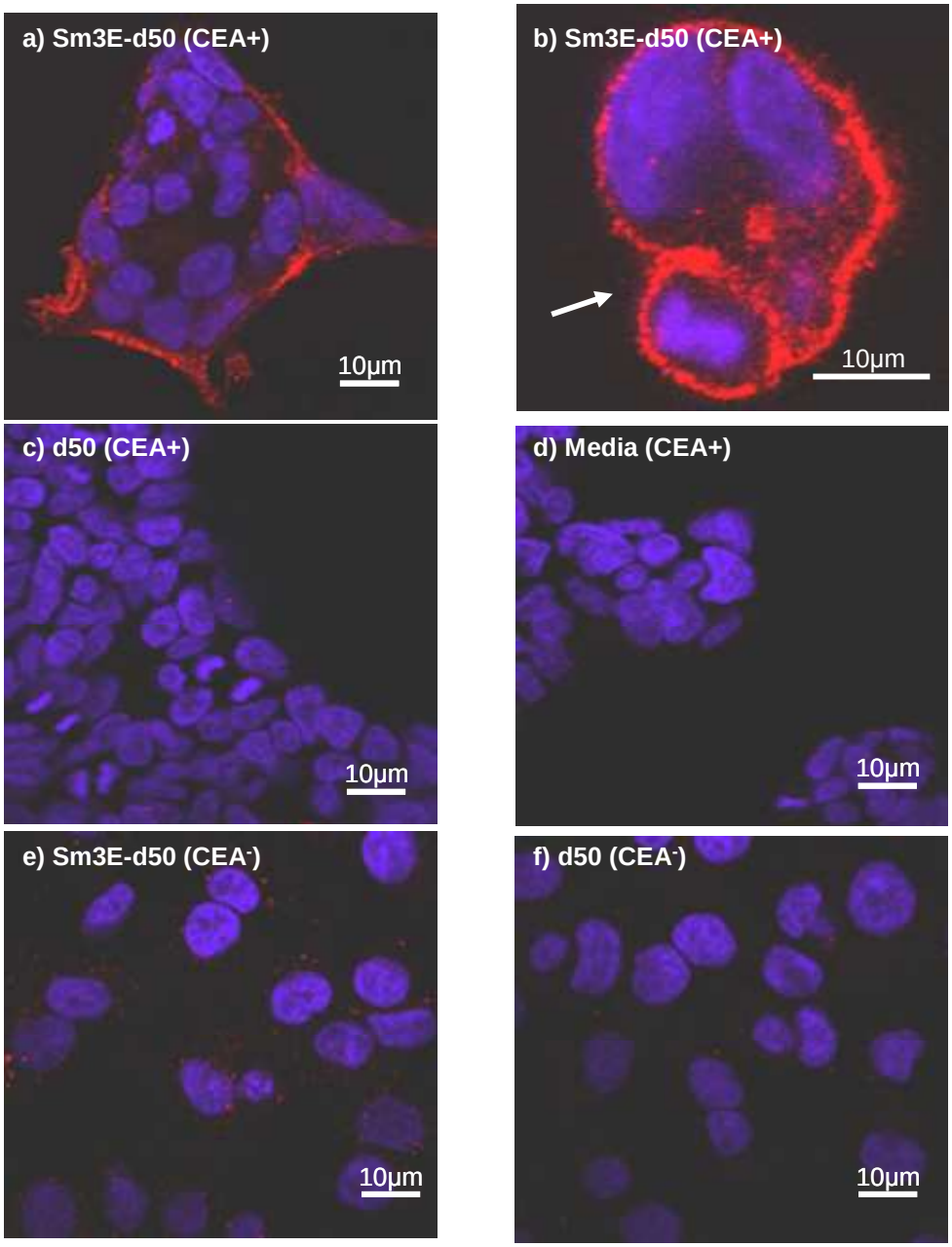

Fig. 4.2. CLSM images of CEA+ve LS174T cells incubated in, a & b) Sm3E-d50, c) d50, d) media only and CEA-ve A375M cells incubated in e) Sm3E-d50, f) d50. Detection of specific cell binding was performed with a mouse anti-dextran primary antibody, followed by a goat anti-mouse alexa fluor 594 antibody and nuclei were stained with Hoechst. All SPIONs were applied at 0.1 mg/ml.

The CLSM results also show specific targeting of the Sm3E functionalised d100 to the CEA+ve LS174T cells (Fig. 4.3a). Furthermore, the Sm3E-d100 showed the same cell membrane binding behaviour as the Sm3E-d50. No binding to the CEA+ve LS174T cells was detected with non-functionalised d100 (Fig. 4.3b).

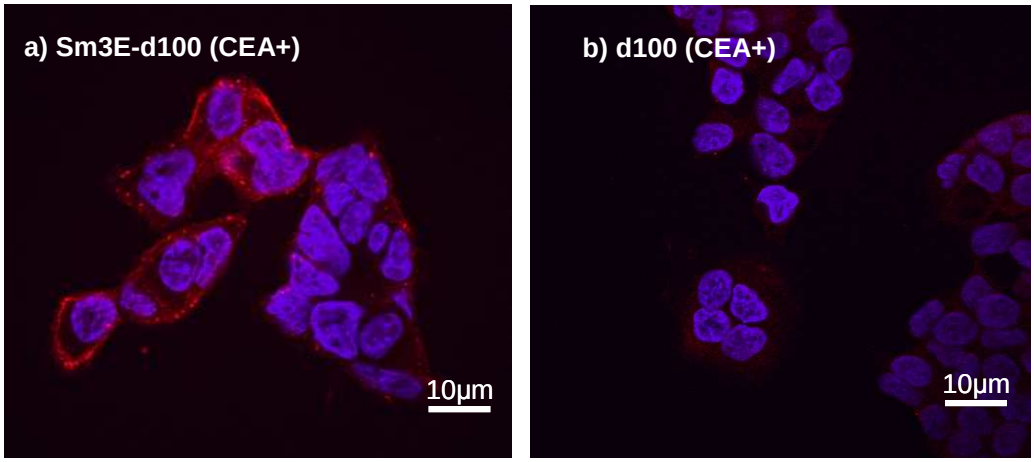

Fig. 4.3. CLSM images of CEA+ve LS174T cells incubated in a) Sm3E-d100 and b) d100. Detection of specific cell binding was performed with a mouse anti-dextran primary antibody, followed by a goat anti-mouse alexa fluor 594 antibody. The nuclei were stained with Hoechst. All SPIONs were applied at 0.1 mg/ml.

4.3.3 Effect of SPION surface chemistry

The surface properties of SPIONs can affect their uptake into cells. Previous reports have suggested PEGylation as well as carboxylation to be involved in spontaneous intracellular uptake (Lentz *et al*., 1994; Mailänder *et al* 2008). Focusing on binding behaviour and relative specificity, the PEG-dSPIONs were investigated and compared with the dSPIONs.

The experiments were performed as in section 4.3.2, with binding behaviour of the PEG-dSPIONs visualised by CLSM. Under the sensitive conditions of CLSM, results revealed both the Sm3E functionalised and non-functionalised PEG-d50 to associate with the CEA+ve LS174T cell line (Fig. 4.4a & 4.4b). These results suggest that the addition of PEG-COOH chains to the d50 SPIONs surface

encouraged non-specificity. However, from quantitative analysis the non-specific uptake was very low <0.01 pg (Table 4.1). Furthermore, PEGylation of the d50 also appeared to promote internalisation (Fig 4.4a & 4.4b).

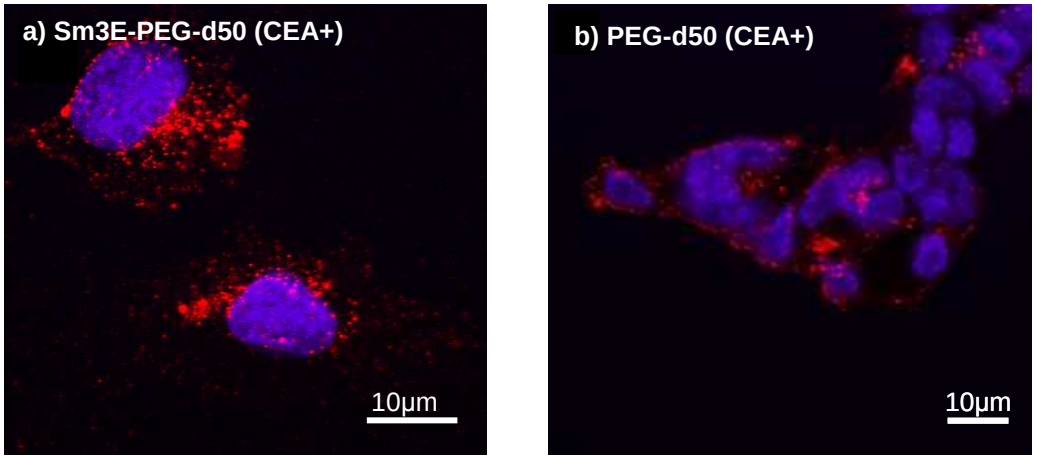

Fig. 4.4. CLSM images of CEA+ve LS174T cells incubated in a) Sm3E-PEG-d50, b) PEG-d50 overnight. Detection of specific cell targeting was performed with a mouse anti-dextran primary antibody, followed by a goat anti-mouse alexa fluor 594 antibody. The nuclei were stained with Hoechst. All SPIONs were applied at 0.1 mg/ml.

In comparison, CLSM images of the smaller Sm3E functionalised PEG-d20 revealed the SPION to specifically bind and internalise into CEA+ve LS174T cells (Fig. 4.5a), with minimal uptake of the non-functionalised PEG-d20 (4.5b). Furthermore, neither Sm3E-PEG-d20 nor the non-functionalised PEG-d20 bound to the control CEA-ve A375M cells (Fig 4.5c & 4.5d). These results therefore, indicate that the specific uptake of the functionalised PEG-d20 is due to the Sm3E-CEA interaction.

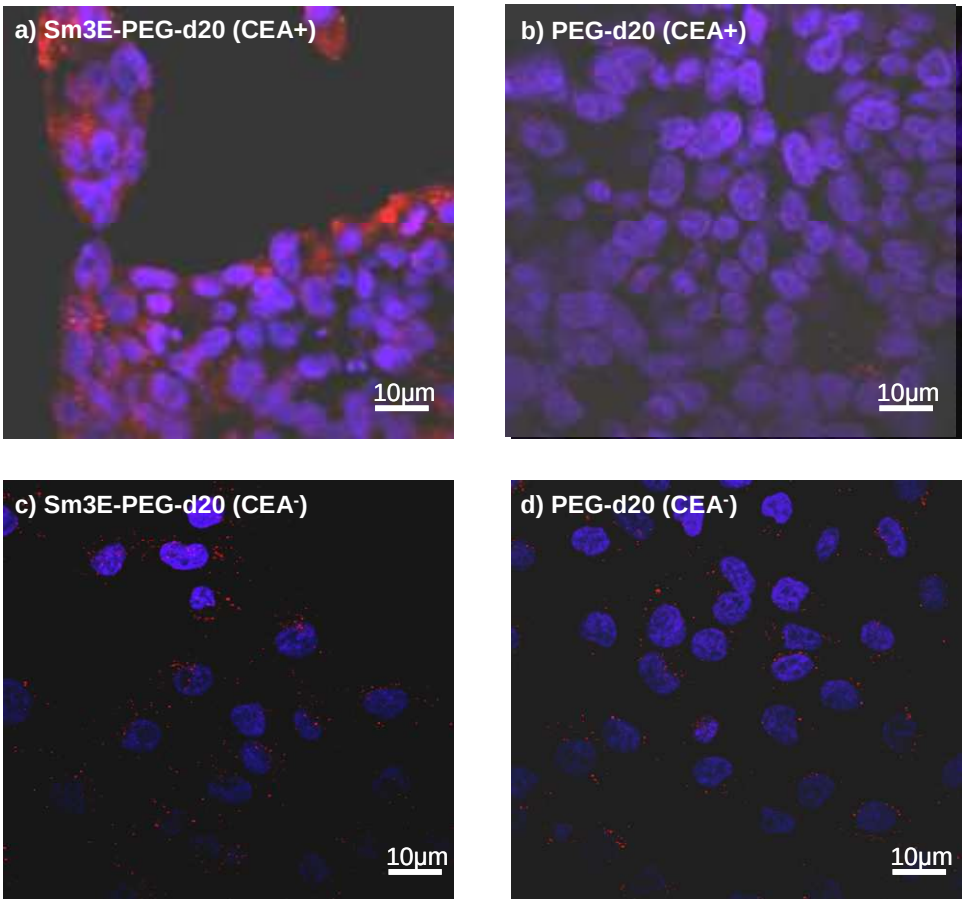

Fig. 4.5. CLSM images of CEA+ve LS174T cells incubated in a) Sm3E-PEG-d20, b) PEG-d20 and CEA-ve A375M cells incubated in c) Sm3E-PEG-d20 and d) PEG-d20. Detection of specific cell binding was performed with a mouse anti-dextran primary antibody, followed by a goat anti-mouse alexa fluor 594 antibody. The nuclei were stained with Hoechst. All SPIONs were applied at 0.1 mg/ml.

4.3.4 Intracellular trafficking

On the CLSM images, the internalised Sm3E-PEG-d50 appeared to localise to punctate structures distributed throughout the cytoplasm of the cells (Fig. 4.6a). To determine whether these represent endosomal compartments the cells were co-immunostained with anti-dextran (Fig. 4.6a, red) and anti LAMP1 (Fig. 4.6b, green) antibodies. Co-localisation was observed between the antibodies (Fig. 4.6d, white arrows) indicating that the Sm3E-PEG-d50 are trafficked to late endosomal compartments.

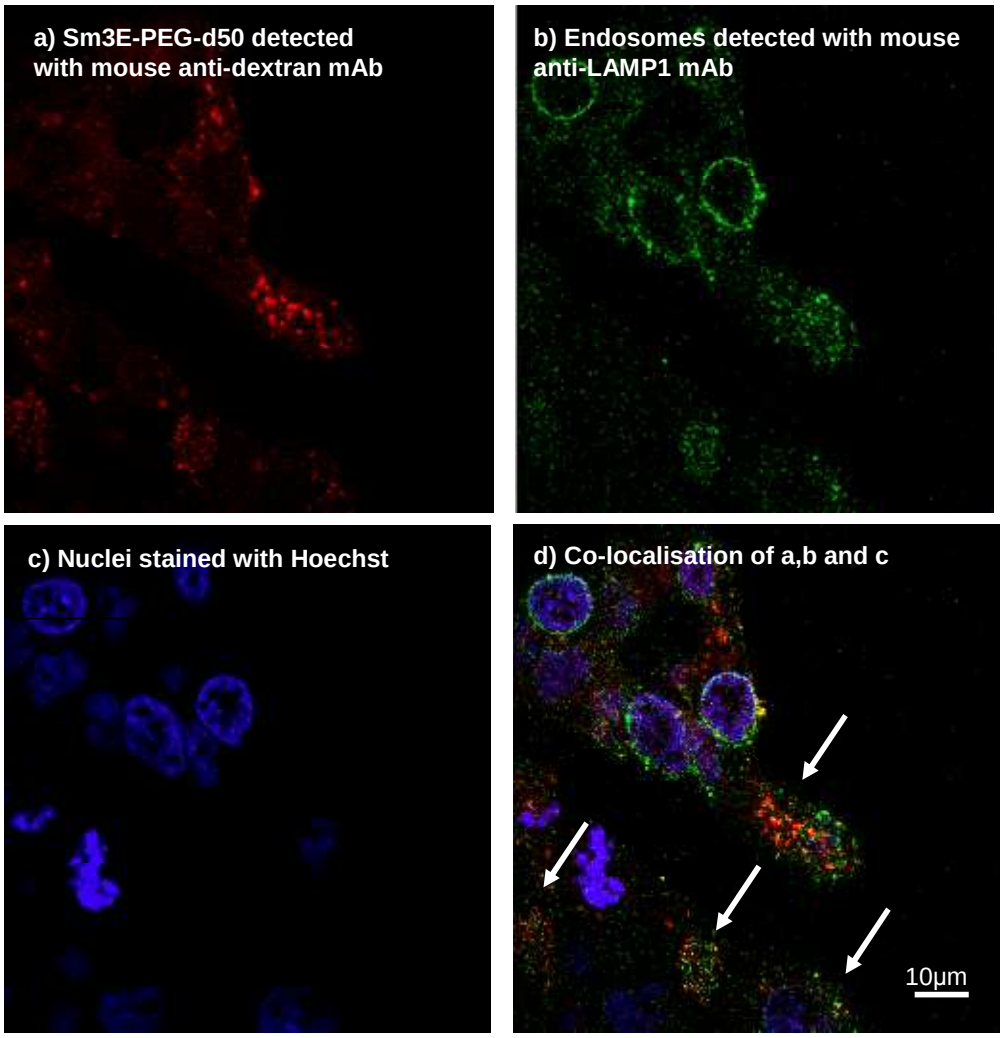

Fig. 4.6. CLSM images of Sm3E-PEG-d50 localising in endosomal compartments (shown by white arrows). Sm3E-PEG-d50 SPIONs are shown in red (a), endosomes in green (b) and cell nuclei in blue (c). CEA+ve LS174T cells were incubated in Sm3E-PEG-d50 at a SPION concentration of 0.1 mg/ml. Co-localisation of Sm3E-PEG-d50 with endosomes was detected with a mouse anti-dextran and mouse anti-LAMP1 followed by goat anti-mouse IgG1 Alexa Fluor 594 and goat anti-mouse IgG2b Alexa Fluor 488, respectively. The nuclei were stained with Hoechst.

4.3.5 Surface charge

Negative surface charge has been reported to encourage non-specific electrostatic interaction with cell membranes and facilitate intracellular uptake (Wilhelm *et al*., 2003; Patil *et al*., 2007). The carboxylated PEG coating of the PEG-dSPIONs may have an affect on the SPIONs overall surface charge, and could therefore be responsible for the internalisation and the non-specificity observed with the PEG-d50 and PEG-d20. The surface charge of the SPIONs was determined by zeta potential measurements performed at pH 7 using a Zetasizer Nano ZS. Results showed that, whilst the d50 SPION had a zeta potential (electrical surface charge) of -1.5 mV, the PEG-d20 and PEG-d50 had a surface charge of -4.0 mV and -5.0 mV, respectively. The intracellular uptake observed with the PEG-d20 and PEG-d50 may therefore, be due to increased negative surface charge, attributed by the absorbed PEG-COOH chains.

The results presented in this chapter are summarised in Table 4.2

Table. 4.2. Summary of CLSM results presented in this chapter regarding the binding behaviour of the Sm3E-SPION conjugates to the CEA+ LS174T cells.

SPIONs	Specificity	Cellular behaviour
d50	No binding	N/A
Sm3E-d50	Specific	Membrane bound
d100	No Binding	N/A
Sm3E-d100	Specific	Membrane bound
PEG-d50	Non-specific	Internalised
Sm3E-PEG-d50	Non-specific / specific	Internalised
PEG-d20	No binding	NA
Sm3E-PEG-d20	Specific	Internalised

4.4 Discussion

The results described in this chapter have shown that Sm3E-SPION conjugates specifically bind to CEA expressing tumour cells. In addition, the results indicate that the size and surface properties of the SPIONs exert a substantial effect on the labelling efficiency, specificity and binding behaviour with the cell.

Specific binding to CEA expressing cells for all the SPIONs investigated was successfully achieved by conjugation to Sm3E, as measured by iron uptake. Furthermore, uptake of the non-functionalised SPIONs was minimal at less than 0.01 pg/cell compared to Sm3E functionalised SPIONs at 2-6pg/cell. These results demonstrate that functionalisation of SPION with a targeting ligand such as scFvs is essential for specific uptake into target cells. The negligible uptake of the non-functionalised SPIONs was also observed in HeLa cells (Wilhelm *et al.*, 2003; Mailander *et al*., 2008; Villanueva *et al*., 2009), CD4+ T cells (Garden *et al*., 2006), CHO cells (Reynolds *et al*., 2006) and pancreatic MIA paCa-2 cells (Yang *et al*., 2009).

From iron uptake measurements, more iron was found to be in the cells incubated in the larger scFv functionalised SPIONs. Suggesting cellular uptake of Sm3E functionalised SPIONs to be dependent on the hydrodynamic size of the SPIONs, with the larger SPIONs demonstrating higher uptake. However, calculation of the number of SPIONs taken up per cell found cellular SPION uptake to increase as SPION size decreased. For example, SPION uptake for the Sm3E-PEG-d20 was approximately 2.7 x 10*5, compared to the Sm3E-100d at 6.6 x 10 *3. Results presented in Chapter 3 show the valency of the SPION to increase with hydrodynamic size, with the 20 nm, 50 nm, 100 nm SPIONs binding 2, 29 and 120 Sm3E scFvs, respectively. The increased valency of the SPIONs can improve their avidity to the target cells (Adams *et al*., 1999, 2006), which would suggest SPION uptake to increase with SPION size as observed by Garden *et al*., and Kaittanis *et al*., who reported an increased cell labelling efficiency of SPIONs with increased valence (Garden *et al*., 2006; Kaittanis *et al*., 2009). However, this does not appear to be the case for the conjugates investigated in this chapter. One possible explanation for the

decrease in Sm3E functionalised SPION uptake with increase SPION size could be due to the high number of Sm3E scFvs bound to the SPION, causing steric inhibition. The majority of the scFvs could therefore be functionally block from reacting with the target CEA, thus reducing the SPIONs avidity to the cell compared to if all Sm3E scFvs were functional. Another reason for the difference in SPION uptake could be due to the binding behaviour of the different Sm3E functionalised SPIONs

Further investigation of the Sm3E-SPION conjugates binding behaviour was performed by CLSM. Results revealed the Sm3E targeted dextran coated SPIONs to specifically localise on the extracellular membrane, as has been reported with dextran coated SPIONs functionalised with whole mAbs (Funovics *et al*., 2004). In contrast, the functionalised PEGylated SPIONs internalised into the cell cytoplasm, forming localised clusters. The increase in SPION uptake could therefore be due to the fact the smaller Sm3E PEG-d20 SPIONs are able to be internalised, making available CEA binding sites for more Sm3E-PEG-d20 SPIONs and in addition are able to fill a larger space. In comparison, the Sm3E-d100 SPIONs appear to only bind to the cell membrane and therefore may saturate all binding sites, thus limiting the number of SPIONs from attaching to the cells. The Sm3E-PEG-d50 also shows a slightly higher SPION uptake than its dextran only counterpart Sm3E-d50.

The possible reason for the difference in binding behaviour between the dSPION and PEG-dSPION could be due to their surface chemistry. Both SPIONs are prepared in the same way, except the PEG-dSPIONs have PEG-COOH chains absorbed onto their dextran surface (communication with Dr Cordula Gruettner, Micromod). Under physiological conditions (pH 7), the PEG-COOH chains are mostly in the deprotonated form and therefore negatively charged. In contrast, dextran is generally neutrally charged (Okon *et al*., 1994).

A number of groups have reported that charged SPIONs have a higher affinity to the cell membrane. This is thought to be due to electrostatic attraction, which in turn encourages internalisation by fluid phase endocytosis (Wilhelm *et al*., 2003; Alberola *et al*., 2009). Therefore, one possible cause of the observed internalisation would be the negative surface charge conferred by the carboxylated PEG chain terminals.

Indeed, the results show a reproducible decrease in electrical surface charge from -1 mV to -5 mV upon addition of PEG-COOH, suggesting that this is a likely contributing factor. In line with these observations, dextran has previously been reported to exhibit poor internalisation (Wilhelm *et al*., 2003), an effect attributed to its neutral charge (Okon *et al*., 1994; Mailander *et al*., 2008). Therefore, without functionalisation to internalising targeting ligands, dextran coated SPIONs are unable to attach and internalise into cells.

The high solubility of PEG with the cell membrane lipid bilayer could also be a reason for the intracellular uptake observed with the PEG-dSPIONs. A number of studies have previously reported on the internalisation property PEG exerts on SPIONs (Yamazaki *et al*., 1990: Lentz *et al*., 1994: Zhang *et al*., 2002: Wilhelm *et al*., 2003). PEG can dissolve in both polar and non-polar solvents (Zhang *et al*., 2002) inducing defects in the bilayer, which is thought to mediate cell membrane fusion a process required in endocytosis (Lentz *et al*., 1994). However, a high concentration of PEG is required for PEG mediated membrane fusion to occur (Yamazaki *et al*., 1990), therefore it is unlikely this mechanism alone attributed to the binding behaviour seen with the PEGylated SPIONs.

As well as intracellular uptake, CLSM results revealed the PEG-d50 SPIONs to exhibit non-specific uptake however, this was not the case for the smaller PEG-d20. A likely explanation could be their PEG-COOH content. From the manufacturers data sheet the number of PEG-COOH chains per PEG-d50 was estimated to be 1900, in comparison, PEG-d20 was estimated to have 131 PEG-COOH chains per SPION. The increase in PEG content of the PEG-d50 correlates with the increase in negative surface charge. Therefore, the increase in PEG-COOH chains and furthermore, negative charge is a probable contributing factor to the non-specificity of the PEG-d50 SPIONs. Despite this non-specific uptake of the PEG-d50 was minimal (<0.01 pg/cell).

Following internalisation the PEG-dSPIONs formed clusters within the cytoplasm of the cell. CLSM images, revealed the PEG-dSPIONs to accumulate into the endosomal compartments within the cell, an observation that is well documented (Gupta *et al*., 2004; Mailander *et al*., 2008; Wilhelm *et al*., 2008; Villanueva *et al.*,

2009). Accumulation of PEG-dSPIONs within endocytic compartments are subject to the effects of hydrolytic enzymes and low pH, ultimately leading to break down of the SPIONs into Fe^{2+} and Fe^{3+} ions for use towards natural Fe pathways (Okon *et al*., 1994; Gupta *et al*., 2004; Thorek *et al*., 2006). This has raised questions about the benefits of using internalising SPIONs for MRI and hyperthermic applications, since the SPIONs need to be in the form of magnetite Fe_3O_4 or maghemite γFe_2O_4. However, magnetite metabolism is slow, reporting to take between 4-7 days (Renshaw *et al*., 1986; Briley-Saebo *et al*., 2004), giving sufficient time for MR imaging or hyperthermia treatment. A recent report by Cartiera *et al*., has speculated however, that the SPIONs incorporated into the endocytic compartments of the cell are capable of escaping and localising instead in the Golgi, ER and secretory vesicles therefore, bypassing intracellular digestion (Cartiera *et al*., 2009).

4.5 Summary

The aim of the work presented in this chapter was to quantify and characterise the interaction of the Sm3E functionalised SPIONs with target CEA expressing cancer cells.

Specific binding of SPIONs to CEA+ LS174T cells was achieved via conjugation to with Sm3E. Size, valency and anionic charge of the SPIONs were demonstrated to be important factors in the cellular uptake and binding behaviour of the SPIONs. The Sm3E-d100 and Sm3E-d50 were shown to selectively bind the extracellular membrane. In comparison, the Sm3E-PEG-d50 showed intracellular uptake and some non-specificity, both effects thought to be attributed to the size and anionic charge of the PEG-d50. By conjugation to the smaller, slightly less anionic PEG-d20 intracellular uptake was still observed, whilst the issue of non-specificity was overcome. Upon internalisation, the PEGylated SPIONs accumulated into the endosomal compartments of the cell.

Chapter 5

Imaging Potential of Functionalised SPIONs

5.1 Introduction

The work in the previous chapter showed that scFv functionalised SPIONs could target specifically to antigen expressing cancer cells. The next stage was to investigate whether these findings could be extended to exploit scFv functionalised SPIONs in MRI.

Reports by others have indicated the potential of mAb functionalised SPIONs as targeted contrast agents (Tiefenauer *et al*., 1993; Suwa *et al*., 1998; Funovics *et al*., 2004; Toma *et al*., 2005). More recently, functionalisation of SPIONs with anti EGFR scFvs has shown potential as a tumour-imaging agent (Yang *et al*., 2009). The use of scFvs as targeting moieties has potential advantages over whole antibodies. First, the molecular diameter of a whole IgG is approximately 28nm (Roberts *et al*., 1995), making scFvs relatively small at approximately 5nm. Therefore, attachment of scFvs to SPIONs should not significantly increase the SPIONs diameter. Second, scFvs do not contain the Fc constant domain and therefore are unable to trigger potentially harmful immune responses. Third, scFvs are readily available in recombinant form and can be generated for clinical applications using non-mammalian expression systems (Tolner *et al*., 2006a). To test the potential of the scFv functionalised SPIONs developed in this thesis as tumour targeted contrast agent three functionalised SPIONs i) Sm3E-d50, ii) Sm3E-PEG-d50 and iii) Sm3E-PEG-d20 were taken forward.

To evaluate the selective tumour imaging potential of the Sm3E functionalised SPIONs to CEA+ve LS174T cells, T_2-weighted images and relaxometry measurements were performed. SPION hydrodynamic size and surface properties have shown to substantially affect binding behaviour (*see section*: 4.3 Results). Therefore, the impact of binding behaviour on the SPIONs imaging potential was evaluated by their T_2-weighted images and T_2 values.

To determine whether Sm3E-SPIONs can be used for specific tumour imaging, the targeting potential of the scFv-SPION conjugates *in vivo,* following systemic injection, was investigated by means of their biodistribution.

5.2 Objectives

The objectives of the research described in this chapter were to:

1. Assess the toxicity of Sm3E functionalised SPIONs *in vitro* by MTT assay

4. Show MRI potential of the SPIONs

5. Demonstrate the selective MRI potential of Sm3E functionalised SPIONs *in vitro* using MRI

6. Investigate the biodistribution of Sm3E-SPIONs *in vivo* following systemic injection

5. 3 Results

5.3.1 *In vitro* cytotoxicity

For SPIONs to be suitable as targeted MRI contrast agents, they should show minimal toxicity to the targeted cell. Images taken by CLSM (*see section*: 4.3.2 Specificity of SPION uptake) show that 24 hrs following incubation with 0.1 mg/ml of SPIONs the cells appeared healthy. The degree of cell survival was further evaluated by means of the standard methyl thiazol terazolium bromide (MTT) assay. Though the cells looked healthy at 24 hr, the SPIONs may experience delayed cell death. Therefore, following 24 hr incubation with SPIONs at 0.1 mg/ml, the cells were incubated for a further 96 hrs in fresh media before addition of MTT. The results from the MTT assay show 92-100% cell viability in relation to the control sample (Fig 5.1). This result indicates that there is no statistically significant evidence of SPION toxicity to CEA+ LS174T cells at a concentration of 0.1 mg/ml ($p = 0.36$).

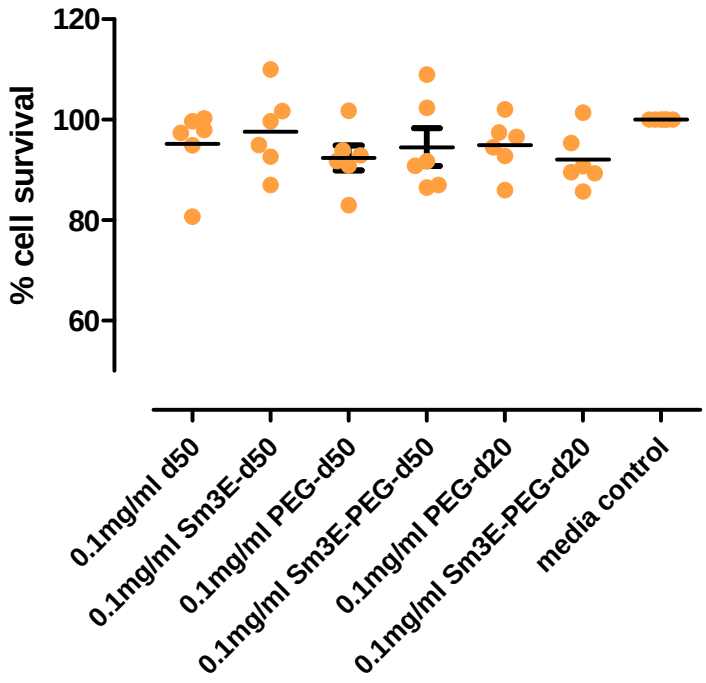

Fig. 5.1. Cell viability of CEA+ve LS174T cells after overnight incubation with Sm3E functionalised and non-functionalised SPIONs at concentrations 0.1 mg/ml. No significant difference in cell viability was observed (ANOVA: p value 0.36)

5.3.2 Magnetic resonance imaging potential of SPIONs

To evaluate the MRI potential of the SPIONs, solutions of increasing concentrations were prepared and their relaxation times measured using a 2.35 T horizontal bore SMIS imaging system. Furthermore, to determine whether the relaxivity of the SPIONs was suitable for diagnostic application, the SPIONs were imaged alongside the clinically approved SPION contrast agent Endorem™ at a concentration of 0.035 mg/ml. Magnetic resonance images were obtained using a phantom similar to that shown in Fig. 5.2. MRI analysis of the various concentrations of SPIONs was performed at TR 1000 msec at multiple TEs. As magnetite was expected to affect mainly T_2 relaxation (*see section*: 1.7.1.Application of SPIONs in MRI), only T_2 measurements were taken. The T_2 relaxation values of the various concentrations of the SPIONs were calculated and are shown in Fig. 5.3. The results show that at a concentration of 0.035 mg/ml the d50, PEG-d50 and PEG-d20 have a T_2 value of 56.2 ms, 58.3 ms and 51.8 ms, respectively. In comparison, Endorem is only slightly higher at 69.4 ms. These results confirm contrast enhancement capabilities of the SPIONs, showing their relaxivity to be comparable to the SPION contrast agent Endorem™. Furthermore, the results show as concentrations of the SPION increase the T_2 relaxation time decreases. The best signal to noise ratio was found to be at 0.04 mg/ml.

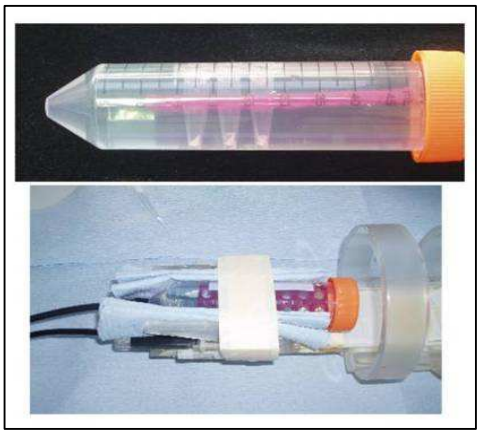

Fig. 5.2. MRI phantom contains a 0.5 ml eppendorf holder placed inside a 50 ml falcon tube. Eppendorf tubes containing samples are placed in the MRI phantom, which is filled with 2.5 g/l $CuSO_4$ to minimise background.

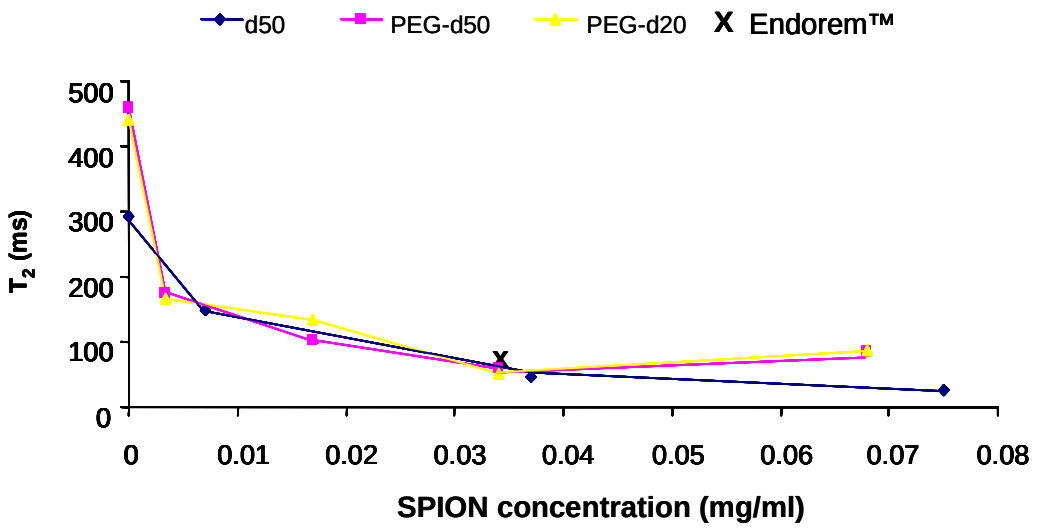

Fig. 5.3. Magnetic Resonance Imaging of serial dilutions of d50, PEG-d50, PEG-d20 and Endorem™ (0.035 mg/ml) on a 2.35 T on a horizontal bore SMIS system. All SPIONs are shown to cause a decrease in the T_2 signal intensity with increasing concentrations of the SPIONs.

5.3.3 *In vitro* MRI of Sm3E-SPIONs

To determine the selective MRI potential of the Sm3E functionalised d50, PEG-d50 and PEG-d20 an *in vitro* MRI study was performed. For this experiment, the CEA+ve LS174T cells and CEA-ve A375M cells were incubated with Sm3E functionalised and non-functionalised SPIONs at 0.1 mg/ml. Following incubation, the cells were spun down, fixed and imaged. Magnetic resonance images were obtained using a phantom consisting of three tubes as shown in Fig. 5.2. The T_2 relaxation values of each sample were calculated and are shown against the corresponding T_2-weighted image in Fig. 5.4.

5.3.3.1 Sm3E-d50

The T_2-weighted MR images of the CEA+ve LS174T cells incubated with the Sm3E functionalised d50 demonstrate a strong negative T_2 contrast (Fig. 5.4), producing a 47% reduction in T_2 values relative to the media only control. Minimal reduction (3%) in T_2 was detected for the CEA+ve LS174T cells incubated in non-functionalised d50.

The T_2-weighted images of the CEA-ve A375M cells (Fig. 5.4) incubated in Sm3E functionalised and non-functionalised d50 show no reduction in the T_2 signal. However, T_2 measurements revealed a slight reduction in the T_2 signal compared to the media only control of 28% and 22% respectively (Fig. 5.4).

5.3.3.2 Sm3E-PEG-d50

In the previous chapter (*see section*: 4.3.4 Intracellular uptake) it was shown that PEGylated SPIONs can internalise, therefore, it was considered that this may affect the MRI signal (Briley-Saebo *et al*., 2004).

The T_2-weighted MR image of the CEA+ve LS174T cell line incubated with Sm3E-PEG-d50 demonstrate a strong negative T_2 contrast of 57% (Fig. 5.4), suggesting intracellular uptake to have no detrimental effect on MRI signal. A minimal T_2 reduction of 11% was detected for the non-functionalised PEG-d50, indicating specificity of the Sm3E-PEG-d50 to the CEA+ve LS174T cells. However, MR images of the CEA-ve A375M cells incubated with the functionalised and non-functionalised PEG-d50 produced a 51% and 49% reduction in T_2. These results reveal non-specific binding of the PEG-d50 with the CEA-ve A375M cells.

5.3.3.3 Sm3E-PEG-d20

From iron uptake measurements (*see section*: 4.3.1 Quantification of SPION uptake) the specific uptake of Sm3E-PEG-d20 was two fold less than the Sm3E-PEG-d50. However, the reduction in T_2 value for the CEA+ve LS174T cells incubated with Sm3E-PEG-d20 was 51%, only marginally lower than the Sm3E-PEG-d50. A negligible T_2 reduction of 17% was detected for the non-functionalised PEG-d20, confirming specificity of the Sm3E-PEG-d20 to CEA+ve LS174T cells.

Incubation of the PEG-d20 with the CEA-ve A375M cells provided only a slight T_2 reduction compared to the media only controls of 27%, this is comparable with the d50.

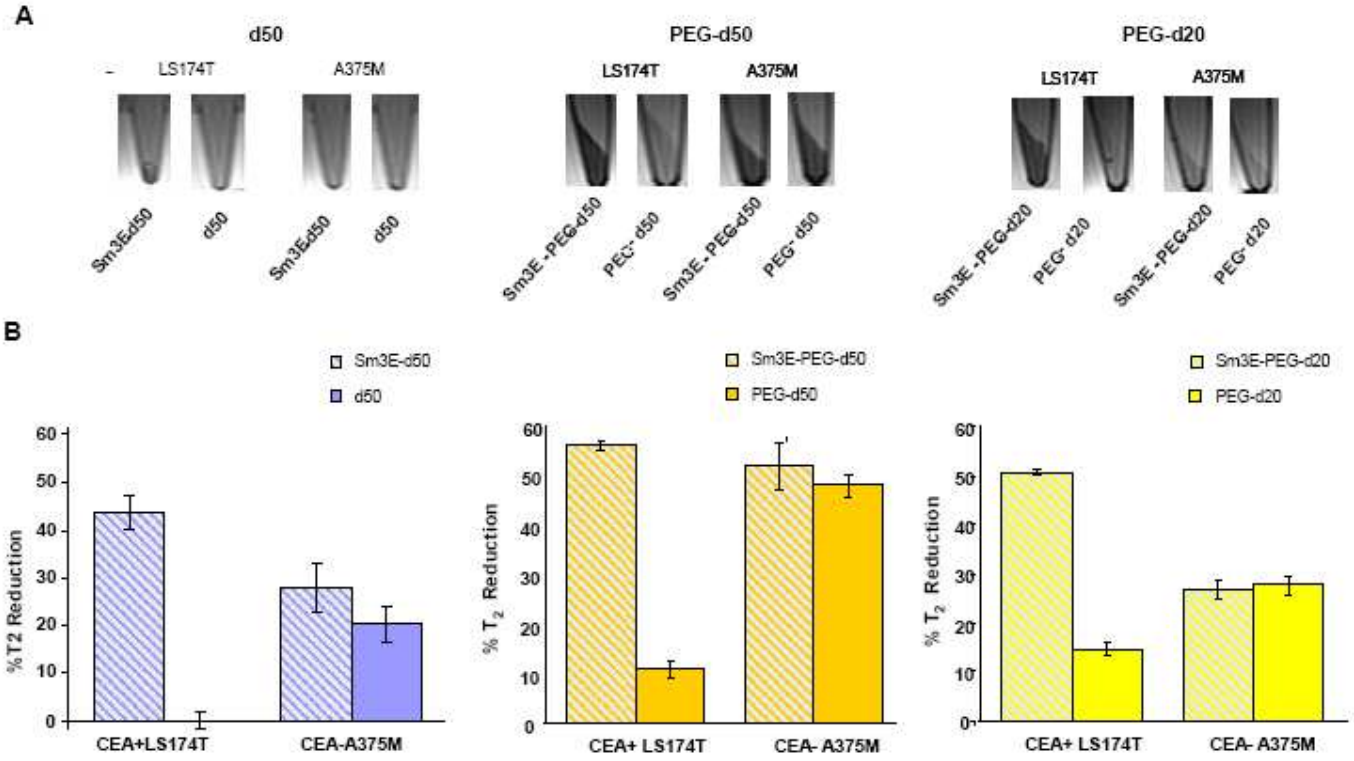

Fig. 5.4. T_2 weighted spin echo images (A) and T_2 values (B) of CEA+ve LS174T cells and CEA-ve A375M cells incubated in 0.1 mg/ml Sm3E functionalised and non-functionalised d50, PEG-d50 and PEG-d20. Percentage T_2 values were calculated and compared to media only control values.

5.3.4 Biodistribution of Sm3E-SPIONs

The Sm3E functionalised SPIONs have shown selective MRI potential *in vitro*. For their use as imaging tools *in vivo* selective uptake into CEA expressing tumour cells, following systemic injection is essential. To investigate the biodistribution of the Sm3E functionalised d50, PEG-d50 and PEG-d20 SPIONs following systemic injection, an *in vivo* study was performed. For this experiment, Sm3E functionalised SPIONs (0.2mg) were injected intravenously into CEA+ve tumour-bearing mice. After 5 min, 1hr and 24 hr the mice were sacrificed, tumours, livers and spleens collected and cryo-sectioned. The tissues were stained with nuclear fast red to detect cells and Prussian blue to detect the SPIONs.

The biodistribution results for the Sm3E functionalised and non-functionalised d50, PEG-d50 and PEG-d20 appeared similar for all time points. Results in Fig 5.5 show uptake for the Sm3E functionalised SPIONs after 1hr. All the SPIONs were found to predominantly localise within the spleen, only a small amount of functionalised SPION accumulated in the tumour and liver. These results suggest that systemic application of the Sm3E functionalised d50, PEG-d50 and PEG-d20 may not be feasible due to rapid clearance via the RES, preventing specific uptake in the tumour.

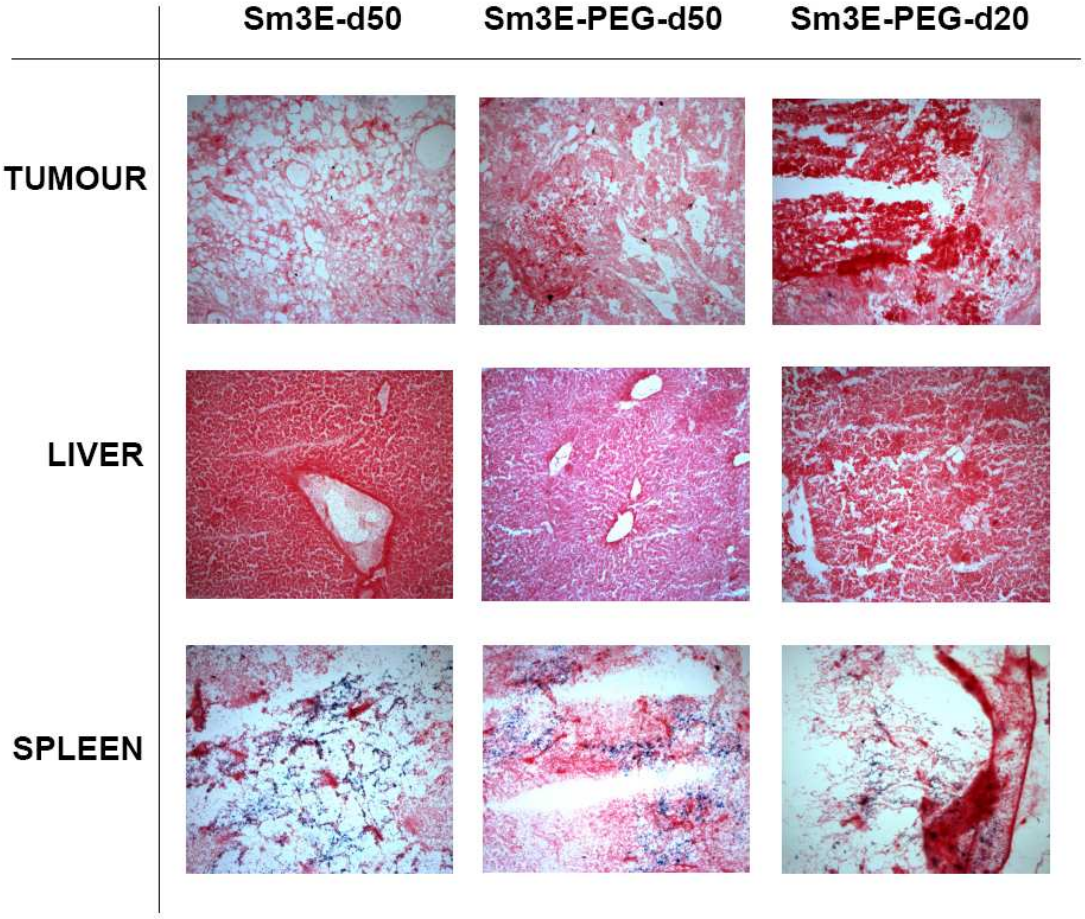

Fig 5.5 Biodistribution study of Sm3E-d50, Sm3E-PEG-d50 and Sm3E-d20 in CEA+ve tumour bearing mice. Tumour, liver and spleen section were stained with H&E to detect cells (red) and Prussion blue to detect SPIONs (blue). The SPIONs predominantly localised in the spleen.

5.4 Discussion

The results described in this chapter demonstrate the potential of Sm3E functionalised d50, PEG-d50 and PEG-d20 to deliver tumour specific MRI. The results also showed that size and surface properties strongly influence non-specific uptake.

Administration of contrast enhancement agents is generally intravenous, allowing the SPIONs to circulate in the blood until they reach their target. To avoid fast clearance from the blood, SPION size and surface properties are important. It has been reported that SPIONs with a hydrodynamic diameter >100 nm, are readily cleared by the reticuloendothelial system (RES) (Gupta *et al*., 2005b) or are unable to move through capillary vessels to reach the tumour (Suwa *et al*., 1998). The d50, PEG-d50 and PEG-d20 were therefore, proposed to be attractive SPIONs for systemic application and for this reason were taken forward for investigation into their tumour specific MRI potential.

Results from MR relaxometry show that colloidal suspensions of the d50, PEG-d20 and PEG-d50 reduce T_2 relaxation in a concentration dependent manner, a pattern previously reported (Wang *et al*., 2001). In addition, SPION size and surface properties had no effect on T_2, with all three SPIONs demonstrating similar T_2 relaxivity values. These results do not support findings by Wang *et al*., who reported MR signal intensities to depend on the composition and size of the SPIONs (Wang *et al.,* 2001). The reduction in T_2 generated by all three SPIONs at 0.035 mg/ml was almost equivalent to that generated by Endorem™ at the same concentration. Therefore, based on the T_2 relaxivity results and their comparability with Endorem™, all three SPIONs exhibited adequate characteristics for application as MRI contrast agents.

For use as a MRI tumour contrast agent, minimal SPION toxicity is a requirement. Cytotoxicity of the SPIONs was evaluated by MTT analysis. Results demonstrate no effect on the cells proliferation or viability when incubated with the functionalised and non-functionalised SPIONs at a concentration of 0.1 mg/ml. These results

therefore, show the Sm3E functionalised d50, PEG-d50 ad PEG-d20 can safely and specifically, label the target CEA+ve LS174T cells. The cytotoxicity results are consistent with previous reports, where dextran and PEGylated SPIONs at concentrations below 0.1 mg/ml exert minimal toxicity (Li *et al*., 2009; Villanueva *et al*., 2009).

The selective MR imaging potential of the Sm3E-d50 conjugates was investigated *in vitro* using the CEA+ve LS174T cells; the CEA-ve A375M cells were used as controls. Incubation of the Sm3E-d50 with the CEA+ve LS174T cells resulted in a marked T_2 signal reduction, correlating with increase in SPION uptake (*see section*: 4.3.1 Quantification of SPION uptake). These results support the findings that the Sm3E functionalised d50 SPIONs specifically bind to CEA+ve LS174T cells and furthermore, induce a specific reduction in T_2 contrast. Incubation of the d50 with the CEA-ve A375M cells resulted in a slight drop in T_2 relaxivity however; this was negligible and consistent with a recent report by Li *et al*., who demonstrated a slight T_2 reduction with control cells containing no SPIONs (Li *et al*., 2009).

The feasibility of using dextran coated SPIONs as specific tumour contrast agents has been previously demonstrated with different antibodies for example, anti CEA mAb (Tiefenauer *et al*., 1993), anti EGFR mAb (Suwa *et al*., 1998), anti-9.2.27 and anti-her2/neu mAbs (Funovics *et al*., 2004) and anti colorectal mAb A7 (Toma *et al*., 2005). However, dextran coated particles may have limited application for tumour targeting *in vivo*, due to rapid clearance by the RES. One way to address this is use PEGylated SPIONs. For this reason, the selective MRI potential of the PEGylated SPIONs was investigated.

MRI results demonstrated the Sm3E-PEG-d50 to specifically bind the CEA+ve LS174T cells, resulting in a 57% reduction in T_2 values. In contrast the non-functionalised PEG-d50 resulted in an 11% reduction in T_2, indicating only a limited amount of non-specific interaction with the CEA+ve LS174T cells, consistent with iron uptake measurements. These T_2 result are very similar to that of the d50, suggesting intracellular uptake has no imaging benefit *in vitro* over the non-internalising SPIONs. However, unlike the d50, there was an approximate 50% reduction in T_2 value for the CEA-ve A375M cells following incubation with both

the Sm3E-PEG-d50 and non-functionalised PEG-d50. These results strongly suggest non-specific uptake by the CEA-ve A375M cell line and also support the non-specific binding behaviour observed in the CLSM images (*see section*: 4.3.3 Effect of SPION surface chemistry)

The PEGylated SPIONs have shown to internalise and localise in endosomal compartments of the cells (*see section*: 4.3.4 Intracellular trafficking). Thus it was postulated that if further trafficked to the lysosomes the SPIONs were likely to be digested into their Fe2+ and Fe3+ states (Okon *et al*., 1994; Gupta *et al*., 2004). The disintegration of the magnetite cores has been reported to cause 10 fold loss in signal (Briley-Saebo *et al*., 2004). This however, was not evident from the MRI results. The sufficient MRI potential of the PEG-dSPIONs following internalisation is supported by a number of other studies (Garden *et al*., 2006; Li *et al*., 2009; Yang *et al*., 2009). The fact the SPIONs are still functional could suggest the SPIONs have escaped from lysosomal degradation (Cartiera *et al*., 2009).

As demonstrated in section 4.3.3 (Effect of SPION surface chemistry) non-specific uptake was dependent on hydrodynamic radii and PEG content of the PEG-dSPION. Indeed, the smaller Sm3E-PEGd20 was readily visible on MRI when targeted to CEA+ve LS174T cells, resulting in a 51% reduction. This was not the case for either the non-targeted PEG-d20 or the CEA-ve A375M cells, demonstrating the Sm3E-PEG-d20s specificity to the CEA+ve LS174T cells. In conclusion, its small size, PEG coating and specific MRI potential makes the Sm3E-PEGd20 an attractive SPION for application as a specific tumour contrast agent.

It was evident from the MRI results that all the SPIONs showed binding to the A375M cells. This non-specific uptake by the A375M cell line compared to the LS174T line may be related to the particular cells and the size and charge of the SPIONs. Consistent with this, a number of groups have reported that the rate and extent of SPION uptake due to PEGylation (Zhang *et al*., 2002) and surface charge (Villanueva *et al*., 2009) can differ among cell lines (Cartiera *et al*., 2009).

The results in this chapter show the Sm3E-SPION conjugates to deliver tumour specific MRI *in vitro*. However, whether this can be translated *in vivo* is uncertain.

From the biodistribution results the Sm3E-d50, Sm3E-PEG-d50 and Sm3E-PEG-d20 demonstrate minimal uptake in the CEA+ve tumour cells, predominantly clearing to the spleen via the RES. The similar biodistribution of all the SPIONs was unexpected, as PEGylation and small hydrodynamic size are reported to improve RES evasion, and in turn, increase blood circulation time. Nanoparticles with prolonged circulation time have been shown to exhibit increased accumulation within tumour tissues via the enhanced permeability and retention effect (Modi *et al.*, 2006) and when functionalised with a targeting ligand are retained by the tumour cells (Pun *et al*., 2004). However, this was not observed with the Sm3E-SPION conjugates investigated, results suggest the PEG-d20 SPION to be just as exposed to RES uptake as the non-PEGylated and larger d50. A possible reason for poor RES evasion shown by the PEGylated SPIONs could be due to the density and length of the PEG chains. The lengths of the PEG chains absorbed onto the SPIONs used in this study are approximately 300 MW. It has been reported that for PEGylated SPIONs to evade the RES a PEG chain MW of 2000 or greater is required (Owens *et al*., 2006; Er *et al*., 2009). The longer length PEG chains form a denser protective layer around the SPIONs, effectively blocking opsonisation from occurring. Therefore, it is likely that the short PEG chains are not adequately masking the dextran matrix from plasma protein opsonisation.

5.5 Summary

The aim of the work presented in this chapter was to test the potential of scFv functionalised SPION for specific MR imaging of cancer cells.

To achieve this, SPIONs were functionalised with Sm3E an anti CEA scFv and tested for their imaging potential with CEA+ve LS174T cells and CEA-ve A375M cells. The level of SPION specificity to the target cell was illustrated by T_2 weighted images and relaxometry values.

The Sm3E functionalised d50 and PEG-d20 exhibited excellent specificity to the target CEA+ve LS174T cells causing approximately 50% reduction in T_2 relaxation, whereas negligible reduction was seen for the controls. The PEG-d50 however, caused substantial T_2 signal reduction of CEA-ve A375M control cells, revealing its

non-specific binding behaviour. Intracellular uptake of SPIONs had no imaging advantage or disadvantage over membrane bound SPIONs, with T_2 reduction for all three SPIONs found to be similar. In addition, viability of the cells was unaffected by exposure to the d50, PEG-d50 and PEG-d20 at a concentration of 0.1 mg/ml. Biodistribution results however, demonstrated minimal uptake of the Sm3E functionalised SPION into the tumour cells, with the majority accumulating in the spleen. Further optimisation of the Sm3E-SPION conjugates surface properties is required to improve their tumour targeting potential *in vivo*.

Chapter 6

Therapeutic Potential of Functionalised SPIONs

6.1 Introduction

Previous work in this thesis has shown that SPIONs can target specifically to cancer cells. The aim of the work presented in the present chapter was to test whether scFv-targeted SPIONs could have the potential to deliver hyperthermic therapy to cancer cells when subjected to an alternating magnetic field (AMF) (*see section*: Application of SPIONs in hyperthermia).

It has been shown by others that the hyperthermic potential of the SPIONs is dependent on the current and frequency parameters of the AMF they are subjected to (Hergt et al., 2004b). To test this and identify a suitable AMF for induction of magnetic fluid hyperthermia MFH, two AMF strengths were investigated.

Another important factor that can affect the hyperthermic potential of the SPIONs is the SPIONs chemical and physical characteristics (Wang *et al*., 2005; Pankhurst *et al.*, 2003; Fortin et al 2007; Motoyama *et al*., 2008). To test this six SPIONs of different size and chemical composition were investigated and SPION characteristics suitable for AMF induced SPION heating were identified.

In addition, cell loading of SPIONs is also reported to be a crucial factor that can affect their hyperthermic potential (Kalambur *et al*., 2007; Kettering *et al*., 2007). Functionalisation of the SPIONs with Sm3E substantially increased specific cell uptake (*see section*: 4.3.1 Quantification of SPION Uptake). Furthermore, depending on their surface properties the SPIONs localised either extracellularly or intracellularly. The therapeutic impact of cell loading and intracellular uptake for MFH was investigated by viability measurements and cellular response of the heat shock protein 70 (HSP70).

6.2 Objectives

The objectives of the research described in this chapter were to:

1. Determine whether hyperthermia can affect cell viability

2. Identify the AMF strength for optimal SPION heating

3. Identify optimal SPION characteristics for magnetic fluid hyperthermia

4. Measure the magnetic fluid hyperthermia cell response on;
   a) Viability
   b) Heat shock protein expression

6.3 Results

6.3.1 Temperature effect on cell viability

To establish whether heat treatment can affect cancer cells, the CEA+ve LS174T cells were exposed to temperatures of 37°C through to 47°C for 20 min. To determine cell viability, live cell numbers were counted 30 min after heat treatment and MTT assays were performed 96 hrs following heat treatment. All results were compared against a non-treated control. Results from both the cell viability counts and MTT assay show that heat can lead to cell death, with both assays showing complete cell death at 46°C (Fig 6.1). Therefore, a temperature increase of 9°C is enough to cause approx 95-100% cell death. A temperature increase of 5-6°C was sufficient to cause approx 50% cell death. Both assays agree that a 3°C temperature rise has no short term detrimental affect on cell survival. From comparison of cell viability results taken at 30 min and 96 hrs following treatment, no significant difference in cell viability was observed. These results therefore, suggest cell death via heat is an immediate effect.

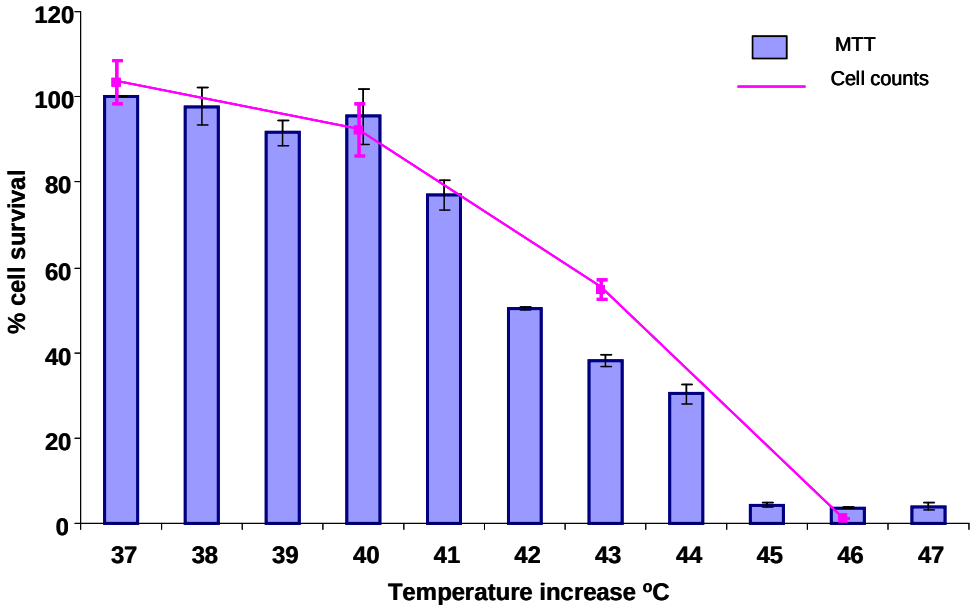

Fig 6.1 Effect of environmental temperature on cell survival as measured by cell viability counts (pink line) and MTT assay (blue bars).

6.3.2 Temperature effect on cellular HSP70 response

Although environmental temperatures below 40^{o}C caused minimal cell death the low increase in temperature may cause stress to the cells. When cells become stressed, they up regulate a number of proteins including HSP70. To determine whether an increase in environmental temperature can cause cells to become stressed and express HSP70 an *in vitro* assay was designed (*see section*: 2.2.8.3). For this experiment CEA+ve LS174T cells were grown on coverslips and incubated at 37^{o}C, 40 ^{o}C and 43 ^{o}C. HSP70 expression was detected using an anti HSP70 mAb (red) and visualised by CLSM.

Results from CLSM analysis show that a 3^{o}C temperature rise induces HSP70 expression, as indicated by the red fluorescence (Fig. 6.2). Furthermore, results reveal HSP70 expression to increase with increasing temperatures, indicating the cells to become more stressed with increasing temperatures. CLSM results also show cell viability to reduce with temperature increase, as fewer cells are observed at 43^{o}C.

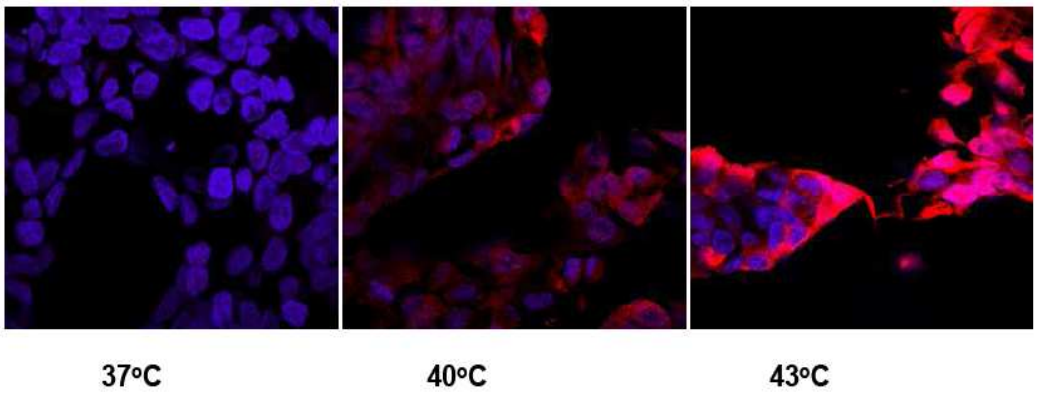

Fig. 6.2. Induced HSP70 expression in CEA+ve LS174T cells following heat treatment as illustrated by CLSM. The CEA+ve LS174T cells were incubated at temperatures 37^{o}C, 40^{o}C. and 43^{o}C. Samples were heated for 20 min, and left for 4 hr at 37 ^{o}C to allow for HSP70 expression. Detection of induced HSP70 (red) was performed with a mouse anti HSP70 primary antibody, followed by a anti mouse alexa fluor 594 antibody. Nuclei were stained with Hoechst (blue).

6.3.3 Magnetic fluid hyperthermia using AMF system 1

To investigate the MFH potential of the SPIONs studied in this thesis the AMF system 1 (Fig. 6.3) was used, this applies an AMF strength of 300 V, 0.62 A and 139.8 kHz.

6.3.3.1 AMF induced heating of d100 and DX100

To test whether the AMF strength of 300 V, 0.62 A and 139.8 kHz is suitable to induce magnetic heating of SPIONs, increasing concentrations of the d100 and DX100 were placed in the AMF coil for 20 min. The temperature increase over time was measured using temperature probes. To remove any false heating due to the coil, which gets hot itself, the coil was kept cool through constant cycling of cold tap water.

AMF System 1: 300 V, 0.62 A and 139.8 kHz

A) **B)**

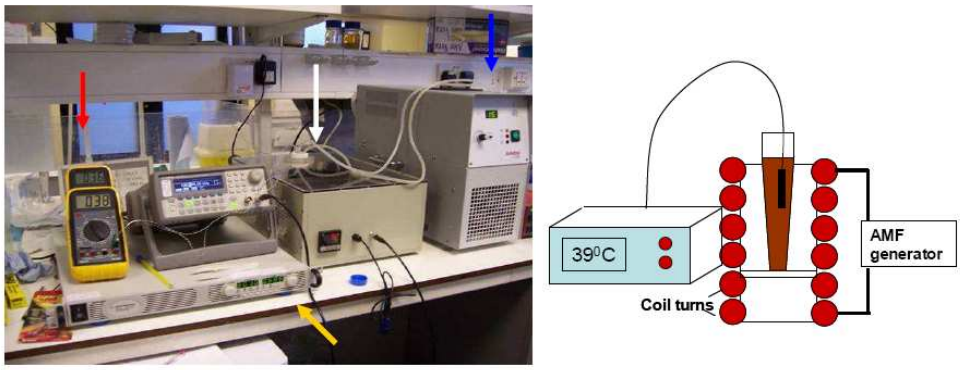

Fig. 6.3. Image A: AMF system 1, applies a field strength of 300 V, 0.62 A and 139.8 kHz. SPION samples at 1 ml are placed into the coil (white arrow), AMF field is applied by power generator for 20 min (yellow arrow). Fluid temperature increase was measured using temperature probes (red arrow). The coil was kept cool by water cooler (blue arrow). Image B: Schematic representation of SPION sample placed into AMF heating coil.

Following AMF treatment, results from the temperature probes show when starting at room temperature the d100 SPIONs to cause no increase in fluid temperature at concentrations of 1 mg/ml and 5 mg/ml, and only a 2^{o}C temperature rise at a concentration of 25 mg/ml (Fig. 6.4). In comparison, the temperature probes showed the DX100 to cause slightly better heating when subjected to the AMF. At a concentration of 5 mg/ml, the AMF treated DX100 generated a temperature increase of 2^{o}C (Fig. 6.4) and at concentrations of 25 mg/ml a temperature increase of 8^{o}C was measured. These results show the SPIONs are capable of generating heat when in an AMF of 300 V, 0.62 A and 139.8 kHz. The heating observed was also shown to be concentration dependent.

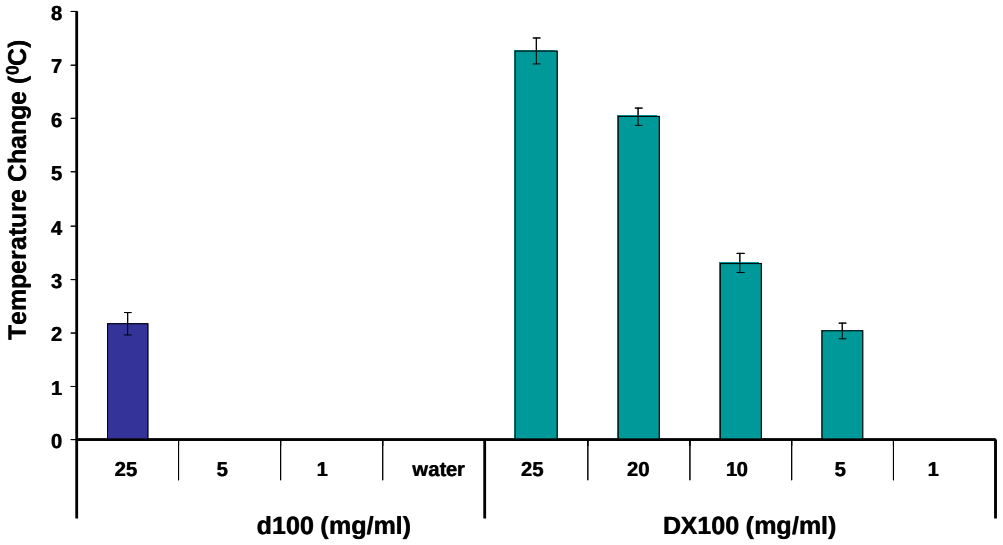

Fig. 6.4. Temperature increase of 1 ml of water by the d100 and DX100 at concentrations 1 mg/ml to 25 mg/ml during AMF treatment (300 V, 0.62 A, 139.8 kHz). Change in temperature was measured using probes placed into solution. Experiments were started at room temperature.

6.3.3.2. Cell viability following magnetic fluid hyperthermia

To determine whether the temperature increase generated by the DX100 when subjected to AMF system 1 would be enough to cause cell kill, an *in vitro* MFH assay was developed and cell viability determined by live cell counts. For this

experiment the CEA+ve LS174T cells were suspended in 1 ml non-functionalised DX100 SPIONs at 1 mg/ml, 5 mg/ml, 10 mg/ml, 25 mg/ml and media as a control. The samples were placed into the coil of the AMF system. A probe was placed in the sample and in the coil to monitor the environmental temperature. The samples were subjected to the AMF for 20 min. Following AMF treatment, viable cells were counted.

Results in Fig 6.5 show that before AMF treatment the DX100 SPIONs exhibited cytotoxicity. At a concentration of 10 mg/ml and 25 mg/ml over 95% cell death was observed and at 5 mg/ml cell death was approximately 75%. Following AMF exposure, the DX100 showed no significant effect on cell viability at 1mg/ml. Furthermore, no effect on cell viability at DX100 SPION concentrations 5mg/ml and above following AMF treatment could be observed due to toxicity. This result suggests that the heat generated by the DX100 SPIONs following exposure to AMF system 1 is not sufficient to cause MFH cell death at 1mg/ml. In addition, DX100 SPIONS 'as are' are toxic to cells at concentrations of 5mg/ml or higher.

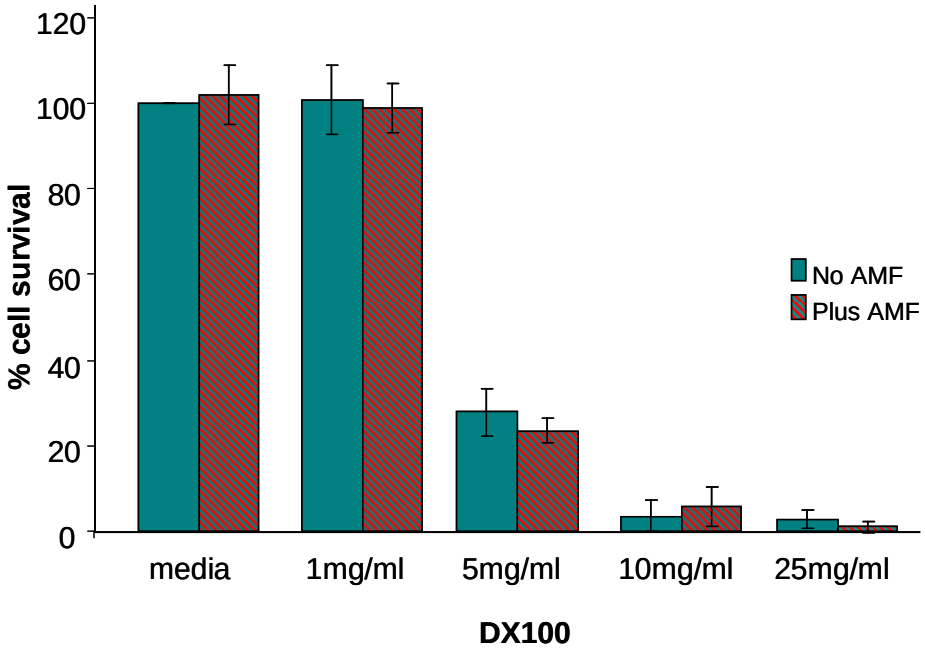

Fig. 6.5 Percentage cell survival of CEA+ve LS174T cells suspended in DX100 before and after AMF hyperthermic treatment. Following treatment cell viability counts were performed and the percentage cell survival determined against media only control.

6.3.3.3 Induction of HSP by magnetic fluid hyperthermia

Although no cell death was apparent following MFH in AMF system 1 using DX100 SPIONs, the cells could be showing signs of stress. As observed is section 6.3.2, a small temperature increase can lead to cellular stress and expression of the HSP70. To determine whether DX100 SPIONs when subjected to the AMF can up-regulate HSP70 expression, an *in vitro* assay was designed (*see section*: 2.2.8.5). For this experiment, CEA+ve LS174T cells were grown on coverslips and incubated in either 1 mg/ml DX100 or 0.1mg/ml Sm3E-DX100. For targeted MFH using the Sm3E-DX100, the cells were washed to remove unbound particles and incubated in fresh culture media before AMF treatment. The cells were placed in the AMF for 20min. Four controls were used i) media only, ii) media + AMF iii) 1mg/ml DX100 no AMF and iv) 0.1mg/ml Sm3E-DX100 no AMF. The expression of the HSP70 was detected using mouse anti HSP70 (red) and visualised by CLSM.

Results from CLSM revealed expression of HSP70 to be minimal for control cells treated in media only (Fig. 6.6a). Following exposure to the AMF, the media only controls showed a small amount of HSP70 expression, as indicated by the red fluorescence (Fig. 6.6b); suggesting AMF alone to cause stress to the cells. The cells also showed up-regulation of HSP70 expression following incubation in 1 mg/ml DX100 (Fig. 6.6c), demonstrating the DX100 SPIONs to also cause stress to the cells. However, following exposure of the cells incubated with DX100 to the AMF, a further increase in HSP70 expression was observed (Fig. 6.6d). Furthermore, following AMF treatment of cells bound to the Sm3E-DX100, a substantial increase in HSP70 was evident. These results therefore demonstrate that even when MFH does not cause cell death the cells do experience stress, as shown by induction of HSP70 expression. In addition, cellular stress can be further enhanced by AMF treatment of CEA+ve LS174T cells specifically labelled with Sm3E functionalised SPIONs.

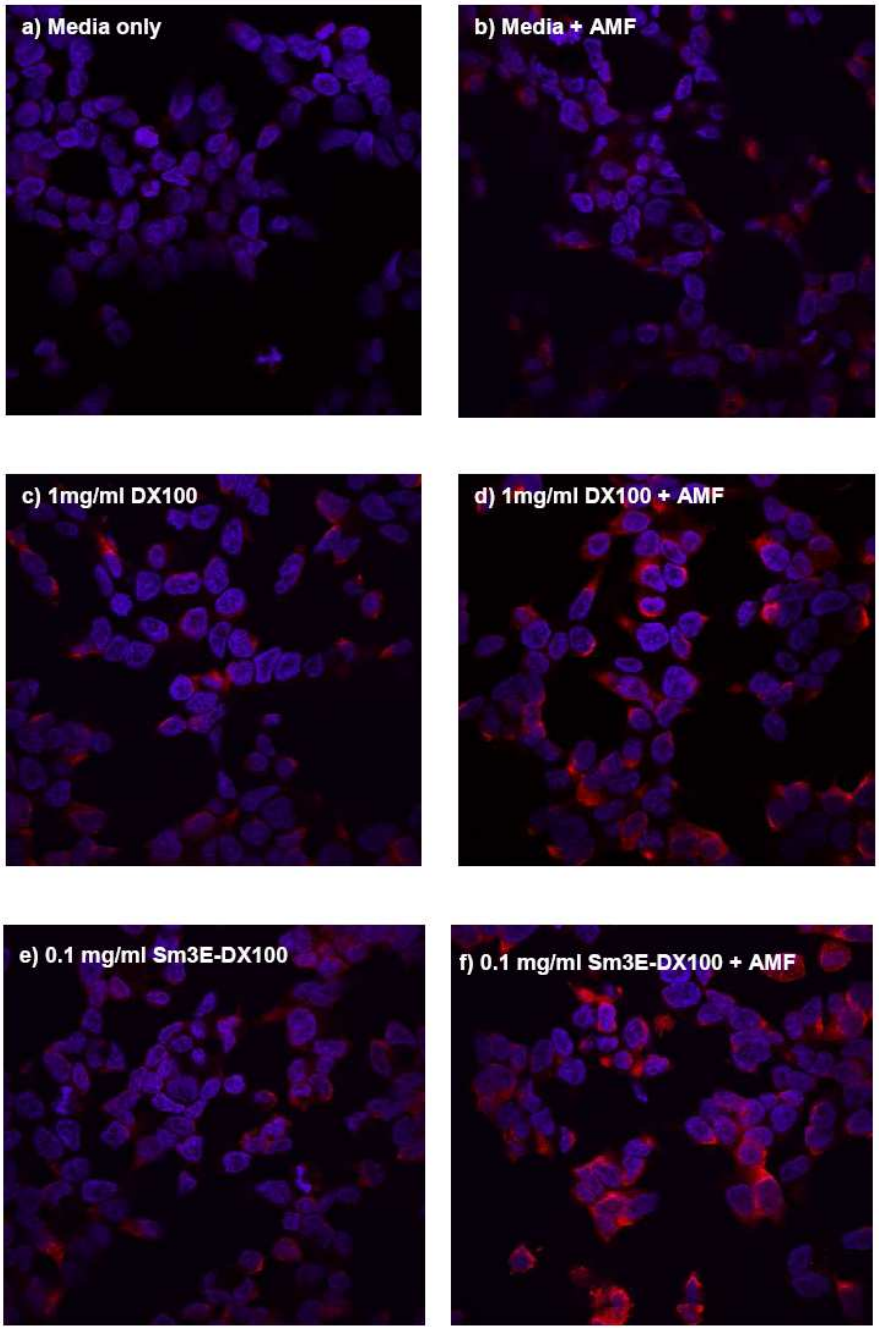

Fig. 6.6. CLSM images showing induced expression of the HSP70 following MFH. The CEA+ve LS174T cells were incubated in a) media only, b) media only plus AMF treatment, c) 1 mg/ml DX100, d) 1 mg/ml DX100 plus AMF treatment, e) 0.1mg/ml Sm3E-DX100 and f) 0.1mg/ml Sm3E-DX100 plus AMF.. Samples were incubated for a further 4hrs following AMF treatment at 37^{o}C. Detection of induced HSP70 was performed with a mouse anti-HSP70 primary antibody, followed with an anti-mouse alexa fluor 594. Nuclei were stained with Hoechst.

6.3.4 Magnetic fluid hyperthermia using AMF system 2

To investigate if the heating potential of the SPIONs could be improved using a larger AMF, a second system was developed in collaboration with Professor Quentin Pankhurst (The Royal Institution of Great Britain). The AMF system 2 (Fig 6.7) applies a higher field strength of 150 V, 0.74 A, 1 MHz. In addition, AMF system 2 also has an Air-Therm ATX attached, which pumps a constant air-flow of 37^{o}C through the coil area, allowing the surrounding temperature to be maintained at 37^{o}C. The application of the Air-Therm ATX was a crude way to represent how blood flow may affect the heating potential of the SPIONs, demonstrating the effect dissipation of heat would have on the overall rise in fluid temperature.

AMF System 2: 150 V, 0.74 A and 1 MHz

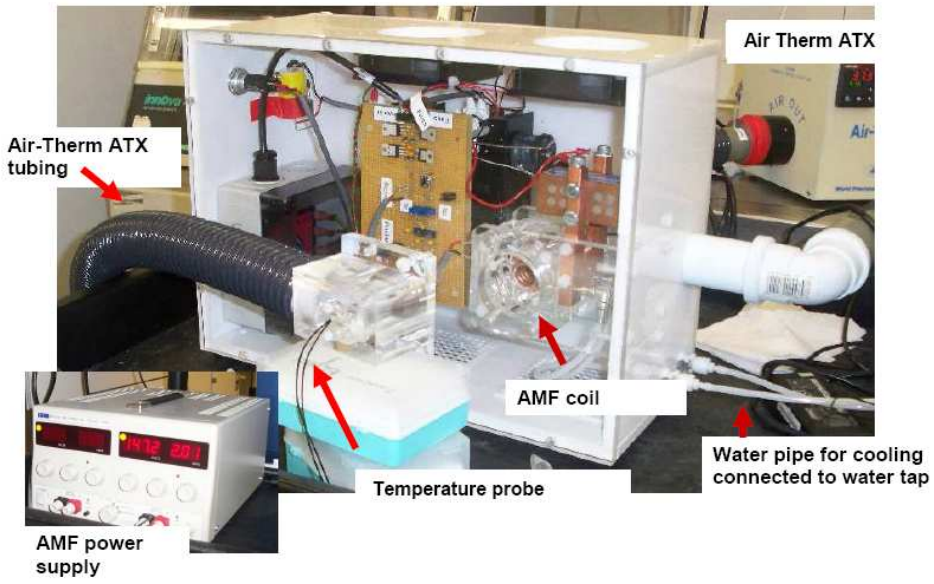

Fig. 6.7. Image of AMF system 2, applies AMF strength 150 V, 0.74 A, 1 MHz. 0.5-1 ml SPION samples are placed into the coil, the environmental temperature was maintained at 37^{o}C by Air-Therm ATX and the AMF coil was kept cool by connection to water supply. The AMF was applied for 20 min and temperature increase was measured by Luxtron thermometer probes.

6.3.4.1 AMF induced heating of d100

The heating potential of the d100 was tested in AMF system 2 and the effect of the Air-Therm ATX was evaluated. Colloidal suspensions of the d100 at 0.05 - 5 mg/ml were placed in AMF system 2 and subjected to AMF for 20 min. This experiment was performed with and without the Air-Therm ATX.

Results showed that without the 37^{o}C Air-Therm ATX, the d100 at 5 mg/ml caused a fluid temperature increase of 35^{o}C when subjected to AMF 2 (Fig 6.8). Furthermore, a temperature increase of 1^{o}C was recorded at a d100 concentration of 0.1 mg/ml. These results demonstrate that application of the higher AMF strength, using AMF system 2, vastly improves the heating potential of the d100. However, following application of the Air-Therm ATX, the fluid temperature increase generated by d100 at 5 mg/ml reduced by 50% to 14^{o}C. The 50% drop in temperature rise is most likely due to the 37^{o}C airflow, generated by the AIR-Therm ATX. Though the temperature increase of the SPION fluid was less when the Air Therm ATX was applied, the temperature increase measured was still better than with AMF system 1.

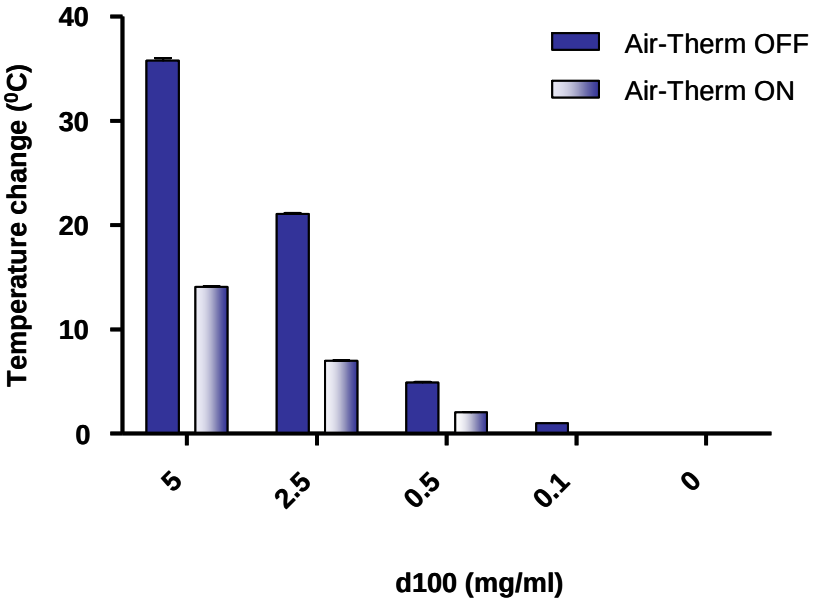

Fig. 6.8. Temperature rise of 0.5 ml of water in 1.5 ml eppendorf tubes by d100 at concentrations 0.1 mg/ml to 5 mg/ml when place in AMF (150 V, 0.74 A, 1M Hz). Change in temperature measured (relative to the starting temperature of 37C) using Luxtron probes placed into solution.

6.3.4.2 AMF induced heating of d50, PEG-d50 and PEG-d20

Following on from the d100, the heating potential of the d50, PEG-d50 and PEG-d20 were also tested using AMF system 2 plus Air-Therm ATX. Results showed a dramatic difference in the heat generated between the different sized SPIONs (Fig. 6.9). In comparison to d100, which at 5 mg/ml caused a fluid temperature increase of approximately 14^{o}C when exposed to AMF 2, the d50, PEG-d50 and PEG-d20 at 5 mg/ml caused only a 3^{o}C - 4^{o}C temperature rise. Results also show the heating potential of the d50 and PEG-d50 to be similar; indicating the adsorption of PEG has little effect on the heat generated.

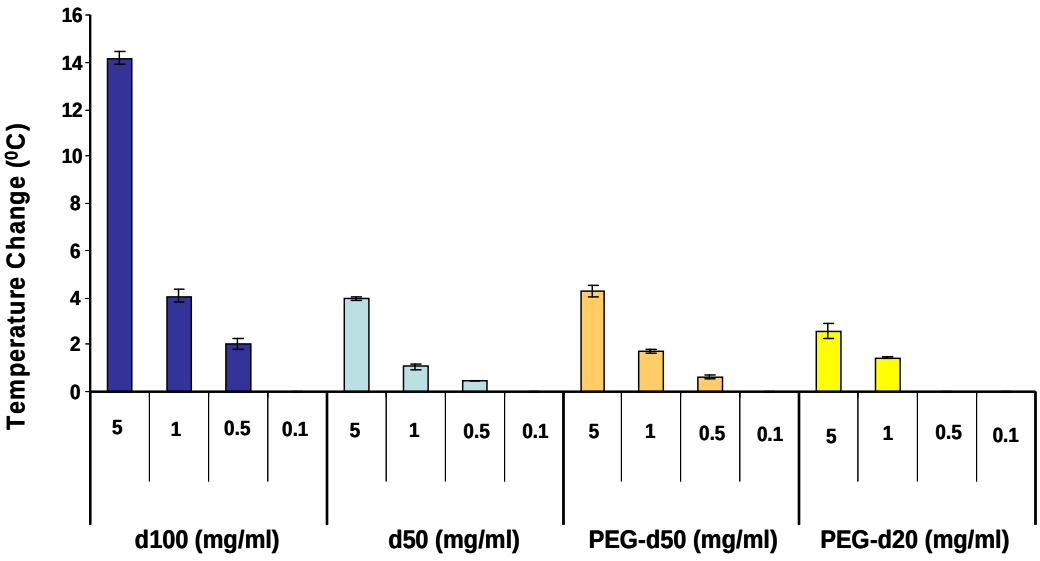

Fig. 6.9. Temperature rise of 0.5 ml of water induced by AMF treatment of the d100, d50, PEG-d50 and PEG-d20 at concentrations 0.1-5 mg/ml. Environmental temperature was maintained at 37^{o}C with the Air-Therm ATX. The Change in fluid temperature was measured (relative to the starting temperature of 37 ^{o}C) using Luxtron probes placed in solution.

6.3.4.3 AMF induced heating of DX100

The heating potential of the DX100 using AMF system 2 was also tested. Results showed AMF system 2 to substantially improve the heating potential of the DX100. Results presented in Fig. 6.10 demonstrate even with the Air-Therm ATX attached,

the DX100 at a concentration of 5 mg/ml caused a fluid temperature increase of 25^{o}C when exposed to AMF 2. Furthermore, the DX100 at a concentration of 0.25 mg/ml and 0.05 mg/ml caused a temperature increase of 2^{o}C and 0.5^{o}C (Fig 6.5). From comparing the heating profiles of all the SPION tested, the DX100 was found to be the superior heater.

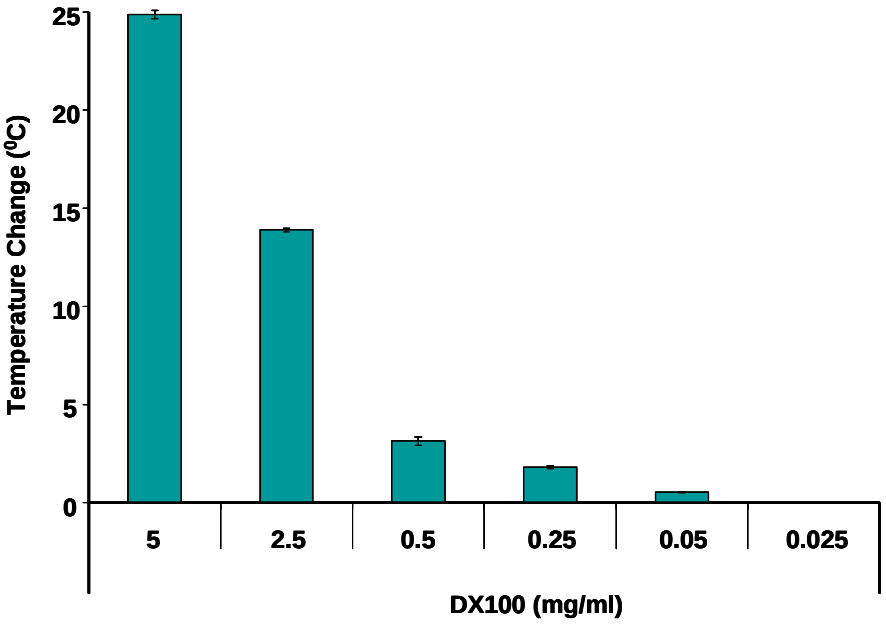

Fig. 6.10. Temperature rise of 0.5 ml of water in 1.5 ml eppendorf tube by DX100 at concentrations 0.025 mg/ml to 5 mg/ml during exposure to AMF of 150 V, 0.74 A, 1 MHz. Temperature of solution started at 37^{o}C using Air-Therm ATX. Change in temperature measured using Luxtron probes placed into solution. Water was used as control sample.

6.3.4.3. Cell viability following magnetic fluid hyperthermia

To determine whether the temperature increase generated by the d100, DX100, d50, PEG-d50 and PEG-d20 when subjected to AMF 2 would be enough to cause cell kill an *in vitro* MFH assay was developed (*see section*: 2.2.8.4) and cell viability determined by the MTT assay. For this experiment, non-functionalised SPIONs at a concentration of 0.1-5 mg/ml and Sm3E functionalised SPIONs at a concentration of

0.1 mg/ml were incubated with the CEA+ve LS174T cell line. Only for the Sm3E functionalised SPIONs were the cells washed and incubated in fresh media before AMF treatment, this was to allow only the Sm3E-SPIONs bound to the cell to cause any hyperthermic affect. The cells were subjected to AMF 2 for 20 min and cell viability determined 96 hrs later by MTT assay.

The MTT results presented in Fig. 6.11 show the DX100 at 2.5 mg/ml caused a 25% drop in cell viability even before exposure to the AMF, suggesting cytotoxicity of the DX100 at 2.5mg/ml this is in accordance with Fig 6.5 which showed DX100 cytotoxicity at 5mg/ml. Cell death was further increased when the DX100 were subjected to AMF 2. AMF treatment of the DX100 at 1-2.5 mg/ml was shown to cause approx 95% cell death, most likely due to MFH. However, at a DX100 concentration <0.5 mg/ml, treatment with AMF 2 did not appear to cause cell death. Furthermore, binding of Sm3E functionalised DX100 to the cells showed no effect on cell viability before and after AMF treatment. These results suggest that the DX100 have the potential to cause cell death via MFH when exposed to AMF 2, but only at concentrations above 1 mg/ml.

In comparison to the DX100, the d100 was slightly more cytotoxic (Fig 6.11). The MTT results show that before exposure to AMF 2 the d100 at 5 mg/ml and 2.5 mg/ml caused approx 95% and 50% cell death. Following AMF treatment of the remaining 50% of cells incubated in the d100 at 2.5mg/ml, complete cell kill was observed, again most likely due to MFH. However, cells incubated in d100 at concentration <1 mg/ml and when bound to Sm3E functionalised d100 showed no cell death before or after treatment in AMF 2.

.

Investigation into the MFH potential of the d50, PEG-d50 and PEG-d20 revealed all three SPIONs at a concentration of 5-2.5 mg/ml to exhibit some level of cytotoxicity before AMF treatment (Fig. 6.12). In addition, results showed cytotoxicity to increase with SPION size. Following AMF treatment of the d50, PEG-d50 and PEG-d20 no effect on cell viability was observed. These results suggest that d50, PEG-d50 and PEG-d20 are not capable of inducing MFH cell death when subjected to AMF system 2.

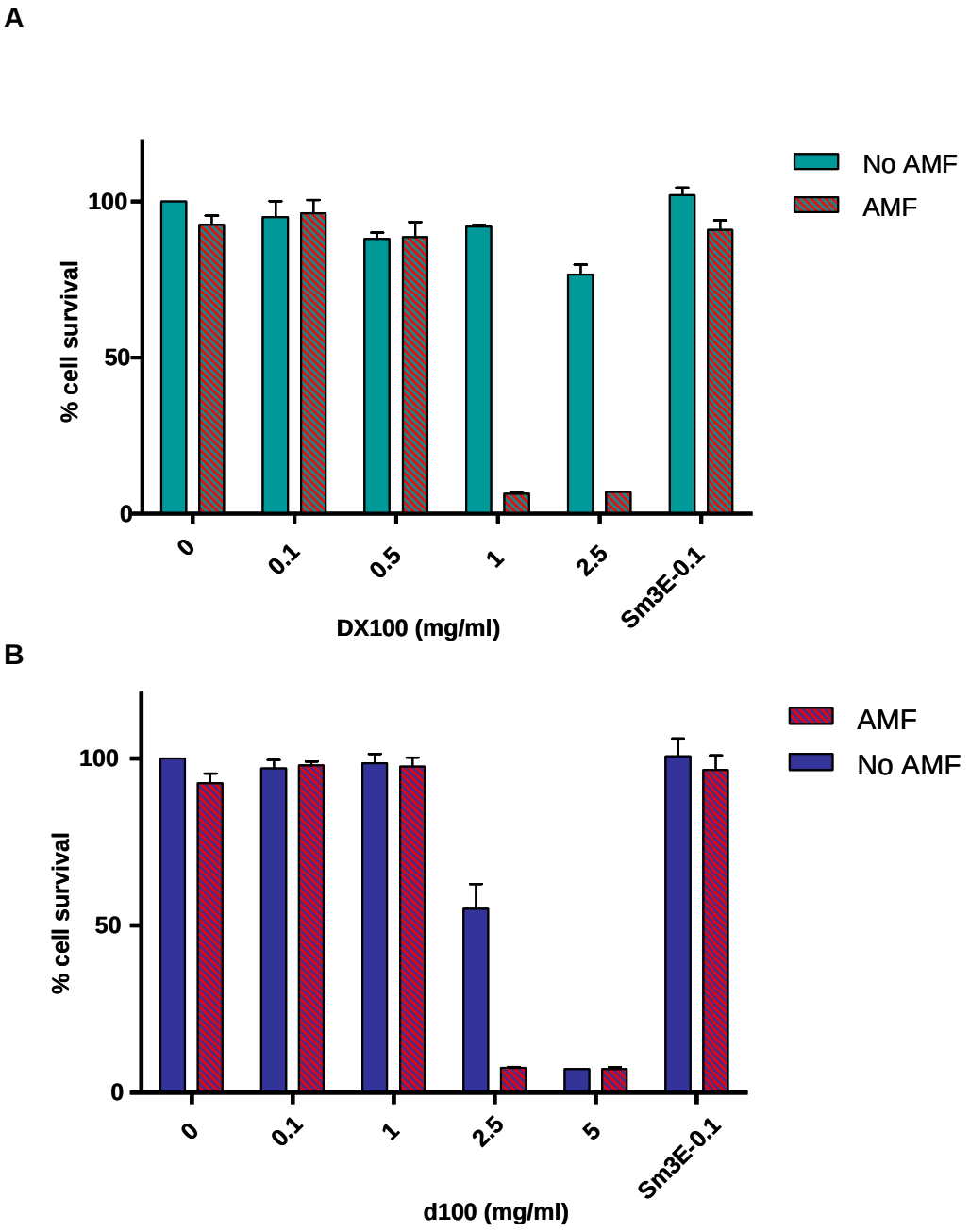

Fig. 6.11. Percentage Cell survival of CEA+ve LS174T cells incubated in A) DX100 and Sm3E-DX100 and B) d100 and Sm3E-d100 before and after AMF hyperthermic treatment. Only the cells incubated with 0.1mg/ml Sm3E functionalised SPIONs were washed and incubated in fresh media before AMF treatment, this was to allow only the Sm3E-SPIONs bound to the cell to cause any hyperthermic affect. Following treatment MTT assay was performed; absorbance was read at 550 nm and percentage cell survival determined against media only control.

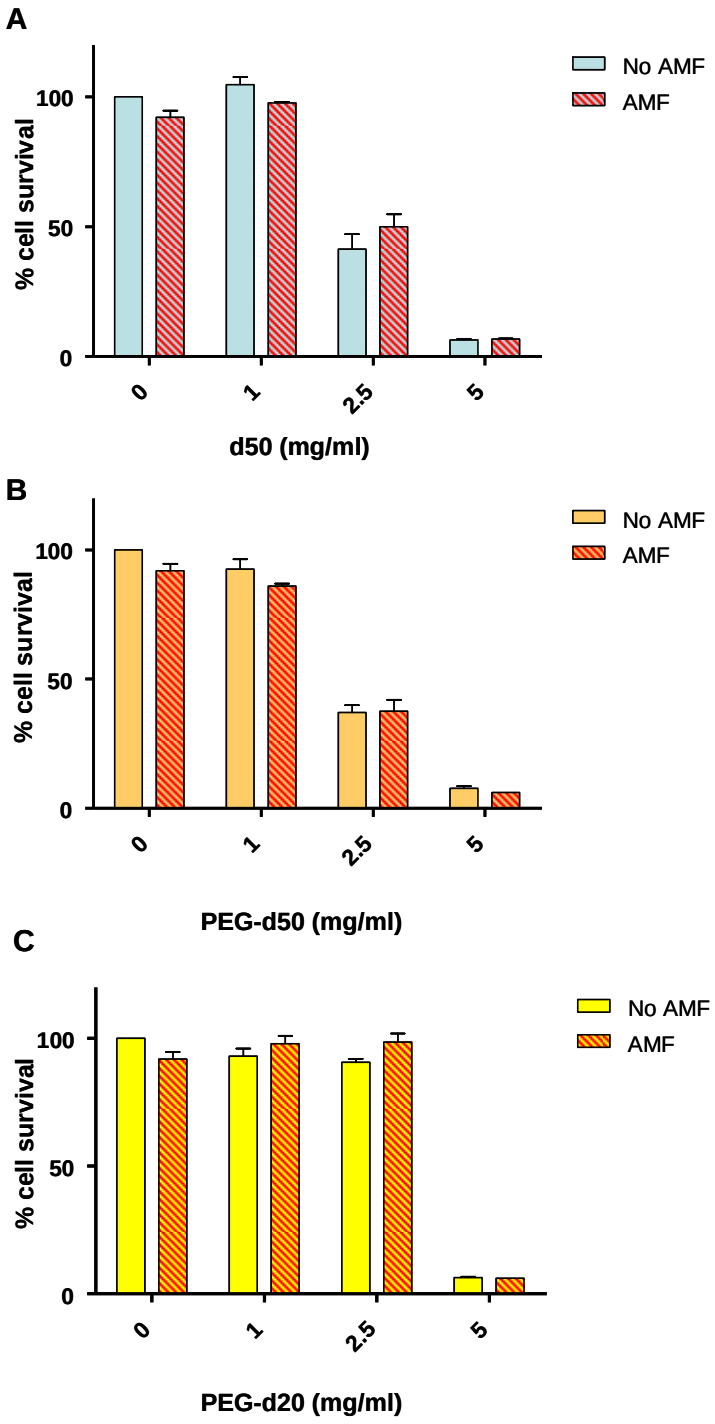

Fig. 6.12. Percentage Cell survival of CEA+ve LS174T cells incubated in A) d50 B) PEG-d50 and C) PEG-d20 before and after AMF hyperthermic treatment. Following AMF treatment MTT assay was performed; absorbance was read at 550 nm and percentage cell survival determined against media only control.

6.3.5 Effect of cellular uptake of SPIONs on magnetic fluid hyperthermia

6.3.5.1 Cell loading

From the previous results (*see section*: 6.3.3.3) AMF treatment of CEA+ve LS174T cells bound to Sm3E functionalised SPIONs caused expression of HSP70 in AMF system 1 but no cell kill *in vitro*. Furthermore, no cell kill was evident with the Sm3E-SPION labelled cells following treatment with AMF system 2, even though exceptional heating was observed. The lack of cell kill could be due to insufficient SPION uptake, the cells tested in section 6.3.3.3 were labelled with approx 6 pg of SPIONs per cell (*see section*: 4.3.1). To increase the cell uptake of SPIONs the cells were incubated at 37^{o}C overnight with Sm3E-DX100 or DX100 as a control, at a concentration of 2 mg/ml, 1 mg/ml or 0.5 mg/ml. Following incubation, results show SPION uptake to be approx 250 pg/cell, 240 pg/cell and 180 pg/cell respectively (Fig. 6.13).

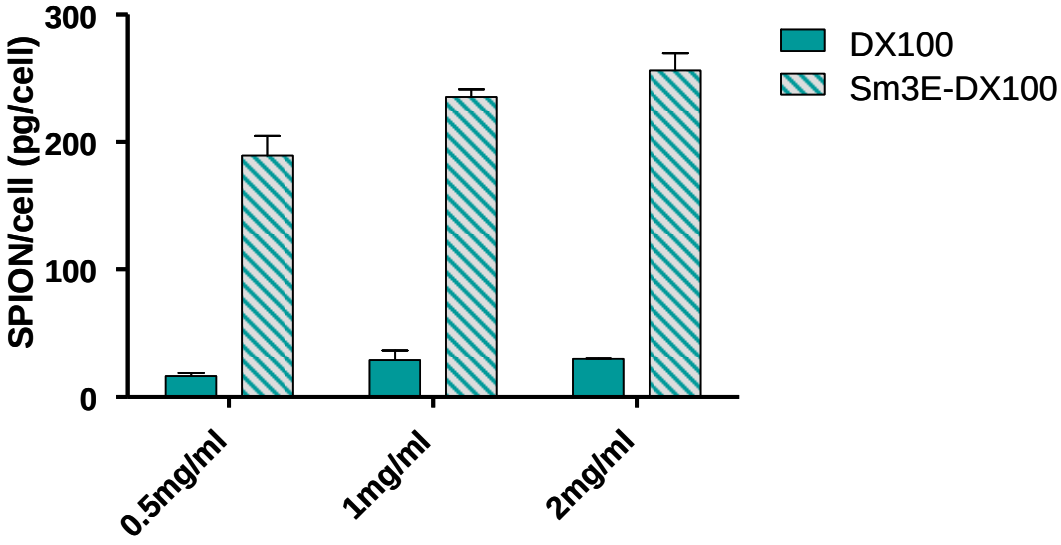

Fig. 6.13. Uptake of Sm3E-DX100 SPIONs by CEA+ LS174T cells as quantified by ferrozine based assay. With reference against standard curve of ferrozine assayed SPIONs the numbers of SPIONs taken up per cell were calculated following incubation in 0.5mg/ml, 1mg/ml or 2mg/ml.

To determine if increased SPION uptake leads to MFH cell death the SPION loaded cells were subjected to AMF 2. From the MTT results (Fig 6.14) it is apparent that the increase in SPION uptake before AMF treatment resulted in a small amount of cytotoxicity, causing approx 20% cell death. However, following AMF treatment only a slight decrease (10%) in cell viability was observed, and only with the cells containing 250 pg of SPIONs. No effect on cell viability due to MFH was observed for the cells loaded with 180 pg and 240 pg of DX100 after exposure to AMF 2.

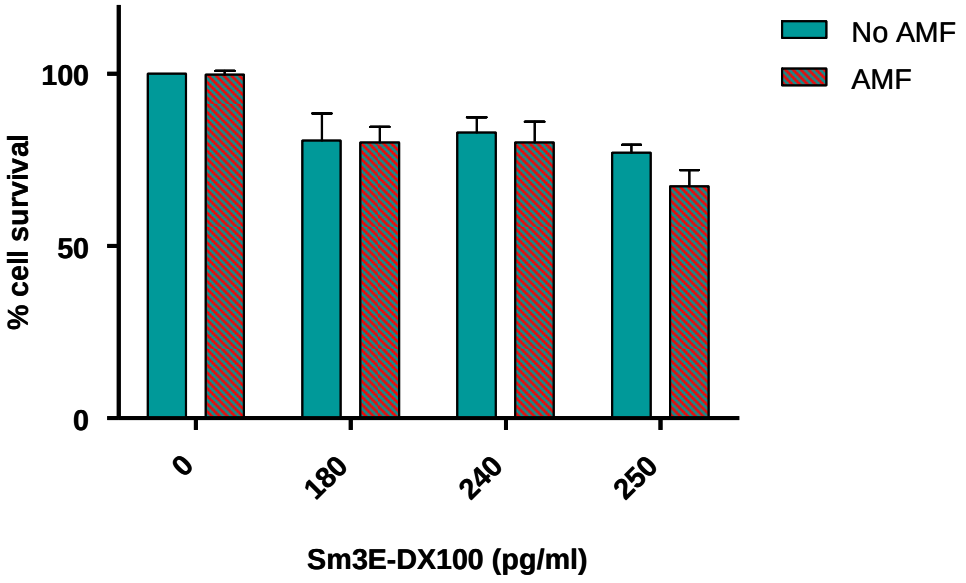

Fig 6.14. Percentage cell survival of CEA+ LS174T loaded with Sm3E-DX100 before and after AMF hyperthermic treatment. Following AMF treatment MTT assay was performed; absorbance was read at 550 nm and percentage cell survival calculated against media only control.

6.3.5.2 Heating mechanism

The lack of cell death following AMF treatment of the SPION loaded cells suggests the SPIONs are not heating when bound to the cells. One possible reason could be the attachment of the Sm3E-SPIONs to the cells, which may restrict the SPIONs movement thus its potential to heat via Brownian motion. To test this, the SPIONs

were suspended in two liquids of different viscosity, water and glycerol. Glycerol is a high viscosity liquid, which should restrict the frictional movement of the SPIONs and thus heating via Brownian motion. Following AMF treatment of the SPIONs, no difference in the SPION heating was observed (Fig. 6.15). These results suggest that reducing the movement of the Sm3E-SPION conjugates by attachment to CEA+ve cells does not affect the SPIONs heating potential when exposed to AMF 2.

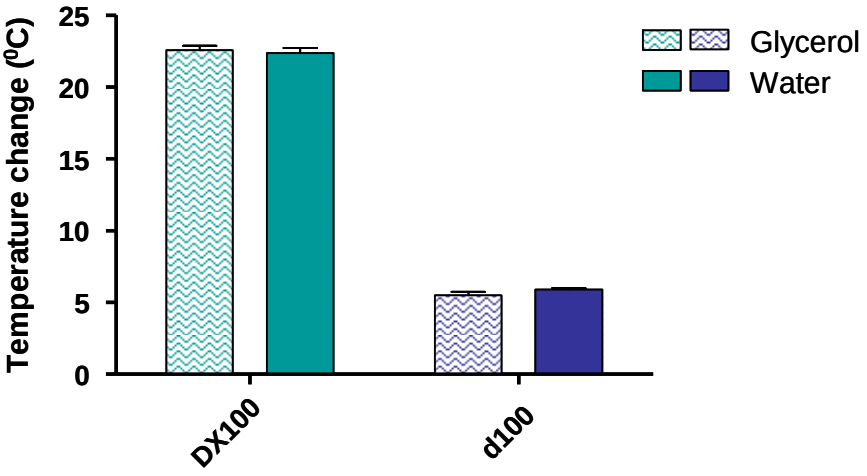

Fig. 6.15. Temperature rise of 5 mg/ml DX100 and 2.5 mg/ml d100 suspended in either water or glycerol following exposure to AMF (150 V, 0.74 A, 1 MHz). Temperature of solution started at 37°C using Air-Therm ATX. Change in temperature was measured using probes placed into solution.

6.4 Discussion

The work presented in this chapter has investigated the heating efficiency of the DX100, d100, d50, PEG-d50 and PEG-d20 within 2 AMFs. The results show that SPION size, concentration and AMF strength are important factors in achieving optimal SPION heating efficiency. Although all the SPIONs caused a fluid temperature increase when in the AMF, only the DX100 and d100 above 1 mg/ml caused hyperthermic cell kill. However, AMF treatment of cells specifically labelled with Sm3E-functionalised SPIONs showed increased HSP70 expression, indicating even a low temperature increase can cause cellular stress and potentially sensitise cells to treatments.

Using heat to destroy or weaken cells towards radiotherapy or chemotherapy has been a common procedure in the clinic (Samanta *et al*., 2008). Furthermore, tumour tissues tend to have a higher sensitivity to heat than normal tissues (Cavaliere *et al*., 1967; Shinkai *et al*., 1995; Wang *et al*., 2005). Viability results following heat treatment of LS174T cells found that a temperature increase of 42-43^{o}C led to a 50% drop in cell viability and a temperature rise over 46^{o}C led to thermoblastation, where over 95% cells were destroyed, a number of other groups have also reported similar results (Jordan *et al*., 1999b; Mornet *et al*., 2004; Lao *et al*., 2004). Although cell viability following a fluid temperature rise of 38^{o}C – 40^{o}C was largely unaffected, analysis of the HSP70 revealed mild hyperthermia to cause cellular stress. Furthermore, the expression of the HSP70 increased with increasing temperature, indicating further stress to the cells. Expression of HSP70 could therefore, be used as a measurement of the effect of hyperthermia on cells. In addition, HSP70 has been reported to induce anti-tumour immunity (*See section:* 1.4 Hyperthermia).

For MFH the heating potential of the SPIONs should be as high as possible, to allow administration of the lowest SPION dose (Hergt *et al*., 1998). However, from the results the tested DX100 and d100 heating potential was very low when exposed to AMF system 1, resulting in an insufficient fluid temperature increase. In AMF system 1, therapeutically favourable temperatures could only be reached at already cytotoxic SPION concentrations. MFH induced cell kill was therefore not achievable

using the d100 and DX100 in AMF system 1. Although no MFH cell kill was achieved using AMF system 1, expression of HSP70 was detected, indicating increased stress in the cells, MFH induced HSP70 expression was also reported by Suzuki *et al*., and Ito *et al*., (Suzuki *et al*., 2003; Ito *et al*., 2004). Furthermore, LS174T cells specifically labelled with a low concentration of Sm3E functionalised SPIONs (6pg/cell) and exposed to AMF system 1 showed a substantial increase in HSP70 expression. This would suggest that Sm3E functionalised SPIONs when specifically attached to CEA are more effective in generating MFH induced cellular stress.

To test whether AMF strength affects the heating potential of the SPIONs a higher AMF strength was investigated. Application of AMF system 2 (150 V, 0.74 A, 1 MHz) substantially improved the heating potential of all the SPIONs and allowed therapeutic temperatures to be reached at non-toxic SPION concentrations. This result indicates the heating efficiency of SPIONs to be highly dependent on the AMF applied. The variation in the SPIONs heating potential when exposed to the two different AMFs could be due to the heating mechanism involved. The two heating mechanisms, Brownian and Neéls relaxation (*See section*; 1.2.2) are encouraged by different field strengths (Hergt *et al*., 2004b). Brownian relaxation predominantly occurs at 1-10 kHz, where as Neéls relaxation peaks at 200 kHz (Hergt *et al*., 2004b). This would suggest that Neéls relaxation is the main heating mechanism for both field strengths even so, results suggest the higher field strength to be more suitable for encouraging Neéls relaxation in the SPION investigated. A number of MFH studies have been reported all using different SPIONs and different AMF strengths, and all showing substantial cell death (Yanase *et al*., 1998; Jordan *et al*., 1999; Hilger *et al*., 2001; Hergt *et al*., 2004; Matsuoka *et al*., 2004; Kalambur *et al*., 2005; Wang *et al*., 2005; Okawa *et al*., 2006; Kettering *et al*., 2007). Therefore, the optimal AMF strength may depend on the characteristics of SPIONs. Indeed, all investigated SPIONs showed different heating profiles when exposed to AMF system 1 and 2.

Thus in addition to the applied AMF, the individual SPION characteristics such as iron content and core size appear to influence the heating ability of the SPIONs when subjected to an AMF. Among all the tested SPIONs the DX100, which has the highest iron content (*see section:* 3.3.3 SPION iron content) demonstrated the best

heating profile. This suggests the iron content to be significant for optimal magnetic heating. However, this contradicts studies by Lao *et al*., who reported that the iron content of SPIONs has no effect on magnetic heating efficiency (Lao *et al*., 2004). Instead, iron core size was identified to be crucial for optimal SPION heating (Shinkai *et al*., 1995; Hergt *et al*., 2004a; Wang *et al*., 2005; Okawa *et al*., 2006; Fortin *et al*., 2007; Kettering *et al*., 2007). According to Gonzales-Weimuller *et al*., and Kallumadil *et al*., the optimal iron core size should be approx 12nm with low polydispersity (Gonzales-Weimuller *et al*., 2009; Kallumadil *et al*., 2009). Indeed, comparison of the d100, d50, PEG-d50 and PEG-d20 AMF heating profiles revealed the d100, which contains predominantly 10-15nm iron oxide cores, to have a better heating efficiency than the PEGd20, which contains iron oxide cores of 5nm (*Personnel communication:* Dr Cordula Gruettner Micromod Partikelteknologie GMbH, Germany). The superior heating potential exhibited by the DX100 may therefore, be due to the DX100 consisting of a higher ratio of optimal sized iron oxide cores.

As well as SPION characteristics and AMF strength, environmental conditions can also affect the SPIONs heating efficiency. To maintain a constant temperature of 37^{o}C (body temperature) through the coil and simulating crudely how blood flow in the body may affect the dissipation of heat the Air-Therm ATX was used. Application of the Air Therm ATX resulted in a 50% drop in the fluid temperature increase, most likely due to the 37^{o}C airflow, quickly dissipating the heat generated. These results suggest that the heating potential of SPIONs when in the body will be less efficient due to the cooling effect of blood flow, a finding that has been previously reported (Andra *et al*., 1999; Moroz *et al*., 2002).

Even with the Air Therm ATX, the DX100 and d100 SPIONs when in AMF system 2, were capable of heating their surrounding fluid to therapeutic temperatures and therefore individually must reach extremely high temperatures. Consequently, when in close proximity to cells, the hot SPIONs should directly cause intracellular cell death, a concept proposed by Gordon *et al*., (Gordon *et al*., 1979). However, from *in vitro* results only the DX100 at >1 mg/ml and the d100 at >2.5 mg/ml caused cell death following AMF treatment. Coincidently, only at these concentrations was the fluid temperature rise therapeutically toxic. These results suggest the cell death

observed was due to heating of the surrounding fluid and not directly by the heat of the SPIONs.

Specific attachment of Sm3E functionalised SPIONs to CEA+ve LS174T cells also showed no effect on cell viability following AMF treatment in AMF system 2. The limitations of intracellular hyperthermia have been speculated to be due to SPION uptake (Kalambur *et al*., 2007), with optimal cell loading for heat transfer reported to be in the range of 60-200 pg/cell (Jordan *et al*., 1997; Kettering *et al*., 2007). However, results revealed that even with specific cell loading of 250 pg of Sm3E functionalised DX100 SPIONs negligible cell death following AMF treatment was observed. Though, it should be mentioned that binding of such a high concentration of SPIONs resulted in agglomeration. Agglomeration of SPIONs can decrease the heating efficiency of SPIONs as the relaxation behaviour of the iron cores become restrained due to inter-particle interactions (Wang *et al*., 2005).

Another explanation for the poor intracellular MFH cell death could be due to loss of Brownian relaxation when the SPIONs are immobilised on or in cells (Hergt *et al*., 2004b). Studies by Kalambur *et al*., found that suspension of SPIONs in higher viscosity fluids, such as glycerol or collagen lead to a reduction in the heat generated when exposed to an AMF (Kalambur *et al*., 2005). This drop in heating was also reported by Fortin *et al*., who encapsulated SPIONs into vesicles to simulate intracellular uptake (Fortin *et al*., 2007). These higher viscosity environments are thought to restrict the frictional movement of the SPIONs, thus preventing Brownian relaxation (Kalambur *et al*., 2005), leaving Neéls relaxation to be the predominant heating mechanism. However, from the findings in this chapter, resuspension of the DX100 and d100 in glycerol caused no difference in their heating efficiency. This further confirms Neéls relaxation to be the main heating mechanism used by the SPIONs in AMF system 2. Therefore, heating by Brownian relaxation mechanism in this study is negligible.

There are a number of reports published detailing the mechanism of AMF hyperthermia induced cell kill (Gordon *et al*., 1979; Rabin *et al*., 2002; Wang *et al*., 2005; Fortin *et al*., 2007). Though, at present the relationship between nanoscale heat response and macroscopic heat release is still not clear (Kalambur *et al*., 2005).

Theoretical studies by Rabin *et al*., showed for the transfer of enough heat to cause cell death a tumour diameter of over 0.9mm fully occupied with SPIONs would be required (Rabin *et al*., 2002). This would enable enough SPIONs to be able to diffuse a large amount of heat, collectively raising the tissue temperature above the threshold to cause hyperthermia or thermoblastation (Rabin *et al*., 2002). However, in the presence of blood flow a larger target region packed with SPIONs would be required for hyperthermic cell death to be evident (Rabin *et al*., 2002). The lack of cell death following targeted MFH *in vitro* may therefore, be due to the number of cells loaded with SPIONs being too low to collectively increase their environmental temperature to cause hyperthermic cell kill. This confirms a postulation by Jordan *et al*. and furthermore supports the results presented in this chapter; that AMF induced hyperthermic cell kill is due to fluid heating and not by intracellular heating as speculated by Gordon *et al*. (Gordon *et al*., 1979; Jordan *et al*., 1999).

At present, only one group has reported success with antibody targeted MFH (DeNardo *et al*., 2005). DeNardo *et al*. reported a decrease in tumour growth after AMF treatment of tumours labelled with ChL6-PEG-d20 conjugate (DeNardo *et al*., 2005; Ivkov *et al*., 2005). However, results in this chapter have shown the PEG-d20 when exposed to an AMF of 150 V, 0.74 A and 1 MHz do not generate enough heat to cause hyperthermic cell death. Natarajan *et al*., describes the tumour growth delay reported in DeNardo *et al*., 2005 to be in response to Eddy currents (Natarajan *et al*., 2008) and therefore, not due to Brownian and Neéls relaxation. Exposure of tissue to the high AMF employed by DeNardo *et al*. can cause tissues to heat up through eddy currents. Furthermore, if the tissues such as tumours contain SPIONs the heat generated can be further enhanced (Natarajan *et al*., 2008), thus, delivering toxic heat specifically to the tumour. Eddy currents however, have been reported to be dangerous to healthy tissues (Hergt *et al*., 2004) therefore, whether this approach is clinically viable still needs to be investigated.

6.5 Summary

The aim of the work presented in this chapter was to first, identify optimal conditions and SPION characteristics for maximal SPIONs heating and second, investigate the MFH potential of the SPIONs and scFv-SPION conjugates when exposed to an AMF.

All the SPIONs investigated in this chapter were shown to be effective generators of heat when exposed to AMF system 2 (150 V, 0.74 A and 1 MHz). However, SPION size and concentration greatly influenced the SPIONs magnetic heating potential. The d100 and DX100 caused a substantially higher fluid temperature increase compared to the smaller SPIONs and in addition, were the only SPIONs to initiate hyperthermic cell kill though, only at concentrations above 1 mg/ml.

Specific targeted MFH using Sm3E functionalised SPIONs exposed to AMF system 1 was found to cause increased expression of the HSP70, indicating cellular stress. However, increased uptake of Sm3E functionalised SPION and exposure to the higher AMF strength did not lead to MFH cell kill *in vitro.* The benefits of Sm3E functionalised SPIONs for MFH maybe more apparent *in vivo*, with increased retention of SPIONs within the tumour and anti-tumour immunity induced by HSP70 expression.

Chapter 7

Conclusion and Future Challenges

The work in this thesis has been designed and executed to investigate the hypotheses that scFv-targeted SPIONs would have potential for imaging and therapy of cancer. To test the hypotheses, a combination of nanotechnology and protein engineering was applied to generate stable scFv-SPION conjugates with retained immunoreactivity to the target CEA. Imaging potential of the scFv-SPION conjugates was demonstrated by confocal microscopy and MRI; therapeutic potential was demonstrated by developing systems to generate toxic heat by exposure of the targeted SPIONs to AMF. The results supported the hypotheses tested and indicate that scFv SPIONs have potential to be developed for cancer imaging and therapy, where there is a great need for novel treatments.

My work has shown that SPIONs may be successfully targeted to cancer cells using scFv. However, for most effectiveness, in MRI or hyperthermia, the scFv-SPION conjugates should be targeted systemically *in vivo*. This is the next challenge; in particular to address the uptake of nanoparticles by the RES which is a widely reported problem (Gupta *et al*., 2007; Barry, 2008). An approach that has been applied to this problem, with varying degrees of success is to coat the nanoparticles with agents that render them relatively less visible to the RES, a property often referred to as 'stealth'. A variety of materials have been used to achieve stealth and the most successfully reported of these is high MW PEG (Owens *et al.,* 2006). However, although PEGylation has shown promise, with increased blood circulation times (Zhang *et al*., 2002; Berry *et al*., 2003), complete RES evasion is yet to be reported. Despite this limitation, systemic application of targeted SPIONs has been demonstrated in studies using mAb targeted SPIONs for MRI (Toma *et al*., 2005; Reynolds *et al*., 2006; Yang *et al*., 2009). Although a strong T2 signal was also reported in the liver and spleen, indicating clearance by the RES (Yang *et al*., 2009).

For specific MR imaging, low concentrations of SPIONs at the tumour site are sufficient (Pinkernelle *et al*., 2005). Though, for MFH to be effective for cell kill, high concentrations of SPIONs are required (Rabin *et al*., 2002). The accumulation of a high concentration of systemically targeted SPIONs within the tumour is not only affected by RES uptake, but also target antigen concentration and distribution within the tumour. Targeting MFH systemically to cause cell kill may therefore, not be a viable approach. Intra-tumoural injection of SPIONs for MFH cell kill has been

demonstrated *in vivo* and furthermore, has shown promising results in the clinic with glioblastoma and prostate cancer (Thiesen *et al*., 2008). However, possible diffusion of the SPIONs out of the tumour due to tumour vascular permeability could result in an overall lower concentration of SPIONs in the tumour and unwanted toxicity thus, affecting the efficacy of MFH treatment. Antibody targeting of SPIONs has been shown to improve the retention time of SPIONs within the tumour via antibody-antigen interaction (Li *et al*., 2009). Therefore, specific attachment of scFv-SPION conjugates to tumour cells would potentially reduce the diffusion of the SPIONs through or out of the tumour, maintaining the concentration required to cause MFH. Furthermore, work in this thesis has shown specific attachment of scFv-SPION conjugates to cells also increases cellular stress when subjected to an AMF this would potentially enhance the potency of MFH.

Although high concentrations of SPIONs are required to cause intense heat for MFH cell kill, lower temperature rises and thus low SPION doses could lead to therapeutic effects. Thus unlike MFH cell kill, mild MFH could be achievable using systemically targeted scFv-SPION conjugates. Small temperature increases of 2-5 degrees have been shown to increase tumour blood flow and vessel permeability (Bicher *et al*., 1980; Vaupel *et al*., 1984; Vaupel *et al*., 1997) leading to increased oxygen concentration and cytotoxic drug delivery into the tumour (Wust *et al*., 2002; Song *et al*., 2005). Consequently, systemically targeted mild MFH could be used as an adjuvant with chemotherapy and radiotherapy regimes. Indeed, studies by Johannson *et al*., showed combined MFH with external radiation to be significantly more effective than radiation alone (Johannson *et al*., 2006). Furthermore, the application of an AMF can be localised to tumour regions, avoiding undesirable heating of RES organs. The potential of systemically targeted mild MFH to increase the toxicity of chemotherapy and radiotherapy in localised areas would therefore, allow for lower drug dosing, reducing the often debilitating side effects.

Mild hyperthermia can also induce expression of HSP70 as evident in this thesis and by others (Ito *et al*., 2001, 2003, 2004). Induction of HSP70 expression by mild MFH has been shown to activate cell mediated and humoral immune responses (*See section:* 1.4 Hyperthermia). Mild MFH can therefore, lead to a vaccination effect resulting in anti-tumour immunity (Yanase *et al*., 1998; Suzuki *et al*., 2003). Indeed,

Yanase *et al.*, showed that following MFH, there was not only a reduction in growth for the heated tumours but also for the non-heated tumours there was a similar size reduction (Yanase *et al*., 1998). In addition, Suzuki *et al*., observed cytotoxic activity when MFH treated mice were re-challenged with the same tumour cells (Suzuki *et al*., 2003). The generation of anti-tumour immunity could revolutionise the treatment of metastatic tumours, as once activated, the immune system could target and specifically destroy the cancer cells.

To take this work forward extensive characterisation of the SPIONs is essential, especially if these SPIONs are taken into the clinic. Charaterisation would include; 1. Measurements of the iron core and overall hydrodynamic size before and after conjugation as these properties are important in the magnetic heating properties of the SPION and clearance by the RES. 2. Accurate calculation of the number of SPION in 1mg SPION solution as the values stated on the data sheet are only estimates. 3. The surface electrical charge "zeta potential" of all the SPIONs investigated before, during and after conjugation to scFvs should be measured, as surface charge can dramatically affect cell binding behaviour of the scFv-SPION conjugates,

Furthermore, to have better control over the number and orientation of the scFvs attached to the SPIONs, development of site specific attachments would be advantageous. One approach could involve engineering of a cysteine group to the N terminus of the scFv thus, enabling attachment to the SPION via disulphide bond.

Other future work would include an *in vivo* heating study, whereby functionalised and non functionalised SPIONs are directly injected into a tumour followed by treatment with an AMF. From heating measurements and histological analysis of cell necrosis and HSP70 expression the adavantge of using tumour specific SPION could be identified along with the feasibility of using tumour specific MFH as an approach to induce anti-tumour immunity .

In conclusion, my work has shown that scFv targeted SPIONs are effective for specific imaging *in vitro* by MRI. Furthermore, I have established parameters for MFH therapy *in vitro*. My results indicate that scFv targeted SPION have potential

for tumour specific MRI and MFH and support the central hypothesis for this thesis, that antibody-targeted SPIONs can be used for diagnosis and therapy of cancer. It is envisaged that when the challenge of creating stealth particles for *in vivo* delivery is met, the work in this thesis will form a future platform of understanding for further development of SPIONs.

Appendix 1

References

Adams GP, Schier R (1999) Generating improved single-chain Fv molecules for tumor targeting. *J Immunol Methods* **231**: 249-260

Adams GP, Schier R, Marshall K, Wolf EJ, McCall AM, Marks JD, Weiner LM (1998) Increased affinity leads to improved selective tumor delivery of single-chain Fv antibodies. *Cancer Res* **58**: 485-490

Adams GP, Shaller CC, Chappell LL, Wu C, Horak EM, Simmons HH, Litwin S, Marks JD, Weiner LM, Brechbiel MW (2000) Delivery of the alpha-emitting radioisotope bismuth-213 to solid tumors via single-chain Fv and diabody molecules. *Nucl Med Biol* **27**: 339-346

Adams GP, Tai MS, McCartney JE, Marks JD, Stafford WF, III, Houston LL, Huston JS, Weiner LM (2006) Avidity-mediated enhancement of in vivo tumor targeting by single-chain Fv dimers. *Clin Cancer Res* **12**: 1599-1605

Adams GP, Weiner LM (2005) Monoclonal antibody therapy of cancer. *Nat Biotechnol* **23**: 1147-1157

Alberola AP, Radler JO (2009) The defined presentation of nanoparticles to cells and their surface controlled uptake. *Biomaterials* **30**: 3766-3770

Amin Z, Donald JJ, Masters A, Kant R, Steger AC, Bown SG, Lees WR (1993) Hepatic metastases: interstitial laser photocoagulation with real-time US monitoring and dynamic CT evaluation of treatment. *Radiology* **187**: 339-347

Andrä W, Ambly CG, Hergt R, Hilger I, Kaiser WA (1999) Temperature distribution as function of time around a small spherical heat source of local magnetic hyperthermia. *J Magn Magn Mater* **194:** 197-203

Arakawa F, Kuroki M, Misumi Y, Oikawa S, Nakazato H, Matsuoka Y (1990) Characterization of a cDNA clone encoding a new species of the nonspecific cross-reacting antigen (NCA), a member of the CEA gene family. *Biochem Biophys Res Commun* **166**: 1063-1071

Arnould L, Gelly M, Penault-Llorca F, Benoit L, Bonnetain F, Migeon C, Cabaret V, Fermeaux V, Bertheau P, Garnier J, Jeannin JF, Coudert B (2006) Trastuzumab-based treatment of HER2-positive breast cancer: an antibody-dependent cellular cytotoxicity mechanism? *Br J Cancer* **94**: 259-267

Artemov D (2003) Molecular magnetic resonance imaging with targeted contrast agents. *J Cell Biochem* **90**: 518-524

Artemov D, Mori N, Ravi R, Bhujwalla ZM (2003) Magnetic resonance molecular imaging of the HER-2/neu receptor. *Cancer Res* **63**: 2723-2727

Atwell JL, Breheney KA, Lawrence LJ, McCoy AJ, Kortt AA, Hudson PJ (1999) scFv multimers of the anti-neuraminidase antibody NC10: length of the linker between VH and VL domains dictates precisely the transition between diabodies and triabodies. *Protein Eng* **12**: 597-604

Axen R, Porath J, Ernback S (1967) Chemical coupling of peptides and proteins to polysaccharides by means of cyanogen halides. *Nature* **214**: 1302-1304

Bailon P, Won CY (2009) PEG-modified biopharmaceuticals. *Expert Opin Drug Deliv* **6**: 1-16

Bagshawe KD (1995) Antibody-directed enzyme prodrug therapy for cancer: its theoretical basis and application. *Mol Med Today* **1**: 424-431

Bagshawe KD, Springer CJ, Searle F, Antoniw P, Sharma SK, Melton RG, Sherwood RF (1988) A cytotoxic agent can be generated selectively at cancer sites. *Br J Cancer* **58**: 700-703

Bates PA, Luo J, Sternberg MJ (1992) A predicted three-dimensional structure for the carcinoembryonic antigen (CEA). *FEBS Lett* **301**: 207-214

Beauchemin N, Benchimol S, Cournoyer D, Fuks A, Stanners CP (1987) Isolation and characterization of full-length functional cDNA clones for human carcinoembryonic antigen. *Mol Cell Biol* **7**: 3221-3230

Beere HM (2004) "The stress of dying": the role of heat shock proteins in the regulation of apoptosis. *J Cell Sci* **117**: 2641-2651

Begent RH, Verhaar MJ, Chester KA, Casey JL, Green AJ, Napier MP, Hope-Stone LD, Cushen N, Keep PA, Johnson CJ, Hawkins RE, Hilson AJ, Robson L (1996) Clinical evidence of efficient tumor targeting based on single-chain Fv antibody selected from a combinatorial library. *Nat Med* **2**: 979-984

Benchimol S, Fuks A, Jothy S, Beauchemin N, Shirota K, Stanners CP (1989) Carcinoembryonic antigen, a human tumor marker, functions as an intercellular adhesion molecule. *Cell* **57**: 327-334

Berling B, Kolbinger F, Grunert F, Thompson JA, Brombacher F, Buchegger F, von KS, Zimmermann W (1990) Cloning of a carcinoembryonic antigen gene family member expressed in leukocytes of chronic myeloid leukemia patients and bone marrow. *Cancer Res* **50**: 6534-6539

Berry CC, Wells S, Charles S, Aitchison G, Curtis AS (2004) Cell response to dextran-derivatised iron oxide nanoparticles post internalisation. *Biomaterials* **25**: 5405-5413

Berry CC, Wells S, Charles S, Curtis AS (2003) Dextran and albumin derivatised iron oxide nanoparticles: influence on fibroblasts in vitro. *Biomaterials* **24**: 4551-4557

Bhatia SS, Vidyashankar C, Sharma RK, Dubey AK (2000) Systemic toxicity with cyclopentolate eye drops. *Indian Pediatr* **37**: 329-331

Bicher HI, Hetzel FW, Sandhu TS, Frinak S, Vaupel P, O'Hara MD, O'Brien T (1980) Effects of hyperthermia on normal and tumor microenvironment. *Radiology* **137**: 523-530

Bird RE, Hardman KD, Jacobson JW, Johnson S, Kaufman BM, Lee SM, Lee T, Pope SH, Riordan GS, Whitlow M (1988) Single-chain antigen-binding proteins. *Science* **242**: 423-426

Bobbitt JM (1956) Periodate oxidation of carbohydrates. *Adv Carbohydr Chem* **48**: 1-41

Boder ET, Midelfort KS, Wittrup KD (2000) Directed evolution of antibody fragments with monovalent femtomolar antigen-binding affinity. *Proc Natl Acad Sci U S A* **97**: 10701-10705

Boehm MK, Corper AL, Wan T, Sohi MK, Sutton BJ, Thornton JD, Keep PA, Chester KA, Begent RH, Perkins SJ (2000) Crystal structure of the anti-(carcinoembryonic antigen) single-chain Fv antibody MFE-23 and a model for antigen binding based on intermolecular contacts. *Biochem J* **346 Pt 2**: 519-528

Boulianne GL, Hozumi N, Shulman MJ (1984) Production of functional chimaeric mouse/human antibody. *Nature* **312**: 643-646

Brannon-Peppas L, Blanchette JO (2004) Nanoparticle and targeted systems for cancer therapy. *Adv Drug Deliv Rev* **56**: 1649-1659

Brigger I, Dubernet C, Couvreur P (2002) Nanoparticles in cancer therapy and diagnosis. *Adv Drug Deliv Rev* **54**: 631-651

Briley-Saebo K, Bjornerud A, Grant D, Ahlstrom H, Berg T, Kindberg GM (2004) Hepatic cellular distribution and degradation of iron oxide nanoparticles following single intravenous injection in rats: implications for magnetic resonance imaging. *Cell Tissue Res* **316**: 315-323

Bulte JW, Kraitchman DL (2004) Iron oxide MR contrast agents for molecular and cellular imaging. *NMR Biomed* **17**: 484-499

Camacho-Leal P, Stanners CP (2008) The human carcinoembryonic antigen (CEA) GPI anchor mediates anoikis inhibition by inactivation of the intrinsic death pathway. *Oncogene* **27**: 1545-1553

Capdevila J, Elez E, Macarulla T, Ramos FJ, Ruiz-Echarri M, Tabernero J (2009) Anti-epidermal growth factor receptor monoclonal antibodies in cancer treatment. *Cancer Treat Rev* **35**: 354-363

Carter P, Kelley RF, Rodrigues ML, Snedecor B, Covarrubias M, Velligan MD, Wong WL, Rowland AM, Kotts CE, Carver ME, . (1992) High level Escherichia coli expression and production of a bivalent humanized antibody fragment. *Biotechnology (N Y)* **10**: 163-167

Cartiera MS, Johnson KM, Rajendran V, Caplan MJ, Saltzman WM (2009) The uptake and intracellular fate of PLGA nanoparticles in epithelial cells. *Biomaterials* **30**: 2790-2798

Cattel L, Ceruti M, Dosio F (2004) From conventional to stealth liposomes: a new Frontier in cancer chemotherapy. *J Chemother* **16 Suppl 4**: 94-97

Cavaliere R, Ciocatto EC, Giovanella BC, Heidelberger C, Johnson RO, Margottini M, Mondovi B, Moricca G, Rossi-Fanelli A (1967) Selective heat sensitivity of cancer cells. Biochemical and clinical studies. *Cancer* **20**: 1351-1381

Cerdan S, Lotscher HR, Kunnecke B, Seelig J (1989) Monoclonal antibody-coated magnetite particles as contrast agents in magnetic resonance imaging of tumors. *Magn Reson Med* **12**: 151-163

Chakravarty P, Marches R, Zimmerman NS, Swafford AD, Bajaj P, Musselman IH, Pantano P, Draper RK, Vitetta ES (2008) Thermal ablation of tumor cells with antibody-functionalized single-walled carbon nanotubes. *Proc Natl Acad Sci U S A* **105**: 8697-8702

Chan CH, Camacho-Leal P, Stanners CP (2007) Colorectal hyperplasia and dysplasia due to human carcinoembryonic antigen (CEA) family member expression in transgenic mice. *PLoS One* **2**: e1353

Chester KA, Begent RH, Robson L, Keep P, Pedley RB, Boden JA, Boxer G, Green A, Winter G, Cochet O, . (1994) Phage libraries for generation of clinically useful antibodies. *Lancet* **343**: 455-456

Chester KA, Bhatia J, Boxer G, Cooke SP, Flynn AA, Huhalov A, Mayer A, Pedley RB, Robson L, Sharma SK, Spencer DI, Begent RH (2000a) Clinical applications of phage-derived sFvs and sFv fusion proteins. *Dis Markers* **16**: 53-62

Chester KA, Mayer A, Bhatia J, Robson L, Spencer DI, Cooke SP, Flynn AA, Sharma SK, Boxer G, Pedley RB, Begent RH (2000b) Recombinant anti-carcinoembryonic antigen antibodies for targeting cancer. *Cancer Chemother Pharmacol* **46 Suppl**: S8-12

Chung KY, Saltz LB (2005) Antibody-based therapies for colorectal cancer. *Oncologist* **10**: 701-709

Colcher D, Pavlinkova G, Beresford G, Booth BJ, Choudhury A, Batra SK (1998) Pharmacokinetics and biodistribution of genetically-engineered antibodies. *Q J Nucl Med* **42**: 225-241

Cook GP, Tomlinson IM (1995) The human immunoglobulin VH repertoire. *Immunol Today* **16**: 237-242

Cooke SP, Pedley RB, Boden R, Begent RH, Chester KA (2002) In vivo tumor delivery of a recombinant single chain Fv::tumor necrosis factor-alpha fusion [correction of factor: a fusion] protein. *Bioconjug Chem* **13**: 7-15

Costello RT, Gastaut JA, Olive D (1999) Tumor escape from immune surveillance. *Arch Immunol Ther Exp (Warsz)* **47**: 83-88

DeNardo SJ, DeNardo GL, Miers LA, Natarajan A, Foreman AR, Gruettner C, Adamson GN, Ivkov R (2005) Development of tumor targeting bioprobes ((111)In-chimeric L6 monoclonal antibody nanoparticles) for alternating magnetic field cancer therapy. *Clin Cancer Res* **11**: 7087s-7092s

Deonarain MP, Rowlinson-Busza G, George AJ, Epenetos AA (1997) Redesigned anti-human placental alkaline phosphatase single-chain Fv: soluble expression, characterization and in vivo tumour targeting. *Protein Eng* **10**: 89-98

Di GN, Cittera E, Nota R, Vecchi A, Grieco V, Scanziani E, Botto M, Introna M, Golay J (2003) Complement activation determines the therapeutic activity of rituximab in vivo. *J Immunol* **171**: 1581-1587

Dolezal O, Pearce LA, Lawrence LJ, McCoy AJ, Hudson PJ, Kortt AA (2000) ScFv multimers of the anti-neuraminidase antibody NC10: shortening of the linker in single-chain Fv fragment assembled in V(L) to V(H) orientation drives the formation of dimers, trimers, tetramers and higher molecular mass multimers. *Protein Eng* **13**: 565-574

Dufner P, Jermutus L, Minter RR (2006) Harnessing phage and ribosome display for antibody optimisation. *Trends Biotechnol* **24**: 523-529

Dutton AH, Tokuyasu KT, Singer SJ (1979) Iron-dextran antibody conjugates: General method for simultaneous staining of two components in high-resolution immunoelectron microscopy. *Proc Natl Acad Sci U S A* **76**: 3392-3396

Edelman GM (1973) Antibody structure and molecular immunology. *Science* **180**: 830-840

Edelman GM, Poulik MD (1961) Studies on structural units of the gamma-globulins. *J Exp Med* **113**: 861-884

Eidelman FJ, Fuks A, DeMarte L, Taheri M, Stanners CP (1993) Human carcinoembryonic antigen, an intercellular adhesion molecule, blocks fusion and differentiation of rat myoblasts. *J Cell Biol* **123**: 467-475

Er Y, Barnes TJ, Fornasiero D, Prestidge CA (2009) The encapsulation and release of guanosine from PEGylated liposomes. *J Liposome Res* **19**: 29-36

Fang J, Jin HB, Song JD (2003) Construction, expression and tumor targeting of a single-chain Fv against human colorectal carcinoma. *World J Gastroenterol* **9**: 726-730

FitzGerald K, Holliger P, Winter G (1997) Improved tumour targeting by disulphide stabilized diabodies expressed in Pichia pastoris. *Protein Eng* **10**: 1221-1225

Folkman J (1992) The role of angiogenesis in tumor growth. *Semin Cancer Biol* **3**: 65-71

Fortin JP, Gazeau F, Wilhelm C (2008) Intracellular heating of living cells through Neel relaxation of magnetic nanoparticles. *Eur Biophys J* **37**: 223-228

Frieze DA, McCune JS (2006) Current status of cetuximab for the treatment of patients with solid tumors. *Ann Pharmacother* **40**: 241-250

Funovics MA, Kapeller B, Hoeller C, Su HS, Kunstfeld R, Puig S, Macfelda K (2004) MR imaging of the her2/neu and 9.2.27 tumor antigens using immunospecific contrast agents. *Magn Reson Imaging* **22**: 843-850

Gabizon AA (2001) Stealth liposomes and tumor targeting: one step further in the quest for the magic bullet. *Clin Cancer Res* **7**: 223-225

Garcia-Lora A, Algarra I, Garrido F (2003) MHC class I antigens, immune surveillance, and tumor immune escape. *J Cell Physiol* **195**: 346-355

Garden OA, Reynolds PR, Yates J, Larkman DJ, Marelli-Berg FM, Haskard DO, Edwards AD, George AJ (2006) A rapid method for labelling CD4+ T cells with ultrasmall paramagnetic iron oxide nanoparticles for magnetic resonance imaging that preserves proliferative, regulatory and migratory behaviour in vitro. *J Immunol Methods* **314**: 123-133

Gaur U, Sahoo SK, De TK, Ghosh PC, Maitra A, Ghosh PK (2000) Biodistribution of fluoresceinated dextran using novel nanoparticles evading reticuloendothelial system. *Int J Pharm* **202**: 1-10

Gazelle GS, Goldberg SN, Solbiati L, Livraghi T (2000) Tumor ablation with radio-frequency energy. *Radiology* **217**: 633-646

George AJ, Lee L, Pitzalis C (2003) Isolating ligands specific for human vasculature using in vivo phage selection. *Trends Biotechnol* **21**: 199-203

George AJ, Bhakoo KK, Haskard DO, Larkman DJ, Reynolds PR (2006) Imaging molecular and cellular events in transplantation. *Transplantation* **82**: 1124-1129

Gilchrist RK, Medal R, Shorey WD, Hanselman RC, Parrott JC, Taylor CB (1957) Selective inductive heating of lymph nodes. *Ann Surg* **146**: 596-606

Gilles MA, Hudson AQ, Borders CL, Jr. (1990) Stability of water-soluble carbodiimides in aqueous solution. *Anal Biochem* **184**: 244-248

Gneveckow U, Jordan A, Scholz R, Bruss V, Waldofner N, Ricke J, Feussner A, Hildebrandt B, Rau B, Wust P (2004) Description and characterization of the novel hyperthermia- and thermoablation-system MFH 300F for clinical magnetic fluid hyperthermia. *Med Phys* **31**: 1444-1451

Golay J, Cittera E, Di GN, Manganini M, Mosca M, Nebuloni M, van RN, Vago L, Introna M (2006) The role of complement in the therapeutic activity of rituximab in a murine B lymphoma model homing in lymph nodes. *Haematologica* **91**: 176-183

Gold P, Freedman SO (1965a) Demonstration of tumor-specific antigens in human colonic carcinomata by immunological tolerance and absorption techniques.. *J Exp Med* **121**: 439-462

Gold P, Freedman SO (1965b) Specific carcinoembryonic antigens of the human digestive system. *J Exp Med* **122**: 467-481

Gonzales-Weimuller M, Zeisberger M, Krishnan KM (2009) Size-dependent heating rates of iron oxide nanoparticles for magnetic fluid hyperthermia. *J Magn Magn Mater* **321**: 1947-1950

Gordon RT, Hines JR, Gordon D (1979) Intracellular hyperthermia. A biophysical approach to cancer treatment via intracellular temperature and biophysical alterations. *Med Hypotheses* **5**: 83-102

Goshima S, Kanematsu M, Matsuo M, Kondo H, Kato H, Yokoyama R, Hoshi H, Moriyama N (2004) Nodule-in-nodule appearance of hepatocellular carcinomas: comparison of gadolinium-enhanced and ferumoxides-enhanced magnetic resonance imaging. *J Magn Reson Imaging* **20**: 250-255

Grady WM, Carethers JM (2008) Genomic and epigenetic instability in colorectal cancer pathogenesis. *Gastroenterology* **135**: 1079-1099

Graff CP, Chester K, Begent R, Wittrup KD (2004) Directed evolution of an anti-carcinoembryonic antigen scFv with a 4-day monovalent dissociation half-time at 37 degrees C. *Protein Eng Des Sel* **17**: 293-304

Graff CP, Wittrup KD (2003) Theoretical analysis of antibody targeting of tumor spheroids: importance of dosage for penetration, and affinity for retention. *Cancer Res* **63**: 1288-1296

Gref R, Luck M, Quellec P, Marchand M, Dellacherie E, Harnisch S, Blunk T, Muller RH (2000) 'Stealth' corona-core nanoparticles surface modified by polyethylene glycol (PEG): influences of the corona (PEG chain length and surface density) and of the core composition on phagocytic uptake and plasma protein adsorption. *Colloids Surf B Biointerfaces* **18**: 301-313

Gregoriadis G (2008) Liposome research in drug delivery: the early days. *J Drug Target* **16**: 520-524

Griffin RJ, Corry PM (2009) Commentary on classic paper in hyperthermic oncology 'Tumour oxygenation is increased by hyperthermia at mild temperatures' by CW Song et al., 1996. *Int J Hyperthermia* **25**: 96-98

Gupta AK, Curtis AS (2004) Surface modified superparamagnetic nanoparticles for drug delivery: interaction studies with human fibroblasts in culture. *J Mater Sci Mater Med* **15**: 493-496

Gupta AK, Gupta M (2005a) Cytotoxicity suppression and cellular uptake enhancement of surface modified magnetic nanoparticles. *Biomaterials* **26**: 1565-1573

Gupta AK, Gupta M (2005b) Synthesis and surface engineering of iron oxide nanoparticles for biomedical applications. *Biomaterials* **26**: 3995-4021

Gupta AK, Naregalkar RR, Vaidya VD, Gupta M (2007) Recent advances on surface engineering of magnetic iron oxide nanoparticles and their biomedical applications. *Nanomed* **2**: 23-39

Hamers-Casterman C, Atarhouch T, Muyldermans S, Robinson G, Hamers C, Songa EB, Bendahman N, Hamers R (1993) Naturally occurring antibodies devoid of light chains. *Nature* **363**: 446-448

Hammarstrom S (1999) The carcinoembryonic antigen (CEA) family: structures, suggested functions and expression in normal and malignant tissues. *Semin Cancer Biol* **9**: 67-81

Hanahan D, Weinberg RA (2000) The hallmarks of cancer. *Cell* **100**: 57-70

Haugland RP (2001) Antibody conjugates for cell biology. *Curr Protoc Cell Biol* **Chapter 16**: Unit

Harmsen MM, De Haard HJ (2007) Properties, production, and applications of camelid single-domain antibody fragments. *Appl Microbiol Biotechnol* **77**: 13-22

Harris LJ, Larson SB, Hasel KW, McPherson A (1997) Refined structure of an intact IgG2a monoclonal antibody. *Biochemistry* **36**: 1581-1597

Hefta SA, Hefta LJ, Lee TD, Paxton RJ, Shively JE (1988) Carcinoembryonic antigen is anchored to membranes by covalent attachment to a glycosylphosphatidylinositol moiety: identification of the ethanolamine linkage site. *Proc Natl Acad Sci U S A* **85**: 4648-4652

Hennecke F, Krebber C, Pluckthun A (1998) Non-repetitive single-chain Fv linkers selected by selectively infective phage (SIP) technology. *Protein Eng* **11**: 405-410

Hergt R, Andrä W, d'Ambly C, Hilger I, Kaiser W, Richter U, Schmidt H (1998) Physical limits of hyperthermia using magnetite fine particles. *IEEE Trans Magn* **34** (5): 3745-3754

Hergt R, Dutz S (2007) Magnetic particle hyperthermia-biophysical limitations of a visionary tumour therapy. *J. Magn Magn Mater* **311:** 187-192

Hergt R, Hiergeist R, Hilger I, Kaiser W, Lapatnikov Y, Margel S, Richter U (2004) Maghemite nanoparticles with very high AC-losses for application in RF-magnetite hyperthermia. *J. Magn Magn Mater* **270:** 345-357

Hergt R, Hiergeist R, Zeisberger M, Glöckl G, Weitschies W, Ramirez LP, Hilger I, Kaiser WA (2004) Enhancement of AC-losses of magnetic nanoparticles for heating applications.*J Magn Magn Mater* **280:** 358-368

Hilger I, Andra W, Hergt R, Hiergeist R, Schubert H, Kaiser WA (2001) Electromagnetic heating of breast tumors in interventional radiology: in vitro and in vivo studies in human cadavers and mice. *Radiology* **218**: 570-575

Hilger I, Hergt R, Kaiser WA (2005) Use of magnetic nanoparticle heating in the treatment of breast cancer. *IEE Proc Nanobiotechnol* **152**: 33-39

Hinoda Y, Neumaier M, Hefta SA, Drzeniek Z, Wagener C, Shively L, Hefta LJ, Shively JE, Paxton RJ (1988) Molecular cloning of a cDNA coding biliary

glycoprotein I: primary structure of a glycoprotein immunologically crossreactive with carcinoembryonic antigen. *Proc Natl Acad Sci U S A* **85**: 6959-6963

Hirsch LR, Stafford RJ, Bankson JA, Sershen SR, Rivera B, Price RE, Hazle JD, Halas NJ, West JL (2003) Nanoshell-mediated near-infrared thermal therapy of tumors under magnetic resonance guidance. *Proc Natl Acad Sci U S A* **100**: 13549-13554

Hoare DG, Koshland DE, Jr. (1967) A method for the quantitative modification and estimation of carboxylic acid groups in proteins. *J Biol Chem* **242**: 2447-2453

Holliger P, Hudson PJ (2005) Engineered antibody fragments and the rise of single domains. *Nat Biotechnol* **23**: 1126-1136

Holt LJ, Herring C, Jespers LS, Woolven BP, Tomlinson IM (2003) Domain antibodies: proteins for therapy. *Trends Biotechnol* **21**: 484-490

Hoogenboom HR (2005) Selecting and screening recombinant antibody libraries. *Nat Biotechnol* **23**: 1105-1116

Hostetter RB, Augustus LB, Mankarious R, Chi KF, Fan D, Toth C, Thomas P, Jessup JM (1990) Carcinoembryonic antigen as a selective enhancer of colorectal cancer metastasis. *J Natl Cancer Inst* **82**: 380-385

Huang BC, Davern S, Kennel SJ (2006) Mono and bivalent binding of a scFv and covalent diabody to murine laminin-1 using radioiodinated proteins and SPR measurements: effects on tissue retention in vivo. *J Immunol Methods* **313**: 149-160

Huang X, El-Sayed IH, Qian W, El-Sayed MA (2006) Cancer cell imaging and photothermal therapy in the near-infrared region by using gold nanorods. *J Am Chem Soc* **128**: 2115-2120

Hust M, Jostock T, Menzel C, Voedisch B, Mohr A, Brenneis M, Kirsch MI, Meier D, Dubel S (2007) Single chain Fab (scFab) fragment. *BMC Biotechnol* **7**: 14

Huston JS, Levinson D, Mudgett-Hunter M, Tai MS, Novotny J, Margolies MN, Ridge RJ, Bruccoleri RE, Haber E, Crea R (1988) Protein engineering of antibody binding sites: recovery of specific activity in an anti-digoxin single-chain Fv analogue produced in Escherichia coli. *Proc Natl Acad Sci U S A* **85**: 5879-5883

Ilantzis C, DeMarte L, Screaton RA, Stanners CP (2002) Deregulated expression of the human tumor marker CEA and CEA family member CEACAM6 disrupts tissue architecture and blocks colonocyte differentiation. *Neoplasia* **4**: 151-163

Imao M, Nagaki M, Moriwaki H (2006) Dual effects of heat stress on tumor necrosis factor-alpha-induced hepatocyte apoptosis in mice. *Lab Invest* **86**: 959-967

Inazawa J, Abe T, Inoue K, Misawa S, Oikawa S, Nakazato H, Yoshida MC (1989) Regional assignment of nonspecific cross-reacting antigen (NCA) of the CEA gene family to chromosome 19 at band q13.2. *Cytogenet Cell Genet* **52**: 28-31

Ito A, Honda H, Kobayashi T (2006) Cancer immunotherapy based on intracellular hyperthermia using magnetite nanoparticles: a novel concept of "heat-controlled necrosis" with heat shock protein expression. *Cancer Immunol Immunother* **55**: 320-328

Ito A, Kuga Y, Honda H, Kikkawa H, Horiuchi A, Watanabe Y, Kobayashi T (2004) Magnetite nanoparticle-loaded anti-HER2 immunoliposomes for combination of antibody therapy with hyperthermia. *Cancer Lett* **212**: 167-175

Ito A, Shinkai M, Honda H, Kobayashi T (2005) Medical application of functionalized magnetic nanoparticles. *J Biosci Bioeng* **100**: 1-11

Ito A, Shinkai M, Honda H, Wakabayashi T, Yoshida J, Kobayashi T (2001) Augmentation of MHC class I antigen presentation via heat shock protein expression by hyperthermia. *Cancer Immunol Immunother* **50**: 515-522

Ito A, Shinkai M, Honda H, Yoshikawa K, Saga S, Wakabayashi T, Yoshida J, Kobayashi T (2003a) Heat shock protein 70 expression induces antitumor immunity during intracellular hyperthermia using magnetite nanoparticles. *Cancer Immunol Immunother* **52**: 80-88

Ito A, Tanaka K, Kondo K, Shinkai M, Honda H, Matsumoto K, Saida T, Kobayashi T (2003b) Tumor regression by combined immunotherapy and hyperthermia using magnetic nanoparticles in an experimental subcutaneous murine melanoma. *Cancer Sci* **94**: 308-313

Ivkov R, DeNardo SJ, Daum W, Foreman AR, Goldstein RC, Nemkov VS, DeNardo GL (2005) Application of high amplitude alternating magnetic fields for heat induction of nanoparticles localized in cancer. *Clin Cancer Res* **11**: 7093s-7103s

Jean GW, Shah SR (2008) Epidermal growth factor receptor monoclonal antibodies for the treatment of metastatic colorectal cancer. *Pharmacotherapy* **28**: 742-754

Jespers L, Schon O, Famm K, Winter G (2004) Aggregation-resistant domain antibodies selected on phage by heat denaturation. *Nat Biotechnol* **22**: 1161-1165

Johannsen M, Gneveckow U, Eckelt L, Feussner A, Waldofner N, Scholz R, Deger S, Wust P, Loening SA, Jordan A (2005) Clinical hyperthermia of prostate cancer using magnetic nanoparticles: presentation of a new interstitial technique. *Int J Hyperthermia* **21**: 637-647

Johannsen M, Gneveckow U, Thiesen B, Taymoorian K, Cho CH, Waldofner N, Scholz R, Jordan A, Loening SA, Wust P (2007) Thermotherapy of prostate cancer using magnetic nanoparticles: feasibility, imaging, and three-dimensional temperature distribution. *Eur Urol* **52**: 1653-1661

Jolesz FA, Hynynen K (2002) Magnetic resonance image-guided focused ultrasound surgery. *Cancer J* **8 Suppl 1**: S100-S112

Jones PL, Gallagher BM, Sands H (1986) Autoradiographic analysis of monoclonal antibody distribution in human colon and breast tumor xenografts. *Cancer Immunol Immunother* **22**: 139-143

Jordan A, Maier-Hauff K (2007) Magnetic nanoparticles for intracranial thermotherapy. *J Nanosci Nanotechnol* **7**: 4604-4606

Jordan A, Scholz R, Maier-Hauff K, van Landeghem FK, Waldoefner N, Teichgraeber U, Pinkernelle J, Bruhn H, Neumann F, Thiesen B, von DA, Felix R (2006) The effect of thermotherapy using magnetic nanoparticles on rat malignant glioma. *J Neurooncol* **78**: 7-14

Jordan A, Scholz R, Wust P, Fahling H, Krause J, Wlodarczyk W, Sander B, Vogl T, Felix R (1997) Effects of magnetic fluid hyperthermia (MFH) on C3H mammary carcinoma in vivo. *Int J Hyperthermia* **13**: 587-605

Jordan A, Scholz R, Wust P, Schirra H, Schiestel T, Schmidt H, Felix R (1999) Endocytosis of dextran and silan-coated magnetite nanoparticles and the effect of intracellular hyperthermia on human mammary carcinoma cells in vitro. *J Magn Magn Mater* **194**: 185-196

Jordan A, Scholz R, Wust P, Fähling H, Felix R (1999) Magnetic fluid hyperthermia (MFH): Cancer treatment with AC magnetic field induced exceitation of biocompatible superparamagnetic nanoparticles. *J Magn Magn Mater* **201**: 413-419

Jordan A, Wust P, Scholz R, Tesche B, Fahling H, Mitrovics T, Vogl T, Cervos-Navarro J, Felix R (1996) Cellular uptake of magnetic fluid particles and their effects on human adenocarcinoma cells exposed to AC magnetic fields in vitro. *Int J Hyperthermia* **12**: 705-722

Jordan E, Al-Halabi L, Schirrmann T, Hust M, Dubel S (2007) Production of single chain Fab (scFab) fragments in Bacillus megaterium. *Microb Cell Fact* **6**: 38

Joyce JA, Pollard JW (2009) Microenvironmental regulation of metastasis. *Nat Rev Cancer* **9**: 239-252

Jung CW (1995) Surface properties of superparamagnetic iron oxide MR contrast agents: ferumoxides, ferumoxtran, ferumoxsil. *Magn Reson Imaging* **13**: 675-691

Jung CW, Jacobs P (1995) Physical and chemical properties of superparamagnetic iron oxide MR contrast agents: ferumoxides, ferumoxtran, ferumoxsil. *Magn Reson Imaging* **13**: 661-674

Kaittanis C, Santra S, Perez JM (2009) Role of Nanoparticle Valency in the Nondestructive Magnetic-Relaxation-Mediated Detection and Magnetic Isolation of Cells in Complex Media. *J Am Chem Soc*

Kalambur VS, Longmire EK, Bischof JC (2007) Cellular level loading and heating of superparamagnetic iron oxide nanoparticles. *Langmuir* **23**: 12329-12336

Kalambur VS, Han B, Hammer B, Shield TW, Bischof JC (2005) In Vitro characterization of movement, heating and visualisation of magnetic nanoparticles for biomedical applications. *Nanotechnology* **16**: 1221-1233

Kallumadil M, Tada M, Nakagawa T, Abe M, Southern P, Pankhurst QA (2009) Suitability of commercial colloids for magnetic hyperthermia. *J. Magn Magn Mater* **321**: 1509-1513

Kamarck ME, Elting JJ, Hart JT, Goebel SJ, Rae PM, Nothdurft MA, Nedwin JJ, Barnett TR (1987) Carcinoembryonic antigen family: expression in a mouse L-cell transfectant and characterization of a partial cDNA in bacteriophage lambda gt11. *Proc Natl Acad Sci U S A* **84**: 5350-5354

Kettering M, Winter J, Zeisberger M, Bremer-Streck S, Oehring H, Bergemann C, Alexiou C, Hergt R, Halbhuber KJ, Kaiser WA, Hilger I (2007) Magnetic nanoparticles as biomodal tools in magnetically induced labelling and magnetic heating of tumour cells: an in vitro study. *Nanotechnology* **18:** 1-9

Khan WN, Hammarstrom S (1990) Identification of a new carcinoembryonic antigen (CEA) family member in human fetal liver--cloning and sequence determination of pregnancy-specific glycoprotein 7. *Biochem Biophys Res Commun* **168**: 214-225

Klein CA (2009) Parallel progression of primary tumours and metastases. *Nat Rev Cancer* **9**: 302-312

Kohler G, Milstein C (1975) Continuous cultures of fused cells secreting antibody of predefined specificity. *Nature* **256**: 495-497

Kohler N, Fryxell GE, Zhang M (2004) A bifunctional poly(ethylene glycol) silane immobilized on metallic oxide-based nanoparticles for conjugation with cell targeting agents. *J Am Chem Soc* **126**: 7206-7211

Koneracká M, Kopčanský, Antalik M, Timko M, Ramchand CN, Lobo D, Mehta RV, Upadhyay RV (1999) Immobilization of proteins and enzymes to fine magnetic particles. *J Magn Magn Mater* **201:** 427-430

Kortt AA, Dolezal O, Power BE, Hudson PJ (2001) Dimeric and trimeric antibodies: high avidity scFvs for cancer targeting. *Biomol Eng* **18**: 95-108

Kostarelos K (2008) The long and short of carbon nanotube toxicity. *Nat Biotechnol* **26**: 774-776

Kousparou CA, Epenetos AA, Deonarain MP (2002) Antibody-guided enzyme therapy of cancer producing cyanide results in necrosis of targeted cells. *Int J Cancer* **99**: 138-148

Krapp S, Mimura Y, Jefferis R, Huber R, Sondermann P (2003) Structural analysis of human IgG-Fc glycoforms reveals a correlation between glycosylation and structural integrity. *J Mol Biol* **325**: 979-989

Kreitman RJ, Pastan I (1998) Accumulation of a recombinant immunotoxin in a tumor in vivo: fewer than 1000 molecules per cell are sufficient for complete responses. *Cancer Res* **58**: 968-975

Kresse M, Wagner S, Pfefferer D, Lawaczeck R, Elste V, Semmler W (1998) Targeting of ultrasmall superparamagnetic iron oxide (USPIO) particles to tumor cells in vivo by using transferrin receptor pathways. *Magn Reson Med* **40**: 236-242

Kubetzko S, Balic E, Waibel R, Zangemeister-Wittke U, Pluckthun A (2006) PEGylation and multimerization of the anti-p185HER-2 single chain Fv fragment 4D5: effects on tumor targeting. *J Biol Chem* **281**: 35186-35201

Lanza GM, Winter PM, Caruthers SD, Morawski AM, Schmieder AH, Crowder KC, Wickline SA (2004) Magnetic resonance molecular imaging with nanoparticles. *J Nucl Cardiol* **11**: 733-743

Lao LL, Ramanujan RV (2004) Magnetic and hydrogel composite materials for hyperthermia applications. *J Mater Sci Mater Med* **15**: 1061-1064

Lee LS, Conover C, Shi C, Whitlow M, Filpula D (1999) Prolonged circulating lives of single-chain Fv proteins conjugated with polyethylene glycol: a comparison of conjugation chemistries and compounds. *Bioconjug Chem* **10**: 973-981

Lemieux B, Coiffier B (2005) Radio-immunotherapy in low-grade non-Hodgkin's lymphoma. *Best Pract Res Clin Haematol* **18**: 81-95

Lentz BR (1994) Polymer-induced membrane fusion: potential mechanism and relation to cell fusion events. *Chem Phys Lipids* **73**: 91-106

Lentz BR, Lee JK (1999) Poly(ethylene glycol) (PEG)-mediated fusion between pure lipid bilayers: a mechanism in common with viral fusion and secretory vesicle release? *Mol Membr Biol* **16**: 279-296

Leuschner C, Kumar CS, Hansel W, Soboyejo W, Zhou J, Hormes J (2006) LHRH-conjugated magnetic iron oxide nanoparticles for detection of breast cancer metastases. *Breast Cancer Res Treat* **99**: 163-176

Li X, Du X, Huo T, Liu X, Zhang S, Yuan F (2009) Specific Targeting of Breast Tumor by Octreotide-Conjugated Ultrasmall Superparamagnetic Iron Oxide Particles Using a Clinical 3.0-Tesla Magnetic Resonance Scanner. *Acta Radiol* 1-12

Lotan R, Debray H, Cacan M, Cacan R, Sharons N (1975) Labeling of soybean agglutinin by oxidation with sodium periodate followed by reduction with sodium [3-H]borohydride. *J Biol Chem* **250**: 1955-1957

Magdelaine-Beuzelin C, Kaas Q, Wehbi V, Ohresser M, Jefferis R, Lefranc MP, Watier H (2007) Structure-function relationships of the variable domains of monoclonal antibodies approved for cancer treatment. *Crit Rev Oncol Hematol* **64**: 210-225

Maier-Hauff K, Rothe R, Scholz R, Gneveckow U, Wust P, Thiesen B, Feussner A, von DA, Waldoefner N, Felix R, Jordan A (2007) Intracranial thermotherapy using magnetic nanoparticles combined with external beam radiotherapy: results of a feasibility study on patients with glioblastoma multiforme. *J Neurooncol* **81**: 53-60

Mailander V, Lorenz MR, Holzapfel V, Musyanovych A, Fuchs K, Wiesneth M, Walther P, Landfester K, Schrezenmeier H (2008) Carboxylated superparamagnetic iron oxide particles label cells intracellularly without transfection agents. *Mol Imaging Biol* **10**: 138-146

Malumbres M, Barbacid M (2009) Cell cycle, CDKs and cancer: a changing paradigm. *Nat Rev Cancer* **9**: 153-166

Mao S, Gao C, Lo CH, Wirsching P, Wong CH, Janda KD (1999) Phage-display library selection of high-affinity human single-chain antibodies to tumor-associated carbohydrate antigens sialyl Lewisx and Lewisx. *Proc Natl Acad Sci U S A* **96**: 6953-6958

Maruyama K, Takizawa T, Yuda T, Kennel SJ, Huang L, Iwatsuru M (1995) Targetability of novel immunoliposomes modified with amphipathic poly(ethylene glycol)s conjugated at their distal terminals to monoclonal antibodies. *Biochim Biophys Acta* **1234**: 74-80

Matsuoka F, Shinkai M, Honda H, Kubo T, Sugita T, Kobayashi T (2004) Hyperthermia using magnetite cationic liposomes for hamster osteosarcoma. *Biomagn Res Technol* **2**: 3

Mayer A, Francis RJ, Sharma SK, Tolner B, Springer CJ, Martin J, Boxer GM, Bell J, Green AJ, Hartley JA, Cruickshank C, Wren J, Chester KA, Begent RH (2006) A phase I study of single administration of antibody-directed enzyme prodrug therapy with the recombinant anti-carcinoembryonic antigen antibody-enzyme fusion protein MFECP1 and a bis-iodo phenol mustard prodrug. *Clin Cancer Res* **12**: 6509-6516

Mayer A, Tsiompanou E, O'Malley D, Boxer GM, Bhatia J, Flynn AA, Chester KA, Davidson BR, Lewis AA, Winslet MC, Dhillon AP, Hilson AJ, Begent RH (2000) Radioimmunoguided surgery in colorectal cancer using a genetically engineered anti-CEA single-chain Fv antibody. *Clin Cancer Res* **6**: 1711-1719

McBain SC, Yiu HH, Dobson J (2008) Magnetic nanoparticles for gene and drug delivery. *Int J Nanomedicine* **3**: 169-180

McCafferty J, Griffiths AD, Winter G, Chiswell DJ (1990) Phage antibodies: filamentous phage displaying antibody variable domains. *Nature* **348**: 552-554

Mehta RV, Upadhyay RV, Charles SW, Ramchand CN (1997) Direct binding of proteins to magnetic particles. *Biotech Tech* **11** (7): 493-496

Michael NP, Chester KA, Melton RG, Robson L, Nicholas W, Boden JA, Pedley RB, Begent RH, Sherwood RF, Minton NP (1996) In vitro and in vivo characterisation of a recombinant carboxypeptidase G2::anti-CEA scFv fusion protein. *Immunotechnology* **2**: 47-57

Modi S, Prakash JJ, Domb AJ, Kumar N (2006) Exploiting EPR in polymer drug conjugate delivery for tumor targeting. *Curr Pharm Des* **12**: 4785-4796

Molday RS, MacKenzie D (1982) Immunospecific ferromagnetic iron-dextran reagents for the labeling and magnetic separation of cells. *J Immunol Methods* **52**: 353-367

Moore A, Marecos E, Bogdanov A, Jr., Weissleder R (2000) Tumoral distribution of long-circulating dextran-coated iron oxide nanoparticles in a rodent model. *Radiology* **214**: 568-574

Moore A, Weissleder R, Bogdanov A, Jr. (1997) Uptake of dextran-coated monocrystalline iron oxides in tumor cells and macrophages. *J Magn Reson Imaging* **7**: 1140-1145

Mornet S, Vasseur S, Grasset F, Duguet E (2004) Magnetic nanoparticle design for medical diagnosis and therapy. *J Mater Chem* **14**: 2161-2175

Moroz P, Jones SK, Gray BN (2002) Magnetically mediated hyperthermia: current status and future directions. *Int J Hyperthermia* **18**: 267-284

Mosmann T (1983) Rapid colorimetric assay for cellular growth and survival: application to proliferation and cytotoxicity assays. *J Immunol Methods* **65**: 55-63

Motoyama J, Hakata T, Kato R, Yamashita N, Morino T, Kobayashi T, Honda H (2008) Size dependent heat generation of magnetite nanoparticles under AC magnetic field for cancer therapy. *Biomagn Res Technol* **6**: 4

Mountain A, Adair JR (1992) Engineering antibodies for therapy. *Biotechnol Genet Eng Rev* **10**: 1-142

Muyldermans S (2001) Single domain camel antibodies: current status. *J Biotechnol* **74**: 277-302

Muyldermans S, Atarhouch T, Saldanha J, Barbosa JA, Hamers R (1994) Sequence and structure of VH domain from naturally occurring camel heavy chain immunoglobulins lacking light chains. *Protein Eng* **7**: 1129-1135

Nahta R, Esteva FJ (2006) Herceptin: mechanisms of action and resistance. *Cancer Lett* **232**: 123-138

Natarajan A, Gruettner C, Ivkov R, DeNardo GL, Mirick G, Yuan A, Foreman A, DeNardo SJ (2008a) NanoFerrite particle based radioimmunonanoparticles: binding affinity and in vivo pharmacokinetics. *Bioconjug Chem* **19**: 1211-1218

Natarajan A, Xiong CY, Gruettner C, DeNardo GL, DeNardo SJ (2008b) Development of multivalent radioimmunonanoparticles for cancer imaging and therapy. *Cancer Biother Radiopharm* **23**: 82-91

Nelson AL, Reichert JM (2009) Development trends for therapeutic antibody fragments. *Nat Biotechnol* **27**: 331-337

Neuberger MS, Ehrenstein MR, Klix N, Jolly CJ, Yelamos J, Rada C, Milstein C (1998) Monitoring and interpreting the intrinsic features of somatic hypermutation. *Immunol Rev* **162**: 107-116

Neumaier M, Zimmermann W, Shively L, Hinoda Y, Riggs AD, Shively JE (1988) Characterization of a cDNA clone for the nonspecific cross-reacting antigen (NCA) and a comparison of NCA and carcinoembryonic antigen. *J Biol Chem* **263**: 3202-3207

Nielsen UB, Adams GP, Weiner LM, Marks JD (2000) Targeting of bivalent anti-ErbB2 diabody antibody fragments to tumor cells is independent of the intrinsic antibody affinity. *Cancer Res* **60**: 6434-6440

Nilsson F, Tarli L, Viti F, Neri D (2000) The use of phage display for the development of tumour targeting agents. *Adv Drug Deliv Rev* **43**: 165-196

Oikawa S, Imajo S, Noguchi T, Kosaki G, Nakazato H (1987a) The carcinoembryonic antigen (CEA) contains multiple immunoglobulin-like domains. *Biochem Biophys Res Commun* **144**: 634-642

Oikawa S, Kosaki G, Nakazato H (1987b) Molecular cloning of a gene for a member of carcinoembryonic antigen (CEA) gene family; signal peptide and N-terminal domain sequences of nonspecific crossreacting antigen (NCA). *Biochem Biophys Res Commun* **146**: 464-469

Oikawa S, Nakazato H, Kosaki G (1987c) Primary structure of human carcinoembryonic antigen (CEA) deduced from cDNA sequence. *Biochem Biophys Res Commun* **142**: 511-518

Okayama T, Kokura S, Ishikawa T, Adachi S, Hattori T, Takagi T, Handa O, Naito Y, Yoshikawa T (2009) Antitumor effect of pretreatment for colon cancer cells with hyperthermia plus geranylgeranylacetone in experimental metastasis models and a subcutaneous tumor model of colon cancer in mice. *Int J Hyperthermia* **25**: 141-149

Okawa K, Sekine M, Maeda M, Tda M, Abe M (2006) Heating ability of magnetite nanobeads with various sizes for magnetic hyperthermia at 120kHz, a noninvasive frequency. *J Appl Phys* **99** (102):1-3

Okon E, Pouliquen D, Okon P, Kovaleva ZV, Stepanova TP, Lavit SG, Kudryavtsev BN, Jallet P (1994) Biodegradation of magnetite dextran nanoparticles in the rat. A histologic and biophysical study. *Lab Invest* **71**: 895-903

Olsen A, Teglund S, Nelson D, Gordon L, Copeland A, Georgescu A, Carrano A, Hammarstrom S (1994) Gene organization of the pregnancy-specific glycoprotein region on human chromosome 19: assembly and analysis of a 700-kb cosmid contig spanning the region. *Genomics* **23**: 659-668

Owens DE, III, Peppas NA (2006) Opsonization, biodistribution, and pharmacokinetics of polymeric nanoparticles. *Int J Pharm* **307**: 93-102

Panagi Z, Beletsi A, Evangelatos G, Livaniou E, Ithakissios DS, Avgoustakis K (2001) Effect of dose on the biodistribution and pharmacokinetics of PLGA and PLGA-mPEG nanoparticles. *Int J Pharm* **221**: 143-152

Pankhurst Q, Connolly J, Jones SK, Dobson J (2003) Application of magnetic nanoparticles in biomedicine. *J Phys D Appl Phys* **36:** R167-R181

Pantoliano MW, Bird RE, Johnson S, Asel ED, Dodd SW, Wood JF, Hardman KD (1991) Conformational stability, folding, and ligand-binding affinity of single-chain Fv immunoglobulin fragments expressed in Escherichia coli. *Biochemistry* **30**: 10117-10125

Pardoe H, Chua-anusorn W, St Pierre TG, Dobson J (2003) Detection limits for ferrimagnetic particle concentrations using magnetic resonance imaging based proton transverse relaxation rate measurements. *Phys Med Biol* **48**: N89-N95

Park JW, Hong K, Kirpotin DB, Colbern G, Shalaby R, Baselga J, Shao Y, Nielsen UB, Marks JD, Moore D, Papahadjopoulos D, Benz CC (2002) Anti-HER2 immunoliposomes: enhanced efficacy attributable to targeted delivery. *Clin Cancer Res* **8**: 1172-1181

Patil S, Sandberg A, Heckert E, Self W, Seal S (2007) Protein adsorption and cellular uptake of cerium oxide nanoparticles as a function of zeta potential. *Biomaterials* **28**: 4600-4607

Paxton RJ, Mooser G, Pande H, Lee TD, Shively JE (1987) Sequence analysis of carcinoembryonic antigen: identification of glycosylation sites and homology with the immunoglobulin supergene family. *Proc Natl Acad Sci U S A* **84**: 920-924

Peng XH, Qian X, Mao H, Wang AY, Chen ZG, Nie S, Shin DM (2008) Targeted magnetic iron oxide nanoparticles for tumor imaging and therapy. *Int J Nanomedicine* **3**: 311-321

Pinkernelle J, Teichgraber U, Neumann F, Lehmkuhl L, Ricke J, Scholz R, Jordan A, Bruhn H (2005) Imaging of single human carcinoma cells in vitro using a clinical whole-body magnetic resonance scanner at 3.0 T. *Magn Reson Med* **53**: 1187-1192

Pluckthun A, Pack P (1997) New protein engineering approaches to multivalent and bispecific antibody fragments. *Immunotechnology* **3**: 83-105

Pohlman B, Sweetenham J, Macklis RM (2006) Review of clinical radioimmunotherapy. *Expert Rev Anticancer Ther* **6**: 445-461

Porter RJ (1962) Prolonged suppression by x-ray of adaptation for the secondary antibody response. *Proc Soc Exp Biol Med* **111**: 583-584

Porter RR (1958) Separation and isolation of fractions of rabbit gamma-globulin containing the antibody and antigenic combining sites. *Nature* **182**: 670-671

Pun SH, Tack F, Bellocq NC, Cheng J, Grubbs BH, Jensen GS, Davis ME, Brewster M, Janicot M, Janssens B, Floren W, Bakker A (2004) Targeted delivery of RNA-cleaving DNA enzyme (DNAzyme) to tumor tissue by transferrin-modified, cyclodextrin-based particles. *Cancer Biol Ther* **3**: 641-650

Rabin Y (2002) Is intracellular hyperthermia superior to extracellular hyperthermia in the thermal sense? *Int J Hyperthermia* **18**: 194-202

Renshaw PF, Owen CS, McLaughlin AC, Frey TG, Leigh JS, Jr. (1986) Ferromagnetic contrast agents: a new approach. *Magn Reson Med* **3**: 217-225

Reynolds PR, Larkman DJ, Haskard DO, Hajnal JV, Kennea NL, George AJ, Edwards AD (2006) Detection of vascular expression of E-selectin in vivo with MR imaging. *Radiology* **241**: 469-476

Riechmann L, Foote J, Winter G (1988) Expression of an antibody Fv fragment in myeloma cells. *J Mol Biol* **203**: 825-828

Riemer J, Hoepken HH, Czerwinska H, Robinson SR, Dringen R (2004) Colorimetric ferrozine-based assay for the quantitation of iron in cultured cells. *Anal Biochem* **331**: 370-375

Rockall AG, Sohaib SA, Harisinghani MG, Babar SA, Singh N, Jeyarajah AR, Oram DH, Jacobs IJ, Shepherd JH, Reznek RH (2005) Diagnostic performance of nanoparticle-enhanced magnetic resonance imaging in the diagnosis of lymph node metastases in patients with endometrial and cervical cancer. *J Clin Oncol* **23**: 2813-2821

Rothfus JA, Smith EL (1963) Glycopeptides. IV. The periodate oxidation of glycopeptides from human gamma-globulin. *J Biol Chem* **238**: 1402-1410

Sack TL, Gum JR, Low MG, Kim YS (1988) Release of carcinoembryonic antigen from human colon cancer cells by phosphatidylinositol-specific phospholipase C. *J Clin Invest* **82**: 586-593

Sainz-Pastor N, Tolner B, Huhalov A, Kogelberg H, Lee YC, Zhu D, Begent RH, Chester KA (2006) Deglycosylation to obtain stable and homogeneous Pichia pastoris-expressed N-A1 domains of carcinoembryonic antigen. *Int J Biol Macromol* **39**: 141-150

Samanta B, Yan H, Fischer NO, Shi J, Jerry DJ, Rotello VM (2008) Protein-passivated Fe(3)O(4) nanoparticles: low toxicity and rapid heating for thermal therapy. *J Mater Chem* **18**: 1204-1208

Sblattero D, Bradbury A (2000) Exploiting recombination in single bacteria to make large phage antibody libraries. *Nat Biotechnol* **18**: 75-80

Scherf U, Benhar I, Webber KO, Pastan I, Brinkmann U (1996) Cytotoxic and antitumor activity of a recombinant tumor necrosis factor-B1(Fv) fusion protein on LeY antigen-expressing human cancer cells. *Clin Cancer Res* **2**: 1523-1531

Sebastian M, Kiewe P, Schuette W, Brust D, Peschel C, Schneller F, Ruhle KH, Nilius G, Ewert R, Lodziewski S, Passlick B, Sienel W, Wiewrodt R, Jager M, Lindhofer H, Friccius-Quecke H, Schmittel A (2009) Treatment of malignant pleural effusion with the trifunctional antibody catumaxomab (Removab) (anti-EpCAM x Anti-CD3): results of a phase 1/2 study. *J Immunother* **32**: 195-202

Seki T, Wakabayashi M, Nakagawa T, Imamura M, Tamai T, Nishimura A, Yamashiki N, Okamura A, Inoue K (1999) Percutaneous microwave coagulation therapy for patients with small hepatocellular carcinoma: comparison with percutaneous ethanol injection therapy. *Cancer* **85**: 1694-1702

Senter PD (1990) Activation of prodrugs by antibody-enzyme conjugates: a new approach to cancer therapy. *FASEB J* **4**: 188-193

Senter PD, Saulnier MG, Schreiber GJ, Hirschberg DL, Brown JP, Hellstrom I, Hellstrom KE (1988) Anti-tumor effects of antibody-alkaline phosphatase conjugates in combination with etoposide phosphate. *Proc Natl Acad Sci U S A* **85**: 4842-4846

Sharkey RM, Goldenberg DM (2006) Targeted therapy of cancer: new prospects for antibodies and immunoconjugates. *CA Cancer J Clin* **56**: 226-243

Sharma SK, Pedley RB, Bhatia J, Boxer GM, El-Emir E, Qureshi U, Tolner B, Lowe H, Michael NP, Minton N, Begent RH, Chester KA (2005) Sustained tumor regression of human colorectal cancer xenografts using a multifunctional mannosylated fusion protein in antibody-directed enzyme prodrug therapy. *Clin Cancer Res* **11**: 814-825

Shinkai M, Ito A (2004) Functional magnetic particles for medical application. *Adv Biochem Eng Biotechnol* **91**: 191-220

Shinkai M, Le B, Honda H, Yoshikawa K, Shimizu K, Saga S, Wakabayashi T, Yoshida J, Kobayashi T (2001) Targeting hyperthermia for renal cell carcinoma using human MN antigen-specific magnetoliposomes. *Jpn J Cancer Res* **92**: 1138-1145

Shinkai M, Suzuki M, Iijima S, Kobayashi T (1995) Antibody-conjugated magnetoliposomes for targeting cancer cells and their application in hyperthermia. *Biotechnol Appl Biochem* **21 (Pt 2)**: 125-137

Shinkai M, Ueda K, Ohtsu S, Honda H, Kohri K, Kobayashi T (1999) Effect of functional magnetic particles on radiofrequency capacitive heating. *Jpn J Cancer Res* **90**: 699-704

Shinkai M, Ueda K, Ohtsu S, Honda H, Kohri K, Kobayashi T (2002) Effect of functional magnetic particles on radiofrequency capacitive heating: an in vivo study. *Jpn J Cancer Res* **93**: 103-108

Shinkai M, Yanase M, Honda H, Wakabayashi T, Yoshida J, Kobayashi T (1996) Intracellular hyperthermia for cancer using magnetite cationic liposomes: in vitro study. *Jpn J Cancer Res* **87**: 1179-1183

Shmeeda H, Tzemach D, Mak L, Gabizon A (2009) Her2-targeted pegylated liposomal doxorubicin: Retention of target-specific binding and cytotoxicity after in vivo passage. *J Control Release*

Skerra A (1993) Bacterial expression of immunoglobulin fragments. *Curr Opin Immunol* **5**: 256-262

Skerra A, Pluckthun A (1988) Assembly of a functional immunoglobulin Fv fragment in Escherichia coli. *Science* **240**: 1038-1041

Smith GP (1985) Filamentous fusion phage: novel expression vectors that display cloned antigens on the virion surface. *Science* **228**: 1315-1317

Smith SC, Theodorescu D (2009) Learning therapeutic lessons from metastasis suppressor proteins. *Nat Rev Cancer* **9**: 253-264

Sofou S, Thomas JL, Lin HY, McDevitt MR, Scheinberg DA, Sgouros G (2004) Engineered liposomes for potential alpha-particle therapy of metastatic cancer. *J Nucl Med* **45**: 253-260

Song CW, Shakil A, Osborn JL, Iwata K (1996) Tumour oxygenation is increased by hyperthermia at mild temperatures. *Int J Hyperthermia* **12**: 367-373

Song CW, Park HJ, Lee CK, Griffin R (2005) Implications of increased tumor blood flow and oxygenation caused by mild temperature hyperthermia in tumor treatment. *Int J Hyperthermia* **21**: 761-767

Srivastava PK, Menoret A, Basu S, Binder RJ, McQuade KL (1998) Heat shock proteins come of age: primitive functions acquire new roles in an adaptive world. *Immunity* **8**: 657-665

Staros JV, Wright RW, Swingle DM (1986) Enhancement by N-hydroxysulfosuccinimide of water-soluble carbodiimide-mediated coupling reactions. *Anal Biochem* **156**: 220-222

Stijlemans B, Conrath K, Cortez-Retamozo V, Van XH, Wyns L, Senter P, Revets H, De BP, Muyldermans S, Magez S (2004) Efficient targeting of conserved cryptic epitopes of infectious agents by single domain antibodies. African trypanosomes as paradigm. *J Biol Chem* **279**: 1256-1261

Stratton MR, Campbell PJ, Futreal PA (2009) The cancer genome. *Nature* **458**: 719-724

Strebhardt K, Ullrich A (2008) Paul Ehrlich's magic bullet concept: 100 years of progress. *Nat Rev Cancer* **8**: 473-480

Sun C, Wirsching P, Janda KD (2003) Enabling ScFvs as multi-drug carriers: a dendritic approach. *Bioorg Med Chem* **11**: 1761-1768

Suwa T, Ozawa S, Ueda M, Ando N, Kitajima M (1998) Magnetic resonance imaging of esophageal squamous cell carcinoma using magnetite particles coated with anti-epidermal growth factor receptor antibody. *Int J Cancer* **75**: 626-634

Suzuki M, Honda H, Kobayashi T, Wakabayashi T, Yoshida J, Takahashi M (1996) Development of a target-directed magnetic resonance contrast agent using monoclonal antibody-conjugated magnetic particles. *Noshuyo Byori* **13**: 127-132

Suzuki M, Shinkai M, Honda H, Kobayashi T (2003) Anticancer effect and immune induction by hyperthermia of malignant melanoma using magnetite cationic liposomes. *Melanoma Res* **13**: 129-135

Svenberg T (1976) Carcinoembryonic antigen-like substances of human bile. Isolation and partial characterization. *Int J Cancer* **17**: 588-596

Tabuchi Y, Takasaki I, Wada S, Zhao QL, Hori T, Nomura T, Ohtsuka K, Kondo T (2008) Genes and genetic networks responsive to mild hyperthermia in human lymphoma U937 cells. *Int J Hyperthermia* **24**: 613-622

Taheri M, Saragovi HU, Stanners CP (2003) The adhesion and differentiation-inhibitory activities of the immunoglobulin superfamily member, carcinoembryonic antigen, can be independently blocked. *J Biol Chem* **278**: 14632-14639

Takami N, Misumi Y, Kuroki M, Matsuoka Y, Ikehara Y (1988) Evidence for carboxyl-terminal processing and glycolipid-anchoring of human carcinoembryonic antigen. *J Biol Chem* **263**: 12716-12720

Tang Y, Jiang N, Parakh C, Hilvert D (1996) Selection of linkers for a catalytic single-chain antibody using phage display technology. *J Biol Chem* **271**: 15682-15686

Tao MH, Morrison SL (1989) Studies of aglycosylated chimeric mouse-human IgG. Role of carbohydrate in the structure and effector functions mediated by the human IgG constant region. *J Immunol* **143**: 2595-2601

Teglund S, Olsen A, Khan WN, Frangsmyr L, Hammarstrom S (1994) The pregnancy-specific glycoprotein (PSG) gene cluster on human chromosome 19: fine structure of the 11 PSG genes and identification of 6 new genes forming a third subgroup within the carcinoembryonic antigen (CEA) family. *Genomics* **23**: 669-684

Thiesen B, Jordan A (2008) Clinical applications of magnetic nanoparticles for hyperthermia. *Int J Hyperthermia* **24**: 467-474

Thompson JA, Pande H, Paxton RJ, Shively L, Padma A, Simmer RL, Todd CW, Riggs AD, Shively JE (1987) Molecular cloning of a gene belonging to the carcinoembryonic antigen gene family and discussion of a domain model. *Proc Natl Acad Sci U S A* **84**: 2965-2969

Thorek DL, Chen AK, Czupryna J, Tsourkas A (2006) Superparamagnetic iron oxide nanoparticle probes for molecular imaging. *Ann Biomed Eng* **34**: 23-38

Tiefenauer LX, Kuhne G, Andres RY (1993) Antibody-magnetite nanoparticles: in vitro characterization of a potential tumor-specific contrast agent for magnetic resonance imaging. *Bioconjug Chem* **4**: 347-352

Tiefenauer LX, Tschirky A, Kuhne G, Andres RY (1996) In vivo evaluation of magnetite nanoparticles for use as a tumor contrast agent in MRI. *Magn Reson Imaging* **14**: 391-402

Tjandra JJ, Ramadi L, McKenzie IF (1990) Development of human anti-murine antibody (HAMA) response in patients. *Immunol Cell Biol* **68 (Pt 6)**: 367-376

Todorovska A, Roovers RC, Dolezal O, Kortt AA, Hoogenboom HR, Hudson PJ (2001) Design and application of diabodies, triabodies and tetrabodies for cancer targeting. *J Immunol Methods* **248**: 47-66

Todryk S, Melcher AA, Hardwick N, Linardakis E, Bateman A, Colombo MP, Stoppacciaro A, Vile RG (1999) Heat shock protein 70 induced during tumor cell killing induces Th1 cytokines and targets immature dendritic cell precursors to enhance antigen uptake. *J Immunol* **163**: 1398-1408

Tolner B, Smith L, Begent RH, Chester KA (2006a) Expanded-bed adsorption immobilized-metal affinity chromatography. *Nat Protoc* **1**: 1213-1222

Tolner B, Smith L, Begent RH, Chester KA (2006b) Production of recombinant protein in Pichia pastoris by fermentation. *Nat Protoc* **1**: 1006-1021

Tolner B, Smith L, Hillyer T, Bhatia J, Beckett P, Robson L, Sharma SK, Griffin N, Vervecken W, Contreras R, Pedley RB, Begent RH, Chester KA (2007) From laboratory to Phase I/II cancer trials with recombinant biotherapeutics. *Eur J Cancer* **43**: 2515-2522

Toma A, Otsuji E, Kuriu Y, Okamoto K, Ichikawa D, Hagiwara A, Ito H, Nishimura T, Yamagishi H (2005) Monoclonal antibody A7-superparamagnetic iron oxide as contrast agent of MR imaging of rectal carcinoma. *Br J Cancer* **93**: 131-136

Tonegawa S (1983) Somatic generation of antibody diversity. *Nature* **302**: 575-581

Turner DJ, Ritter MA, George AJ (1997) Importance of the linker in expression of single-chain Fv antibody fragments: optimisation of peptide sequence using phage display technology. *J Immunol Methods* **205**: 43-54

Van Lenten L, Ashwell G (1971) Studies on the chemical and enzymatic modification of glycoproteins. A general method for the tritiation of sialic acid-containing glycoproteins. *J Biol Chem* **246**: 1889-1894

van den Beucken T, van NN, Sablon E, Desmet J, Celis L, Hoogenboom HR, Hufton SE (2001) Building novel binding ligands to B7.1 and B7.2 based on human antibody single variable light chain domains. *J Mol Biol* **310**: 591-601

Vaupel P, Muller-Klieser W, Otte J, Manz R (1984) Impact of various thermal doses on the oxygenation and blood flow in malignant tumors upon localized hyperthermia. *Adv Exp Med Biol* **169**: 621-629

Vaupel PW (1997) The influence of tumor blood flow and microenvironmental factors on the efficacy of radiation, drugs and localized hyperthermia. *Klin Padiatr* **209**: 243-249

Vernon CC, Hand JW, Field SB, Machin D, Whaley JB, van der ZJ, van Putten WL, van Rhoon GC, van Dijk JD, Gonzalez GD, Liu FF, Goodman P, Sherar M (1996) Radiotherapy with or without hyperthermia in the treatment of superficial localized breast cancer: results from five randomized controlled trials. International Collaborative Hyperthermia Group. *Int J Radiat Oncol Biol Phys* **35**: 731-744

Villanueva A, Canete M, Roca AG, Calero M, Veintemillas-Verdaguer S, Serna CJ, Morales MP, Miranda R (2009) The influence of surface functionalization on the enhanced internalization of magnetic nanoparticles in cancer cells. *Nanotechnology* **20**: 115103

Virji M (2001) CEA and innate immunity. *Trends Microbiol* **9**: 258-259

Vogl TJ, Mack MG, Muller PK, Straub R, Engelmann K, Eichler K (1999) Interventional MR: interstitial therapy. *Eur Radiol* **9**: 1479-1487

von Kleist S, Chavanel G, Burtin P (1972) Identification of an antigen from normal human tissue that crossreacts with the carcinoembryonic antigen. *Proc Natl Acad Sci U S A* **69**: 2492-2494

von Mehren M, Adams GP, Weiner LM (2003) Monoclonal antibody therapy for cancer. *Annu Rev Med* **54**: 343-369

Wallis F, Gilbert FJ (1999) Magnetic resonance imaging in oncology: an overview. *J R Coll Surg Edinb* **44**: 117-125

Wang X, Gu H, Yang Z (2005) The heating effect of magnetic fluids in an alternating magnetic field. *J Magn Magn Mater* **293**: 334-340

Wang XY, Kaneko Y, Repasky E, Subjeck JR (2000) Heat shock proteins and cancer immunotherapy. *Immunol Invest* **29**: 131-137

Wang YX, Hussain SM, Krestin GP (2001) Superparamagnetic iron oxide contrast agents: physicochemical characteristics and applications in MR imaging. *Eur Radiol* **11**: 2319-2331

Ward ES, Gussow D, Griffiths AD, Jones PT, Winter G (1989) Binding activities of a repertoire of single immunoglobulin variable domains secreted from Escherichia coli. *Nature* **341**: 544-546

Weissleder R, Elizondo G, Wittenberg J, Rabito CA, Bengele HH, Josephson L (1990) Ultrasmall superparamagnetic iron oxide: characterization of a new class of contrast agents for MR imaging. *Radiology* **175**: 489-493

Weissleder R, Lee AS, Khaw BA, Shen T, Brady TJ (1992) Antimyosin-labeled monocrystalline iron oxide allows detection of myocardial infarct: MR antibody imaging. *Radiology* **182**: 381-385

Weng KC, Noble CO, Papahadjopoulos-Sternberg B, Chen FF, Drummond DC, Kirpotin DB, Wang D, Hom YK, Hann B, Park JW (2008) Targeted tumor cell internalization and imaging of multifunctional quantum dot-conjugated immunoliposomes in vitro and in vivo. *Nano Lett* **8**: 2851-2857

Whitlow M, Bell BA, Feng SL, Filpula D, Hardman KD, Hubert SL, Rollence ML, Wood JF, Schott ME, Milenic DE, . (1993) An improved linker for single-chain Fv with reduced aggregation and enhanced proteolytic stability. *Protein Eng* **6**: 989-995

Wilhelm C, Billotey C, Roger J, Pons JN, Bacri JC, Gazeau F (2003) Intracellular uptake of anionic superparamagnetic nanoparticles as a function of their surface coating. *Biomaterials* **24**: 1001-1011

Wilhelm C, Gazeau F (2008) Universal cell labelling with anionic magnetic nanoparticles. *Biomaterials* **29**: 3161-3174

Winter G, Griffiths AD, Hawkins RE, Hoogenboom HR (1994) Making antibodies by phage display technology. *Annu Rev Immunol* **12**: 433-455

Worn A, Pluckthun A (2001) Stability engineering of antibody single-chain Fv fragments. *J Mol Biol* **305**: 989-1010

Wu AM, Senter PD (2005) Arming antibodies: prospects and challenges for immunoconjugates. *Nat Biotechnol* **23**: 1137-1146

Wu TT, Kabat EA (1970) An analysis of the sequences of the variable regions of Bence Jones proteins and myeloma light chains and their implications for antibody complementarity. *J Exp Med* **132**: 211-250

Wust P, Gneveckow U, Johannsen M, Bohmer D, Henkel T, Kahmann F, Sehouli J, Felix R, Ricke J, Jordan A (2006) Magnetic nanoparticles for interstitial thermotherapy--feasibility, tolerance and achieved temperatures. *Int J Hyperthermia* **22**: 673-685

Wust P, Hildebrandt B, Sreenivasa G, Rau B, Gellermann J, Riess H, Felix R, Schlag PM (2002) Hyperthermia in combined treatment of cancer. *Lancet Oncol* **3**: 487-497

Yamazaki M, Ito T (1990) Deformation and instability in membrane structure of phospholipid vesicles caused by osmophobic association: mechanical stress model for the mechanism of poly(ethylene glycol)-induced membrane fusion. *Biochemistry* **29**: 1309-1314

Yanase M, Shinkai M, Honda H, Wakabayashi T, Yoshida J, Kobayashi T (1997) Intracellular hyperthermia for cancer using magnetite cationic liposomes: ex vivo study. *Jpn J Cancer Res* **88**: 630-632

Yanase M, Shinkai M, Honda H, Wakabayashi T, Yoshida J, Kobayashi T (1998a) Antitumor immunity induction by intracellular hyperthermia using magnetite cationic liposomes. *Jpn J Cancer Res* **89**: 775-782

Yanase M, Shinkai M, Honda H, Wakabayashi T, Yoshida J, Kobayashi T (1998b) Intracellular hyperthermia for cancer using magnetite cationic liposomes: an in vivo study. *Jpn J Cancer Res* **89**: 463-469

Yang AS, Lattime EC (2003) Tumor-induced interleukin 10 suppresses the ability of splenic dendritic cells to stimulate CD4 and CD8 T-cell responses. *Cancer Res* **63**: 2150-2157

Yang L, Mao H, Wang YA, Cao Z, Peng X, Wang X, Duan H, Ni C, Yuan Q, Adams G, Smith MQ, Wood WC, Gao X, Nie S (2009) Single chain epidermal growth factor receptor antibody conjugated nanoparticles for in vivo tumor targeting and imaging. *Small* **5**: 235-243

Yip YL, Ward RL (2002) Application of phage display technology to cancer research. *Curr Pharm Biotechnol* **3**: 29-43

Yokota T, Milenic DE, Whitlow M, Schlom J (1992) Rapid tumor penetration of a single-chain Fv and comparison with other immunoglobulin forms. *Cancer Res* **52**: 3402-3408

Zahnd C, Amstutz P, Pluckthun A (2007) Ribosome display: selecting and evolving proteins in vitro that specifically bind to a target. *Nat Methods* **4**: 269-279

Zalipsky S (1993) Synthesis of an end-group functionalized polyethylene glycol-lipid conjugate for preparation of polymer-grafted liposomes. *Bioconjug Chem* **4**: 296-299

Zee van der J (2002) Heating the patient: a promising approach? *Annals Oncol* **13:**1173-1184

Zhang Y, Kohler N, Zhang M (2002) Surface modification of superparamagnetic magnetite nanoparticles and their intracellular uptake. *Biomaterials* **23**: 1553-1561

Zhou J, Leuschner C, Kumar C, Hormes JF, Soboyejo WO (2006) Sub-cellular accumulation of magnetic nanoparticles in breast tumors and metastases. *Biomaterials* **27**: 2001-2008

Zhou Y, Drummond DC, Zou H, Hayes ME, Adams GP, Kirpotin DB, Marks JD (2007) Impact of Single-chain Fv Antibody Fragment Affinity on Nanoparticle Targeting of Epidermal Growth Factor Receptor-expressing Tumor Cells. *J Mol Biol* **371**: 934-947

Zimmermann W, Weber B, Ortlieb B, Rudert F, Schempp W, Fiebig HH, Shively JE, von KS, Thompson JA (1988) Chromosomal localization of the carcinoembryonic antigen gene family and differential expression in various tumors. *Cancer Res* **48**: 2550-2554

Appendix 2

Presentations and Publications

Oral Presentation

Vigor K, Kyrtatos P, Minogue S, Kallumadil, Al-Jamal K, Kogelberg H, Tolner B, Kostarelos K, Lythgoe M, Pankhurst Q, Chester K. Antibody targeted magnetic nanoparticles for imaging and therapy of cancer. Int, Conference on Nanomedicine, Greece, Sept 2007

Vigor K, Farrell D, Huhalov A, Tolner B , Kogelberg H , Pankhurst Q, Parkin I, Begent R, Chester K. Antibody nanoparticle conjugation for hyperthermic treatment of tumours.. ECSAPS, London, Sept 2006

Vigor K. Farrell D, Huhalov A, Tolner B , Kogelberg H , Pankhurst Q, Parkin I, Begent R, Chester K. Antibody nanoparticle conjugation for hyperthermic treatment of tumours. 6th Int, conference on the scientific and clinical application of magnetic carriers, Austria, May 2006

Poster presentation

K.Vigor, D Farrell, K Chester, I Parkin, Q Pankhurst, , Antibody nanoparticle conjugation for hyperthermic treatment of tumours. RSCBioNanoscience, Brighton, Sept 2005.

K.Vigor D Farrell, A Huhalov, B Tolner , H Kogelberg , Q Pankhurst, I Parkin, R Begent, K Chester. Antibody nanoparticle conjugation for hyperthermic treatment of tumours. Poster presentation, NCRI, Birmingham UK, Oct 2005.

Vigor K, Kyrtatos P, Minogue S Kogelberg H, Tolner B, Pankhurst Q, Chester K, Lythgoe M. Antibody targeted magnetic nanoparticles for imaging of cancer. ISMRM-ESMRMB. Berlin, Germany. May 2007

Publication

Vigor K, Kyrtatos P, Minogue S, Kallumadil, Al-Jamal K, Kogelberg H, Tolner B, Kostarelos K, Begent R H, Lythgoe M, Pankhurst Q, Chester K. Nanoparticles functionalised with recombinant single chain Fv antibody fragments (scFv) for the magnetic resonance imaging of cancer cells. Biomaterials 2010; 31: 1307-1315